Summary of the Bulletin of the International Seismological Centre

2015

January – June

Volume 52 Issue I

www.isc.ac.uk

isc-mirror.iris.washington.edu

ISSN 2309-236X

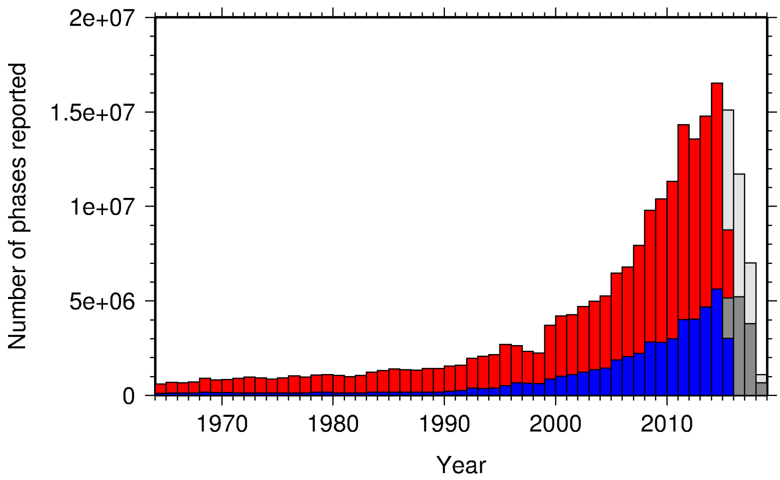

The number of phases (red) and number of amplitudes (blue) collected by the ISC for events each year since 1964. The data in grey covers the current period where data are still being collected before the ISC review takes place and are accurate at the time of publication. See Section 8.3.

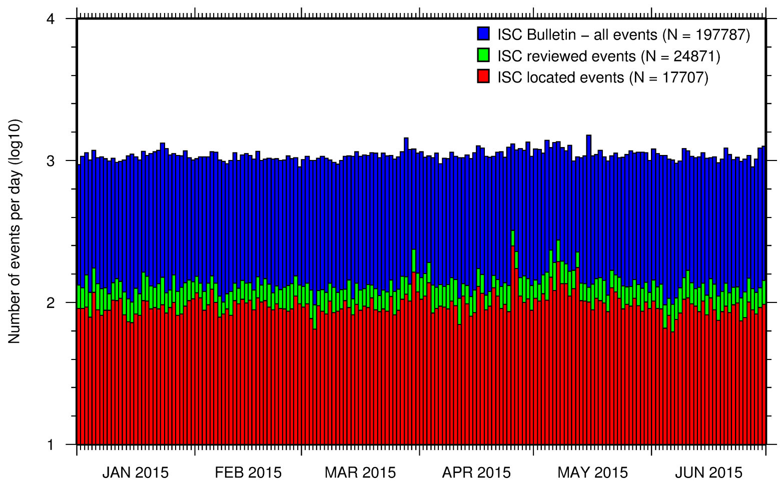

The number of events within the Bulletin for the current summary period. The vertical scale is logarithmic. See Section 9.1.

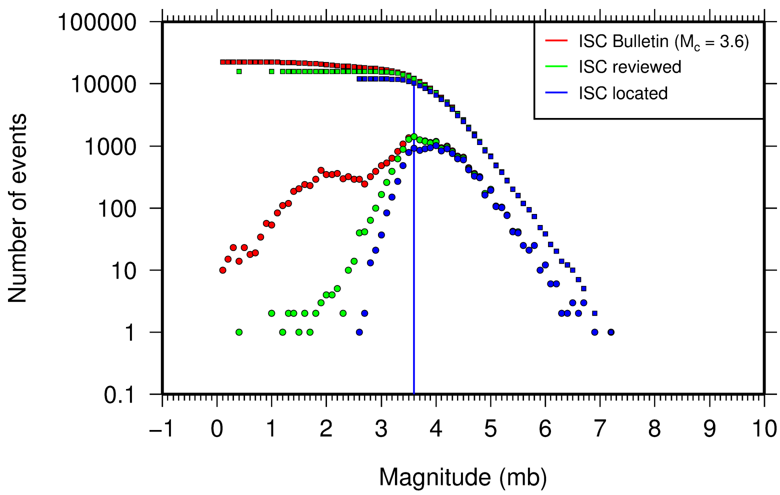

Frequency and cumulative frequency magnitude distribution for all events in the ISC Bulletin, ISC reviewed events and events located by the ISC. The magnitude of completeness (M_C) is shown for the ISC Bulletin. Note: only events with values of m_b are represented in the figure. See Section 9.4.

Summary of the Bulletin of the International Seismological Centre

2015

January - June

Volume 52 Issue I

Produced and edited by:
Kathrin Lieser, James Harris and Dmitry Storchak

Published by
International Seismological Centre

ISC Data Products

http://www.isc.ac.uk/products/

ISC Bulletin:

http://www.isc.ac.uk/iscbulletin/search

ISC Bulletin and Catalogue monthly files, to the last reviewed month in FFB or ISF1 format:

ftp://www.isc.ac.uk/pub/[isf|ffb]/bulletin/*yyyy*/*yyyymm*.gz

ftp://www.isc.ac.uk/pub/[isf|ffb]/catalogue/*yyyy*/*yyyymm*.gz

Datafiles for the ISC data before the rebuild:

ftp://www.isc.ac.uk/pub/prerebuild/[isf|ffb]/bulletin/*yyyy*/*yyyymm*.gz

ftp://www.isc.ac.uk/pub/prerebuild/[isf|ffb]/catalogue/*yyyy*/*yyyymm*.gz

ISC-EHB Bulletin:

http://www.isc.ac.uk/isc-ehb/search/

IASPEI Reference Event List (GT bulletin):

http://www.isc.ac.uk/gtevents/search/

ISC-GEM Global Instrumental Earthquake Catalogue:

http://http://www.isc.ac.uk/iscgem/download.php

ISC Event Bibliography:

http://www.isc.ac.uk/event_bibliography/bibsearch.php

International Seismograph Station Registry:

http://www.isc.ac.uk/registries/search/

Seismological Contacts:

http://www.isc.ac.uk/projects/seismocontacts/

International Seismological Centre
Pipers Lane
Thatcham
RG19 4NS
United Kingdom
www.isc.ac.uk

ISSN 2309-236X

Printed and bound in Wales by Cambrian Printers.

Contents

1

Preface

Dear Colleague,

This is the first 2015 issue of the Summary of the ISC Bulletin, which remains the most fundamental reason for continued operations at the ISC. This issue covers earthquakes and other seismic events that occurred during the period from January to June 2015. The full annual DVD-ROM will be attached to the second 2015 issue. In the mean time, the monthly files for January to June period are available from the ISC ftp site. For instructions, please see the www.isc.ac.uk/iscbulletin/.

This publication contains information on the ISC, its staff, Members, Sponsors and Data providers. It offers analysis of the data contributed to the ISC by many seismological agencies worldwide as well as analysis of the data in the ISC Bulletin itself. This issue also includes seismological standards and procedures used by the ISC in its operations.

Notably, this issue contains information on the recently released Rebuilt ISC Bulletin for the period 1964-1979 that replaced the original ISC Bulletin data.

We continue publishing invited articles describing the history, current status and operational procedures at those networks that contribute data to the ISC. This time it is the turn for the Norwegian seismic network at the University of Bergen and Finnish seismic network at the University of Helsinki.

We hope that you find this relatively new publication useful in your work. If your home-institution or company is unable, for one reason or another, to support the long-term international operations of the ISC in full by becoming a Member or a Sponsor, then, please, consider subscribing to this publication by contacting us at admin@isc.ac.uk.

With kind regards to our Data Contributors, Members, Sponsors and users,

Dr Dmitry A. Storchak
Director
International Seismological Centre (ISC)

2

The International Seismological Centre

2.1 The ISC Mandate

The International Seismological Centre (ISC) was set up in 1964 with the assistance of UNESCO as a successor to the International Seismological Summary (ISS) to carry forward the pioneering work of Prof. John Milne, Sir Harold Jeffreys and other British scientists in collecting, archiving and processing seismic station and network bulletins and preparing and distributing the definitive summary of world seismicity.

Under the umbrella of the International Association of Seismology and Physics of the Earth Interior (IASPEI/IUGG), the ISC has played an important role in setting international standards such as the International Seismic Bulletin Format (ISF), the IASPEI Standard Seismic Phase List (SSPL) and both the old and New IASPEI Manual of the Seismological Observatory Practice (NMSOP-2) (www.iaspei.org/projects/NMSOP.html).

The ISC has contributed to scientific research and prominent scientists such as John Hodgson, Eugine Herrin, Hal Thirlaway, Jack Oliver, Anton Hales, Ola Dahlman, Shigeji Suehiro, Nadia Kondorskaya, Vit Karnik, Stephan Müller, David Denham, Bob Engdahl, Adam Dziewonski, John Woodhouse and Guy Masters all considered it an important duty to serve on the ISC Executive Committee and the Governing Council.

The current mission of the ISC is to maintain:

- the ISC **Bulletin** – the longest continuous definitive summary of World seismicity (collaborating with 130 seismic networks and data centres around the world). (www.isc.ac.uk/iscbulletin/)
- the International Seismographic Station Registry (**IR**, jointly with the World Data Center for Seismology, Denver). (www.isc.ac.uk/registries/)
- the IASPEI Reference Event List (Ground Truth, **GT**, jointly with IASPEI). (www.isc.ac.uk/gtevents/)

These are fundamentally important tasks. Bulletin data produced, archived and distributed by the ISC for almost 50 years are the definitive source of such information and are used by thousands of seismologists worldwide for seismic hazard estimation, for tectonic studies and for regional and global imaging of the Earth's structure. Key information in global tomographic imaging is derived from the analysis of ISC data. The ISC Bulletin served as a major source of data for such well known products as the ak135 global 1-D velocity model and the EHB (*Engdahl et al.*, 1998) and Centennial (*Engdahl and Villaseñor*, 2002) catalogues. It presents an important quality-control benchmark for the Comprehensive Nuclear-Test-Ban Treaty Organization (CTBTO). Hypocentre parameters from the ISC Bulletin are used by the Data Management Center of the Incorporated Research Institutions for Seismology (IRIS DMC) to serve event-oriented user-requests for waveform data. The ISC-GEM Bulletin is a cornerstone of the ISC-GEM Global Instrumental Reference Earthquake Catalogue for Global Earthquake risk Model (GEM).

The ISC Bulletin contains over 6 million seismic events: earthquakes, chemical and nuclear explosions, mine blasts and mining induced events. At least 1.7 million of them are regional and teleseismically recorded events that have been reviewed by the ISC analysts. The ISC Bulletin contains approximately 200 million individual seismic station readings of arrival times, amplitudes, periods, SNR, slowness and azimuth, reported by approximately 17,000 seismic stations currently registered in the IR. Over 6,000 stations have contributed to the ISC Bulletin in recent years. This number includes the numerous sites of the USArray. The IASPEI GT List currently contains 8816 events for which latitude, longitude and depth of origin are known with high confidence (to 5 km or better) and seismic signals were recorded at regional and/or teleseismic distances.

2.2 Brief History of the ISC

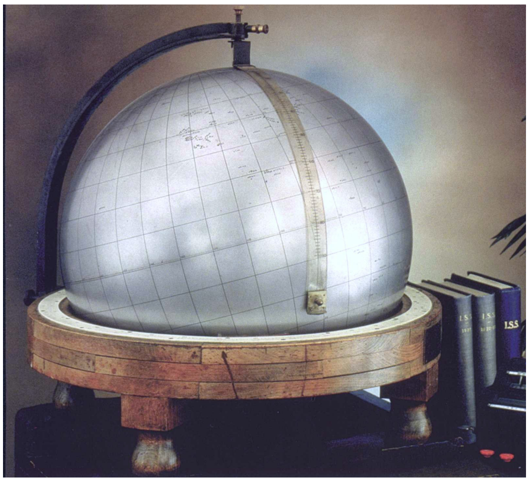

Figure 2.1: *The steel globe bearing positions of early seismic stations was used for locating positions of earthquakes for the International Seismological Summaries.*

Earthquake effects have been noted and documented from the earliest times, but it is only since the development of earthquake recording instruments in the latter half of the 19th century that a proper study of their occurrence has been possible. After the first teleseismic observation of an earthquake in 1889, the need for international exchange of readings was recognised in 1895 by Prof. John Milne and by Ernst von Rebeur Paschwitz together with Georg Gerland, resulting in the publication of the first international seismic bulletins. Milne's "Shide Circulars" were issued under the auspices of the Seismological Committee of the British Association for the Advancement of Science (BAAS), while co-workers of Gerland at the Central Bureau of the International Association of Seismology worked independently in Strasbourg (BCIS).

Following Milne's death in 1913, Seismological Bulletins of the BAAS were continued under Prof. H.H. Turner, later based at Oxford University. Upon formal post-war dissolution of the International Association of Seismology in 1922 the newly founded Seismological Section of the International Union of Geodesy and Geophysics (IUGG) set up the International Seismological Summary (ISS) to continue at Oxford under Turner, to produce the definitive global catalogues from the 1918 data-year onwards, under the auspices of IUGG and with the support of the BAAS.

ISS production, led by several professors at Oxford University, and Sir Harold Jeffreys at Cambridge

University, continued until it was superseded by the ISC Bulletin, after the ISC was formed in Edinburgh in 1964 with Dr P.L. Willmore as its first director.

During the period 1964 to 1970, with the help of UNESCO and other international scientific bodies, the ISC was reconstituted as an international non-governmental body, funded by interested institutions from various countries. Initially there were supporting members from seven countries, now there are almost 60, and member institutions include national academies, research foundations, government departments and research institutes, national observatories and universities. Each member, contributing a minimum unit of subscription or more, appoints a representative to the ISC's Governing Council, which meets every two years to decide the ISC's policy and operational programme. Representatives from the International Association of Seismology and Physics of the Earth's Interior also attend these meetings. The Governing Council appoints the Director and a small Executive Committee to oversee the ISC's operations.

Figure 2.2: *ISC building in Thatcham, Berkshire, UK.*

In 1975, the ISC moved to Newbury in southern England to make use of better computing facilities there. The ISC subsequently acquired its own computer and in 1986 moved to its own building at Pipers Lane, Thatcham, near Newbury. The internal layout of the new premises was designed for the ISC and includes not only office space but provision for the storage of extensive stocks of ISS and ISC publications and a library of seismological observatory bulletins, journals and books collected over many tens of years.

In 1997 the first set of the ISC Bulletin CD-ROMs was produced (not counting an earlier effort at USGS). The first ISC website appeared in 1998 and the first ISC database was put in day-to-day operations from 2001.

Throughout 2009-2011 a major internal reconstruction of the ISC building was undertaken to allow for more members of staff working in mainstream ISC operations as well as major development projects such as the CTBTO Link, ISC-GEM Catalogue and the ISC Bulletin Rebuild.

2.3 Former Directors of the ISC and its U.K. Predecessors

John Milne
Publisher of the Shide Circular Reports on Earthquakes
1899-1913

Herbert Hall Turner

Seismological Bulletins of the BAAS

1913-1922
Director of the ISS
1922-1930

Harry Hemley Plaskett
Director of the ISS
1931-1946

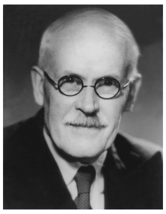

Harold Jeffreys
Director of the ISS
1946-1957

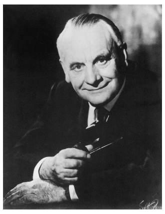

Robert Stoneley
Director of the ISS
1957-1963

P.L. (Pat) Willmore
Director of the ISS
1963-1970
Director of the ISC
1964-1970

Edouard P. Arnold
Director of the ISC
1970-1977

Anthony A. Hughes
Director of the ISC
1977-1997

Raymond J. Willemann
Director of the ISC
1998-2003

Avi Shapira
Director of the ISC
2004-2007

2.4 Member Institutions of the ISC

Article IV(a-b) of the ISC Working Statutes stipulates that any national academy, agency, scientific institution or other non-profit organisation may become a Member of the ISC on payment to the ISC of a sum equal to at least one unit of subscription and the nomination of a voting representative to serve on the ISC's governing body. Membership shall be effective for one year from the date of receipt at the ISC of the annual contribution of the Member and is thereafter renewable for periods of one year.

The ISC is currently supported with funding from its 62 Member Institutions and a four-year Grant Award EAR-1417970 from the US National Science Foundation.

Figures 2.3 and 2.4 show major sectors to which the ISC Member Institutions belong and proportional financial contributions that each of these sectors make towards the ISC's annual budget.

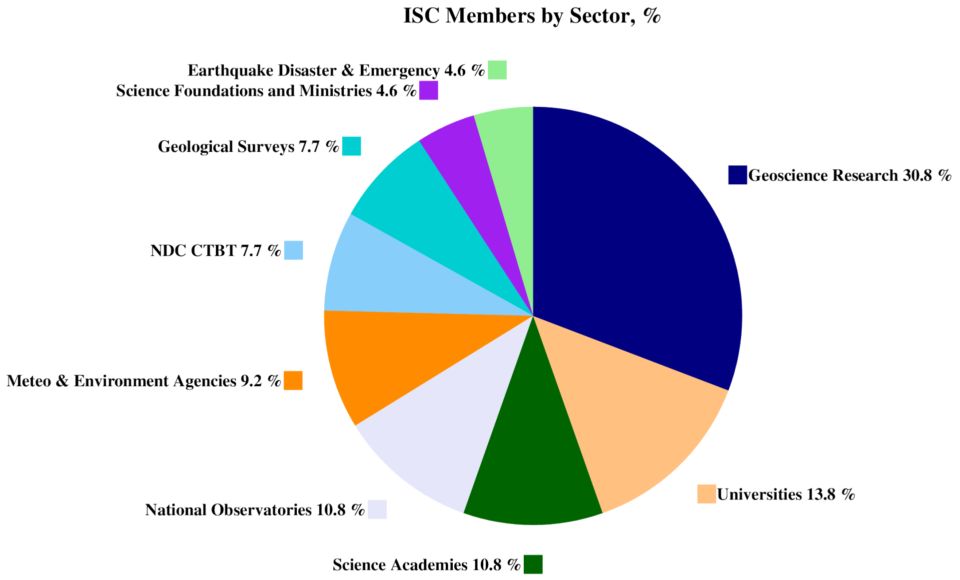

Figure 2.3: *Distribution of the ISC Member Institutions by sector in year 2013 as a percentage of total number of Members.*

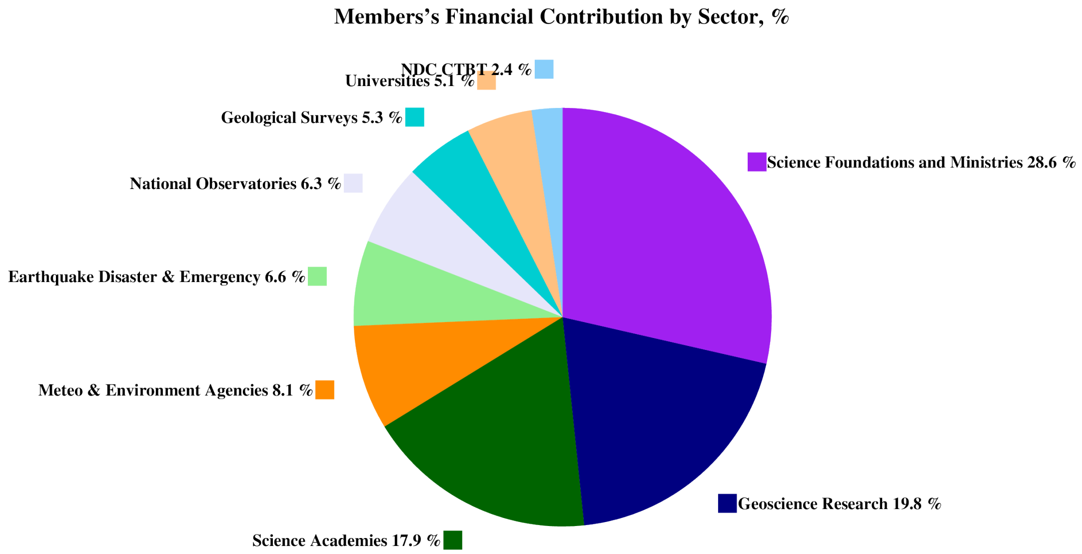

Figure 2.4: *Distribution of Member's financial contributions to the ISC by sector in year 2013 as a percentage of total annual Member contributions.*

There follows a list of all current Member Institutions with a category (1 through 9) assigned according to the ISC Working Statutes. Each category relates to the number of membership units contributed.

Centre de Recherche en Astronomie, Astrophysique et Géophysique (CRAAG)
Algeria
www.craag.dz
Category: 1

Instituto Nacional de Prevención Sísmica (INPRES)
Argentina
www.inpres.gov.ar
Category: 1

Geoscience Australia
Australia
www.ga.gov.au
Category: 4

Bundesministerium für Wissenschaft, Forschung und Wirtschaft (BMWFW)
Austria
www.bmbwk.gv.at
Category: 2

Centre of Geophysical Monitoring (CGM) of the National Academy of Sciences of Belarus
Belarus
www.cgm.org.by
Category: 1

Belgian Science Policy Office (BELSPO)
Belgium

Category: 1

Universidade de São Paulo, Centro de Sismologia
Brazil
www.sismo.iag.usp.br
Category: 1

Seismological Observatory, Institute of Geosciences, University of Brasilia
Brazil
www.obsis.unb.br
Category: 1

The Geological Survey of Canada
Canada
gsc.nrcan.gc.ca
Category: 4

Centro Sismologico Nacional, Universidad de Chile
Chile
ingenieria.uchile.cl
Category: 1

China Earthquake Administration
China
www.cea.gov.cn
Category: 4

Institute of Earth Sciences, Academia Sinica
Chinese Taipei
www.earth.sinica.edu.tw
Category: 1

Geological Survey Department
Cyprus
www.moa.gov.cy
Category: 1

Insitute of Geophysics, Academy of Sciences of the Czech Republic
Czech Republic
www.avcr.cz
Category: 1

Geological Survey of Denmark and Greenland (GEUS)
Denmark
www.geus.dk
Category: 2

National Research Institute for Astronomy and Geophysics (NRIAG), Cairo
Egypt
www.nriag.sci.eg
Category: 1

The University of Helsinki
Finland
www.helsinki.fi
Category: 2

Laboratoire de Détection et de Géophysique/CEA
France
www-dase.cea.fr
Category: 2

Institute National des Sciences de l'Univers
France
www.insu.cnrs.fr
Category: 4

GeoForschungsZentrum Potsdam
Germany
www.gfz-potsdam.de
Category: 2

Bundesanstalt für Geowissenschaften und Rohstoffe
Germany
www.bgr.bund.de
Category: 4

The Seismological Institute, National Observatory of Athens
Greece
www.noa.gr
Category: 1

The Hungarian Academy of Sciences
Hungary
www.mta.hu
Category: 1

The Icelandic Meteorological Office
Iceland
www.vedur.is
Category: 1

National Centre for Seismology, Ministry of Earth Sciences of India
India
www.moes.gov.in
Category: 4

Iraqi Meteorological Organization and Seismology
Iraq
www.imos-tm.com
Category: 1

The Geophysical Institute of Israel
Israel
www.gii.co.il
Category: 1

Soreq Nuclear Research Centre (SNRC)
Israel
www.soreq.gov.il
Category: 1

Istituto Nazionale di Geofisica e Vulcanologia
Italy
www.ingv.it
Category: 3

Istituto Nazionale di Oceanografia e di Geofisica Sperimentale
Italy
www.ogs.trieste.it
Category: 1

University of the West Indies at Mona
Jamaica
www.mona.uwi.edu
Category: 1

Japan Agency for Marine-Earth Science and Technology (JAMSTEC)
Japan
www.jamstec.go.jp
Category: 2

Earthquake Research Institute, University of Tokyo
Japan
www.eri.u-tokyo.ac.jp
Category: 3

The Japan Meteorological Agency (JMA)
Japan
www.jma.go.jp
Category: 5

National Institute of Polar Research (NIPR)
Japan
www.nipr.ac.jp
Category: 1

Royal Scientific Society
Jordan
www.rss.jo
Category: 1

Centro de Investigación Científica y de Educación Superior de Ensenada (CICESE)
Mexico
resnom.cicese.mx
Category: 1

Institute of Geophysics, National University of Mexico
Mexico
www.igeofcu.unam.mx
Category: 1

The Royal Netherlands Meteorological Institute (KNMI)
Netherlands
www.knmi.nl
Category: 2

GNS Science
New Zealand
www.gns.cri.nz
Category: 3

The University of Bergen
Norway
www.uib.no
Category: 2

Stiftelsen NORSAR
Norway
www.norsar.no
Category: 2

Institute of Geophysics, Polish Academy of Sciences
Poland
www.igf.edu.pl
Category: 1

Instituto Português do Mar e da Atmosfera
Portugal
www.ipma.pt
Category: 2

Red Sísmica de Puerto Rico
Puerto Rico
redsismica.uprm.edu
Category: 1

Korean Meterological Administration
Republic of Korea
www.kma.go.kr
Category: 1

National Institute for Earth Physics
Romania
www.infp.ro
Category: 1

Russian Academy of Sciences
Russia
www.ras.ru
Category: 5

Earth Observatory of Singapore (EOS), an autonomous Institute of Nanyang Technological University
Singapore
www.earthobservatory.sg
Category: 1

Environmental Agency of Slovenia
Slovenia
www.arso.gov.si
Category: 1

Council for Geoscience
South Africa
www.geoscience.org.za
Category: 1

Institut Cartogràfic i Geològic de Catalunya (ICGC)
Spain
www.icgc.cat
Category: 1

Institute of Earth Sciences Jaume Almera
Spain
www.ictja.csic.es
Category: 1

Uppsala Universitet
Sweden
www.uu.se
Category: 2

National Defence Research Establishment (FOI)
Sweden
www.foi.se
Category: 1

The Swiss Academy of Sciences
Switzerland
www.scnat.ch
Category: 2

The Seismic Research Centre, University of the West Indies at St. Augustine
Trinidad and Tobago
www.uwiseismic.com
Category: 1

Kandilli Observatory and Earthquake Research Institute
Turkey
www.koeri.boun.edu.tr
Category: 1

Disaster and Emergency Management Authority (AFAD)
Turkey
www.deprem.gov.tr
Category: 2

AWE Blacknest
United Kingdom
www.blacknest.gov.uk
Category: 1

The Royal Society
United Kingdom
www.royalsociety.org
Category: 6

British Geological Survey
United Kingdom
www.bgs.ac.uk
Category: 2

Incorporated Research Institutions for Seismology
U.S.A.
www.iris.edu
Category: 1

National Earthquake Information Center, U.S. Geological Survey
U.S.A.
www.neic.usgs.gov
Category: 1

The National Science Foundation of the United States. (Grant No. EAR-1417970)
U.S.A.
www.nsf.gov
Category: 9

In addition the ISC is currently in receipt of grants from the International Data Centre (IDC) of the Preparatory Commission of the Comprehensive Nuclear-Test-Ban Treaty Organization (CTBTO), FM Global, Lighthill risk Network, OYO, USGS (Award G15AC00202) and BGR.

2.5 Sponsoring Organisations

Article IV(c) of the ISC Working Statutes stipulates any commercial organisation with an interest in the objectives and/or output of the ISC may become an Associate Member of the ISC on payment of an Associate membership fee, but without entitlement to representation with a vote on the ISC's governing body.

www.reftek.com

REF TEK designs and manufactures application specific, high-performance, battery-operated, field-portable geophysical data acquisition devices for the global market. With over 35 years of experience, REF TEK provides customers with complete turnkey solutions that include high resolution recorders, broadband sensors, state-of-the-art communications (V-SAT, GPRS, etc), installation, training, and continued customer support. Over 7,000 REF TEK instruments are currently being used globally for multiple applications. From portable earthquake monitoring to telemetry earthquake monitoring, earthquake aftershock recording to structural monitoring and more, REF TEK equipment is suitable for a wide variety of application needs.

GeoSIG swiss made to measure http://www.geosig.com/

GeoSIG provides earthquake, seismic, structural, dynamic and static monitoring and measuring solutions As an ISO Certified company, GeoSIG is a world leader in design and manufacture of a diverse range of high quality, precision instruments for vibration and earthquake monitoring. GeoSIG instruments are at work today in more than 100 countries around the world with well-known projects such as the NetQuakes installation with USGS and Oresund Bridge in Denmark. GeoSIG offers off-the-shelf solutions as well as highly customised solutions to fulfil the challenging requirements in many vertical markets including the following:

- Earthquake Early Warning and Rapid Response (EEWRR)
- Seismic and Earthquake Monitoring and Measuring
- Industrial Facility Seismic Monitoring and Shutdown
- Structural Analysis and Ambient Vibration Testing
- Induced Vibration Monitoring
- Research and Scientific Applications

güralp http://www.guralp.com/

Güralp has been developing revolutionary force-feedback broadband seismic instrumentation for more than thirty years. Our sensors record seismic signals of all kinds, from teleseismic events occurring on the other side of the planet, to microseisms induced by unconventional hydrocarbon extraction. Our sophisticated digitisers record these signals with the highest resolution and accurate timing.

We supply individual instruments or complete seismic systems. Our services include field support such as installation and maintenance, to complete network and data management.

We design our instruments to meet increasingly complex requirements for deployment in the most challenging circumstances. As a result, you will find Güralp instruments gathering seismic data in the harshest of environments, from the Antarctic ice sheet; to boreholes 100s of metres deep; to the world's most active volcanoes and deepest ocean trenches.

http://src.com.au/

The Seismology Research Centre is an Australian earthquake observatory that began developing their own seismic recorders and data processing software in the late 1970s when digital recorders were uncommon. The Gecko is the SRC's 7th generation of seismic recorder, now available with a variety of integrated sensors to meet every monitoring requirement, including:

- Strong Motion Accelerographs
- 2Hz and 4.5Hz Blast Vibration Monitors
- Short Period 1Hz Seismographs
- Broadband 200s-1500Hz Optical Seismographs

Visit src.com.au/downloads/waves to grab a free copy of the SRC's MiniSEED waveform viewing and analysis software application, Waves.

2.6 Data Contributing Agencies

In addition to its Members and Sponsors, the ISC owes its existence and successful long-term operations to its 149 seismic bulletin data contributors. These include government agencies responsible for national seismic networks, geoscience research institutions, geological surveys, meteorological agencies, universities, national data centres for monitoring the CTBT and individual observatories. There would be no ISC Bulletin available without the regular stream of data that are unselfishly and generously contributed to the ISC on a free basis.

East African Network
EAF

The Institute of Seismology, Academy of Sciences of Albania
Albania
TIR

Centre de Recherche en Astronomie, Astrophysique et Géophysique
Algeria
CRAAG

Universidad Nacional de La Plata
Argentina
LPA

Instituto Nacional de Prevención Sísmica
Argentina
SJA

National Survey of Seismic Protection
Armenia
NSSP

Curtin University
Australia
CUPWA

Geoscience Australia
Australia
AUST

Zentralanstalt für Meteorologie und Geodynamik (ZAMG)
Austria
VIE

International Data Centre, CTBTO
Austria
IDC

Republic Center of Seismic Survey
Azerbaijan
AZER

Royal Observatory of Belgium
Belgium
UCC

Observatorio San Calixto
Bolivia
SCB

Republic Hydrometeorological Service, Seismological Observatory, Banja Luka
Bosnia-Herzegovina
RHSSO

Instituto Astronomico e Geofísico
Brazil
VAO

Geophysical Institute, Bulgarian Academy of Sciences
Bulgaria
SOF

Seismological Observatory of Mount Cameroon
Cameroon
SOMC

Canadian Hazards Information Service, Natural Resources Canada
Canada
OTT

Centro Sismológico Nacional, Universidad de Chile
Chile
GUC

China Earthquake Networks Center
China
BJI

Institute of Earth Sciences, Academia Sinica
Chinese Taipei
ASIES

CWB
Chinese Taipei
TAP

Red Sismológica Nacional de Colombia
Colombia
RSNC

Sección de Sismología, Vulcanología y Exploración Geofísica
Costa Rica
UCR

Seismological Survey of the Republic of Croatia
Croatia
ZAG

Servicio Sismológico Nacional Cubano
Cuba
SSNC

Cyprus Geological Survey Department
Cyprus
NIC

Geophysical Institute, Academy of Sciences of the Czech Republic
Czech Republic
PRU

The Institute of Physics of the Earth (IPEC)
Czech Republic
IPEC

Geological Survey of Denmark and Greenland
Denmark
DNK

Observatorio Sismologico Politecnico Loyola
Dominican Republic
OSPL

Servicio Nacional de Sismología y Vulcanología
Ecuador
IGQ

National Research Institute of Astronomy and Geophysics
Egypt
HLW

Servicio Nacional de Estudios Territoriales
El Salvador
SNET

University of Addis Ababa
Ethiopia
AAE

Seismological Observatory Skopje
FYR Macedonia
SKO

Institute of Seismology, University of Helsinki
Finland
HEL

Laboratoire de Détection et de Géophysique/CEA
France
LDG

EOST / RéNaSS
France
STR

Laboratoire de Géophysique/CEA
French Polynesia
PPT

Institute of Earth Sciences/ National Seismic Monitoring Center
Georgia
TIF

Alfred Wegener Institute for Polar and Marine Research
Germany
AWI

Seismological Observatory Berggießhübel, TU Bergakademie Freiberg
Germany
BRG

Geophysikalisches Observatorium Collm
Germany
CLL

Bundesanstalt für Geowissenschaften und Rohstoffe
Germany
BGR

National Observatory of Athens
Greece
ATH

University of Patras, Department of Geology
Greece
UPSL

Department of Geophysics, Aristotle University of Thessaloniki
Greece
THE

INSIVUMEH
Guatemala
GCG

Hong Kong Observatory
Hong Kong
HKC

Geodetic and Geophysical Research Institute
Hungary
BUD

Geodetic and Geophysical Reasearch Institute, Hungarian Academy of Sciences
Hungary
KRSZO

Icelandic Meteorological Office
Iceland
REY

National Geophysical Research Institute
India
HYB

National Centre for Seismology of the Ministry of Earth Sciences of India
India
NDI

Badan Meteorologi, Klimatologi dan Geofisika
Indonesia
DJA

International Institute of Earthquake Engineering and Seismology (IIEES)
Iran
THR

Tehran University
Iran
TEH

Iraqi Meteorological and Seismology Organisation
Iraq
ISN

The Geophysical Institute of Israel
Israel
GII

Istituto Nazionale di Oceanografia e di Geofisica Sperimentale (OGS)
Italy
TRI

Dipartimento per lo Studio del Territorio e delle sue Risorse (RSNI)
Italy
GEN

Istituto Nazionale di Geofisica e Vulcanologia
Italy
ROM

Laboratory of Research on Experimental and Computational Seimology
Italy
RISSC

MedNet Regional Centroid - Moment Tensors
Italy
MED_RCMT

Station Géophysique de Lamto
Ivory Coast
LIC

Jamaica Seismic Network
Jamaica
JSN

National Research Institute for Earth Science and Disaster Prevention
Japan
NIED

National Institute of Polar Research
Japan
SYO

The Matsushiro Seismological Observatory
Japan
MAT

Japan Meteorological Agency
Japan
JMA

Jordan Seismological Observatory
Jordan
JSO

National Nuclear Center
Kazakhstan
NNC

Seismological Experimental Methodological Expedition
Kazakhstan
SOME

Kuwait Institute for Scientific Research
Kuwait
KISR

Kyrgyz Seismic Network
Kyrgyzstan
KNET

Institute of Seismology, Academy of Sciences of Kyrgyz Republic
Kyrgyzstan
KRNET

Latvian Seismic Network
Latvia
LVSN

National Council for Scientific Research
Lebanon
GRAL

Geological Survey of Lithuania
Lithuania
LIT

European Center for Geodynamics and Seismology
Luxembourg
ECGS

Macao Meteorological and Geophysical Bureau
Macao, China
MCO

Geological Survey Department Malawi
Malawi
GSDM

Malaysian Meteorological Service
Malaysia
KLM

Instituto de Geofísica de la UNAM
Mexico
MEX

Centro de Investigación Científica y de Educación Superior de Ensenada
Mexico
ECX

Institute of Geophysics and Geology
Moldova
MOLD

Seismological Institute of Montenegro
Montenegro
PDG

Centre National de Recherche
Morocco
CNRM

The Geological Survey of Namibia
Namibia
NAM

National Seismological Centre, Nepal
Nepal
DMN

IRD Centre de Nouméa
New Caledonia
NOU

Institute of Geological and Nuclear Sciences
New Zealand
WEL

Instituto Nicaraguense de Estudios Territoriales - INETER
Nicaragua
INET

Stiftelsen NORSAR
Norway
NAO

University of Bergen
Norway
BER

Sultan Qaboos University
Oman
OMAN

Micro Seismic Studies Programme, PINSTECH
Pakistan
MSSP

Universidad de Panama
Panama
UPA

Manila Observatory
Philippines
QCP

Philippine Institute of Volcanology and Seismology
Philippines
MAN

Institute of Geophysics, Polish Academy of Sciences
Poland
WAR

Instituto Português do Mar e da Atmosfera, I.P.
Portugal
INMG

Sistema de Vigilância Sismológica dos Açores
Portugal
SVSA

Instituto Geofisico do Infante Dom Luiz
Portugal
IGIL

Centre of Geophysical Monitoring of the National Academy of Sciences of Belarus
Republic of Belarus
BELR

Inst. of Seismology and Geodynamics, V.I. Vernadsky Crimean Federal University
Republic of Crimea
CFUSG

Korea Meteorological Administration
Republic of Korea
KMA

National Institute for Earth Physics
Romania
BUC

Kola Regional Seismic Centre, GS RAS
Russia
KOLA

Mining Institute of the Ural Branch of the Russian Academy of Sciences
Russia
MIRAS

Geophysical Survey of Russian Academy of Sciences
Russia
MOS

North Eastern Regional Seismological Centre, GS RAS
Russia
NERS

Kamchatkan Experimental and Methodical Seismological Department, GS RAS
Russia
KRSC

Institute of Environmental Problems of the North, Russian Academy of Sciences
Russia
IEPN

Sakhalin Experimental and Methodological Seismological Expedition, GS RAS
Russia
SKHL

Baykal Regional Seismological Centre, GS SB RAS
Russia
BYKL

Yakutiya Regional Seismological Center, GS SB RAS
Russia
YARS

Altai-Sayan Seismological Centre, GS SB RAS
Russia
ASRS

Saudi Geological Survey
Saudi Arabia
SGS

Seismological Survey of Serbia
Serbia
BEO

Geophysical Institute, Slovak Academy of Sciences
Slovakia
BRA

Slovenian Environment Agency
Slovenia
LJU

Ministry of Mines, Energy and Rural Electrification
Solomon Islands
HNR

Council for Geoscience
South Africa
PRE

Instituto Geográfico Nacional
Spain
MDD

Real Instituto y Observatorio de la Armada
Spain
SFS

Institut Cartogràfic i Geològic de Catalunya
Spain
MRB

University of Uppsala
Sweden
UPP

Swiss Seismological Service (SED)
Switzerland
ZUR

Thai Meteorological Department
Thailand
BKK

The Seismic Research Centre
Trinidad and Tobago
TRN

Institut National de la Météorologie
Tunisia
TUN

Disaster and Emergency Management Presidency
Turkey
DDA

Kandilli Observatory and Research Institute
Turkey
ISK

Red Sísmica de Puerto Rico
U.S.A.
RSPR

National Earthquake Information Center
U.S.A.
NEIC

Pacific Northwest Seismic Network
U.S.A.
PNSN

IRIS Data Management Center
U.S.A.
IRIS

The Global CMT Project
U.S.A.
GCMT

Subbotin Institute of Geophysics, National Academy of Sciences
Ukraine
SIGU

Main Centre for Special Monitoring
Ukraine
MCSM

Dubai Seismic Network
United Arab Emirates
DSN

British Geological Survey
United Kingdom
BGS

Institute of Seismology, Academy of Sciences, Republic of Uzbekistan
Uzbekistan
ISU

Fundación Venezolana de Investigaciones Sismológicas
Venezuela
FUNV

National Center for Scientific Research
Vietnam
PLV

Geological Survey Department of Zambia
Zambia
LSZ

Goetz Observatory
Zimbabwe
BUL

2.7 ISC Staff

Listed below are the staff (and their country of origin) who were employed at the ISC at the time of this ISC Bulletin Summary.

- Dmitry Storchak
- Director
- Russia/United Kingdom

- Lynn Elms
- Administration Officer
- United Kingdom

- James Harris
- Senior System and Database Administrator
- United Kingdom

- Alfie James Barber
- System Administrator
- United Kingdom

- Gergely Csontos
- Web Developer
- Hungary

- John Eve
- Data Collection Officer
- United Kingdom

- Edith Korger
- Data Collection Seismologist
- Austria

- Domenico Di Giacomo
- Seismologist
- Italy

- Konstantinos Lentas
- Seismologist/Developer
- Greece

- Rosemary Hulin (née Wylie)
- Analyst/Administrator
- United Kingdom

- Blessing Shumba
- Seismologist/Analyst
- Zimbabwe

- Rebecca Verney
- Analyst
- United Kingdom

- Jennifer Weston
- Seismologist/Analyst
- United Kingdom

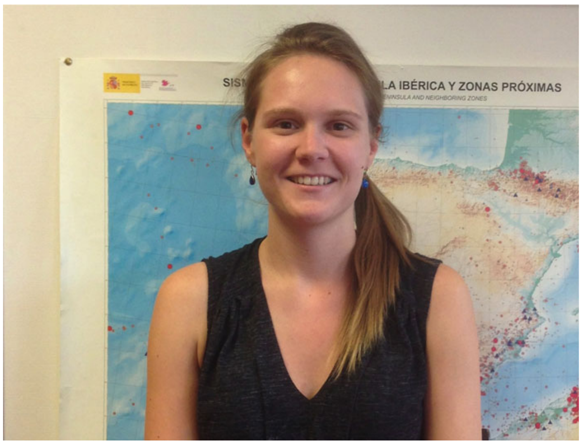

- Elizabeth Entwistle
- Seismologist/Analyst
- United Kingdom

- Elizabeth Ayres (née Ball)
- Analyst/Historical Data Entry Officer
- United Kingdom

- Kathrin Lieser
- Seismologist/Analyst
- Germany

- Lonn Brown
- Seismologist/Analyst
- Canada

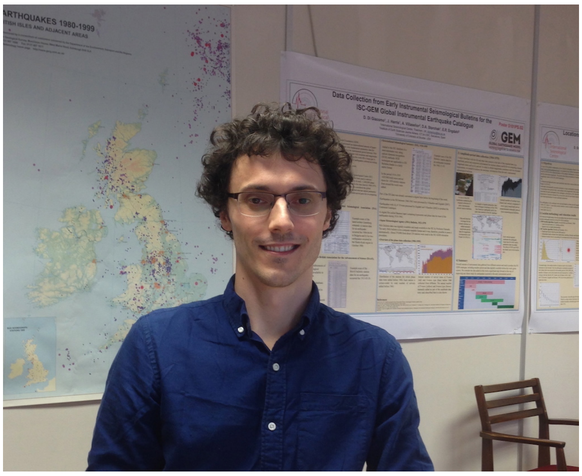

- Charikleia Gkarlaouni
- Seismologist/Analyst
- Greece

- Peter Franek
- Seismologist/Analyst
- Slovakia

- Daniela Olaru
- Historical Data Entry Officer
- Romania

3

Availability of the ISC Bulletin

The ISC Bulletin is available from the following sources:

- Web searches
  The entire ISC Bulletin is available directly from the ISC website via tailored searches.
  (www.isc.ac.uk/iscbulletin/search)
  (isc-mirror.iris.washington.edu/iscbulletin/search)
  - Bulletin search - provides the most verbose output of the ISC Bulletin in ISF or QuakeML.
  - Event catalogue - only outputs the prime hypocentre for each event, producing a simple list of events, locations and magnitudes.
  - Arrivals - search for arrivals in the ISC Bulletin. Users can search for specific phases for selected stations and events.
- CD-ROMs/DVD-ROMs

  CDs/DVDs can be ordered from the ISC for any published volume (one per year), or for all back issues of the Bulletin (not including the latest volume). The data discs contain the Bulletin as a PDF, in IASPEI Seismic Format (ISF), and in Fixed Format Bulletin (FFB) format. An event catalogue is also included, together with the International Registry of seismic station codes.
- FTP site

  The ISC Bulletin is also available to download from the ISC ftp site, which contains the Bulletin in PDF, ISF and FFB formats. (ftp://www.isc.ac.uk)
  (ftp://isc-mirror.iris.washington.edu)

Mirror service

A mirror of the ISC database, website and ftp site is available at IRIS DMC (isc-mirror.iris.washington.edu), which benefits from their high-speed internet connection, providing an alternative method of accessing the ISC Bulletin.

4

Citing the International Seismological Centre

Data from the ISC should always be cited. This includes use by academic or commercial organisations, as well as individuals. A citation should show how the data were retrieved and may be in one of these suggested forms:

Data retrieved from the ISC web site:

- International Seismological Centre, On-line Bulletin, http://www.isc.ac.uk, Internatl. Seismol. Cent., Thatcham, United Kingdom, 2018.

Data transcribed from the IASPEI reference event bulletin:

- International Seismological Centre, Reference Event Bulletin, http://www.isc.ac.uk, Internatl. Seismol. Cent., Thatcham, United Kingdom, 2018.

Data transcribed from the EHB bulletin:

- International Seismological Centre, EHB Bulletin, http://www.isc.ac.uk, Internatl. Seismol. Cent., Thatcham, United Kingdom, 2018.

Data copied from ISC CD-ROMs/DVD-ROMs:

- International Seismological Centre, Bulletin Disks 1-25 [CD-ROM], Internatl. Seismol. Cent., Thatcham, United Kingdom, 2018.

Data transcribed from the printed Bulletin:

- International Seismological Centre, Bull. Internatl. Seismol. Cent., 46(9-12), Thatcham, United Kingdom, 2009.

Data transcribed from the printed Summary of the Bulletin:

- International Seismological Centre, Summ. Bull. Internatl. Seismol. Cent., January - June 2015, 52(I), Thatcham, United Kingdom, 2018.

The ISC is named as a valid data centre for citations within American Geophysical Union (AGU) publications. As such, please follow the AGU guidelines when referencing ISC data in one of their journals. The ISC may be cited as both the institutional author of the Bulletin and the source from which the data were retrieved.

BibTex entry example:

```
@manual{ISCcitation2018,
author = "International Seismological Centre",
title = "On-line Bulletin",
organization = "Internatl. Seismol. Cent.",
note = "http://www.isc.ac.uk",
address = "Thatcham, United Kingdom",
year = "2018"
}
```

5

Operational Procedures of Contributing Agencies

5.1 Seismic Monitoring and Data Processing at the Norwegian National Seismic Network

Lars Ottemöller, Marte Louise Strømme and Berit Marie Storheim
Department of Earth Science, University of Bergen, Bergen, Norway


Lars Ottemöller


Marte Louise Strømme


Berit Marie Storheim

5.1.1 Introduction

The Norwegian National Seismic Network (NNSN) is operated by the University of Bergen (UiB) to monitor the area covering mainland Norway, the North Sea, Norwegian Sea, Barents Sea and the arctic archipelago of Svalbard. Today, the network consists of 34 seismic stations distributed over the Norwegian mainland and the arctic islands Jan Mayen, Bjørnøya, Hopen and Spitsbergen. The main purpose of the network is to monitor the local and regional seismic activity. The Norwegian mainland and coastal areas are only moderately active, and the largest regional earthquakes occur along the Mid-Atlantic ridge. North of Iceland, Jan Mayen is an active volcanic island with most recent eruptions in 1970 and 1985 that is monitored by UiB. With its distribution and high station quality the network also provides data to various scientific studies. The network data are openly available and phase data are submitted to the ISC (agency code BER). This report gives an overview of the network history and current status, the data processing systems and the seismicity that is recorded.

5.1.2 Seismic Network

History

Instrumental seismology in Norway started with the installation of a seismograph at the Bergen Museum in 1905. This became possible due to the Oslo earthquake of 1904 and was in time to record the San Francisco earthquake of 1906. The first seismograph was a Bosch-Omori sensor that remained in

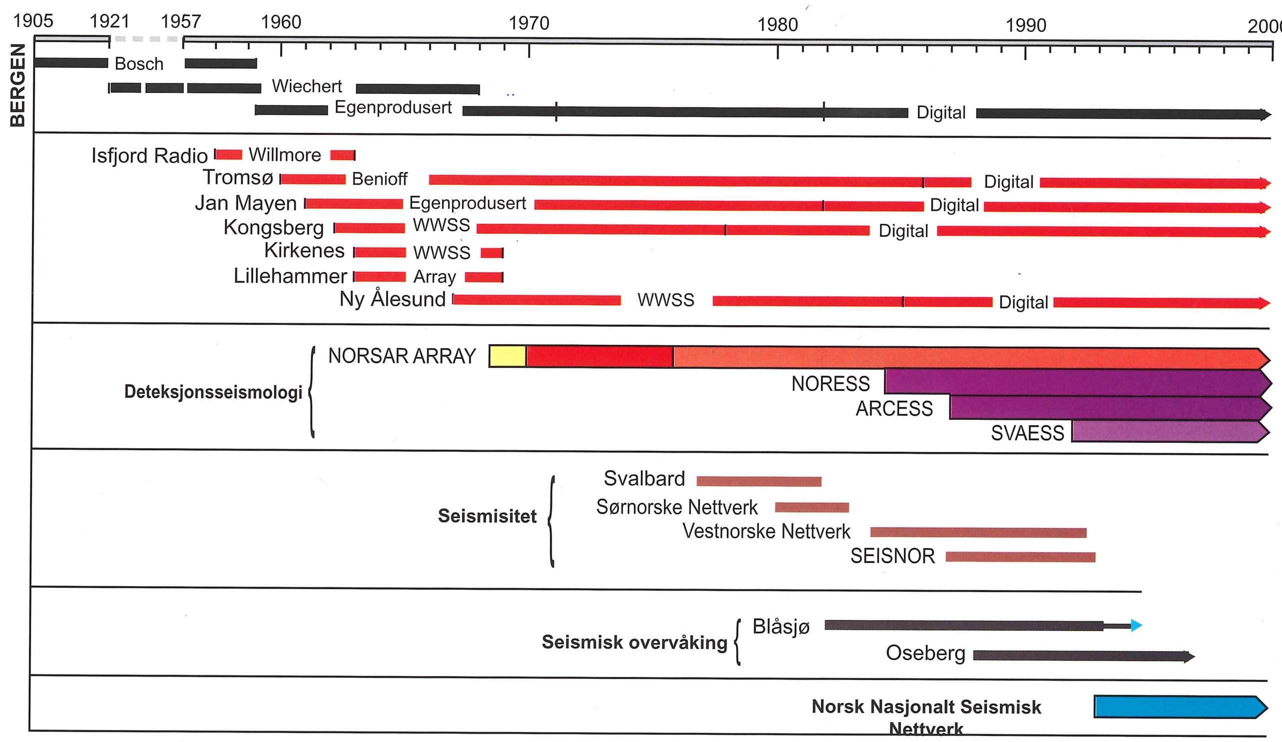

Figure 5.1: *Operation of seismic stations in Noway over time: From the top: black lines indicate stations in Bergen, thin red lines are other UiB stations, thick red lines are NORSAR arrays and thin brown and black lines are time limited local networks operated by both UiB and NORSAR. Abbreviations: WWSSN: World Wide Standard Seismic Network. NORESS, ARCESS and SVAESS are NORSAR operated arrays.*

operation until 1959. In parallel, Wiechert seismometers were operated from 1921. Additional seismic stations were built between 1958 and 1961 on Svalbard, in Tromsø and on Jan Mayen. The complete history of network development is given in *Sellevoll and Sundvor* (2001). Also, a self-built seismometer was in operation in Bergen from 1959. The University of Bergen (UiB) network expanded in the 1980s mostly with the installation of short period seismometers across Norway. Two Global Seismograph Network stations are in operation in Norway, Kongsberg (KONO) is operated by IRIS/USGS/UiB since 1978 and Kings Bay (KBS) by IRIS/USGS/GEOFON/AWI/UIB since 1994. From 1992, the UiB stations were merged into the Norwegian National Seismic Network (NNSN). An overview of the historic development is given in Figure 5.1.

Current Status

The NNSN consists of 34 seismic stations that are distributed over mainland Norway and the Norwegian Arctic regions (Figure 5.2). The majority of stations (28) are equipped with broadband sensors and high quality 24-bit digitizers, while the remaining (6) have short period sensors. Data from all stations are received in near real-time in Bergen through different modes of communication including public Internet, ADSL, GSM and satellite. In addition to the UiB stations, the NNSN receives data from NORSAR stations in Norway, but also from neighbouring networks in the UK, Denmark, Finland, Sweden, Iceland and Poland.

The NNSN instrument vaults were constructed differently over time. Some of the earlier stations have

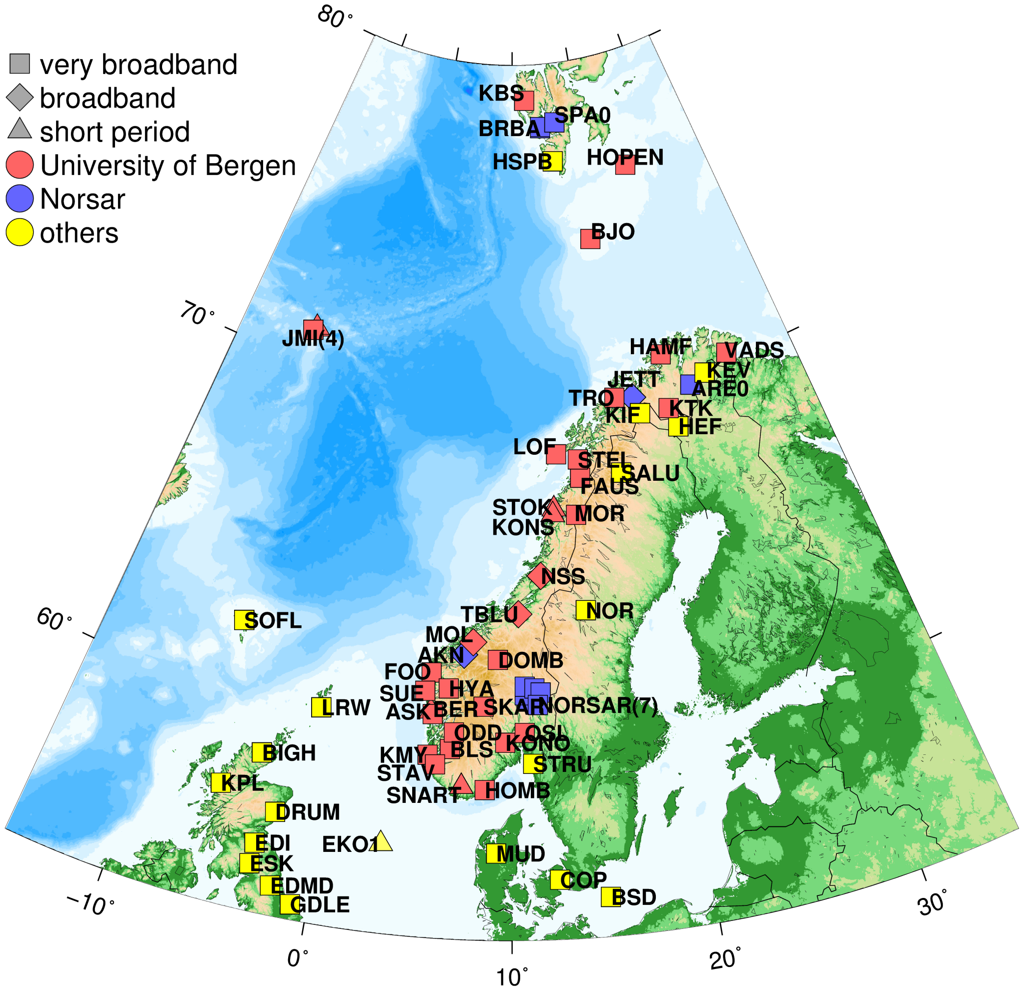

Figure 5.2: *Stations contributing to the NNSN data processing. UiB operates the 34 NNSN stations (red). The remaining stations are operated by NORSAR (blue), and selected stations by the UK, Denmark, Finland, Sweden, Iceland and Poland (yellow).*

high-quality purpose built vaults (e.g., KONO, KBS, TRO, BER). Many of the stations constructed since the 1980s were short period and have simple shallow vaults. Recent new vaults are constructed more specifically to obtain high quality broadband recordings (Figure 5.3). The final data quality results from the combination of instrumentation, vault and the noise conditions. A detailed study by *Demuth et al.* (2016) describes the noise conditions on the NNSN stations and estimates the effect of noise on the detection levels (Figure 5.4). The microseismic peaks in Norway originate from the North Atlantic and a clear correlation of weather conditions and seismic noise can be observed. An example of noise levels for station LOF (Lofoten islands in northern Norway) is given in Figure 5.5. The microseismic peaks on the NNSN stations clearly have higher amplitudes during the winter months.

The NNSN continues to develop and the remaining short period stations will be upgraded in the coming years. A recent development in Norway has been the installation of passive monitoring seafloor installations at a number of oil fields by the operating companies. Some of that data is now received in near real-time to obtain better detection and location capability especially in the offshore areas. The network will also expand in the coming years through the EPOS-Norway (`www.epos-no.org`) project that aims to install new stations in northern Norway and on Svalbard.

Figure 5.3: Pictures from the broadband station VADS in North-eastern Norway, installed in 2016.

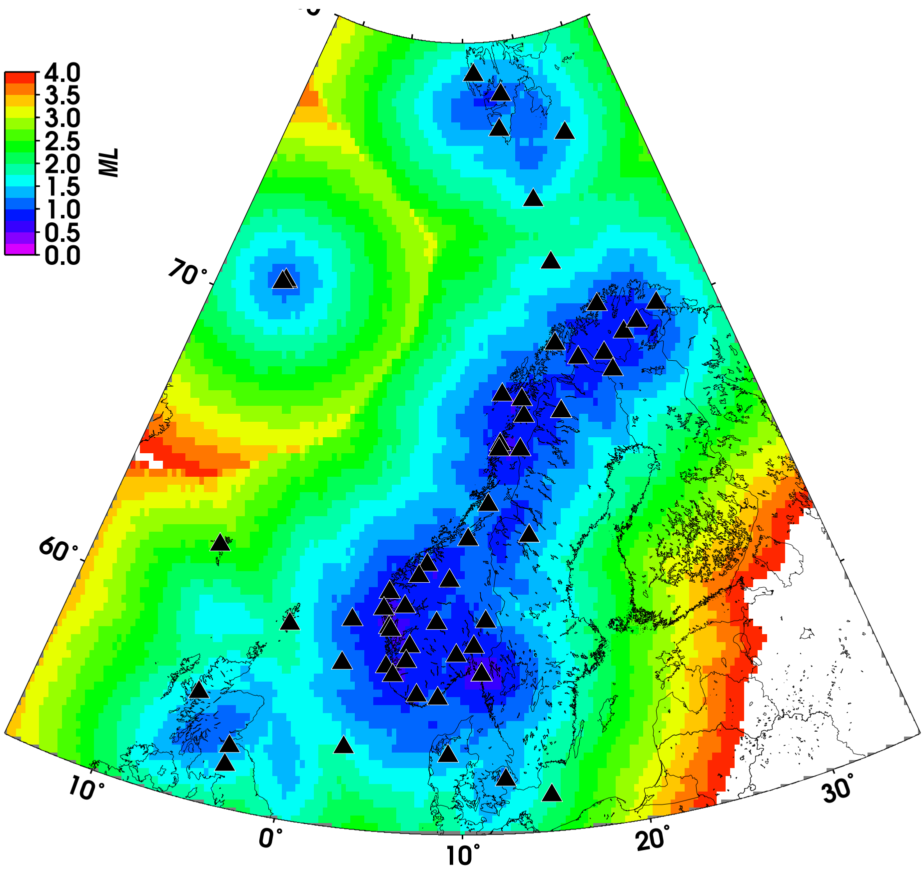

Figure 5.4: Computed detection levels for the network of stations shown as black triangles.

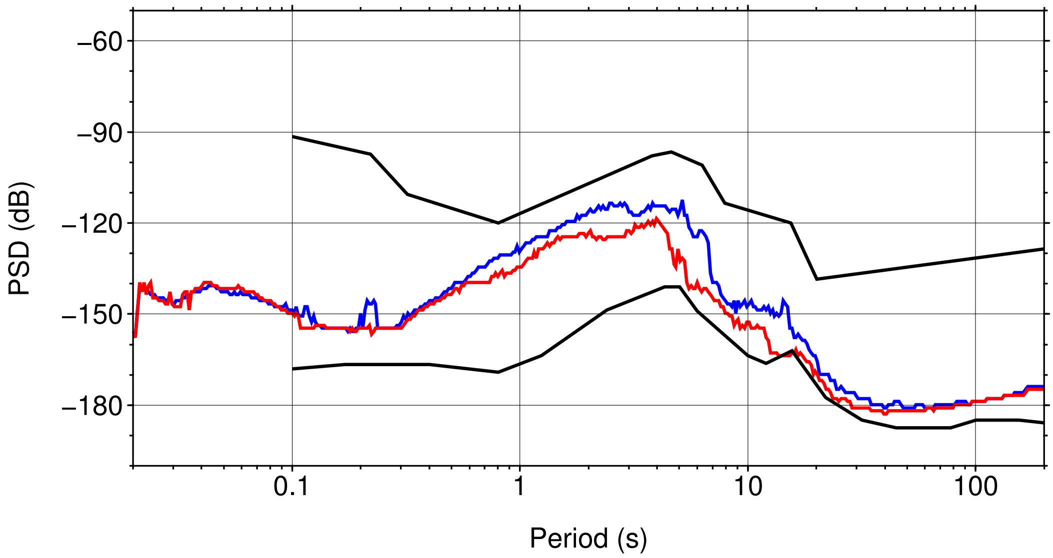

Figure 5.5: *Noise level modes for station LOF for summer (red), 1 April 2017 – 30 September 2017, and winter (blue) , 1 October 2017 – 31 March 2018.*

5.1.3 Data Processing

The real-time data arrives in Bergen and is initially processed automatically. The detected events are located manually on a daily basis, and final bulletins are produced by detailed manual interpretation of the seismograms.

Acquisition and Event Detection

Data from the NNSN and other stations are received at UiB through the seedlink protocol (`www.seiscomp3.org`). Data on the stations are provided through a seedlink server running either on the digitizer or a standard computer connected to the digitizer. Data latency is generally less than 30 seconds for the NNSN stations. All other data are received from seedlink servers running at the respective institutions. Data is archived in the standard SeisComp structure that can be accessed directly from the interactive processing software.

The automatic processing and event detection is done through Earthworm (`www.isti.com/products/earthworm`). Apart from the pre-processing, such as filtering and decimation, the main Earthworm modules used are for the creation of helicorder plots and the detection through the implementation of Carl Johnson's detection (see Earthworm documentation). The detection is configured for a number of regional sub-networks. Detection waveform files are produced, which are then injected into the processing database for further processing.

Routine Processing in SEISAN

The SEISAN software has been developed at UiB since the late 1980s (*Havskov and Ottemöller*, 1999). The development still continues and SEISAN is the main tool for the routine processing of the NNSN data. The software contains all the main tools for routine data processing and a database structure for storing the data. Recently, the SeisanExplorer has been added to provide a more user friendly, but

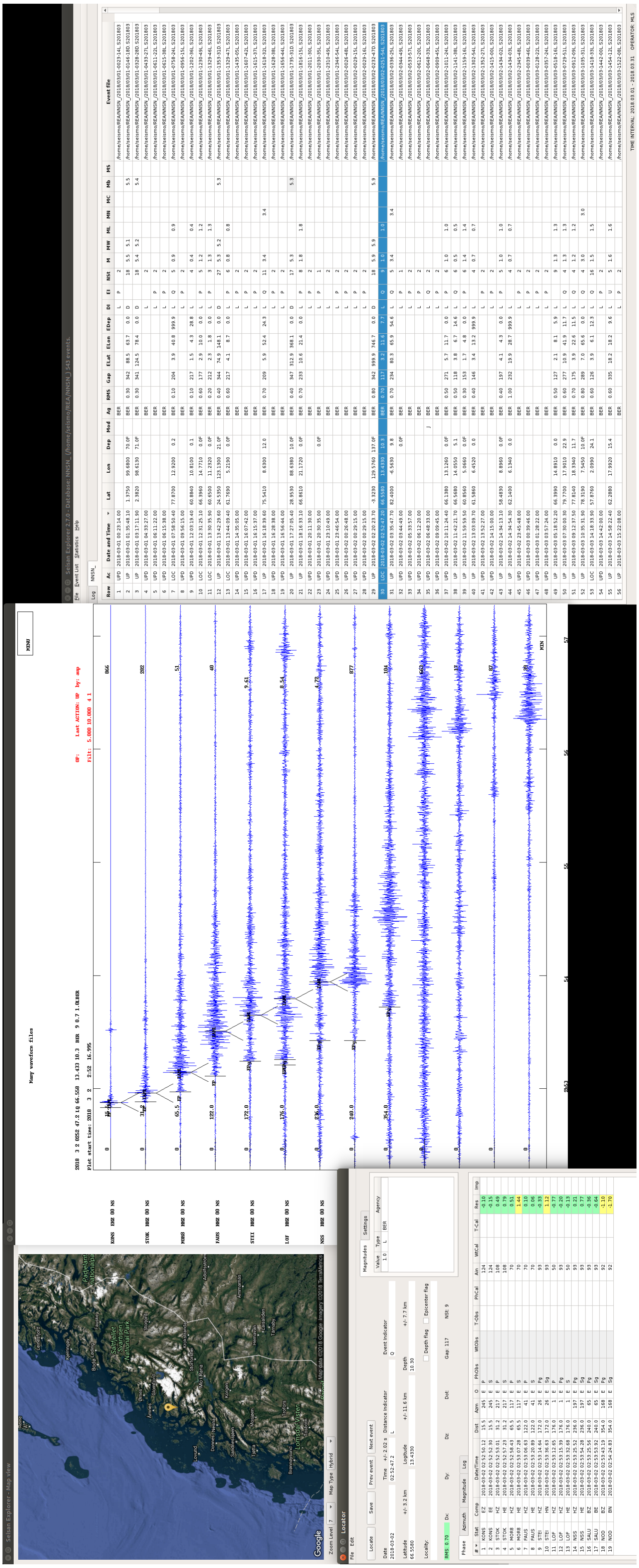

Figure 5.6: *SeisanExplorer setup. Clockwise from top: Interactive map showing location for the current solution, data trace view tool mulplt, SeisanExplorer database window, and locator window.*

still efficient, graphical user interface. With SeisanExplorer it is possible to have the main interlinked tools (database program, trace plotting, locator, mapping) available on screen to efficiently process and evaluate the results (Figure 5.6).

The interactive processing starts with the screening of detection files and dismissing false detections. While the focus of the NNSN is on regional data, teleseismic events are also processed. The routine processing includes manual phase identification and hypocentre location in an iterative manner. Event locations are performed using the HYPOCENTER program (*Lienert and Havskov*, 1995). The velocity model used for locating all local and regional events, except for earthquakes at the Jan Mayen, is given in *Havskov and Bungum* (1987). For local events, phases are picked on all possible stations. The main phases that can be identified are Pg/Pn and Sg/Sn. T-phases are also commonly observed from earthquakes on the mid-Atlantic ridge (Figure 5.7). At teleseismic distances, mostly P is picked for earthquakes below M=6.0, while additional phases are picked for larger events.

Various amplitudes are picked to calculate magnitudes using the standard IASPEI recommended scales (ML, mb, mB, Ms, MS, MW). At local and regional distances, the ML scale by *Alsaker et al.* (1991) is in use for mainland Norway. However, this does not work for the North-Atlantic as Lg does not propagate in the oceanic crust. Therefore, a new scale mb(Pn) where amplitudes are measured from the Pn wave has recently been developed (*Kim and Ottemöller*, 2017). The same method has been used to develop an mb(Sn) scale (so far unpublished), which can be used to recalculate magnitudes in the catalogue. Figure 5.8 shows that magnitudes on average were underestimated by 1.44 magnitude units.

Discrimination of Explosions

The majority of seismic events detected by the NNSN are explosions rather than earthquakes. In 2017, about 30 % of all 8685 detected local and regional events are earthquakes. Some of the mining explosions are reported to the NNSN and then marked as such in the database. While explosions can be interesting to study, they possibly contaminate the earthquake catalogue and their identification is important. Events are marked as either earthquake, probable explosion or confirmed explosion in the database. With the large proportion of explosions, quick identification is also important to minimize the processing work that is spent on them. Much research has been done on the identification of explosions (e.g. *Carr and Garbin*, 1998; *Kim et al.*, 1994; *Baumgardt and Ziegler*, 1988). However, automatic identification remains challenging, also due to the fact that there is a range of explosion source types and wave propagation differences across the area. In Finland, *Kortström et al.* (2016) have recently developed an automatic classification system based on a machine learning approach.

Applying the same algorithm as *Kortström et al.* (2016) for Norwegian data has so far only been partly successful. Instead, the focus is currently on the use of spectrogram plotting as part of the routine processing and this has been implemented into SEISAN (Figure 5.9). The single station spectrograms can be plotted after distance sorting for evaluation of the source characteristics and also to see how the spectral content changes with distance due to wave propagation, including scattering.

One difficulty is that explosions are carried out in different ways. Larger industrial explosions are often fired as sources in series with some time delay (ripple firing) to spread the energy over time to increase fracturing efficiency and reduce ground vibration. The time delay causes waves at certain frequencies

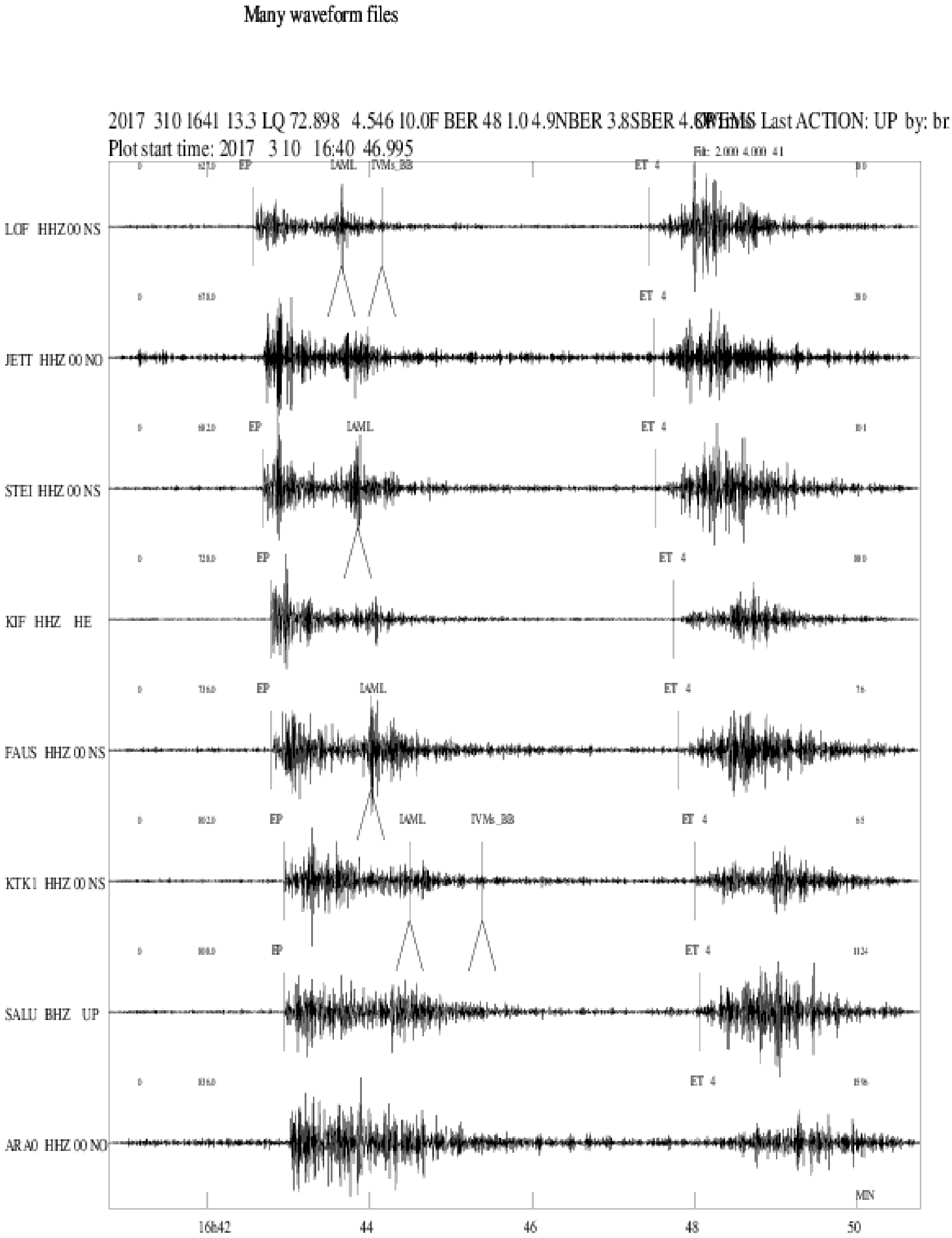

Figure 5.7: *Waveform data from event on 10 March 10 2017 at 16:41 UTC, 4.9NBER, 4.8WEMS, located at 72.898N, 4.546E, Mohns Ridge in the Norwegian Sea. The T-waves are marked with ET toward the later part of the seismograms.*

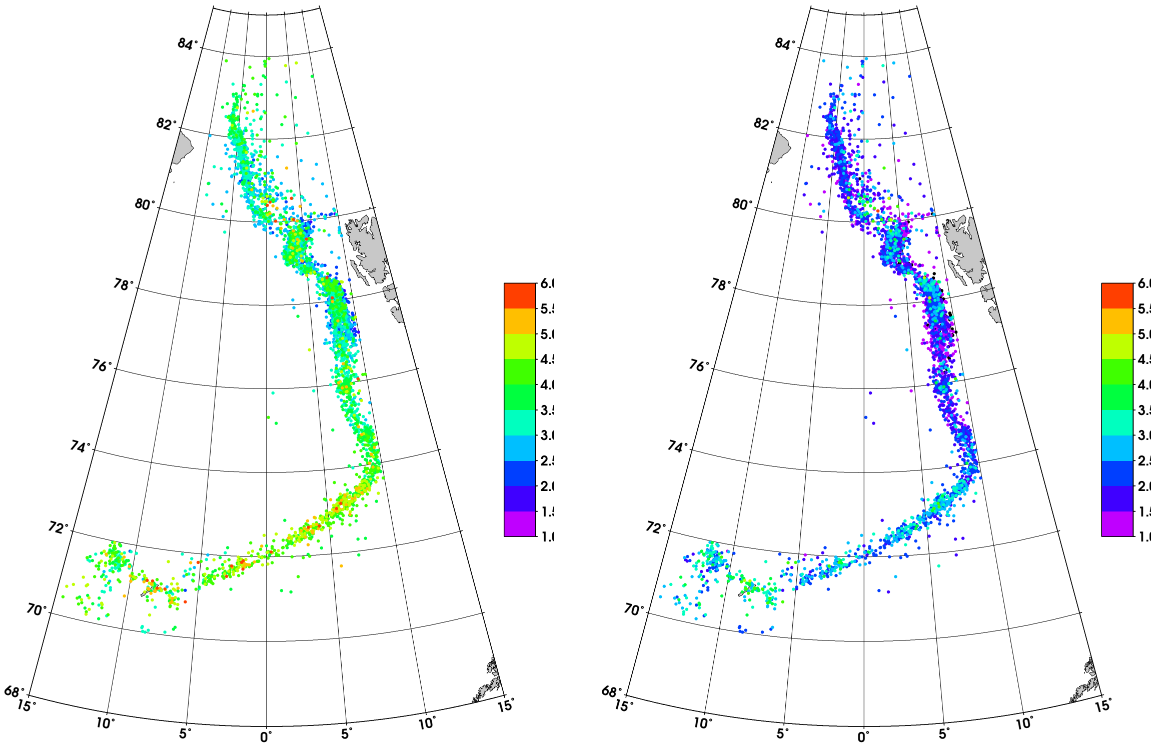

Figure 5.8: *Comparison of magnitudes for events between 1990 and 2017 in the North Atlantic. The map on the left shows the mb(sn) magnitude while the map on the right shows ML results that have been the default in the NNSN catalogue until now.*

to interfere constructively or destructively, seen as horizontal bands in the spectrograms (Figure 5.9, bottom). The ripple fired explosions are generally quite easy to identify, with some extreme cases of very clear bands.

Single charge explosions are also carried out at land or sea. For these, the energy is more evenly distributed over frequency, and they can look more like earthquakes. In some cases clear distinction from earthquakes is not possible and location (in relation to mining quarries), time of day and magnitude have to be considered in addition. However, many earthquakes are more evenly distributed over frequency and scattered S-wave energy, in particular, is seen at higher frequencies than is the case for explosions (Figure 5.9, top).

5.1.4 Seismicity Database

The NNSN maintains a database that contains local, regional and teleseismic earthquakes all in a consistent structure including historic and instrumental times. For 2017, the database contains more than 8500 local and regional earthquakes and just over 1000 teleseismic earthquakes (Figure 5.10). The yearly number of teleseismic earthquakes has been quite consistent since 2000, while local/regional event numbers have increased since 2011 (Figure 5.10). This event increase is explained by a change in the detection routine (that has resulted in a reduced detection level in the North Atlantic region), an increase in and improvement of the number of seismic stations (also in Arctic areas) and some earthquake sequences that present an actual increase in seismicity.

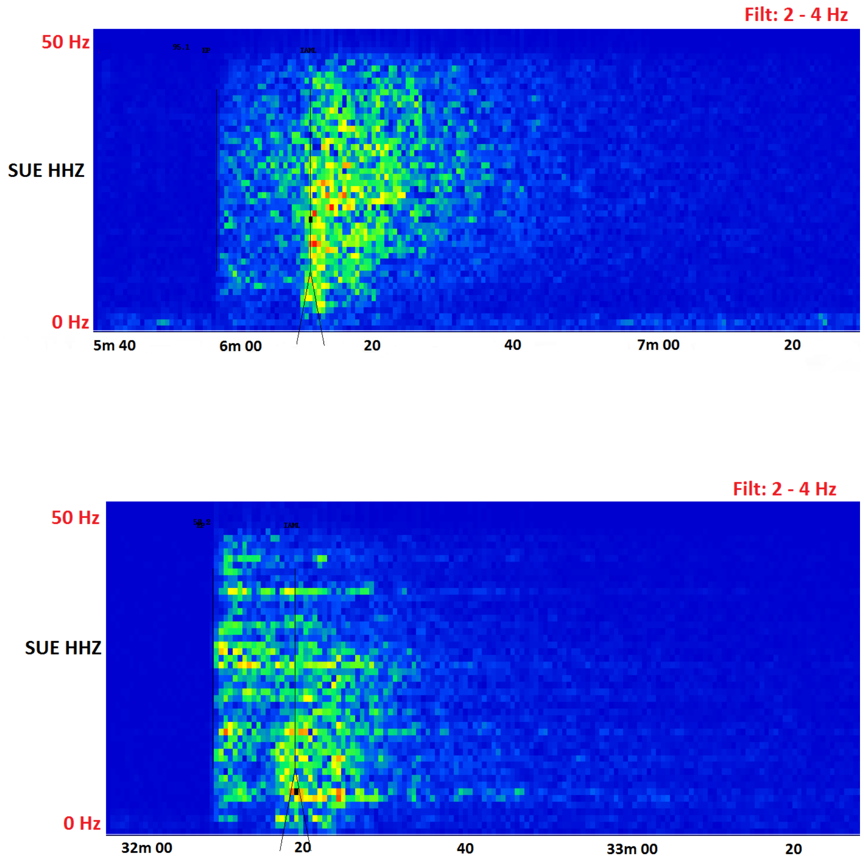

Figure 5.9: *Spectrogram comparison. Top: Probable earthquake in western Norway, station SUE Z-component, 2 min duration, ML 1.2, 95 km distance to epicentre. Bottom: Probable explosion in western Norway, station SUE Z-component, 2 minutes duration, ML 1.4, 58 km distance to epicentre.*

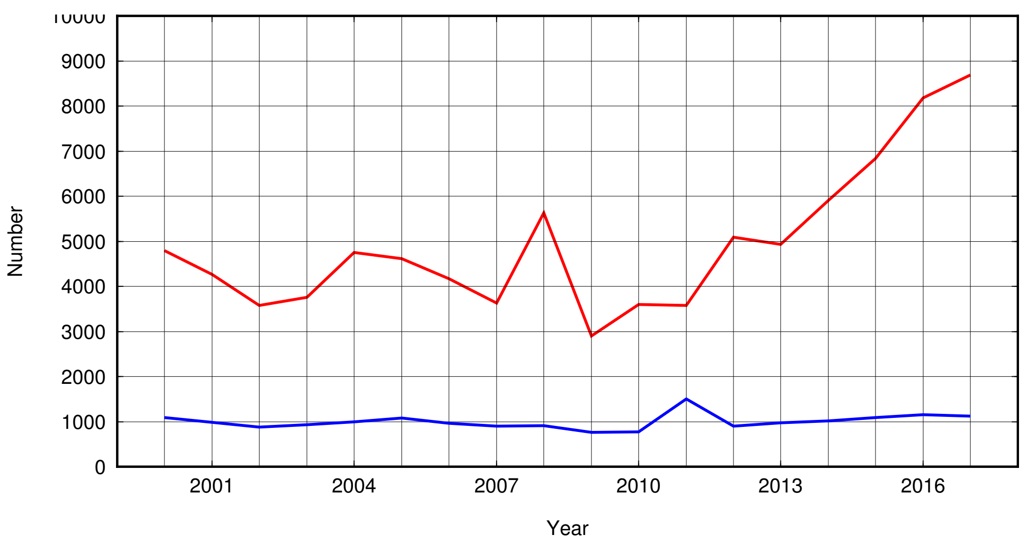

Figure 5.10: *Number of local/regional (red) and teleseismic (blue) events recorded in the NNSN database since 2000.*

Local and Regional Events

The seismicity at the regional scale is dominated by the earthquake activity along the Mid-Atlantic ridge and Jan Mayen fracture zone where earthquakes up to magnitude 7 occur (Figure 5.11). It is possible that these earthquakes are felt on Svalbard and Jan Mayen, but the risk from them is largely negligible, with the exception of Jan Mayen where minor damage has been reported in the past. The activity to the east of the ridge is of intraplate origin. Earthquakes are detected in most parts of Norway onshore. However, it is the coastal areas in northern Norway and south-western Norway that are most active (Figure 5.11). Earthquake monitoring is of particular importance for the companies extracting hydrocarbons in the North Sea, where moderate size earthquakes have occurred. The North Sea activity is considered to be mostly of tectonic origin, with the exception of an induced event in 2001 (*Ottemöller et al.*, 2005). The main characteristics of the earthquakes in Norway were presented by *Bungum et al.* (1991) and *Bungum et al.* (2010). A major earthquake sequence started in the Storfjorden area of the Svalbard archipelago in 2008 with the occurrence of a magnitude ML=6.1 earthquake (*Pirli et al.*, 2010). More than 25 moderate size earthquakes have occurred since then, and the activity still continues in 2018.

Teleseismic Events

The yearly number of teleseismic earthquakes processed by the NNSN is about 1000. Since 1990, the database contains 14,667 teleseismic earthquakes with 198,606 travel time readings that have been reported to the ISC. The distribution of shallow earthquakes and their travel times are given in Figure 5.12. This shows that direct phases (up to about 90 degrees) are recorded from regions as far as away as South America and Indonesia. Core phases are observed from the South Pacific in areas around Kermadec Islands, Fiji, Tonga etc., and in the South Atlantic (Figure 5.12).

Data Availability

Both waveform and parametric data from the NNSN are openly available. The web-portal for recent earthquake information is `http://www.skjelv.no`. Near real-time waveform data can be obtained from a seedlink server at UiB upon request. The continuous and event based waveform data are available from the following ftp server `ftp://ftp.geo.uib.no/pub/seismo/DATA`, while the macroseismic data can be looked at through the Midop interface at `http://nnsn.geo.uib.no/link_6_00b.shtml`. Data access will improve in the near future through the development of an EPOS-Norway data portal.

5.1.5 Acknowledgements

The Norwegian National Seismic Network is financed by the **The Norwegian Oil and Gas Association**, a professional body and employer's association for oil and supply companies, and the University of Bergen. We appreciate the real-time data exchange with the following institutions: NORSAR, British Geological Survey, University of Helsinki, University of Uppsala, and Geological Survey of Denmark and Greenland. The technical development of the NNSN is carried out by Ole Meyer, while the IT systems and processing software are managed by Øyvind Natvik and Terje Utheim.

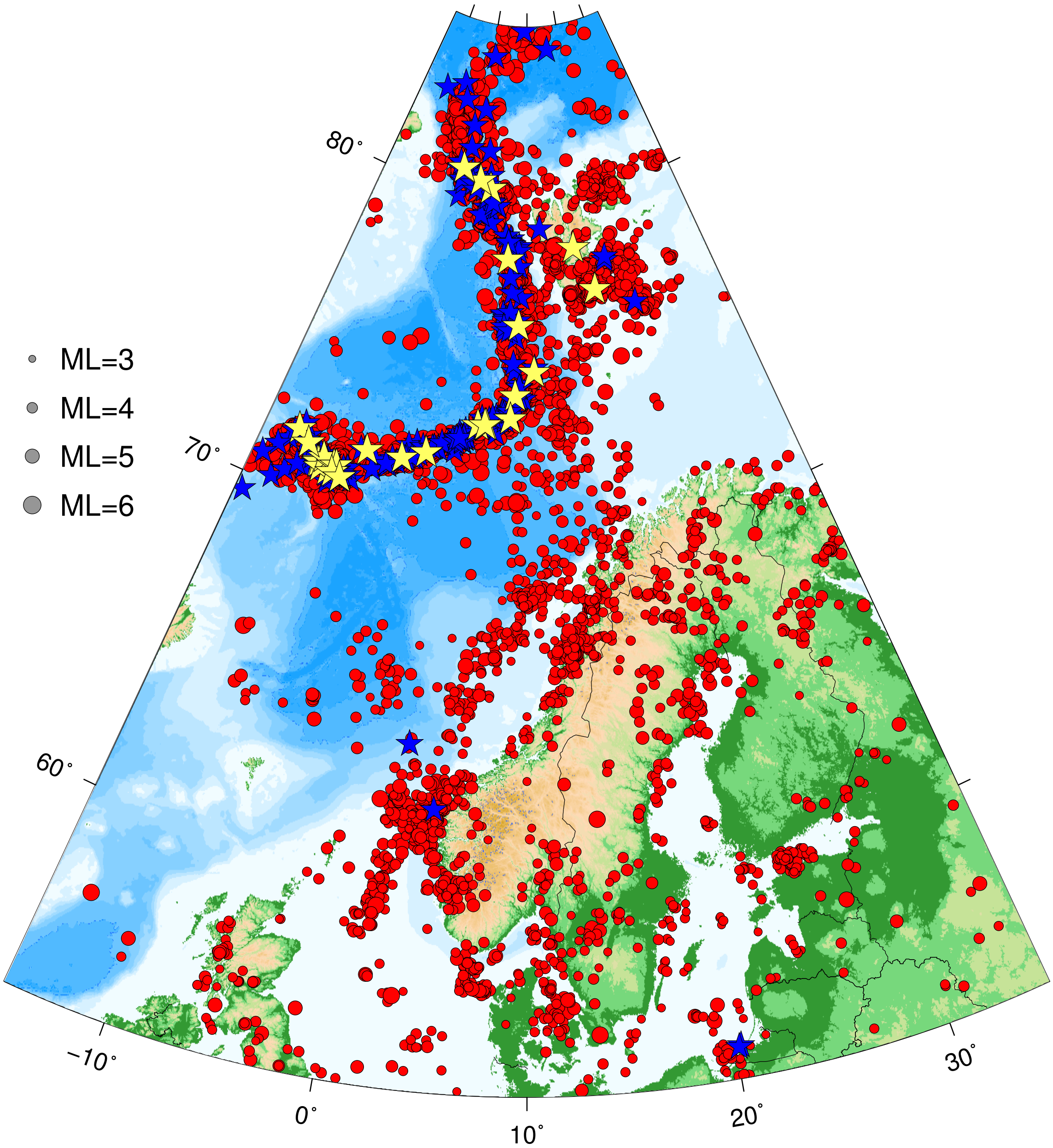

Figure 5.11: *Seismicity of local events ML ≥ 2.5, located by the NNSN from January 1980 to 2017. Confirmed and probable explosions are excluded.*

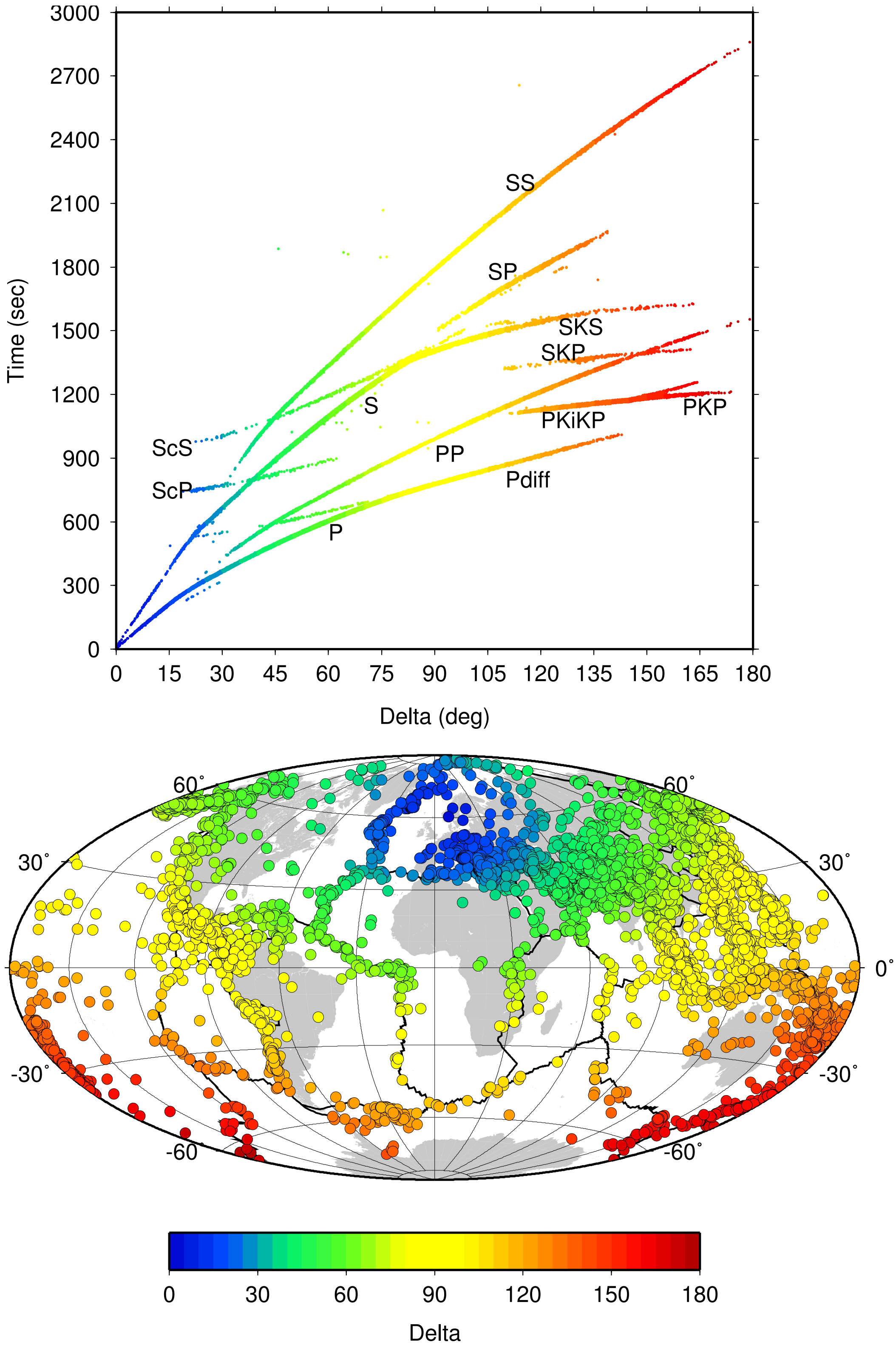

Figure 5.12: *Travel times and locations of shallow (0-60 km) teleseismic earthquakes in the NNSN database between 1990 and 2017. Top: Travel time observations, colour code gives distance from observing stations. Bottom: Location of earthquakes for which travel times are shown, distance from Bergen is colour coded.*

5.1.6 References

Alsaker A., L.B. Kvamme, R.A. Hansen, A. Dahle and H. Bungum (1991), The ML scale in Norway, *Bull. Seism. Soc. Am.*, *81*(2), 379–398.

Baumgardt, D. R. and K.A. Ziegler (1988), Spectral Evidence for Source Multiplicity in Explosions: Application to Regional Discrimination of Earthquakes and Explosions, *Bull.Seism. Soc. Am.*, *78*(5), 1773–1795.

Bungum, H., A. Alsaker, L. B. Kvamme, and R. A. Hansen (1991), Seismicity and seismotectonics of Norway and nearby continental shelf areas, *J. Geophys. Res.*, *96*(B2), 2249–2265, DOI:10.1029/90JB02010.

Bungum, H., O. Olesen, C. Pascal, S. Gibbons, C. Lindholm and O. Vestøl (2010), To what extent is the present seismicity of Norway driven by post-glacial rebound?, *J. Geol. Soc. London*, *167*, 373–384, DOI:10.1144/0016-76492009-009.

Carr, D. B. and H.D. Garbin (1998), Discriminating Ripple-Fired Explosions with High-Frequency (>16Hz) Data, *Bull. Seism. Soc. Am.*, *88*(4), 963–972.

Demuth, A., L. Ottemöller and H. Keers (2016), Ambient noise levels and detection threshold in Norway, *J. Seismol.*, *20*, 889–904, DOI:10.1007/s10950-016-9566-8.

Havskov J. and H. Bungum (1987), Source parameters for earthquakes in the northern North Sea, *Norsk Geologisk Tidskrift*, *67*, 51–58.

Havskov, J. and L. Ottemöller (1999), SEISAN earthquake analysis software, *Seis. Res. Lett.*, ztextit70, 532–534.

Kortström, J., M. Uski and T. Tiira (2016), Automatic classification of seismic events within a regional seismograph network, *Computers & Geoscience*, *87*, 22–30, DOI:10.1016/j.cageo.2015.11.006.

Lienert, B.R. and J. Havskov (1995), HYPOCENTER 3.2 A computer program for locating earthquakes locally, regionally and globally, *Seis. Res. Lett.*, *66*, 26–36.

Kim, W.-Y., D.W. Simpson and P.G. Richards (1994), High-Frequency Spectra of Regional Phases from Earthquakes and Chemical Explosions, *Bull.Seism. Soc. Am.*, *84*(5), 1365–1386.

Kim, W.-Y. and L. Ottemöller (2017), Regional Pn body-wave magnitude scale mb(Pn) for earthquakes along the northern mid-Atlantic Ridge, *J. Geophys. Res.: Solid Earth*, *122*, 10,321–10,340, DOI:10.1002/2017JB014639.

Ottemöller, L., H. H. Nielsen, K. Atakan, J. Braunmiller and J. Havskov (2005), The 7 May 2001 induced seismic event in the Ekofisk oil field, North Sea, *J. Geophys. Res.*, *110*(B10), B10301, DOI:10.1029/2004JB003374.

Pirli M., J. Schweitzer, L. Ottemöller, M. Raeesi, R. Mjelde, K. Atakan, A. Guterch, S. J. Gibbons, B. Paulsen, W. Debski, P. Wiejacz and T. Kværna (2010), Preliminary Analysis of the 21 February 2008 Svalbard (Norway) Seismic Sequence, *Seis. Res. Lett.*, *81*(1), 63–75, DOI:10.1785/gssrl.81.1.63.

Sellevoll, M.A. and E. Sundvor (2001), Jordskjelvstasjonen: Institutt for den faste jords fysikk gjennom ett århundre, University of Bergen, 250 pp.

5.2 The Finnish National Seismic Network

Jari Kortström, Marja Uski and Kati Oinonen
Institute of Seismology, University of Helsinki, Helsinki, Finland

Jari Kortström

Marja Uski

Kati Oinonen

5.2.1 Introduction

The Institute of Seismology, University of Helsinki (ISUH) was founded in 1961 as a response to the growing public concern about environmental hazards caused by nuclear weapon testing. Since then ISUH has been responsible for seismic monitoring in Finland. The current mandate covers government regulatory duties in seismic hazard mitigation and nuclear test ban treaty verification, observatory activities and operation of the Finnish National Seismic Network (FNSN) as well as research and teaching of seismology at the University of Helsinki.

ISUH and its predecessor in seismic monitoring, the Department of Physics at the University of Helsinki, have actively participated in the international seismic data exchange. In the ISC Bulletin, the first phase reading from a Finnish station dates back to 1927 (HEL, Helsinki) and the earliest reported hypocentre from agency HEL to 1958. Manual analysis of teleseismic events was phased out at ISUH in 2010, but teleseismic parameter data from some of FNSN stations are still sent to the ISC through partner networks. In addition, ISUH has been submitting the monthly bulletins of local and regional seismic events to the ISC since 1998.

5.2.2 Seismicity of Finland and Surroundings

Finland is situated in the Fennoscandian shield, which is a stable continental region characterized by weak to moderate size earthquakes and a relatively low rate of natural seismicity. In an average year ISUH detects and locates roughly 16,000 local and regional seismic events, of which only 1-2% are tectonic earthquakes. The majority of events are industrial explosions for construction and mining purposes. In addition, rockbursts and other mining–induced events occur regularly in and around several large-scale mines.

Figure 5.13 shows local and regional earthquakes detected by the FNSN and partner networks since 2000. The seismicity is commonly related to both intraplate and plate margin processes; the opening of the North Atlantic Ocean, postglacial rebound, and local stress caused by e.g. gravitational or compositional variations of the crust. Diffuse seismicity arises all over the region, but a few zones of enhanced seismic activity can also be discerned. Distinct NE–SW-trending earthquake clusters extending from the western coast of the Gulf of Bothnia along the Finland-Sweden border zone to northern Norway are mostly associated with postglacial fault zones. The seismically active Kuusamo-Kandalaksha zone in eastern Finland and NW Russia is spatially associated with a major NE-SW oriented shear zone, which in turn is transected by faults and shear zones of various orientation. Enhanced seismicity in SE Finland is due to shallow earthquake swarms occurring within the Wiborg rapakivi granite batholith. The latest major swarm during 2011 and 2012 comprised more than 200 low magnitude events.

The largest known earthquake in Finland took place on 23 June 1882 in the Bothnian Bay area (see "1" in Fig. 5.13). It was scaled to Mw 4.6 and located offshore but it was still strong enough to cause minor damage to buildings in the coastal towns.

The Fennoscandian earthquakes occur generally in the uppermost 15 km of the crust and only a small portion are located in the middle and lower crust, at depths between 16 and 45 km. The focal mechanisms show mostly a combination of strike-slip and reverse faulting styles with a NW-SE direction of maximum horizontal stress. For a more comprehensive description of the regional seismicity see *Korja et al.* (2015) and references therein.

5.2.3 History of the FNSN and Present Network Status

The first seismograph station in Finland was installed at the premises of the Department of Physics, University of Helsinki in 1924. However, the mechanical Mainka seismographs had low magnification and thus the recordings were of little practical value for the study of local seismicity. The first short-period seismographs were set up between 1956 and 1963. The next significant upgrade of FNSN occurred during the late 1970's when digital tripartite arrays in southern and central Finland became fully operational, allowing for systematic use of instrumental detection, location and magnitude determination methods. By the end of the 1990's, the entire network was operating using digital telemetric or dial-up methods (*Luosto and Hyvönen*, 2001).

The FNSN has expanded significantly during the 21st Century. It now comprises 36 permanent stations and a number of portable sensors used as temporary deployments for monitoring or research purposes (Fig. 5.14). Most of the stations have Streckeisen STS-2, Nanometrics Trillium (Compact/P/PA/QA) or Guralp CMG-3T broad band sensors. Some Teledyne-Geotech S13/GS13 short period sensors are also in use. Data acquisition systems are a combination of Earth Data PS6-24 digitizers and PC with Seiscomp/Seedlink software or Nanometrics Centaurs. The stations are connected to the ISUH with Seedlink via Internet and provide continuous waveform data at 40 Hz (array) or 100–250 Hz sampling frequency. Further information about instrumentation can be found at the Institute's web site (`www.seismo.helsinki.fi`).

The FNSN is under continuous development; new station locations are being investigated and existing stations upgraded. The latest extensions include 9 stations (OBF0-8, Fig. 5.14) deployed around a planned nuclear power plant, 4 stations (RUF, RMF, NIF and KPF, Fig. 5.14) funded by FIN-EPOS to improve the overall station coverage, and 5 stations (HEL1-5, Fig. 5.14) set up in the Helsinki

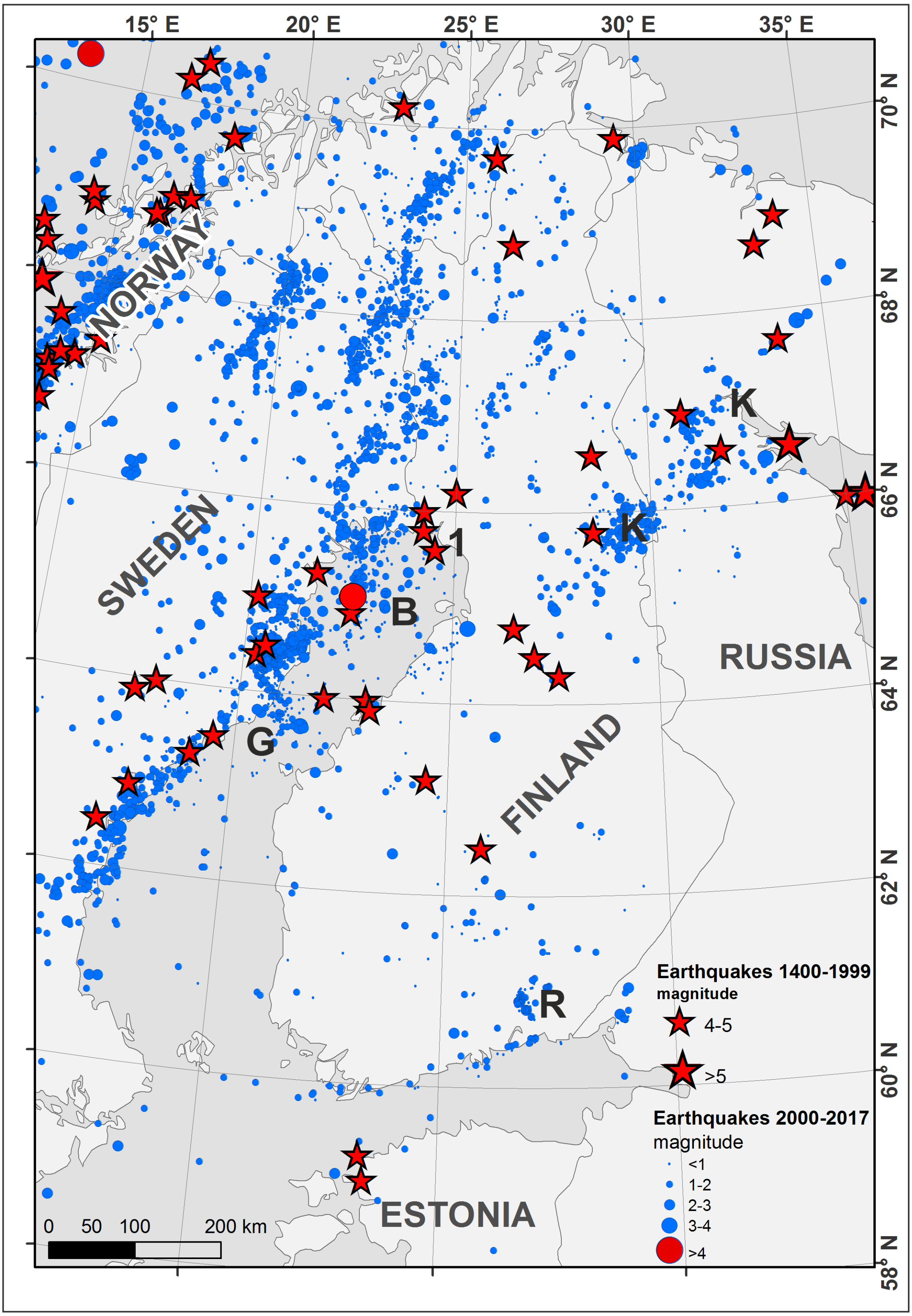

Figure 5.13: *Seismicity of Finland and surroundings. Earthquakes for 2000-2017 (dots) and M > 4 events for 1400-1999 (asterisks). 1-Bothnian Bay earthquake 23-06-1882. Seismicity zones: B-Bothnian Bay; G-Gulf of Bothnia; K-Kuusamo-Kandalaksha; R-Wiborg rapakivi area. Data sources: Fennoscandian earthquake catalogue FENCAT and ISUH preliminary earthquake data for 2014-17.*

metropolitan area to monitor induced seismicity around a deep heat geothermal pilot plant.

The regional coverage is further improved by acquiring available real time data from partner networks; the Northern Finland Seismological Network (NFSN) operated by the University of Oulu and the national seismic networks of Estonia (ENSN), Norway (NNSN) and Sweden (SNSN). In addition, data from two Russian stations (RUS) are accessed through IRIS (`www.iris.edu/hq/programs/gsn`) and Geofon (`geofon.gfz-potsdam.de`). Some of the seismic stations in Finland belong to other global seismic networks as well, transmitting data in real time to the data centres. The station KEV belongs to the IRIS global seismic network whereas FINES, a small aperture array comprising 16 substations, is one of the 50 primary monitoring stations of the Comprehensive Nuclear-Test-Ban-Treaty Organization (CTBTO; `www.ctbto.org`).

The permanent stations have a relatively low background noise level, as demonstrated in Figure 5.15. The examples show the probability density function of power spectral densities calculated from one year of data recorded at MEF, which is one of the noisiest urban stations, and VRF, which is a good example of low noise remote station. Analyses were made using pqlx-software (*McNamara and Boaz*, 2005). All the permanent station installations are in direct contact with bedrock, in most cases utilizing natural outcrops of bedrock.

5.2.4 Automatic Event Detection and Location System

Local and Regional Events

Since 2010, ISUH has employed an automatic system for monitoring local and regional seismic events. The system is based on network processing of three-component (3-C) and array stations and it utilizes the available on-line stations in Finland and neighbouring countries (Fig. 5.14). At a single 3-C site the detections are generated with basic STA/LTA-detector. The code used is an implementation of *Ruud and Husebye* (1992), which uses the "predicted coherence" measure of *Roberts et al.* (1989). The automatic processing of array data is done with DP/EP code provided by NORSAR (*Fyen*, 1989).

An in-house designed routine is used for event association (*Kortström et al.*, 2016a). The routine reads continuously preliminary locations from single station and array bulletins, calculates theoretical P- and S-wave travel times for each source-to-station path, and searches matching P- and S-onset times from the detection logs of other stations. An event is accepted for further analysis if a sufficient number of stations is contributing to the same preliminary origin. The associated phase data are then passed to HYPOSAT location program (*Schweitzer*, 2001). As automatic arrival times are seldom accurate enough for reliable depth estimation, the source depth is always fixed to zero during the iterations.

Finally, the event solution is forwarded to automatic event classification routine (*Kortström et al.*, 2016b). It is based on a supervised pattern recognition technique called the Support Vector Machine (SVM) and the classification relies on differences in signal energy distribution between natural and artificial seismic sources. The tool was designed to reduce work-load and the cost of manual seismic analysis by pre-filtering the fully automatic event lists. Experience gained during the operation period indicates that the SVM tool can discriminate blasts and spurious events from earthquakes with a high level of reliability.

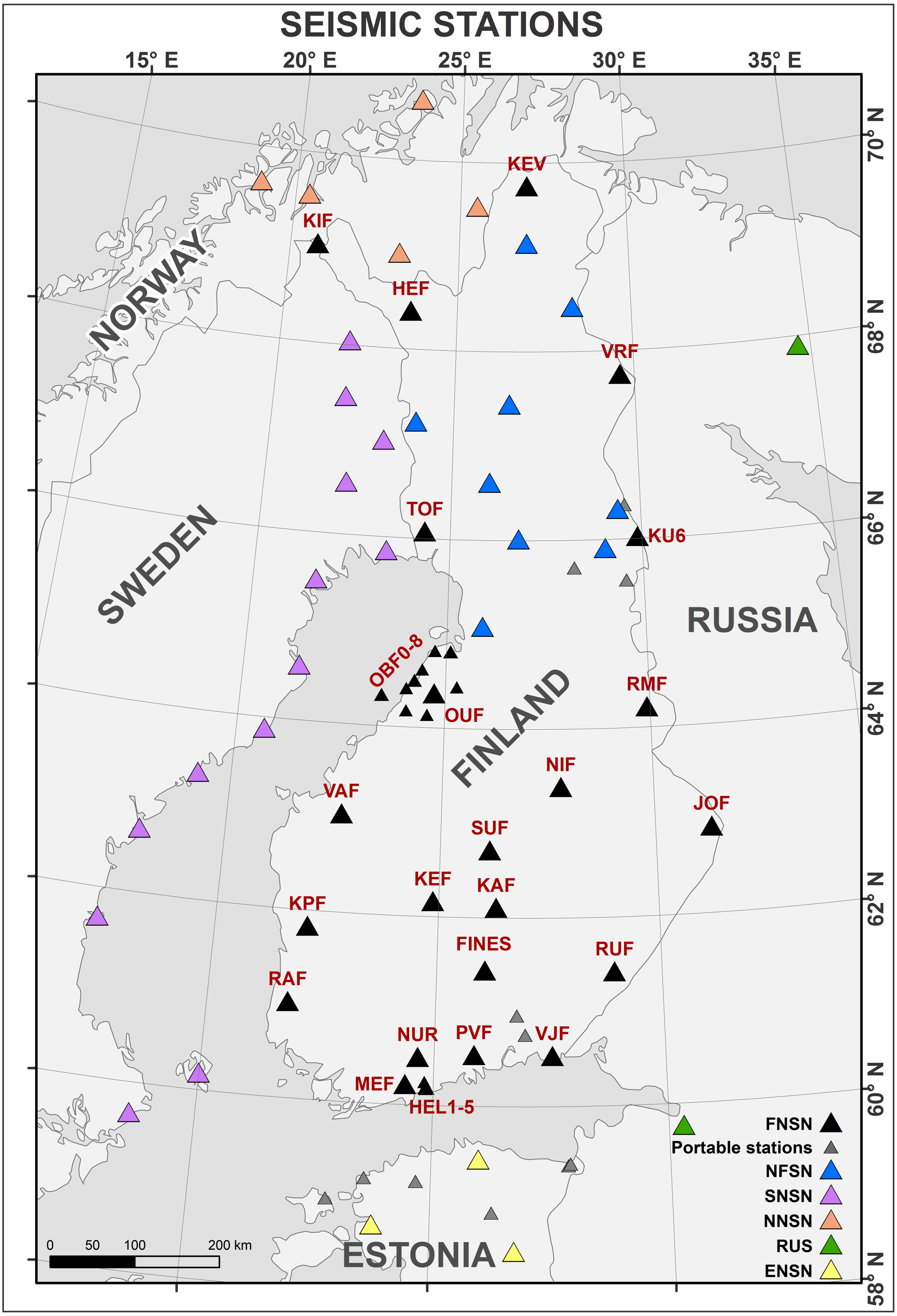

Figure 5.14: FNSN and contributing stations from partner networks. See text for network abbreviations.

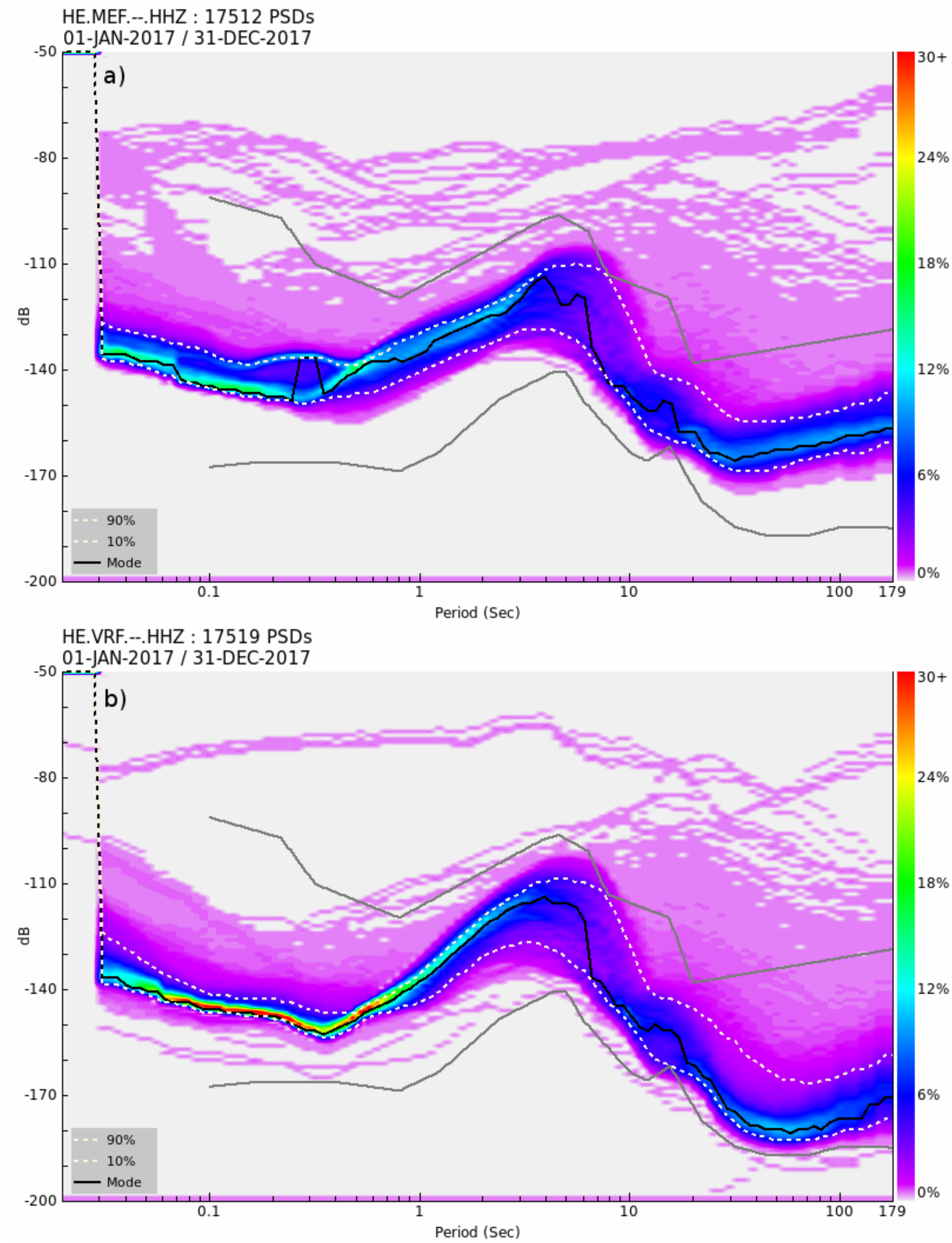

Figure 5.15: *Spectral density functions at station MEF (a) and VRF (b). Regularly observed energy levels (blue, green, yellow and red) indicate background noise and scarcer energy levels (pink and violet) sudden disturbances such as signals of seismic events. Grey lines denote the global average of low and high noise level models (Peterson, 1993).*

The output, a fully automatic event solution, includes origin time, epicenter coordinates, magnitude, event type, arrival-times of P- and S-phases at each station, and error statistics for each of the estimated parameters. The event solutions are published on the Institute's web page within 15 minutes of occurrence and, for significant events, automatic alert message is distributed to the seismologists. As is seen in Figure 5.16, the automatic data processing system provides event detection and location capabilities down to magnitude 1.0 within the network (threshold magnitude calculation method by *Valtonen et al.*, 2013).

Teleseismic Events

Due to decreasing staff resources, manual analysis of teleseismic events was terminated in 2010. However, ISUH has an implementation of SeisComP3 (`www.seismcomp3.org`) system to produce fast automatic alerts of big global earthquakes. These event solutions form the backbone of seismic monitoring in the Finnish Natural Disaster Warning System (LUOVA). LUOVA aims to provide a prompt warning and information on natural hazards and disasters for relevant authorities and emergency response centres. At ISUH there is always a seismologist on call to deliver assessed information about worldwide hazardous earthquakes or nuclear tests to LUOVA.

5.2.5 Interactive Analysis of Local and Regional Events

The precision of automatic source parameters seldom fulfils the criteria required by a good quality seismological event solution. Interactive review of automatic event solutions is therefore essential to e.g. remove spurious events and adjust the automatic phase picks. The coarse interactive analysis scheme used at ISUH is presented in Figure 5.17.

Significant events, such as strong earthquakes or widely felt seismic events are generally analysed within 12 hours of the occurrence with the event solution promptly submitted to relevant authorities, cooperative seismic agencies and media. Felt reports arriving via electronic macroseismic questionnaires or by phone are also given the highest priority in the analysis scheme.

The routine event analysis begins on the first working day after the data day by screening of the automatic event bulletin and associated digital seismograms. Additional waveform data requests are made for events missed by the automatic detector or the association routine. Event type definitions in the automatic bulletins are checked by spectral analysis methods (*Kortström et al.*, 2016b). For events identified as regular mining blasts, the automatic solution is accepted if the location and magnitude fulfil given quality criteria. The events identified as earthquakes as well as mining-induced or suspicious events are subjected to manual reanalysis: adjustment and identification of the automatic phase picks, amplitude and period measurement for local magnitude, and relocation including source depth estimation. After interactive quality-control, the daily event data are published on the web pages and stored into the parametric database.

In a monthly review, the preliminary event solutions are completed with phase readings and source parameters reported by seismic agencies in the neighbouring countries. In addition, waveform data from the offline temporary stations in Finland are screened and phase readings included in the earthquake

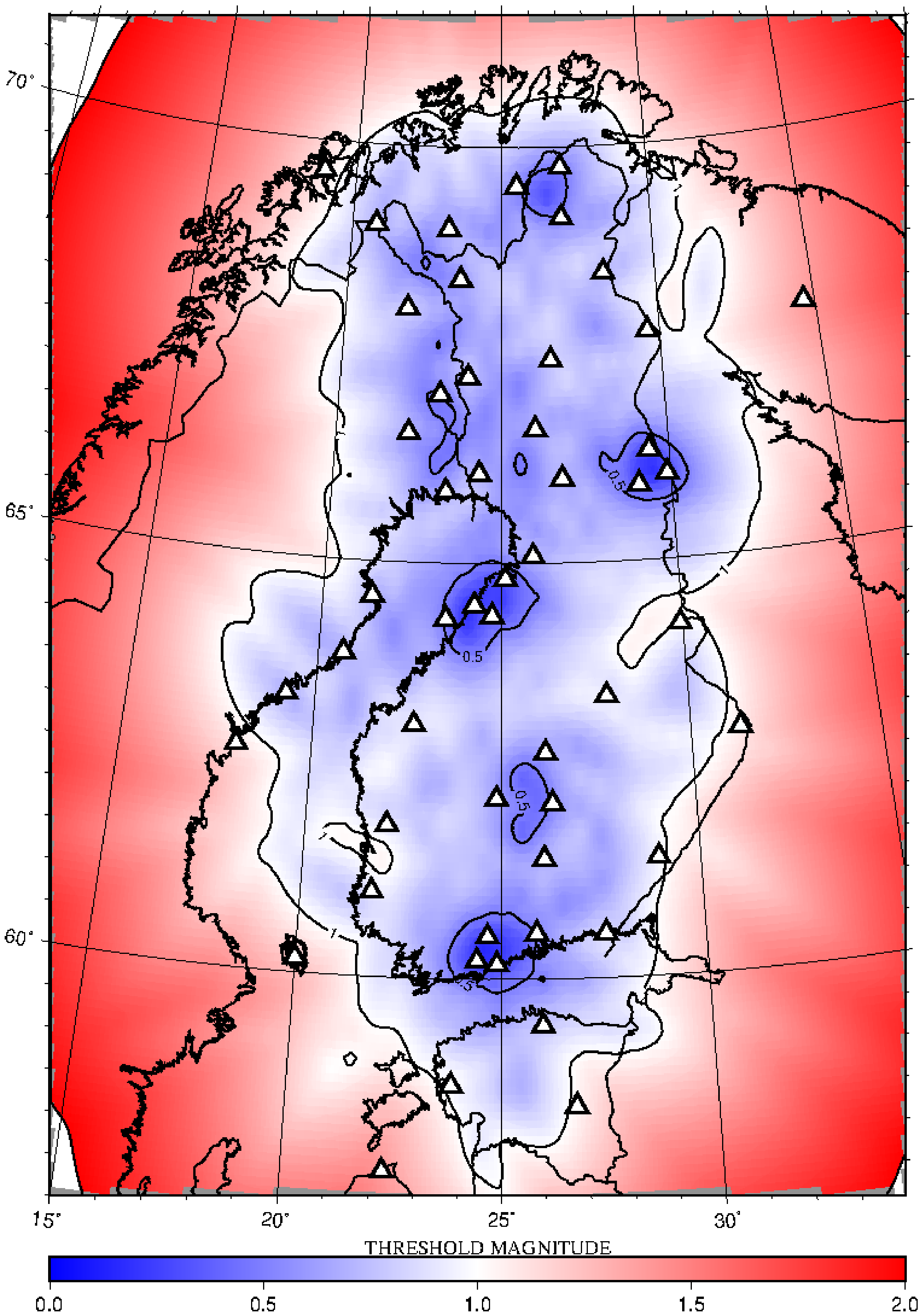

Figure 5.16: *Threshold magnitude for the current automatic detection and location system. Triangles are seismic stations that are used in the processing.*

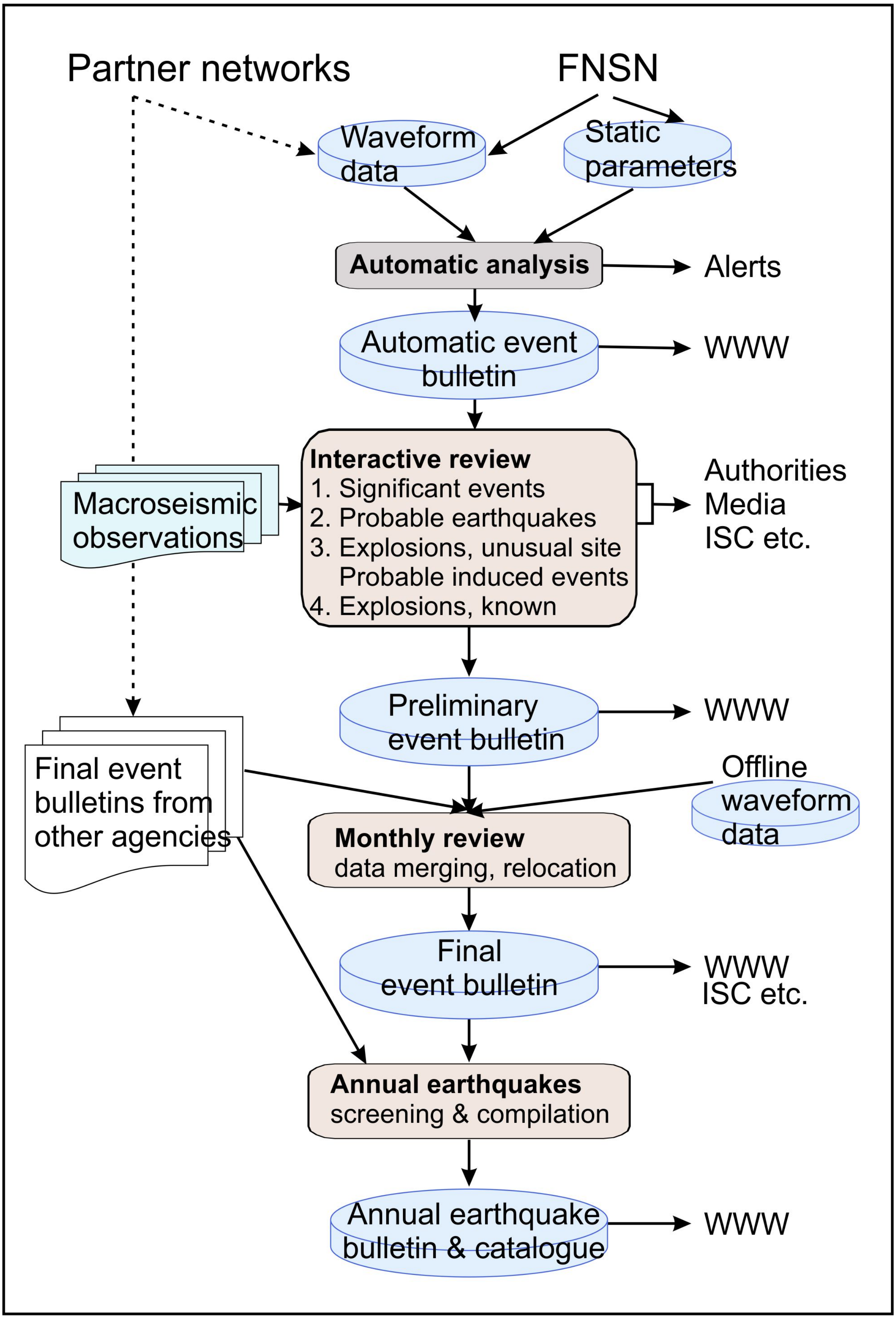

Figure 5.17: *A schematic view of local and regional event analysis at ISUH.*

reports. The final monthly bulletin is submitted to the ISC and other cooperative agencies.

For interactive seismic analysis ISUH uses the Geotool software (*Coyne and Henson*, 1995), which is available for National Data Centers of the CTBTO States Parties. The basic Geotool functions include filtering, phase picking and event location as well as several tools for spectral and array data analyses. The software can be customized and extended. As an example, ISUH has implemented its own event location routine to Geotool.

The local magnitude used at ISUH, ML(HEL), is based on synthetic Wood-Anderson amplitudes (*Uski and Tuppurainen*, 1996). For continental earthquakes the amplitudes are measured from Sg or Lg phase maxima. For offshore events, additional relations are used to estimate ML(HEL) from Sn or Pn wave maximum amplitudes. The magnitude is related to seismic moment through (*Uski et al.*, 2015):

$$\mathrm{ML(HEL)} = 0.83\log(M_0) - 7.98 \qquad \text{for } \log(M_0) \leq 13.5$$
$$\mathrm{ML(HEL)} = 0.59\log(M_0) - 4.73 \qquad \text{for } \log(M_0) > 13.5.$$

5.2.6 Annual Earthquake Bulletin

ISUH is compiling an annual report of earthquakes in Northern Europe (Fig. 5.17). The University of Bergen, the Geological Survey of Estonia and the Department of Earth Sciences, University of Uppsala are the main contributors of supplementary earthquake reports. The annual earthquake data are used to update the Fennoscandian earthquake catalogue FENCAT (*Ahjos and Uski*, 1992). The seismicity record in FENCAT spans more than six centuries and it is the most comprehensive source of earthquake data available in the region. Homogenization of the catalogue data has been a subject in recent seismic hazard studies (e.g. *Uski et al.*, 2015).

5.2.7 Data Availability

ISUH hosts a seedlink server (`finseis.seismo.helsinki.fi:18000`), from which real time data of almost all permanent stations of FNSN are freely available. The data of six stations have been forwarded to GEOFON since 2007. Our intention is to make all FNSN permanent stations available to GEOFON's EIDA data archive (`eida.gfz-potsdam.de`).

All parametric data products, i.e. local and regional event bulletins, annual earthquake bulletins as well as the FENCAT earthquake catalogue are available at the Institute's web pages (`www.seismo.helsinki.fi`).

5.2.8 Acknowledgments

We would like to thank the following institutions for the collaboration in real-time data exchange: GFZ Potsdam, IRIS, Geological Survey of Denmark and Greenland, University of Oulu, University of Uppsala, University of Bergen, NORSAR, and Geological Survey of Estonia. The latter four agencies are also providing parametric seismic data to our bulletin work. We are grateful for the reviews from Kathrin Lieser at the ISC which helped to improve the manuscript.

5.2.9 References

Ahjos, T. and M. Uski (1992), Earthquakes in northern Europe in 1375-1989, *Tectonophysics*, *207*, 1–23, DOI:10.1016/0040-1951(92)90469-M, updates at `www.seismo.helsinki.fi`.

Coyne, J. M. and I. Henson (1995), Geotool Sourcebook: User's Manual, Philips Laboratory, Technical Report PL-TR-96-2021.

Fyen, J. (1989), Event processor program package, *NORSAR Semiannual Technical Summary, 1 Oct 1988 - 31 Mar 1989, Scientific Report 2-88/89*, Kjeller, Norway.

Korja, A. (ed), E. M. Kosonen (ed), N. M. Hellqvist, P. H. Koskinen, P. B. Mäntyniemi, M. R. Uski, O. S. Valtonen, M.-L. Airo, T. Huotari-Halkosaari, M. Nironen, R. Sutinen, S. Grigull, M. Stephens, H. Karin and B. Lund (2015), *Seismotectonic framework and seismic source area models in Fennoscandia, Northern Europe*, Report S-63, Institute of Seismology, University of Helsinki, 284 pp.

Kortström, J., T. Tiira and O. Kaisko (2016a), Automatic data processing and analysis system for monitoring region around a planned nuclear power plant, *Adv. Geosci.*, *1*, 1–9, DOI:10.5194/adgeo-41-73-2016.

Kortström, J., M. Uski and T. Tiira (2016b), Automatic classification of seismic events within a regional seismograph network, *Computers & Geoscience*, *87*, 22–30, DOI:10.1016/j.cageo.2015.11.006.

Luosto, U. and T. Hyvönen (2001), Seismology in Finland in the Twentieth Century, *Geophysica*, *37*(1-2), 147–185.

McNamara, D. E. and R. I. Boaz (2005), Seismic Noise Analysis System, Power Spectral Density Probability Density Function: Stand-Alone Software Package, *United States Geological Survey Open File Report 2005-1438*.

Peterson, J. (1993), Observations and modelling of background seismic noise, *United States Geological Survey Open File Report 93-322*, Albuquerque, New Mexico.

Roberts, R. G., A. Christoffersson and F. Cassidy (1989), Real-time event detection, phase identification and source location estimation using single station three-component seismic data, *Geophys. J. Int.*, *97*, 471–480.

Ruud, B. O. and E. S. Husebye (1992), A new three component detector and automatic single-station bulletin production, *B. Seismol. Soc. Am.*, *82*, 221–237.

Schweitzer, J. (2001), HYPOSAT - An Enhanced Routine to Locate Seismic Events, *Pure and Applied Geophysics*, *158*(1–2), 277–289.

Uski, M. and A. Tuppurainen (1996), A new local magnitude scale for the Finnish seismic network, *Tectonophysics*, *261*, 23–37.

Uski, M., B. Lund and K. Oinonen (2015), Scaling relations for homogeneous moment based magnitude, in J. Saari (Ed), B. Lund, M. Malm, P. Mäntyniemi, K. Oinonen, T. Tiira, M. Uski and T. Vuorinen, *Evaluating Seismic Hazard for the Hanhikivi Nuclear Power Plant Site. Seismological Characteristics of the Seismic Source Areas, Attenuation of Seismic Signal, and Probabilistic Analysis of Seismic*

Hazard, Report NE-4459, ÅF-Consult Ltd, 123 pp.

Valtonen, O., M. Uski, A. Korja, T. Tiira and J. Kortström (2013), Optimal configuration of a micro-earthquake network, *Adv. Geosci.*, *34*, 33–36, DOI:10.5194/adgeo-34-33-2013.

6

The ISC Rebuild Project: first 16 years published

The original ISC Bulletin is a product of many decades of work, over many time periods, and as a result it uses a mixture of methods, velocity models, and quality criteria. Figure 6.1 summarizes the pre-Rebuild state of the ISC Bulletin, and shows the intended state of the ISC Bulletin after the Rebuild Project is finished. Overall, the Rebuild Project aims to modernize and homogenize the ISC Bulletin across more than five decades of data. The first 16 years of the have been reviewed and published, and are now available for public use.

The main tasks of the Rebuild Project include: recomputing ISC hypocentres to guarantee consistency of locations and error estimates, recomputing earthquake magnitudes using a new and more robust procedure, introducing essential additional data sets that were not available at the time of intial relocation, performing general clean up duties including the removal of bogus events, and homogenizing phase identification codes.

Relocations start from the original ISC hypocenters. The location algorithm is run, and events which do not pass our quality criteria are reviewed by an analyst. Our quality criteria employ both hypocentre and residual-based checks, and were tested and refined over many iterations before the project began.

The new procedure for generating ISC magnitudes involves the consistent removal of outliers (i.e. alpha-trimmed median), and the removal of magnitudes based only on 1 or 2 readings (i.e. minimum 3 station amplitude readings are now required for ISC magnitude). Additionally, many new readings have been included, notably resulting in a large number of new Ms magnitudes prior to 1978.

Figure 6.2 shows several regional maps of seismicity which covers covers the 16 data-year period we have currently published, 1964–1979, and highlight some of the improvements we are able to make.

Visible improvements at this scale include improved clustering of events and more consistent depth contours of subduction zones, however a much more detailed look into the results is available in the recent paper published on the Rebuild Project, available freely from Geoscience Letters (Storchak et al., 2017).

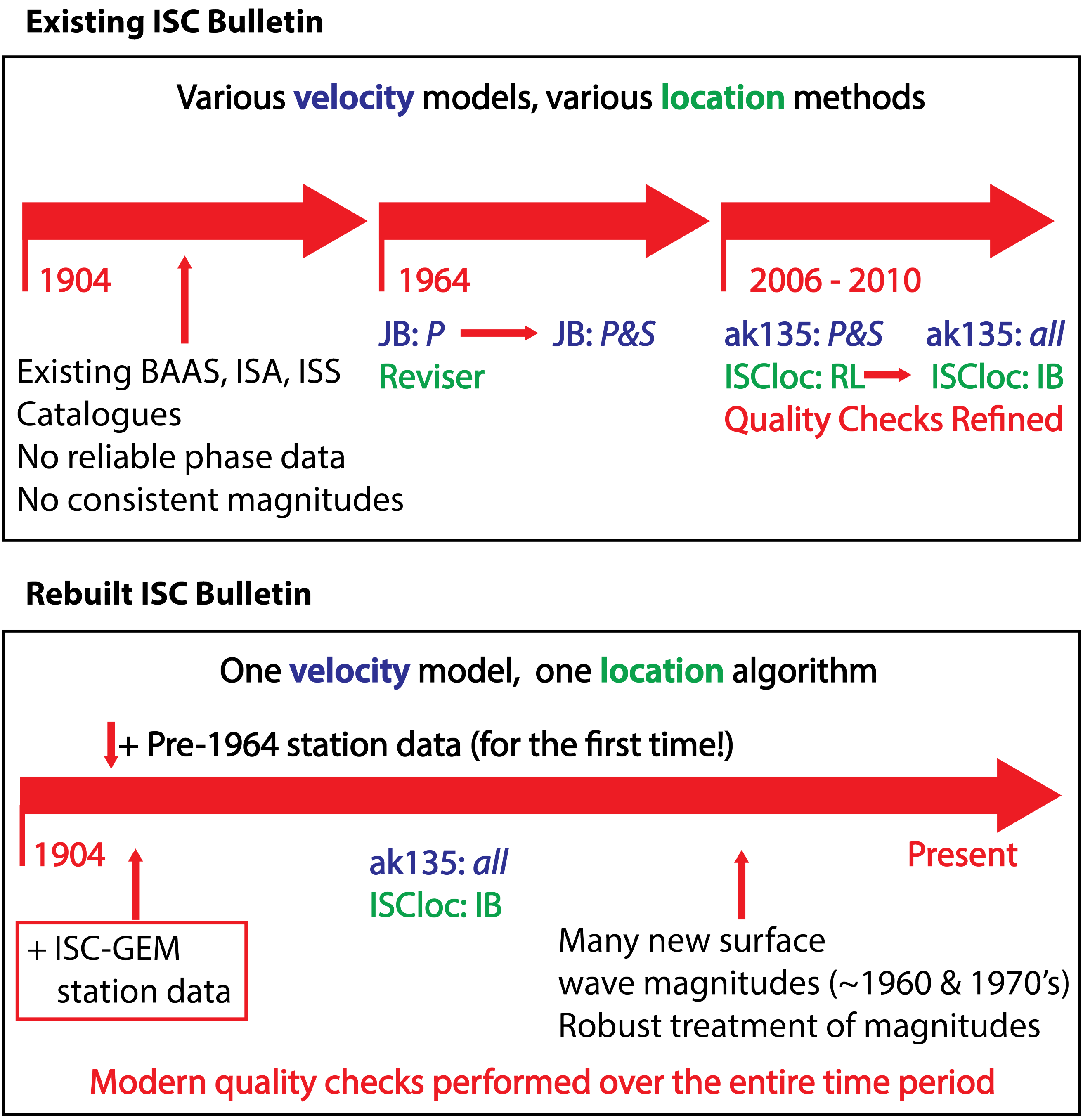

Figure 6.1: *Summary of the state of the original ISC Bulletin, and the projected state of the bulletin after work on the Rebuild Project is complete. Velocity models are in blue, location programs/algorithms are in green. The Reviser locator was written in 1970, and amended throughout the years. ISCloc:IB is from Bondar and Storchak (2011). ak135 velocity model is from Kennet et al. (1995) and Kennet (2005). Note that at the initial introduction of the ak135 velocity in the ISC Bulletin, only P and S phases were used for relocation, until the period near 2010, when all available ak135 phases were used.*

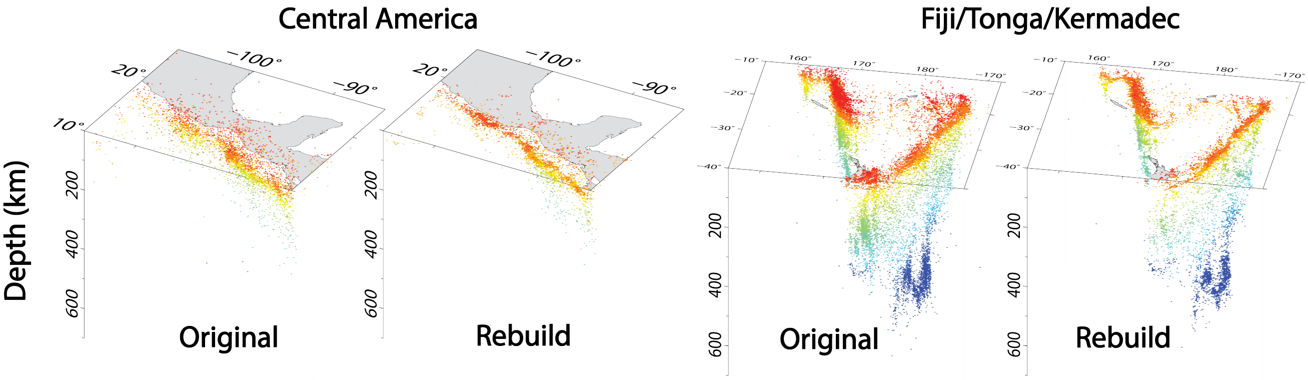

Figure 6.2: *Regional maps of seismicity comparing the original ISC Bulletin and the Rebuild ISC Bulletin in two different geographical regions, covering the years 1964–1979. Number of events is not constant between the two time periods, but instead show the full bulletin as it was, before and after the Rebuild efforts.*

References

Bondár, I. and D.A. Storchak (2011), Improved location procedures at the International Seismological Centre, *Geophys. J. Int.*, *186*, 1220–1244, DOI:10.1111/j.1365-246X.2011.05107.x.

Kennet, B.L.N., Engdahl, E.R. and Buland, R., (1995), Constraints on seismic velocities in the Earth from travel times, *Geophys. J. Int.*, *122*, 108–124.

Kennet, B.L.N., (2005), Seismological tables: ak135, Research School of Earth Sciences, the Australian National University, Canberra.

Storchak, D.A., Harris, J., Brown, L., Lieser, K., Shumba, B., Verney, R., Di Giacomo, D. and Korger., E. (2017), Rebuild of the Bulletin of the International Seismological Centre (ISC), part 1: 1964-1979, *Geoscience Letters*, *4:32*, DOI:10.1186/s40562-017-0098-z.

7

Summary of Seismicity, January - June 2015

In the first half of 2015 ten events with magnitudes larger than M_W 7 (Tab. 7.2) occurred. The two largest events with a magnitude of M_W 7.9 were the shallow Gorkha event in Nepal in April and the deep-focus Ogasawara event in the Bonin Islands region in May. With a focal depth of 686 km (30/05/2015 11:23:02 UTC, 27.8281°N, 140.4939°E, 685.5 km, 3480 stations (ISC)) the latter event is located about 100 km below the deep seismicity common for this area and below the nominal base of the mantle transition zone (MTZ) at 660 km depth above which earthquakes usually occur. This rose the question of the location of the earthquake with respect to the base of the MTZ as well as the location of the base of the MTZ in this area. Several models of the subducting slab at depth were developed: *Ye et al.* (2016) suggested folded or torn and buckled slab models, and *Porrit and Yoshioka* (2016) proposed a pileup of the Pacific slab at a depressed base of the MTZ. *Zhao et al.* (2017) conclude in their study that the generation of the 2015 Bonin deep earthquake was caused by the joint effects of several factors, including the fast deep subduction of the Pacific slab, slab tearing and its related thermal variation, stress changes and phase transformations in the slab near the upper-lower mantle boundary, as well as complex interactions between the subducting slab and the ambient mantle.

Although the Ogasawara event was felt several hundreds miles away in the metropolitan region of Tokyo (*USGS*, 2016) it did not cause damage because of its depth and remote location. For the Nepal event this unfortunately is not true. Due to its shallow focal depth of 13 km (25/04/2015 06:11:26.63 UTC, 28.1302°N, 84.7168°E, 13.4 km, 2182 stations (ISC)) and its location in a populated area with structures that are highly vulnerable to earthquake shaking (*USGS*, 2015), this event caused severe damage and casualties. According to the *Government of Nepal* (2015) over 8,700 casualties and 22,300 injuries were reported and about a third of Nepals population (about 8 m people) was affected by the event and its aftershocks. The main shock occurred along the central Himalayan Arc, where the Indo-Australian and Eurasian plates collide. Slip models suggest that the rupture propagated over 150 km along the fault to the east into the deeper part of the seismogenic zone (e.g. *Wang and Fialko*, 2015; *Lindsey et al.*, 2015; *Fan and Shearer*, 2015). The largest aftershock hit Nepal on 12 May with a magnitude of M_W 7.5 at the eastern end of the rupture area of the main shock, extending the rupture area to the east (*Lindsey et al.*, 2015). The Ghorka event with 226 entries to date in the ISC Event Bibliography (*Di Giacomo et al.*, 2014; *International Seismological Centre*, 2018) and its largest aftershock with 32 entries rose the most interest, by far, in the scientific community during the time period covered by this Summary, followed by the Ogasawara event with 8 entries.

The number of events in this Bulletin Summary categorised by type are given in Table 7.1.

The period between January and June 2015 produced 10 earthquakes with $M_W \geq 7$; these are listed in Table 7.2.

Figure 7.1 shows the number of moderate and large earthquakes in the first half of 2015. The distribution

felt earthquake	104
known earthquake	157823
known chemical explosion	6357
known induced event	3380
known mine explosion	705
known rockburst	306
known experimental explosion	52
suspected earthquake	25449
suspected chemical explosion	660
suspected induced event	4
suspected mine explosion	4283
suspected rockburst	153
total	199276

Table 7.1: *Summary of events by type between January and June 2015.*

Table 7.2: *Summary of the earthquakes of magnitude Mw $\geq$ 7 between January and June 2015.*

Date	lat	lon	depth	Mw	Flinn-Engdahl Region
2015-05-30 11:23:02	27.83	140.49	685	7.9	Bonin Islands region
2015-04-25 06:11:26	28.13	84.72	13	7.9	Nepal
2015-05-05 01:44:04	-5.52	151.86	29	7.5	New Britain region
2015-03-29 23:48:31	-4.78	152.58	41	7.5	New Britain region
2015-05-12 07:05:18	27.80	86.13	12	7.5	Nepal
2015-02-13 18:59:13	52.51	-32.02	16	7.1	Reykjanes Ridge
2015-05-07 07:10:23	-7.30	154.56	30	7.1	Bougainville-Solomon Islands region
2015-06-17 12:51:35	-35.37	-17.81	27	7.0	Southern Mid-Atlantic Ridge
2015-02-27 13:45:05	-7.36	122.49	559	7.0	Flores Sea
2015-05-22 21:45:20	-11.13	163.59	19	7.0	Bougainville-Solomon Islands region

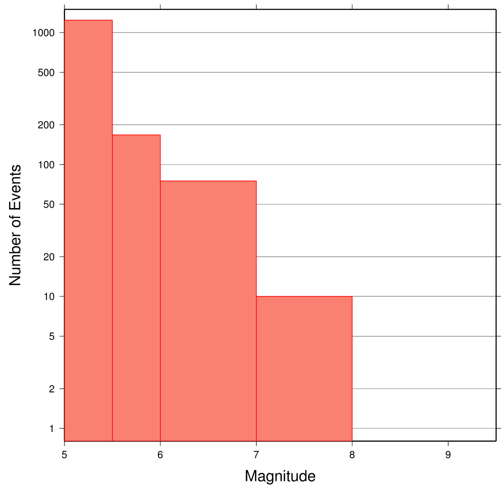

Figure 7.1: *Number of moderate and large earthquakes between January and June 2015. The non-uniform magnitude bias here correspond with the magnitude intervals used in Figures 7.2 to 7.5.*

of the number of earthquakes should follow the Gutenberg-Richter law.

Figures 7.2 to 7.5 show the geographical distribution of moderate and large earthquakes in various magnitude ranges.

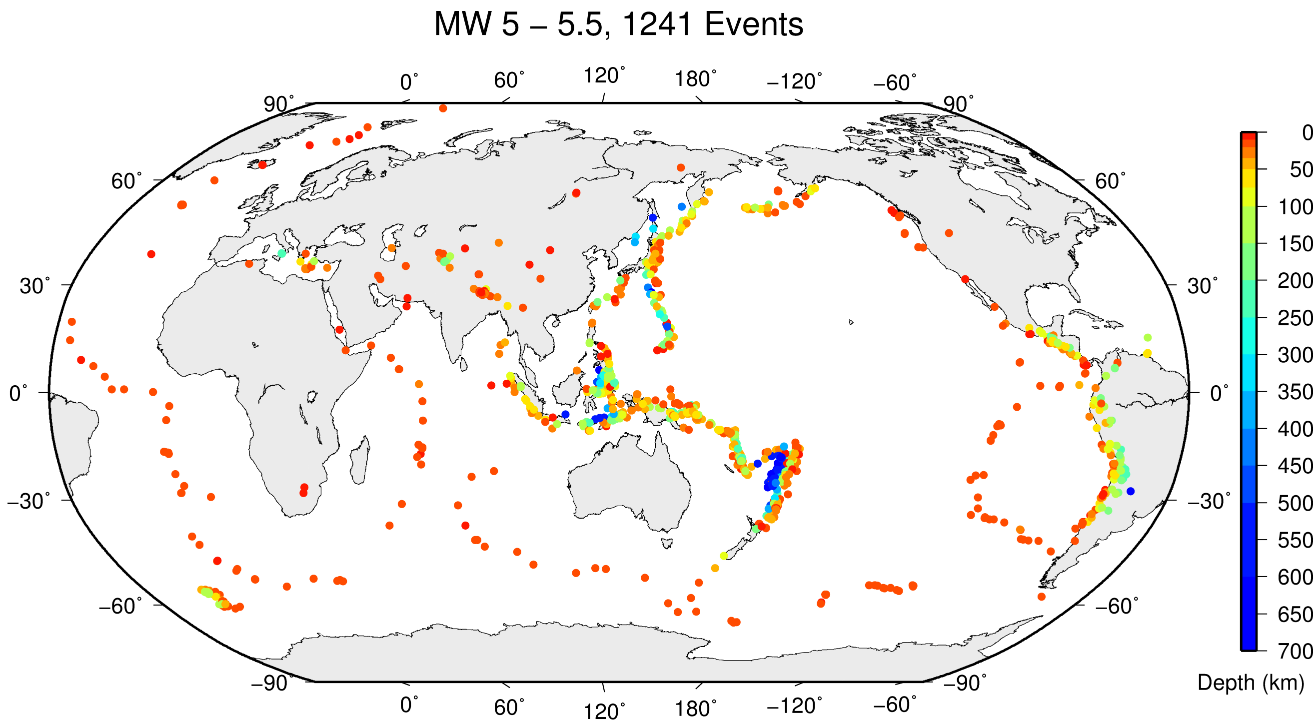

Figure 7.2: *Geographic distribution of magnitude 5-5.5 earthquakes between January and June 2015.*

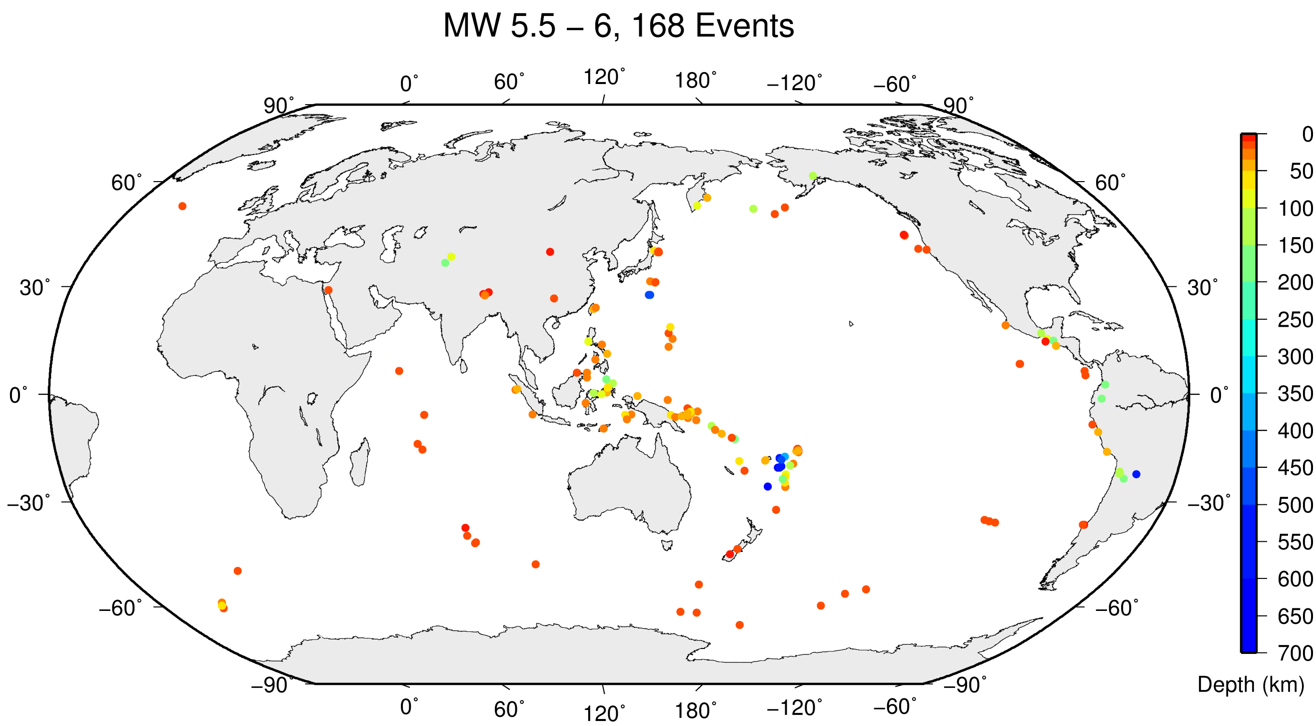

Figure 7.3: *Geographic distribution of magnitude 5.5-6 earthquakes between January and June 2015.*

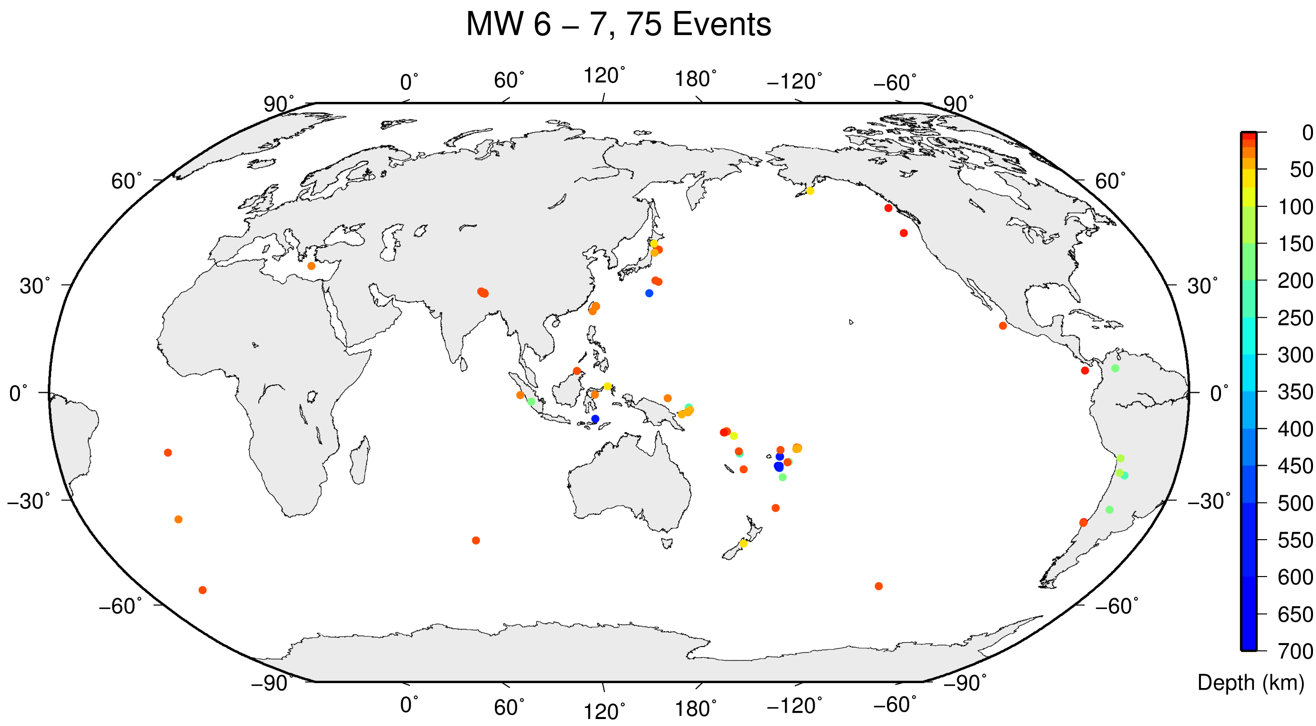

Figure 7.4: *Geographic distribution of magnitude 6-7 earthquakes between January and June 2015.*

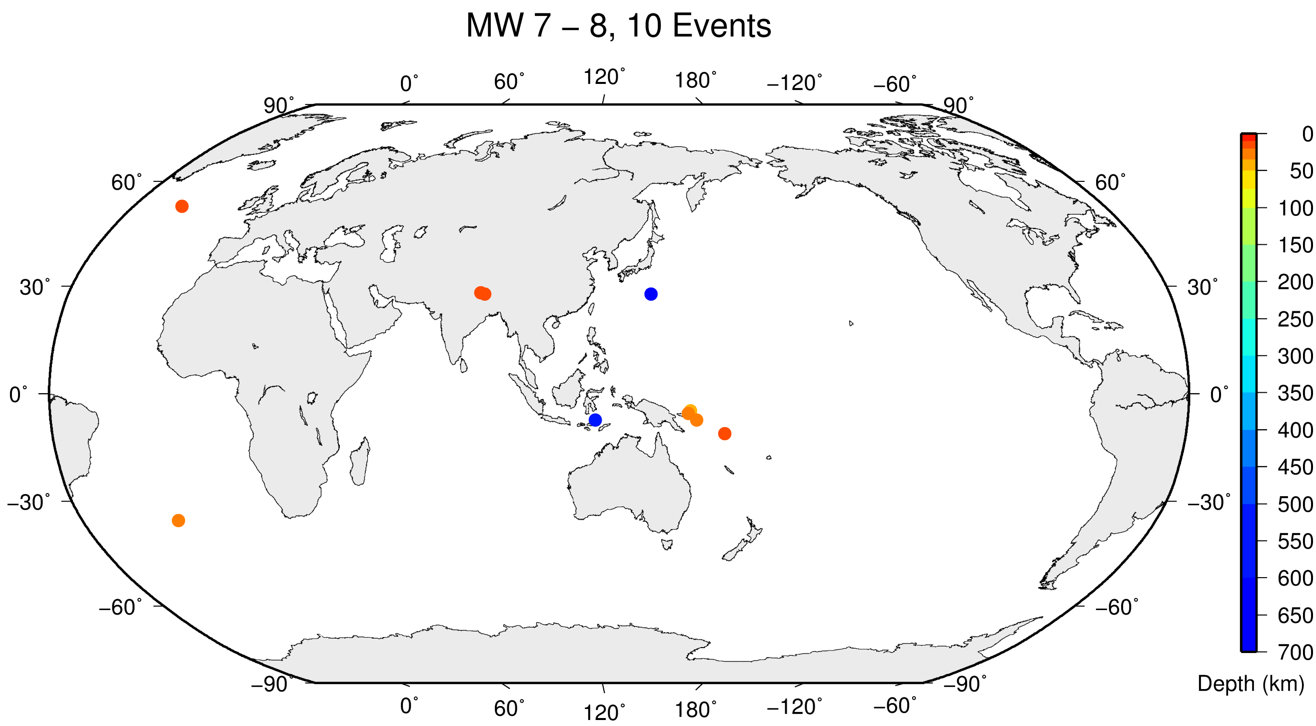

Figure 7.5: *Geographic distribution of magnitude 7-8 earthquakes between January and June 2015.*

References

Di Giacomo, D., D.A. Storchak, N. Safronova, P. Ozgo, J. Harris, R. Verney and I. Bondár (2014), A New ISC Service: The Bibliography of Seismic Events, *Seismol. Res. Lett.*, *85*(2), 354–360, DOI:10.1785/0220130143.

Fan, W. and P. M. Shearer (2015), Detailed rupture imaging of the 25 April 2015 Nepal earthquake using teleseismic P waves, *Geophys. Res. Lett.*, *42*, 5744–5752, DOI:10.1002/2015GL064587.

Government of Nepal (2015), Nepal Earthquake 2015: Post Disaster Needs Assessment, 2015, Vol. A: Key Findings, National Planning Commission, Kathmandu.

International Seismological Centre, On-line Event Bibliography, `www.isc.ac.uk/event_bibliography`, Internatl. Seis. Cent., Thatcham, United Kingdom, 2018.

Lindsey, E.O., R. Natsuaki, X. Xu, M. Shimada, M. Hashimoto, D. Melgar and D. T. Sandwell (2015), Line-of-sight displacement from ALOS-2 interferometry: Mw 7.8 Gorkha Earthquake and Mw 7.3 aftershock, *Geophys. Res. Lett.*, *42*, 6655–6661, DOI:10.1002/2015GL065385.

Porritt, R. and S. Yoshioka (2016), Slab pileup in the mantle transition zone and the 30 May 2015 Chichi-jima earthquake, *Geophys. Res. Lett.*, *43*, 4905–4912, DOI:10.1002/2016GL068168.

USGS (2015), PAGER, `https://earthquake.usgs.gov/earthquakes/eventpage/us20002926#pager`, (visited on 1 June 2018).

USGS (2016), Did you fell it?, `https://earthquake.usgs.gov/earthquakes/eventpage/us20002ki3#dyfi`, (visited on 1 June 2018).

Wang, K. and Y. Fialko (2015), Slipmodel of the 2015 Mw 7.8 Gorkha (Nepal) earthquake from inversions of ALOS-2 and GPS data, *Geophys. Res. Lett.*, *42*, 7452–7458, DOI:10.1002/2015GL065201.

Ye, L., T. Lay, Z. Zhan, H. Kanamori and J.-L. Hao (2016), The isolated 680 km deep 30 May 2015 Mw 7.9 Ogasawara (Bonin) Islands earthquake, *Earth Planet. Sci. Lett.*, 433, 169– 179, DOI:10.1016/j.epsl.2015.10.049.

Zhao, D., M. Fujisawa and G. Toyokuni (2017), Tomography of the subducting Pacific slab and the 2015 Bonin deepest earthquake (Mw 7.9), *Sci. Rep. 7*, 44487, DOI:10.1038/srep44487.

8

Statistics of Collected Data

8.1 Introduction

The ISC Bulletin is based on the parametric data reports received from seismological agencies around the world. With rare exceptions, these reports include the results of waveform review done by analysts at network data centres and observatories. These reports include combinations of various bulletin elements such as event hypocentre estimates, moment tensors, magnitudes, event type and felt and damaging data as well as observations of the various seismic waves recorded at seismic stations.

Data reports are received in different formats that are often agency specific. Once an authorship is recognised, the data are automatically parsed into the ISC database and the original reports filed away to be accessed when necessary. Any reports not recognised or processed automatically are manually checked, corrected and re-processed. This chapter describes the data that are received at the ISC before the production of the reviewed Bulletin.

Notably, the ISC integrates all newly received data reports into the automatic ISC Bulletin (available on-line) soon after these reports are made available to ISC, provided it is done before the submission deadline that currently stands at 12 months following an event occurrence.

With data constantly being reported to the ISC, even after the ISC has published its review, the total data shown as collected, in this chapter, is limited to two years after the time of the associated reading or event, i.e. any hypocentre data collected two years after the event are not reflected in the figures below.

8.2 Summary of Agency Reports to the ISC

A total of 148 agencies have reported data for January 2015 to June 2015. The parsing of these reports into the ISC database is summarised in Table 8.1.

Table 8.1: *Summary of the parsing of reports received by the ISC from a total of 148 agencies, containing data for this summary period.*

	Number of reports
Total collected	2904
Automatically parsed	1936
Manually parsed	968

Data collected by the ISC consists of multiple data types. These are typically one of:

- Bulletin, hypocentres with associated phase arrival observations.

- Catalogue, hypocentres only.
- Unassociated phase arrival observations.

In Table 8.2, the number of different data types reported to the ISC by each agency is listed. The number of each data type reported by each agency is also listed. Agencies reporting indirectly have their data type additionally listed for the agency that reported it. The agencies reporting indirectly may also have 'hypocentres with associated phases' but with no associated phases listed - this is because the association is being made by the agency reporting directly to the ISC. Summary maps of the agencies and the types of data reported are shown in Figure 8.1 and Figure 8.2.

Table 8.2: *Agencies reporting to the ISC for this summary period. Entries in bold are for new or renewed reporting by agencies since the previous six-month period.*

Agency	Country	Directly or indirectly reporting (D/I)	Hypocentres with associated phases	Hypocentres without associated phases	Associated phases	Unassociated phases	Amplitudes
TIR	Albania	D	344	8	4515	18	844
CRAAG	Algeria	D	409	0	1908	190	0
LPA	Argentina	D	0	0	0	507	0
SJA	Argentina	D	373	62	12555	0	2944
NSSP	Armenia	D	77	2	842	0	0
AUST	Australia	D	804	1	20133	0	0
CAN	**Australia**	**I NEIC**	**0**	**0**	**2**	**0**	**0**
CUPWA	Australia	D	28	0	348	0	0
IDC	Austria	D	17838	14	395343	0	329396
VIE	Austria	D	3790	79	35593	656	35578
AZER	Azerbaijan	D	81	1	4357	0	0
UCC	Belgium	D	691	0	7671	213	857
SCB	Bolivia	D	25	0	621	0	109
RHSSO	Bosnia-Herzegovina	D	1036	55	18508	5995	0
VAO	Brazil	D	1011	13	28531	0	0
SOF	Bulgaria	D	232	0	1277	0	0
SOMC	**Cameroon**	**D**	**0**	**0**	**0**	**21**	**0**
OTT	Canada	D	1916	32	41812	0	2273
PGC	Canada	I OTT	1545	1	33414	0	0
GUC	Chile	D	2587	179	70963	2696	19196
BJI	China	D	1650	19	91257	25483	61447
ASIES	Chinese Taipei	D	0	30	0	0	0
TAP	Chinese Taipei	D	20635	37	834390	0	0
RSNC	Colombia	D	6702	2	169168	16639	52707
CASC	Costa Rica	I NEIC	1	0	0	0	0
ICE	Costa Rica	I UCR	0	1	0	0	0
UCR	Costa Rica	D	440	23	13637	0	903
ZAG	Croatia	D	0	0	0	35555	0
SSNC	Cuba	D	146	0	2260	0	995
NIC	Cyprus	D	665	2	15950	0	7740
IPEC	Czech Republic	D	485	13	3331	22370	1491
PRU	Czech Republic	D	5256	38	45549	208	10710
DNK	Denmark	D	1624	1205	17258	28591	10469
OSPL	Dominican Republic	D	280	0	3247	0	976
SDD	**Dominican Republic**	**I OSPL**	**3**	**0**	**0**	**0**	**0**
IGQ	Ecuador	D	5	72	3518	0	0
HLW	Egypt	D	231	2	2714	0	0
SNET	El Salvador	D	1077	50	23789	10	4039
SSS	El Salvador	I UCR	0	7	0	0	0
EST	Estonia	I HEL	331	7	0	0	0
AAE	Ethiopia	D	45	0	309	57	0
SKO	FYR Macedonia	D	1552	0	18495	4219	3261

Table 8.2: (continued)

Agency	Country	Directly or indirectly reporting (D/I)	Hypocentres with associated phases	Hypocentres without associated phases	Associated phases	Unassociated phases	Amplitudes
FIA0	Finland	I HEL	11	1	0	0	0
HEL	Finland	D	5787	4096	114993	0	16506
CSEM	France	I KISR	2090	1085	0	0	0
LDG	France	D	2464	117	50913	8	20682
STR	France	D	1723	0	25789	10	0
PPT	French Polynesia	D	1190	0	9199	844	9980
TIF	Georgia	D	0	614	0	9687	0
AWI	Germany	D	1871	0	7564	385	0
BGR	Germany	D	782	256	20533	0	7480
BNS	Germany	I BGR	6	32	0	0	0
BRG	Germany	D	0	0	0	7668	3576
BUG	Germany	I BGR	19	5	0	0	0
CLL	Germany	D	2	0	79	7412	2519
GDNRW	Germany	I BGR	1	24	0	0	0
GFZ	Germany	I KRSZO	54	9	0	0	0
HLUG	**Germany**	**I BGR**	**1**	**0**	**0**	**0**	**0**
LEDBW	Germany	I BGR	17	4	0	0	0
ATH	Greece	D	11889	25	303117	0	94479
THE	Greece	D	4516	79	97023	5718	29200
UPSL	Greece	D	0	2	0	0	0
GCG	Guatemala	D	460	0	2631	0	0
HKC	Hong Kong	D	0	0	0	48	0
BUD	Hungary	D	0	10	0	942	0
KRSZO	Hungary	D	187	307	14065	0	4019
REY	Iceland	D	160	0	6305	0	0
HYB	India	D	852	177	1238	0	99
MERI	**India**	**I NDI**	**0**	**1**	**0**	**0**	**0**
NDI	India	D	784	602	17668	2053	5767
DJA	Indonesia	D	3554	68	61288	0	79945
TEH	Iran	D	613	34	21873	0	4146
THR	Iran	D	320	18	2495	0	603
ISN	Iraq	D	300	0	1950	0	751
GII	Israel	D	359	0	5260	0	0
GEN	Italy	D	615	1	6306	1856	0
MED_RCMT	Italy	D	0	171	0	0	0
RISSC	Italy	D	3	0	43	0	0
ROM	Italy	D	8241	112	518506	209607	342190
TRI	Italy	D	0	0	0	6808	0
LIC	Ivory Coast	D	737	0	2213	0	1473
JSN	Jamaica	D	110	0	653	6	0
JMA	Japan	D	58687	3	473008	677	0
MAT	Japan	D	0	0	0	10691	0
NIED	Japan	D	0	674	0	0	0
SYO	Japan	D	0	0	0	2001	0
JSO	Jordan	D	3	3	43	0	50
NNC	Kazakhstan	D	8604	0	99725	0	93232
SOME	Kazakhstan	D	5223	146	81618	24	70416
KISR	**Kuwait**	**D**	**531**	**15**	**2662**	**96**	**0**
KNET	Kyrgyzstan	D	1260	0	9885	0	1647
KRNET	Kyrgyzstan	D	4281	0	71492	0	0
LVSN	Latvia	D	217	0	3032	0	1585
GRAL	Lebanon	D	242	0	1614	396	0
LIT	Lithuania	D	450	459	3980	1614	277
ECGS	Luxembourg	D	53	0	438	0	0
MCO	Macao, China	D	0	0	0	33	0
GSDM	Malawi	D	0	0	0	466	0
KLM	Malaysia	D	417	0	1761	0	0
ECX	Mexico	D	778	9	14606	0	2200
MEX	Mexico	D	5270	157	53037	101	0
MOLD	Moldova	D	0	0	0	850	417
PDG	Montenegro	D	377	3	8850	0	4212
NAM	Namibia	D	22	0	100	12	0
DMN	Nepal	D	1312	6	13811	0	9044

Table 8.2: (continued)

Agency	Country	Directly or indirectly reporting (D/I)	Hypocentres with associated phases	Hypocentres without associated phases	Associated phases	Unassociated phases	Amplitudes
DBN	Netherlands	I BGR	0	3	0	0	0
NOU	**New Caledonia**	**D**	**1592**	**1028**	**8436**	**0**	**0**
WEL	New Zealand	D	7539	67	243475	112	260844
INET	Nicaragua	D	0	1013	0	0	0
BER	Norway	D	2397	2209	50766	2647	10953
NAO	Norway	D	1562	1039	5614	0	1149
OMAN	Oman	D	512	0	16069	0	0
MSSP	Pakistan	D	0	0	0	809	0
UPA	Panama	D	562	0	11254	0	52
ARE	Peru	I NEIC	19	45	0	0	0
LIM	Peru	I HYB	0	7	0	0	0
MAN	Philippines	D	0	1555	0	31529	6341
QCP	Philippines	D	0	0	0	18	0
WAR	Poland	D	0	0	0	9994	314
IGIL	Portugal	D	606	0	2494	0	808
INMG	Portugal	D	2829	2	39415	1656	12582
PDA	Portugal	I SVSA	1	1	0	0	0
SVSA	Portugal	D	1520	0	30011	8174	13560
BELR	Republic of Belarus	D	307	2	4235	21798	7484
CFUSG	**Republic of Crimea**	**D**	**35**	**0**	**630**	**0**	**0**
KMA	**Republic of Korea**	**D**	**254**	**0**	**3629**	**0**	**0**
BUC	Romania	D	1156	17	22146	58712	8318
ASRS	Russia	D	131	0	4695	0	1333
BYKL	Russia	D	477	0	37109	0	12672
DRS	Russia	I MOS	73	93	0	0	0
IEPN	Russia	D	123	0	1238	4141	1477
KOLA	Russia	D	137	0	475	0	0
KRSC	Russia	D	615	0	20801	0	0
MIRAS	Russia	D	98	0	708	0	366
MOS	Russia	D	1866	230	312484	0	111806
NERS	Russia	D	24	0	772	0	368
NORS	Russia	I MOS	47	132	0	0	0
SKHL	Russia	D	535	536	14383	0	6795
YARS	Russia	D	534	0	7532	0	4850
SGS	Saudi Arabia	D	24	0	207	0	0
BEO	Serbia	D	1291	48	22784	0	0
BRA	Slovakia	D	0	0	0	21438	0
LJU	Slovenia	D	1147	145	16339	3169	5416
HNR	Solomon Islands	D	0	0	0	1924	0
PRE	South Africa	D	778	0	12587	0	4192
MDD	Spain	D	2681	8	75535	0	56015
MRB	Spain	D	374	0	9709	0	4250
SFS	Spain	D	502	0	3339	347	0
UPP	Sweden	D	1596	2747	17103	0	0
ZUR	Switzerland	D	360	0	9672	0	5059
BKK	Thailand	D	2202	42	31246	0	34122
TRN	Trinidad and Tobago	D	2	1300	195	30744	0
TUN	Tunisia	D	0	33	0	0	0
DDA	Turkey	D	9116	1	202348	0	68517
ISK	Turkey	D	8676	11	127397	6360	73724
IST	**Turkey**	**I NEIC**	**0**	**0**	**1**	**0**	**0**
AEIC	U.S.A.	I NEIC	1499	390	55011	0	0
ANF	U.S.A.	I IRIS	219	874	0	0	0
BUT	U.S.A.	I NEIC	65	16	0	0	0
CERI	U.S.A.	I IRIS	8	0	0	0	0
GCMT	U.S.A.	D	0	2162	0	0	0
HVO	U.S.A.	I NEIC	208	1	16	0	0
IRIS	U.S.A.	D	1416	874	68467	0	0

Table 8.2: *(continued)*

Agency	Country	Directly or indirectly reporting (D/I)	Hypocentres with associated phases	Hypocentres without associated phases	Associated phases	Unassociated phases	Amplitudes
LDO	U.S.A.	I NEIC	5	7	532	0	0
NCEDC	U.S.A.	I NEIC	113	7	2261	0	0
NEIC	U.S.A.	D	15954	9054	1361546	0	634534
OGSO	**U.S.A.**	**I NEIC**	**3**	**0**	**0**	**0**	**0**
PAS	U.S.A.	I NEIC	57	14	8857	0	0
PNSN	U.S.A.	D	0	28	0	0	0
REN	U.S.A.	I NEIC	329	13	731	0	0
RSPR	U.S.A.	D	1871	3	24059	0	0
SCEDC	U.S.A.	I IRIS	71	0	0	0	0
SEA	U.S.A.	I NEIC	45	130	4869	0	0
SLM	U.S.A.	I NEIC	41	7	938	0	0
TUL	U.S.A.	I NEIC	1501	1	0	0	0
UUSS	U.S.A.	I NEIC	35	0	606	0	0
WES	U.S.A.	I IRIS	8	0	0	0	0
MCSM	**Ukraine**	**D**	**7**	**0**	**160**	**0**	**0**
SIGU	Ukraine	D	46	0	1444	0	815
DSN	United Arab Emirates	D	360	0	4861	0	0
BGS	United Kingdom	D	332	14	8801	23	3259
EAF	Unknown	D	389	0	2274	10093	17
ISU	Uzbekistan	D	122	0	1257	0	0
CAR	Venezuela	I NEIC	5	12	0	0	0
FUNV	**Venezuela**	**D**	**188**	**0**	**3615**	**0**	**0**
PLV	Vietnam	D	1	0	12	0	4
LSZ	Zambia	D	45	0	146	33	2
BUL	Zimbabwe	D	166	0	742	456	0

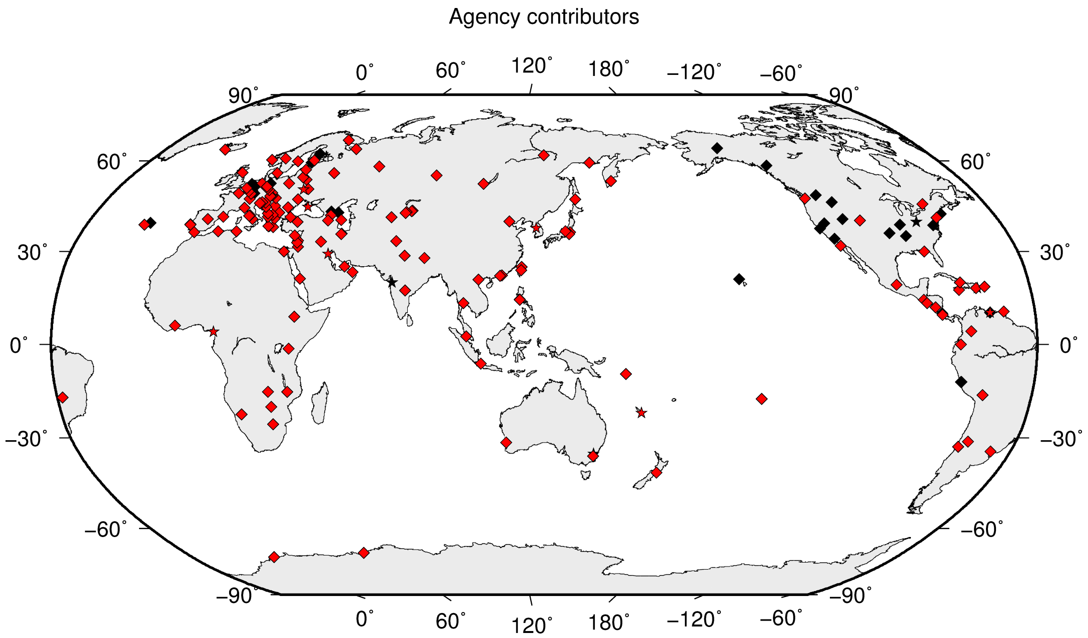

Figure 8.1: *Map of agencies that have contributed data to the ISC for this summary period. Agencies that have reported directly to the ISC are shown in red. Those that have reported indirectly (via another agency) are shown in black. Any new or renewed agencies, since the last six-month period, are shown by a star. Each agency is listed in Table 8.2.*

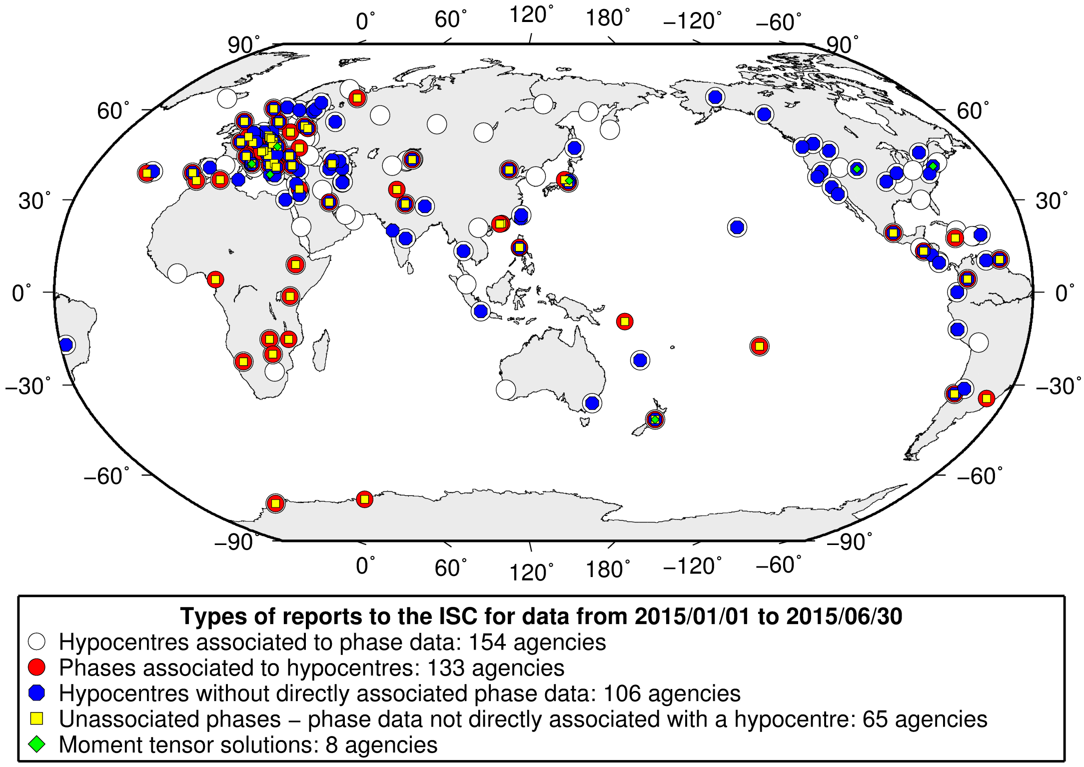

Figure 8.2: *Map of the different data types reported by agencies to the ISC. A full list of the data types reported by each agency is shown in Table 8.2.*

8.3 Arrival Observations

The collection of phase arrival observations at the ISC has increased dramatically with time. The increase in reported phase arrival observations is shown in Figure 8.3.

The reports with phase data are summarised in Table 8.3. This table is split into three sections, providing information on the reports themselves, the phase data, and the stations reporting the phase data. A map of the stations contributing these phase data is shown in Figure 8.5.

The ISC encourages the reporting of phase arrival times together with amplitude and period measurements whenever feasible. Figure 8.6 shows the percentage of events for which phase arrival times from each station are accompanied with amplitude and period measurements.

Figure 8.7 indicates the number of amplitude and period measurement for each station.

Together with the increase in the number of phases (Figure 8.3), there has been an increase in the number of stations reported to the ISC. The increase in the number of stations is shown in Figure 8.4. This increase can also be seen on the maps for stations reported each decade in Figure 8.8.

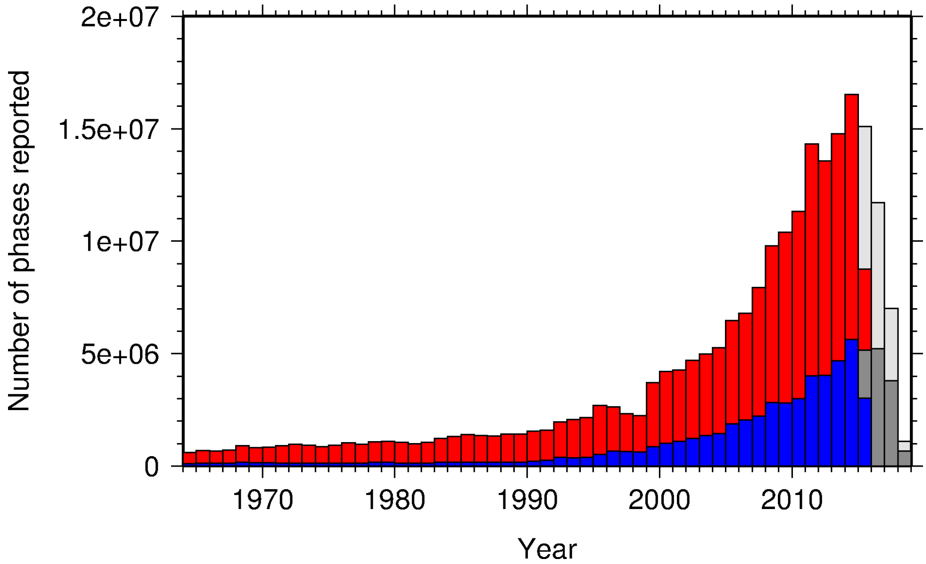

Figure 8.3: *Histogram showing the number of phases (red) and number of amplitudes (blue) collected by the ISC for events each year since 1964. The data in grey covers the current period where data are still being collected before the ISC review takes place and is accurate at the time of publication.*

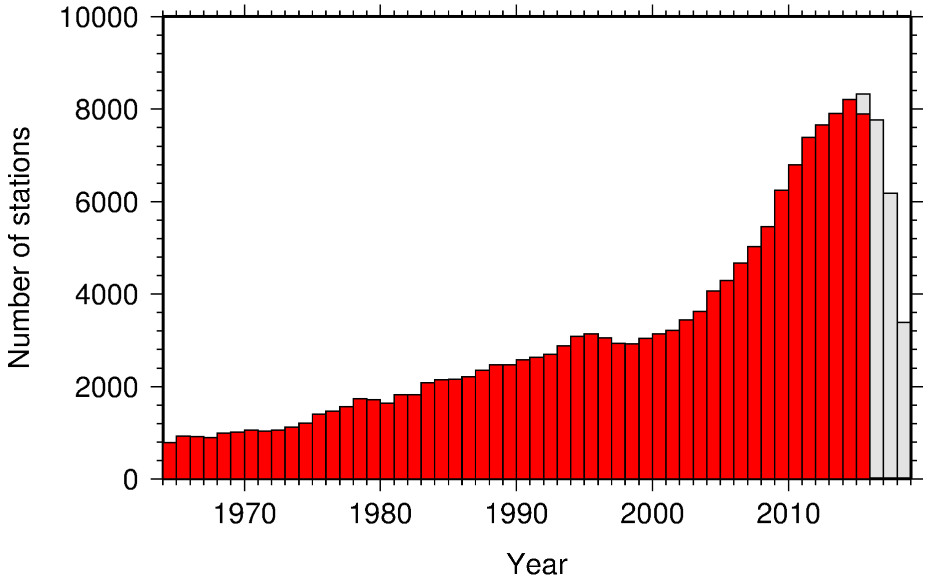

Figure 8.4: *Histogram showing the number of stations reporting to the ISC each year since 1964. The data in grey covers the current period where station information is still being collected before the ISC review of events takes place and is accurate at the time of publication.*

Reports with phase arrivals	2718
Reports with phase arrivals including amplitudes	1048
Reports with only phase arrivals (no hypocentres reported)	217
Total phase arrivals received	7401535
Total phase arrival-times received	6881945
Number of duplicate phase arrival-times	584455 (8.5%)
Number of amplitudes received	2693057
Stations reporting phase arrivals	7690
Stations reporting phase arrivals with amplitude data	4311
Max number of stations per report	1995

Table 8.3: *Summary of reports containing phase arrival observations.*

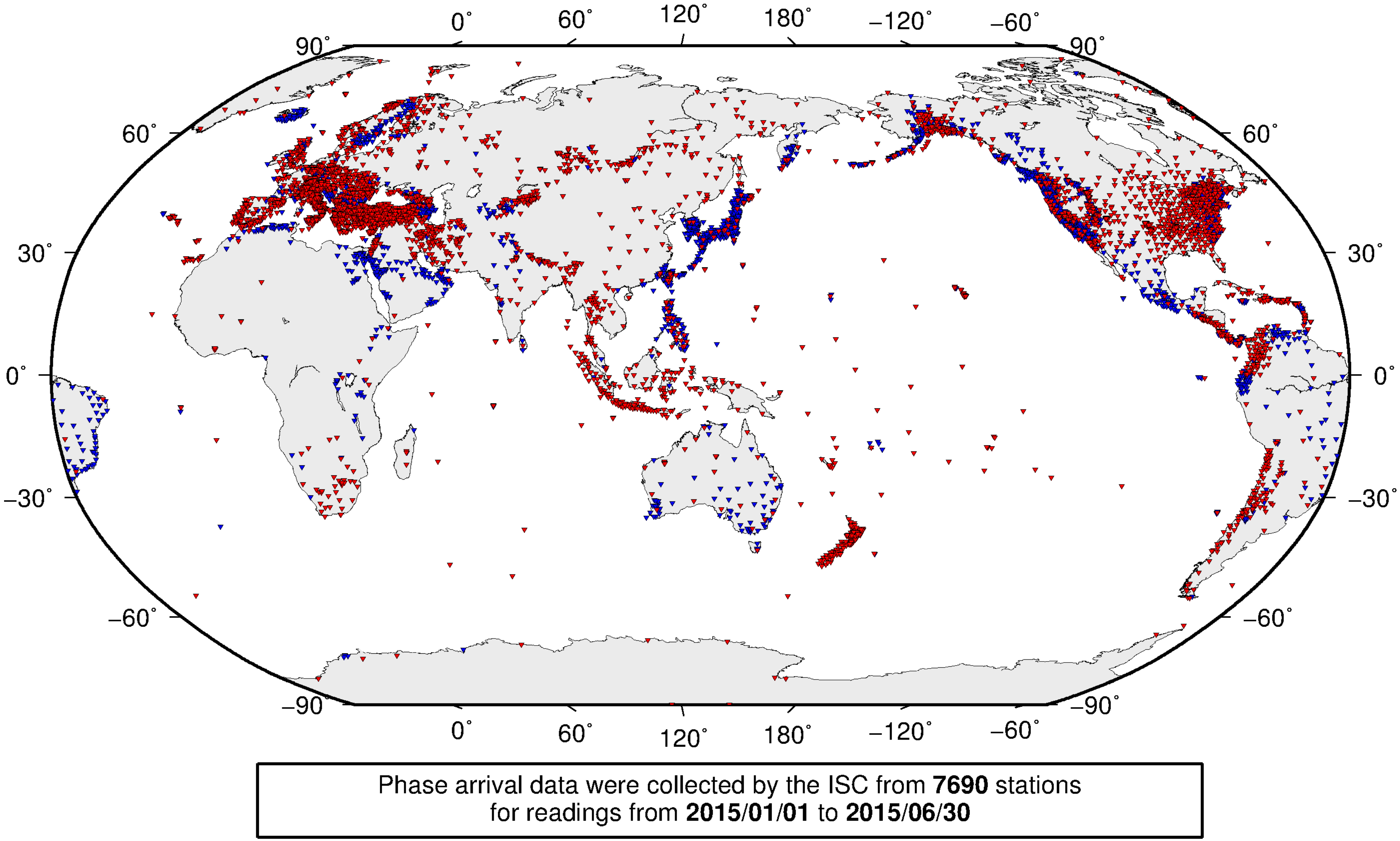

Figure 8.5: *Stations contributing phase data to the ISC for readings from January 2015 to the end of June 2015. Stations in blue provided phase arrival times only; stations in red provided both phase arrival times and amplitude data.*

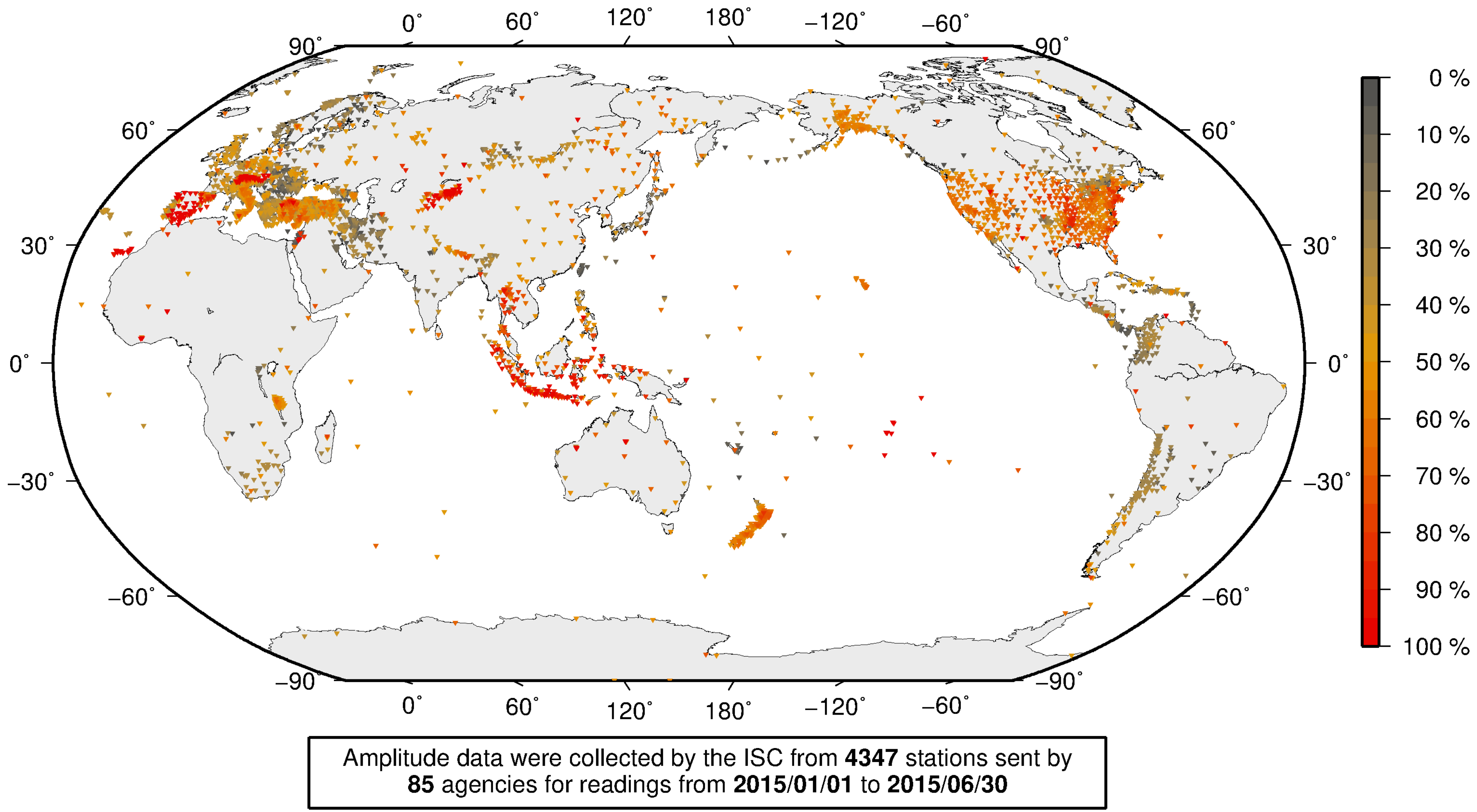

Figure 8.6: *Percentage of events for which phase arrival times from each station are accompanied with amplitude and period measurements.*

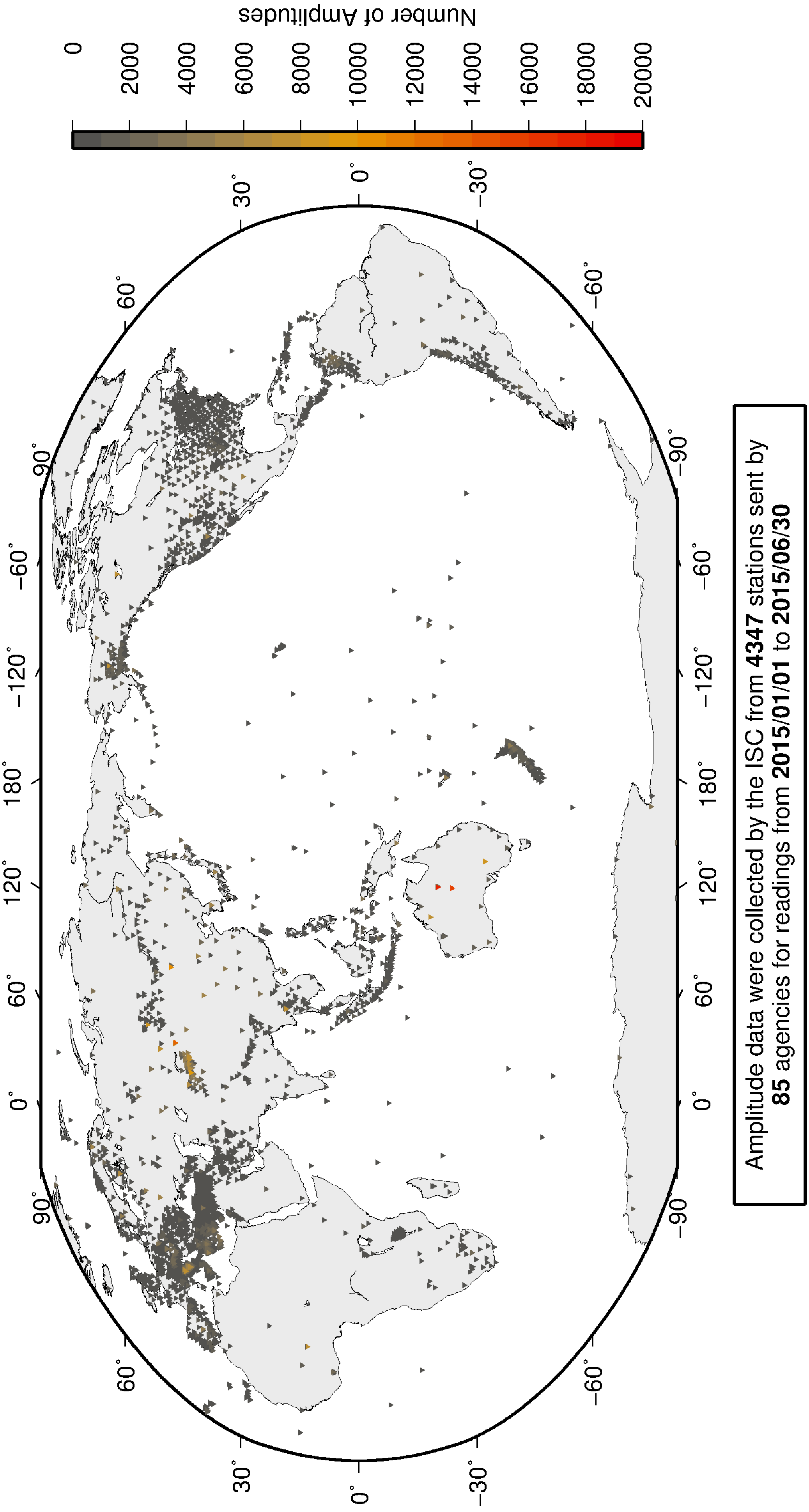

Figure 8.7: *Number of amplitude and period measurements for each station.*

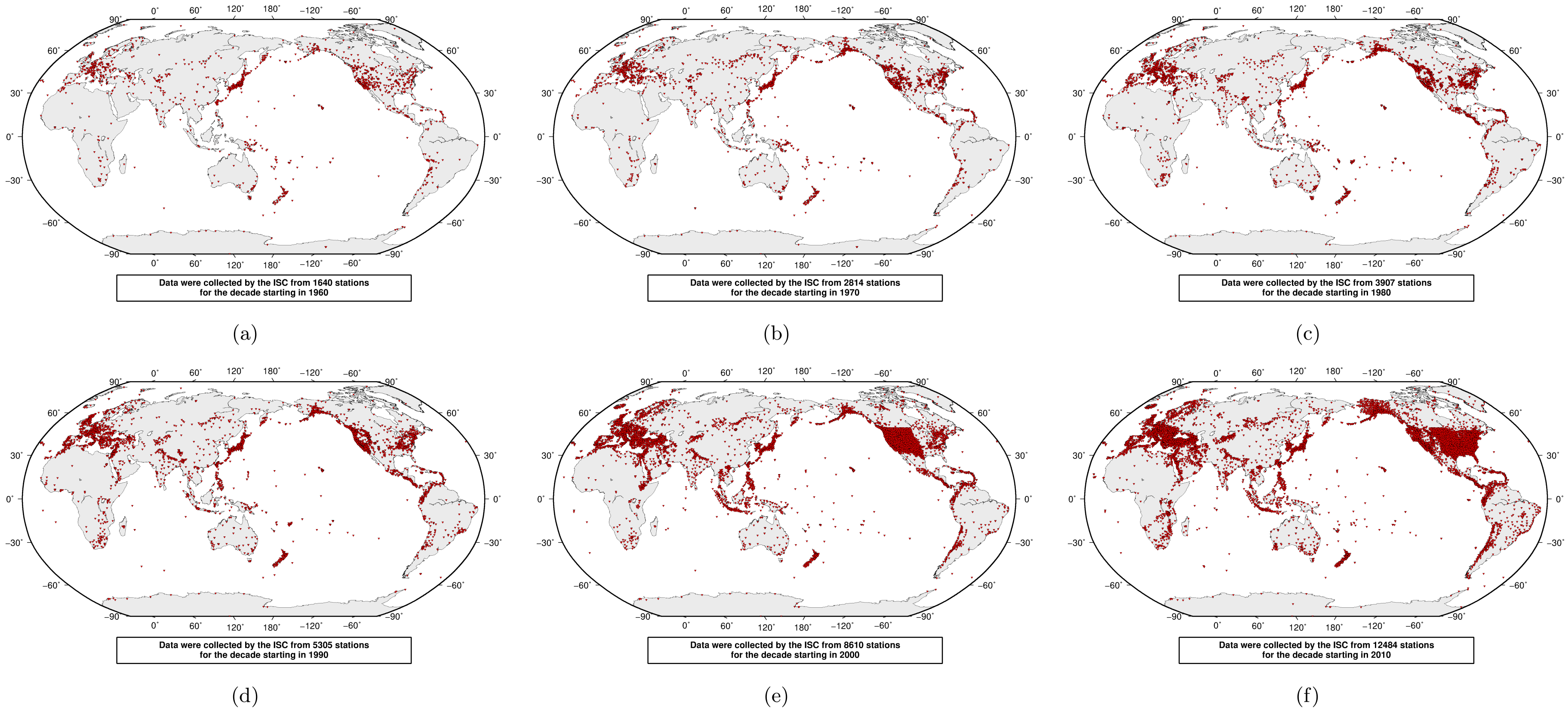

Figure 8.8: *Maps showing the stations reported to the ISC for each decade since 1960. Note that the last map covers a shorter time period.*

8.4 Hypocentres Collected

The ISC Bulletin groups multiple estimates of hypocentres into individual events, with an appropriate prime hypocentre solution selected. The collection of these hypocentre estimates are described in this section.

The reports containing hypocentres are summarised in Table 8.4. The number of hypocentres collected by the ISC has also increased significantly since 1964, as shown in Figure 8.9. A map of all hypocentres reported to the ISC for this summary period is shown in Figure 8.10. Where a network magnitude was reported with the hypocentre, this is also shown on the map, with preference given to reported values, first of M_W followed by M_S, m_b and M_L respectively (where more than one network magnitude was reported).

Table 8.4: *Summary of the reports containing hypocentres.*

Reports with hypocentres	2612
Reports of hypocentres only (no phase readings)	111
Total hypocentres received	302880
Number of duplicate hypocentres	8811 (2.9%)
Agencies determining hypocentres	169

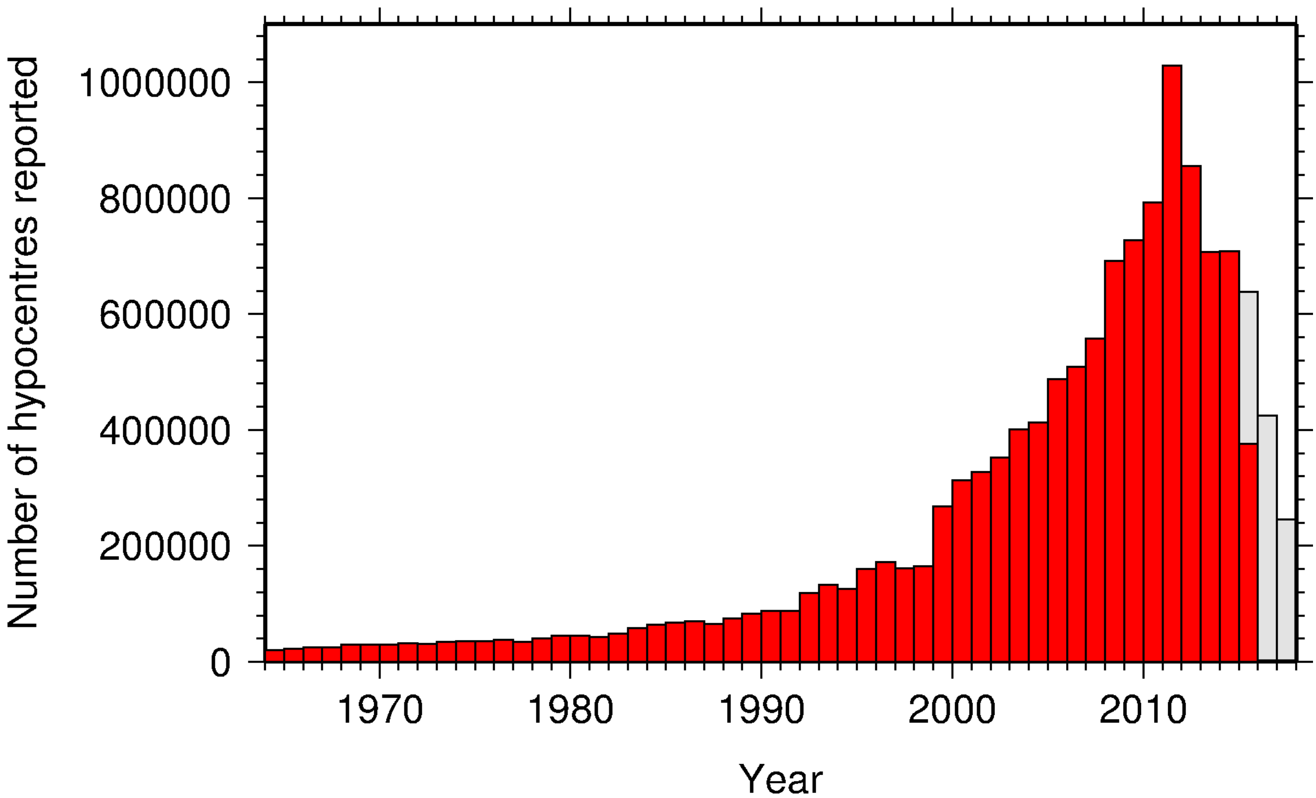

Figure 8.9: *Histogram showing the number of hypocentres collected by the ISC for events each year since 1964. For each event, multiple hypocentres may be reported.*

All the hypocentres that are reported to the ISC are automatically grouped into events, which form the basis of the ISC Bulletin. For this summary period 321506 hypocentres (including ISC) were grouped into 207203 events, the largest of these having 52 hypocentres in one event. The total number of events

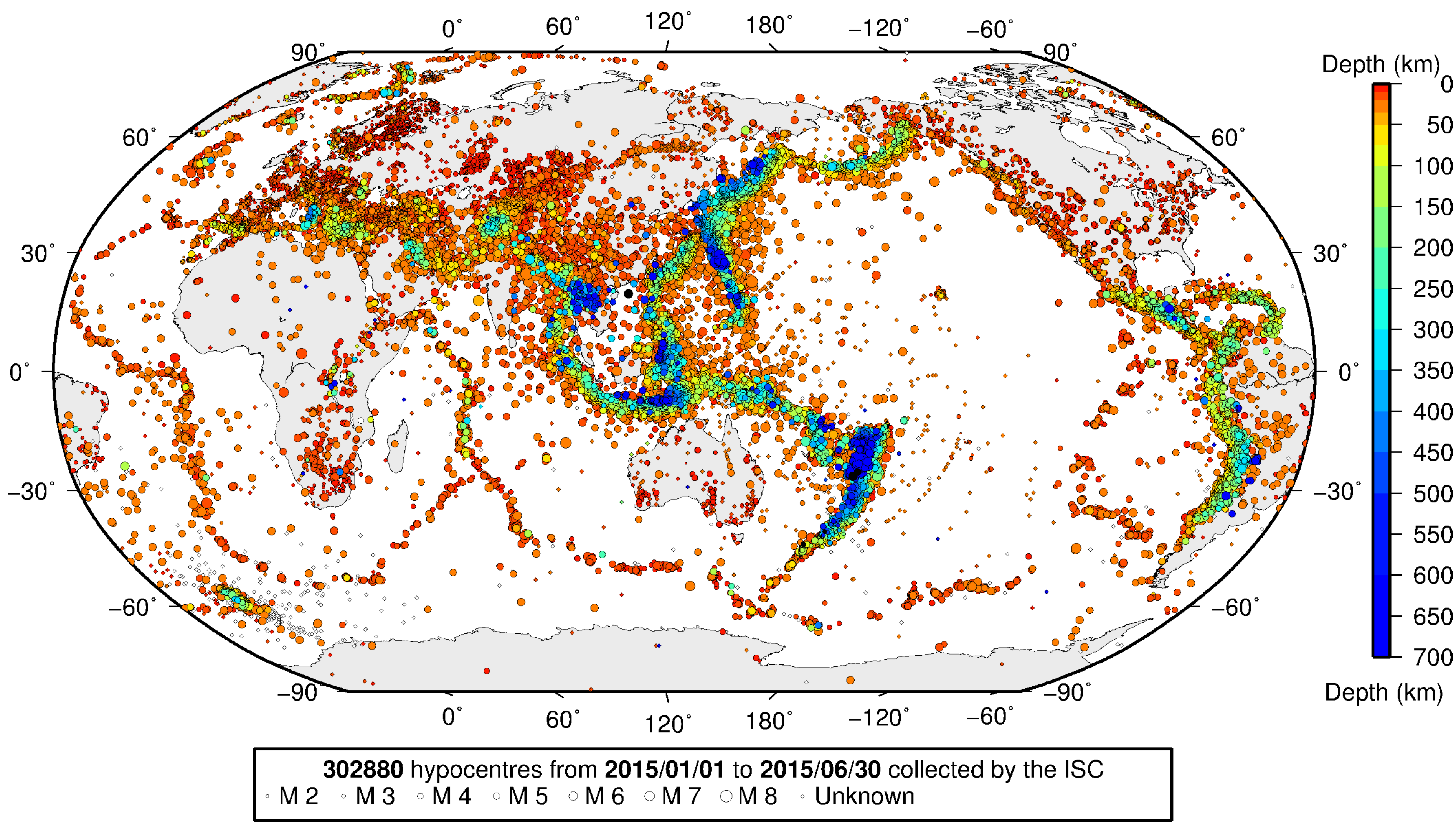

Figure 8.10: *Map of all hypocentres collected by the ISC. The scatter shows the large variation of the multiple hypocentres that are reported for each event. The magnitude corresponds with the reported network magnitude. If more than one network magnitude type was reported, preference was given to values of M_W, M_S, m_b and M_L respectively. Compare with Figure 9.2*

shown here is the result of an automatic grouping algorithm, and will differ from the total events in the published ISC Bulletin, where both the number of events and the number of hypocentre estimates will have changed due to further analysis. The process of grouping is detailed in Section 11.1.3. Figure 9.2 on page 86 shows a map of all prime hypocentres.

8.5 Collection of Network Magnitude Data

Data contributing agencies normally report earthquake hypocentre solutions along with magnitude estimates. For each seismic event, each agency may report one or more magnitudes of the same or different types. This stems from variability in observational practices at regional, national and global level in computing magnitudes based on a multitude of wave types. Differences in the amplitude measurement algorithm, seismogram component(s) used, frequency range, station distance range as well as the instrument type contribute to the diversity of magnitude types. Table 8.5 provides an overview of the complexity of reported network magnitudes reported for seismic events during the summary period.

Table 8.5: *Statistics of magnitude reports to the ISC; M – average magnitude of estimates reported for each event.*

	M<3.0	3.0≤M<5.0	M≥5.0
Number of seismic events	153886	33850	403
Average number of magnitude estimates per event	1.3	4.9	26.5
Average number of magnitudes (by the same agency) per event	1.2	2.7	3.4
Average number of magnitude types per event	1.2	4.0	13.1
Number of magnitude types	25	36	31

Table 8.6 gives the basic description, main features and scientific paper references for the most commonly reported magnitude types.

Table 8.6: *Description of the most common magnitude types reported to the ISC.*

Magnitude type	Description	References	Comments
M	Unspecified		Often used in real or near-real time magnitude estimations
mB	Medium-period and Broad-band body-wave magnitude	*Gutenberg* (1945a); *Gutenberg* (1945b); *IASPEI* (2005); *IASPEI* (2013); *Bormann et al.* (2009); *Bormann and Dewey* (2012)	
mb	Short-period body-wave magnitude	*IASPEI* (2005); *IASPEI* (2013); *Bormann et al.* (2009); *Bormann and Dewey* (2012)	Classical mb based on stations between 21°-100° distance

Table 8.6: *continued*

Magnitude type	Description	References	Comments
mb1	Short-period body-wave magnitude	*IDC* (1999) and references therein	Reported only by the IDC; also includes stations at distances less than 21°
mb1mx	Maximum likelihood short-period body-wave magnitude	*Ringdal* (1976); *IDC* (1999) and references therein	Reported only by the IDC
mbtmp	short-period body-wave magnitude with depth fixed at the surface	*IDC* (1999) and references therein	Reported only by the IDC
mbLg	Lg-wave magnitude	*Nuttli* (1973); *IASPEI* (2005); *IASPEI* (2013); *Bormann and Dewey* (2012)	Also reported as MN
Mc	Coda magnitude		
MD (Md)	Duration magnitude	*Bisztricsany* (1958); *Lee et al.* (1972)	
ME (Me)	Energy magnitude	*Choy and Boatwright* (1995)	Reported only by NEIC
MJMA	JMA magnitude	*Tsuboi* (1954)	Reported only by JMA
ML (Ml)	Local (Richter) magnitude	*Richter* (1935); *Hutton and Boore* (1987); *IASPEI* (2005); *IASPEI* (2013)	
MLSn	Local magnitude calculated for Sn phases	*Balfour et al.* (2008)	Reported by PGC only for earthquakes west of the Cascadia subduction zone
MLv	Local (Richter) magnitude computed from the vertical component		Reported only by DJA and BKK
MN (Mn)	Lg-wave magnitude	*Nuttli* (1973); *IASPEI* (2005)	Also reported as mbLg
MS (Ms)	Surface-wave magnitude	*Gutenberg* (1945c); *Vaněk et al.* (1962); *IASPEI* (2005)	Classical surface-wave magnitude computed from station between 20°-160° distance
Ms1	Surface-wave magnitude	*IDC* (1999) and references therein	Reported only by the IDC; also includes stations at distances less than 20°
ms1mx	Maximum likelihood surface-wave magnitude	*Ringdal* (1976); *IDC* (1999) and references therein	Reported only by the IDC

Table 8.6: *continued*

Magnitude type	Description	References	Comments
Ms7	Surface-wave magnitude	*Bormann et al.* (2007)	Reported only by BJI and computed from records of a Chinese-made long-period seismograph in the distance range 3°-177°
MW (Mw)	Moment magnitude	*Kanamori* (1977); *Dziewonski et al.* (1981)	Computed according to the *IASPEI* (2005) and *IASPEI* (2013) standard formula
Mw(mB)	Proxy Mw based on mB	*Bormann and Saul* (2008)	Reported only by DJA and BKK
Mwp	Moment magnitude from P-waves	*Tsuboi et al.* (1995)	Reported only by DJA and BKK and used in rapid response
mbh	Unknown		
mbv	Unknown		
MG	Unspecified type		Contact contributor
Mm	Unknown		
msh	Unknown		
MSV	Unknown		

Table 8.7 lists all magnitude types reported, the corresponding number of events in the ISC Bulletin and the agency codes along with the number of earthquakes.

Table 8.7: *Summary of magnitude types in the ISC Bulletin for this summary period. The number of events with values for each magnitude type is listed. The agencies reporting these magnitude types are listed, together with the total number of values reported.*

Magnitude type	Events	Agencies reporting magnitude type (number of values)
M	7156	WEL (7020), RSPR (105), PRU (28), KRSZO (2), FDF (1)
mB	2065	BJI (1419), DJA (779), WEL (204), JSO (1), STR (1)
mb	25705	IDC (16802), NEIC (6973), NNC (4498), KRNET (4280), MOS (1530), BJI (1398), DJA (1225), VIE (1053), MAN (588), VAO (429), NOU (379), BGR (320), MDD (215), OMAN (45), NDI (45), SIGU (34), IASPEI (32), CFUSG (21), STR (18), DNK (15), DSN (10), PGC (5), GII (4), CRAAG (2), BGS (1), INET (1), YARS (1), DMN (1), MCSM (1), JSO (1)
MB	4	IPEC (4)
mb1	17675	IDC (17675)
mb1mx	17675	IDC (17675)
mB_BB	16	BGR (16)
mb_Lg	1737	NEIC (1707), TEH (28), OTT (3), OGSO (2), MDD (1)
mbLg	2450	MDD (2450)
mbR	156	VAO (156)

Table 8.7: *Continued.*

Magnitude type	Events	Agencies reporting magnitude type (number of values)
mbtmp	17675	IDC (17675)
Mc	8	OSPL (4), DNK (3), BER (1)
MD	12821	MEX (5324), LDG (1976), TRN (1158), RSPR (915), ECX (737), ROM (677), GCG (448), TIR (308), GRAL (242), SOF (223), HLW (190), GII (151), SSNC (144), PDG (136), EAF (104), JSN (74), SNET (57), SLM (46), SJA (45), INMG (39), TUN (33), CFUSG (26), BUT (25), SEA (24), BUG (24), PNSN (24), NDI (19), UPA (17), INET (16), DDA (16), UCR (16), NCEDC (12), HVO (11), ISK (7), LSZ (7), BUL (6), NIC (3), IGQ (2), DJA (2), UUSS (2)
MJMA	56042	JMA (56042)
ML	103399	TAP (20646), ATH (11608), IDC (9870), DDA (8859), ISK (8654), ROM (7624), RSNC (6671), HEL (5933), WEL (5879), THE (4527), UPP (3583), GUC (2547), LDG (2209), VIE (2081), NEIC (1835), AEIC (1819), BER (1763), TUL (1497), BEO (1290), PGC (1182), BUC (1149), DNK (1147), LJU (1123), ANF (1084), RHSSO (1036), SNET (1033), INMG (887), PRE (777), ECX (744), NIC (663), KRSC (614), GEN (613), MAN (594), TEH (568), IPEC (485), NAO (446), NDI (412), IGIL (395), MRB (374), SFS (347), CRAAG (346), THR (322), PDG (313), ISN (296), OSPL (276), TIR (263), SJA (262), DMN (227), OMAN (222), BJI (214), LVSN (214), REN (214), HVO (198), HLW (178), KISR (175), KRSZO (172), UCR (166), SEA (151), INET (149), SSNC (146), KOLA (137), DSN (136), BGS (135), BGR (134), KNET (129), MIRAS (98), AZER (82), DRS (80), UCC (75), PPT (66), ARE (61), ECGS (53), PAS (52), BUT (50), NOU (43), BNS (38), OTT (37), UPA (35), NCEDC (33), UUSS (30), SCB (25), BUG (24), SGS (21), CUPWA (17), MOS (15), FIA0 (12), SSS (6), VAO (5), RISSC (3), ALG (2), LDO (2), IGQ (2), PDA (2), JMA (2), CSEM (2), CLL (1), CASC (1), SOF (1), PLV (1), YARS (1), TIF (1), OGSO (1), MCSM (1), SKO (1)
MLh	441	ZUR (333), ASRS (108)
MLSn	489	PGC (489)
MLv	11349	WEL (7038), DJA (2618), NOU (1123), STR (914), MCSM (7), KRSZO (2), ASRS (1), JSO (1)
Mm	289	GII (289)
MN	256	OTT (256)
mpv	4776	NNC (4776)
MPVA	234	MOS (183), NORS (179)
MS	9286	IDC (7846), MAN (1507), BJI (1101), MOS (389), BGR (143), NSSP (79), SOME (27), OMAN (23), VIE (14), IASPEI (6), DNK (6), BER (4), IPEC (4), IGIL (2), NDI (2), RSNC (1), BGS (1), PPT (1), DRS (1), DSN (1), LDG (1), YARS (1)
Ms1	7846	IDC (7846)
ms1mx	7846	IDC (7846)

Table 8.7: *Continued.*

Magnitude type	Events	Agencies reporting magnitude type (number of values)
Ms7	1085	BJI (1085)
Ms_20	188	NEIC (188)
MW	4755	GCMT (1081), INET (918), NIED (674), UPA (536), PGC (517), RSNC (321), UCR (281), SJA (262), DDA (238), FUNV (187), SSNC (125), MED_RCMT (83), WEL (49), ASIES (30), GUC (28), ROM (15), IEC (13), DJA (13), SNET (7), THE (7), UPSL (2), GFZ (1), JSO (1)
Mw(mB)	208	WEL (206), STR (1), JSO (1)
Mwb	214	NEIC (214)
Mwc	230	GCMT (230), NEIC (45)
MwMwp	1	JSO (1)
Mwp	138	DJA (127), OMAN (11)
Mwr	335	NEIC (251), SLM (36), NCEDC (20), CAR (10), OTT (10), UCR (7), GUC (6), PAS (5), RSNC (2)
Mww	203	NEIC (203)

The most commonly reported magnitude types are short-period body-wave, surface-wave, local (or Richter), moment, duration and JMA magnitude type. For a given earthquake, the number and type of reported magnitudes greatly vary depending on its size and location. The large earthquake of October 25, 2010 gives an example of the multitude of reported magnitude types for large earthquakes (Listing 8.1). Different magnitude estimates come from global monitoring agencies such as the IDC, NEIC and GCMT, a local agency (GUC) and other agencies, such as MOS and BJI, providing estimates based on the analysis of their networks. The same agency may report different magnitude types as well as several estimates of the same magnitude type, such as NEIC estimates of Mw obtained from W-phase, centroid and body-wave inversions.

Listing 8.1: *Example of reported magnitudes for a large event*

```
Event   15264887 Southern Sumatera
   Date        Time        Err   RMS Latitude Longitude  Smaj  Smin  Az Depth   Err Ndef Nsta Gap  mdist  Mdist Qual   Author      OrigID
2010/10/25 14:42:22.18   0.27 1.813  -3.5248  100.1042 4.045 3.327  54  20.0  1.37 2102 2149  23   0.76 176.43 m i de ISC       01346132
 (#PRIME)

Magnitude  Err Nsta Author      OrigID
mb      6.1       61 BJI      15548963
mB      6.9       68 BJI      15548963
Ms      7.7       85 BJI      15548963
Ms7     7.5       86 BJI      15548963
mb      5.3 0.1   48 IDC      16686694
mb1     5.3 0.1   51 IDC      16686694
mb1mx   5.3 0.0   52 IDC      16686694
mbtmp   5.3 0.1   51 IDC      16686694
ML      5.1 0.2    2 IDC      16686694
MS      7.1 0.0   31 IDC      16686694
Ms1     7.1 0.0   31 IDC      16686694
ms1mx   6.9 0.1   44 IDC      16686694
mb      6.1      243 ISCJB    01677901
MS      7.3      228 ISCJB    01677901
M       7.1      117 DJA      01268475
mb      6.1 0.2  115 DJA      01268475
mB      7.1 0.1  117 DJA      01268475
MLv     7.0 0.2   26 DJA      01268475
        7.1 0.4  117 DJA      01268475
Mwp     6.9 0.2  102 DJA      01268475
mb      6.4       49 MOS      16742129
MS      7.2       70 MOS      16742129
mb      6.5      110 NEIC     01288303
ME      7.3          NEIC     01288303
MS      7.3      143 NEIC     01288303
MW      7.7          NEIC     01288303
MW      7.8      130 GCMT     00125427
mb      5.9          KLM      00255772
ML      6.7          KLM      00255772
MS      7.6          KLM      00255772
mb      6.4       20 BGR      16815854
Ms      7.2        2 BGR      16815854
mb      6.3 0.3  250 ISC      01346132
MS      7.3 0.1  237 ISC      01346132
```

An example of a relatively small earthquake that occurred in northern Italy for which we received magnitude reports of mostly local and duration type from six agencies in Italy, France and Austria is given in Listing 8.2.

Listing 8.2: *Example of reported magnitudes for a small event*

```
Event 15089710 Northern Italy
   Date         Time         Err   RMS Latitude Longitude  Smaj  Smin  Az Depth   Err Ndef Nsta Gap  mdist  Mdist Qual   Author      OrigID
2010/08/08 15:20:46.22   0.94 0.778  45.4846    8.3212 2.900 2.539 110  28.6  9.22  172  110  82   0.41   5.35 m i ke ISC        01249414
 (#PRIME)

Magnitude  Err Nsta Author      OrigID
ML      2.4       10 ZUR       15925566
Md      2.6 0.2   19 ROM       16861451
Ml      2.2 0.2    9 ROM       16861451
ML      2.5          GEN       00554757
ML      2.6 0.3   28 CSEM      00554756
Md      2.3 0.0    3 LDG       14797570
Ml      2.6 0.3   32 LDG       14797570
```

Figure 8.11 shows a distribution of the number of agencies reporting magnitude estimates to the ISC according to the magnitude value. The peak of the distribution corresponds to small earthquakes where many local agencies report local and/or duration magnitudes. The number of contributing agencies rapidly decreases for earthquakes of approximately magnitude 5.5 and above, where magnitudes are mostly given by global monitoring agencies.

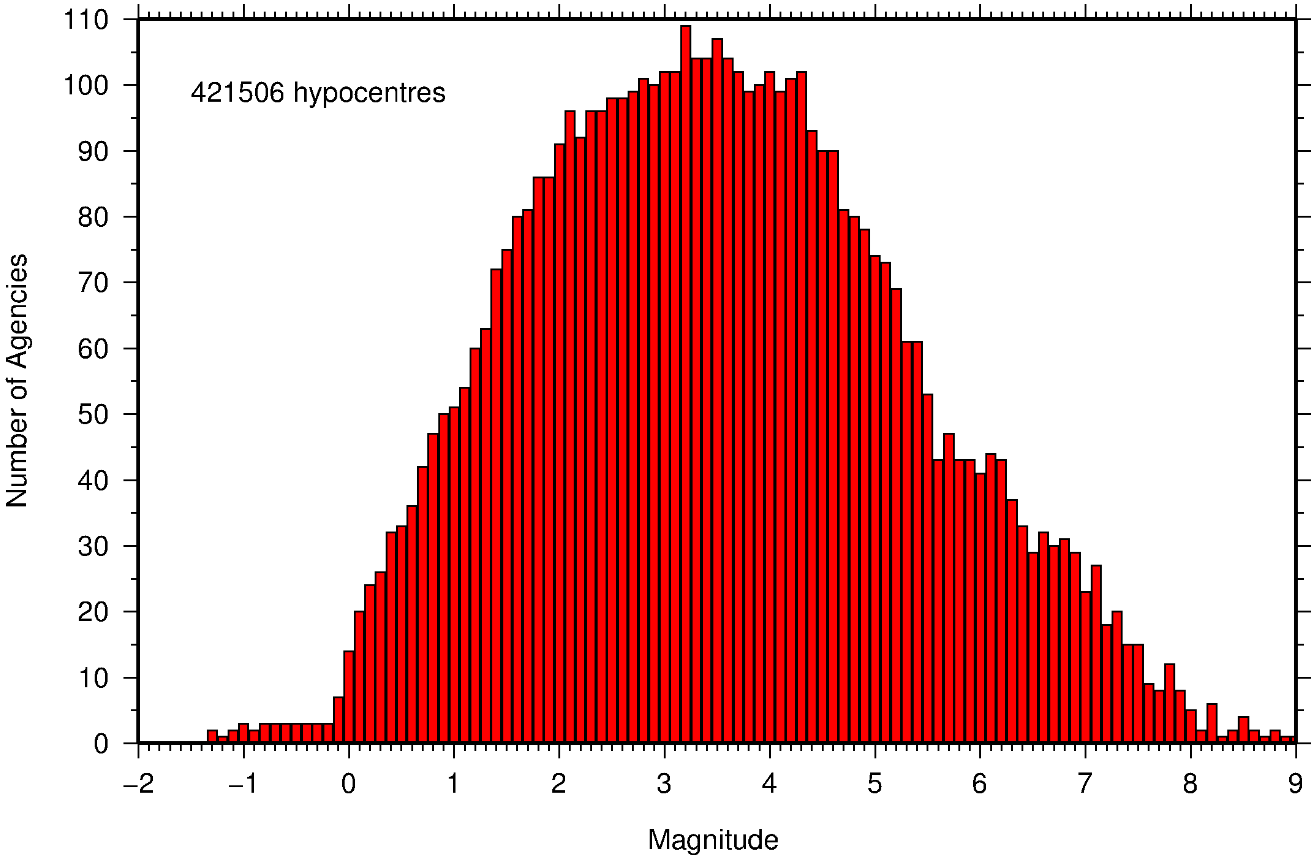

Figure 8.11: *Histogram showing the number of agencies that reported network magnitude values. All magnitude types are included.*

8.6 Moment Tensor Solutions

The ISC Bulletin publishes moment tensor solutions, which are reported to the ISC by other agencies. The collection of moment tensor solutions is summarised in Table 8.8. A histogram showing all moment tensor solutions collected throughout the ISC history is shown in Figure 8.12. Several moment tensor solutions from different authors and different moment tensor solutions calculated by different methods from the same agency may be present for the same event.

Table 8.8: *Summary of reports containing moment tensor solutions.*

Reports with Moment Tensors	48
Total moment tensors received	6260
Agencies reporting moment tensors	8

The number of moment tensors for this summary period, reported by each agency, is shown in Table 8.9. The moment tensor solutions are plotted in Figure 8.13.

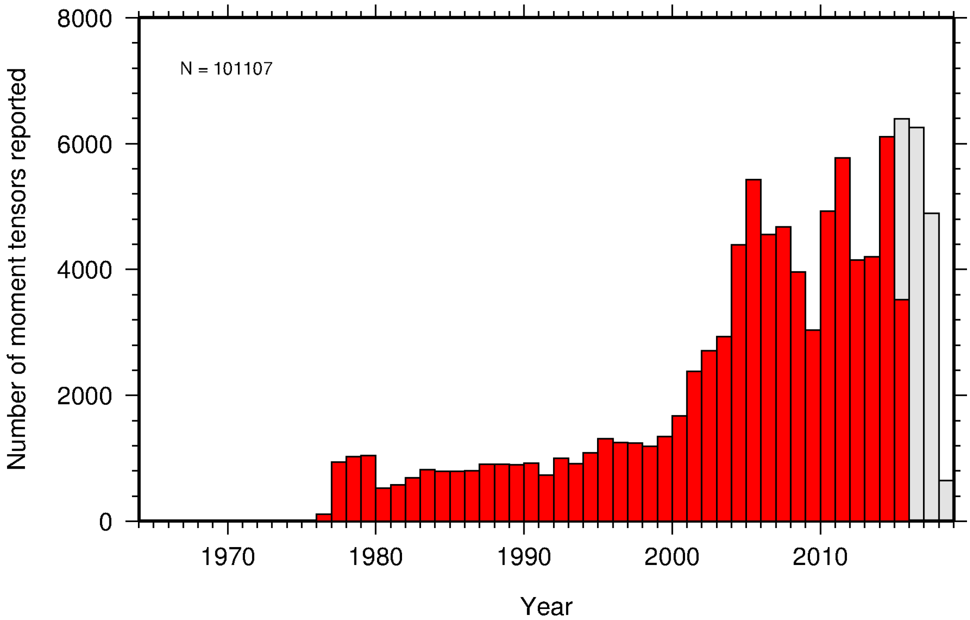

Figure 8.12: *Histogram showing the number of moment tensors reported to the ISC since 1964. The regions in grey represent data that are still being actively collected.*

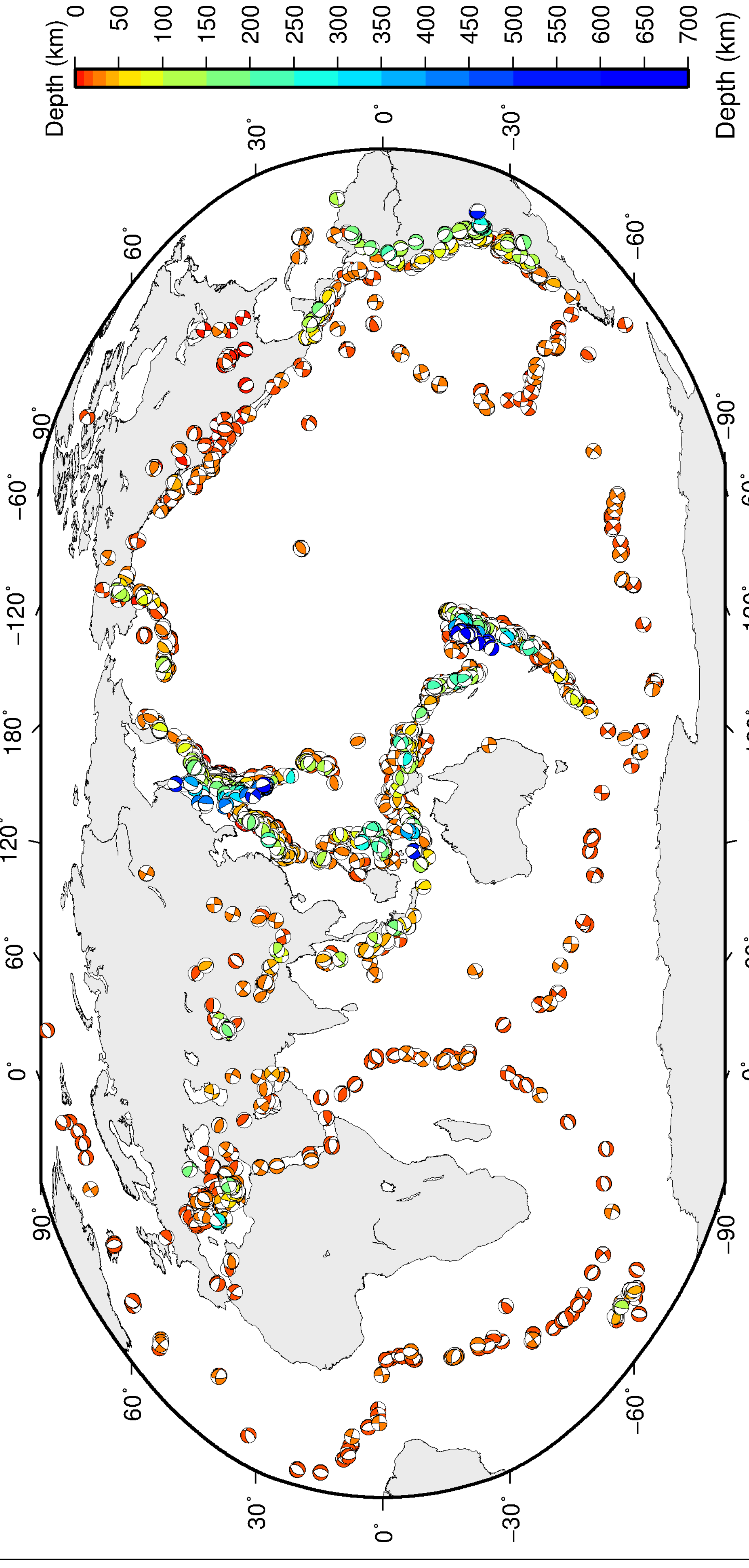

ISC Bulletin: **2995** focal mechanism solutions for **2035** events from **2015/01/01** to **2015/06/30**

Figure 8.13: *Map of all moment tensor solutions in the ISC Bulletin for this summary period.*

Agency	Number of moment tensor solutions
NEIC	1093
GCMT	1081
NIED	674
JMA	396
ISC	190
RSNC	135
MED_RCMT	83
WEL	49
ECX	42
IEC	26
PNSN	24
THE	14
ROM	13
UPA	13
UCR	12
MOS	10
SNET	6
OSPL	3
UPSL	2
JSN	2
BER	1
SJA	1

Table 8.9: *Summary of moment tensor solutions in the ISC Bulletin reported by each agency.*

8.7 Timing of Data Collection

Here we present the timing of reports to the ISC. Please note, this does not include provisional alerts, which are replaced at a later stage. Instead, it reflects the final data sent to the ISC. The absolute timing of all hypocentre reports, regardless of magnitude, is shown in Figure 8.14. In Figure 8.15 the reports are grouped into one of six categories - from within three days of an event origin time, to over one year. The histogram shows the distribution with magnitude (for hypocentres where a network magnitude was reported) for each category, whilst the map shows the geographic distribution of the reported hypocentres.

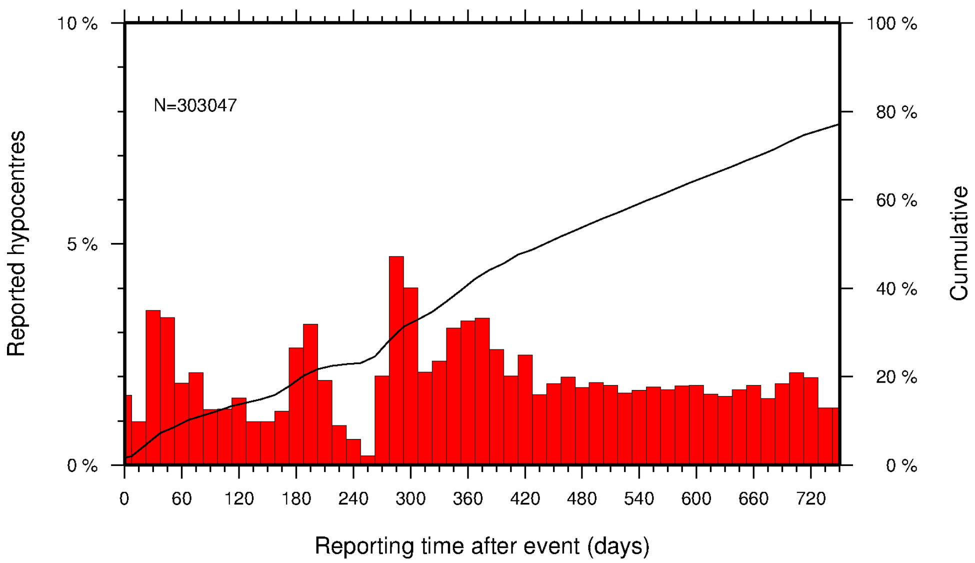

Figure 8.14: *Histogram showing the timing of final reports of the hypocentres (total of N) to the ISC. The cumulative frequency is shown by the solid line.*

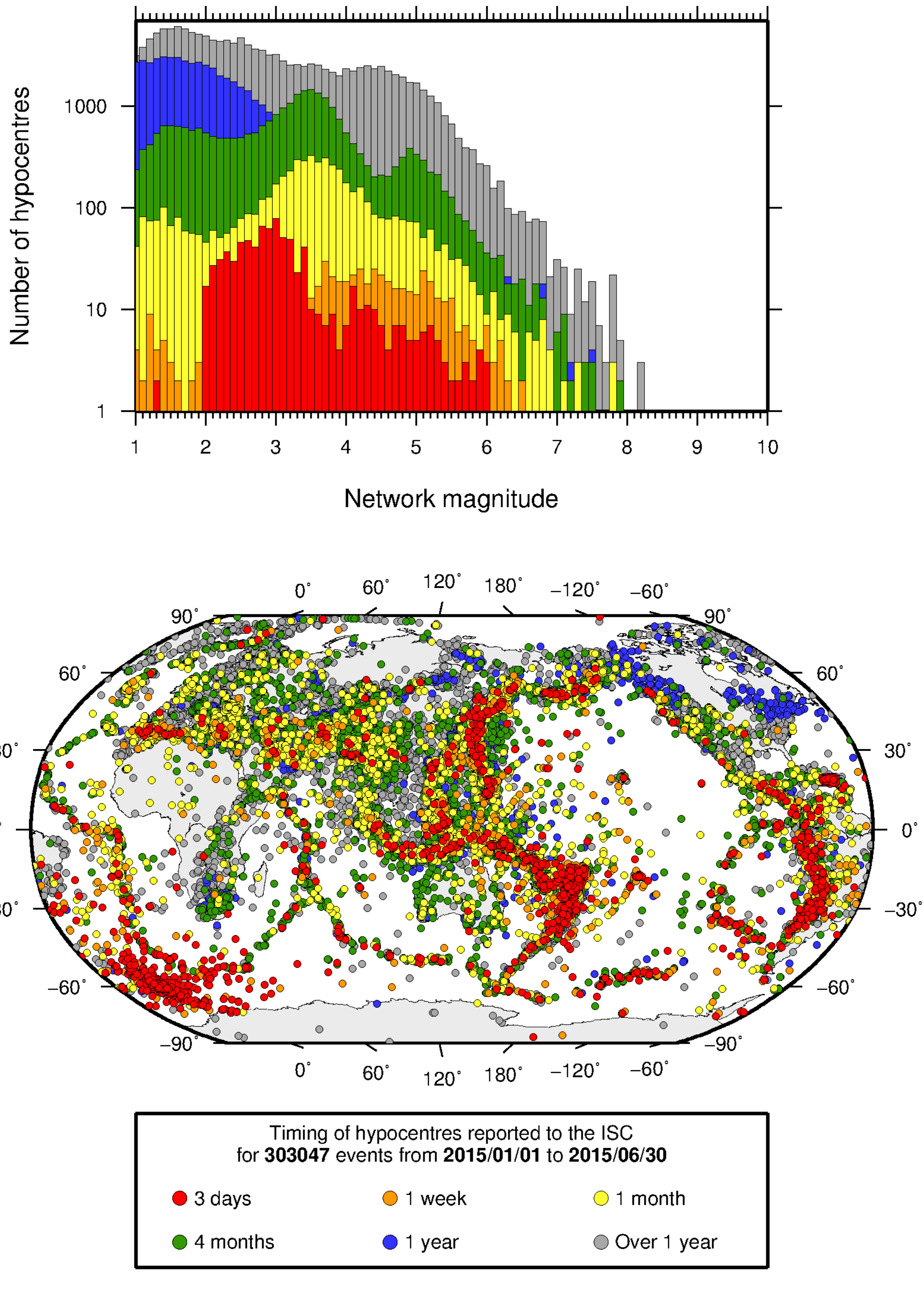

Figure 8.15: *Timing of hypocentres reported to the ISC. The colours show the time after the origin time that the corresponding hypocentre was reported. The histogram shows the distribution with magnitude. If more than one network magnitude was reported, preference was given to a value of M_W followed by M_S, m_b and M_L respectively; all reported hypocentres are included on the map. Note: early reported hypocentres are plotted over later reported hypocentres, on both the map and histogram.*

9

Overview of the ISC Bulletin

This chapter provides an overview of the seismic event data in the ISC Bulletin. We indicate the differences between all ISC events and those ISC events that are reviewed or located. We describe the wealth of phase arrivals and phase amplitudes and periods observed at seismic stations worldwide, reported in the ISC Bulletin and often used in the ISC location and magnitude determination. Finally, we make some comparisons of the ISC magnitudes with those reported by other agencies, and discuss magnitude completeness of the ISC Bulletin.

9.1 Events

The ISC Bulletin had 199277 reported events in the summary period between January and June 2015. Some 92% (183377) of the events were identified as earthquakes, the rest (15900) were of anthropogenic origin (including mining and other chemical explosions, rockbursts and induced events) or of unknown origin. As discussed in Section 11.1.3, typically about 15% of the events are selected for ISC review, and about half of the events selected for review are located by the ISC. In this summary period 12% of the events were reviewed and 8% of the events were located by the ISC. For events that are not located by the ISC, the prime hypocentre is identified according to the rules described in Section 11.1.3.

Of the 7465007 reported phase observations, 37% are associated to ISC-reviewed events, and 35% are associated to events selected for ISC location. Note that all large events are reviewed and located by the ISC. Since large events are globally recorded and thus reported by stations worldwide, they will provide the bulk of observations. This explains why only about one-fifth of the events in any given month is reviewed although the number of phases associated to reviewed events has increased nearly exponentially in the past decades.

Figure 9.1 shows the daily number of events throughout the summary period. Figure 9.2 shows the locations of the events in the ISC Bulletin; the locations of ISC-reviewed and ISC-located events are shown in Figures 9.3 and 9.4, respectively.

Figure 9.5 shows the hypocentral depth distributions of events in the ISC Bulletin for the summary period. The vast majority of events occur in the Earth's crust. Note that the peaks at 0, 10, 35 km, and at every 50 km intervals deeper than 100 km are artifacts of analyst practices of fixing the depth to a nominal value when the depth cannot be reliably resolved.

Figure 9.6 shows the depth distribution of free-depth solutions in the ISC Bulletin. The depth of a hypocentre reported to the ISC is assumed to be determined as a free parameter, unless it is explicitly labelled as a fixed-depth solution. On the other hand, as described in Section 11.1.4, the ISC locator attempts to get a free-depth solution if, and only if, there is resolution for the depth in the data, i.e. if

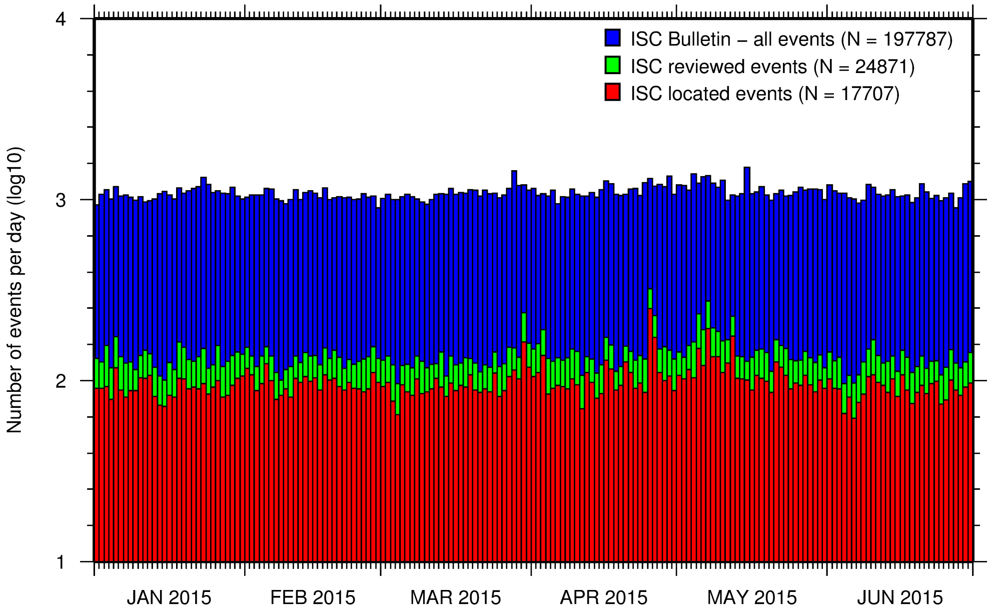

Figure 9.1: *Histogram showing the number of events in the ISC Bulletin for the current summary period. The vertical scale is logarithmic.*

there is a local network and/or sufficient depth-sensitive phases are reported.

Figure 9.7 shows the depth distribution of fixed-depth solutions in the ISC Bulletin. Except for a fraction of events whose depth is fixed to a shallow depth, this set comprises mostly ISC-located events. If there is no resolution for depth in the data, the ISC locator fixes the depth to a value obtained from the ISC default depth grid file, or if no default depth exists for that location, to a nominal default depth assigned to each Flinn-Engdahl region (see details in Section 11.1.4). During the ISC review editors are inclined to accept the depth obtained from the default depth grid, but they typically change the depth of those solutions that have a nominal (10 or 35 km) depth. When doing so, they usually fix the depth to a round number, preferably divisible by 50.

For events selected for ISC location, the number of stations typically increases as arrival data reported by several agencies are grouped together and associated to the prime hypocentre. Consequently, the network geometry, characterised by the secondary azimuthal gap (the largest azimuthal gap a single station closes), is typically improved. Figure 9.8 illustrates that the secondary azimuthal gap is indeed generally smaller for ISC-located events than that for all events in the ISC Bulletin. Figure 9.9 shows the distribution of the number of associated stations. For large events the number of associated stations is usually larger for ISC-located events than for any of the reported event bulletins. On the other hand, events with just a few reporting stations are rarely selected for ISC location. The same is true for the number of defining stations (stations with at least one defining phase that were used in the location). Figure 9.10 indicates that because the reported observations from multiple agencies are associated to the prime, large ISC-located events typically have a larger number of defining stations than any of the reported event bulletins.

The formal uncertainty estimates are also typically smaller for ISC-located events. Figure 9.11 shows the distribution of the area of the 90% confidence error ellipse for ISC-located events during the summary period. The distribution suffers from a long tail indicating a few poorly constrained event locations. Nevertheless, half of the events are characterised by an error ellipse with an area less than 220 km^2, 90%

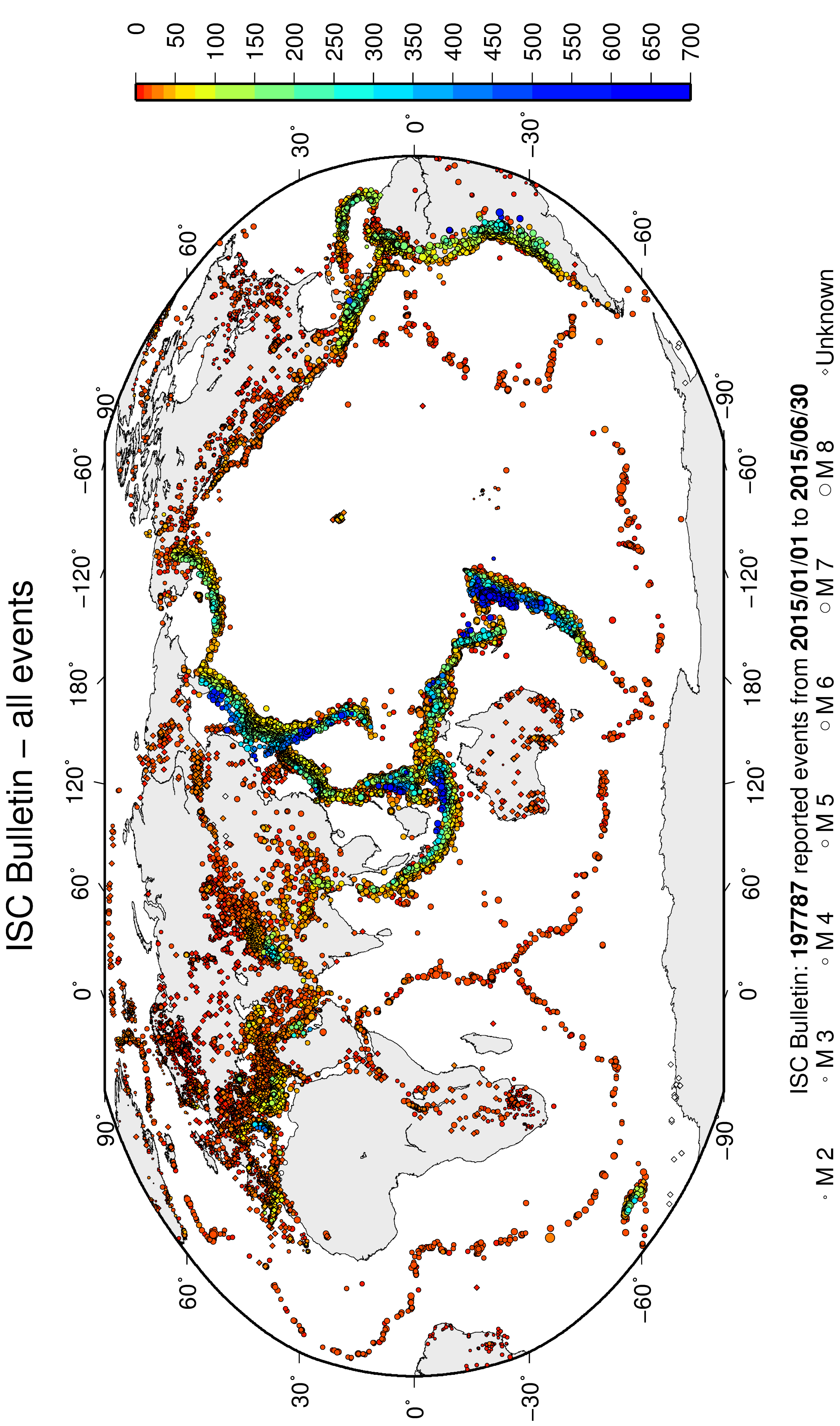

Figure 9.2: *Map of all events in the ISC Bulletin. Prime hypocentre locations are shown. Compare with Figure 8.10.*

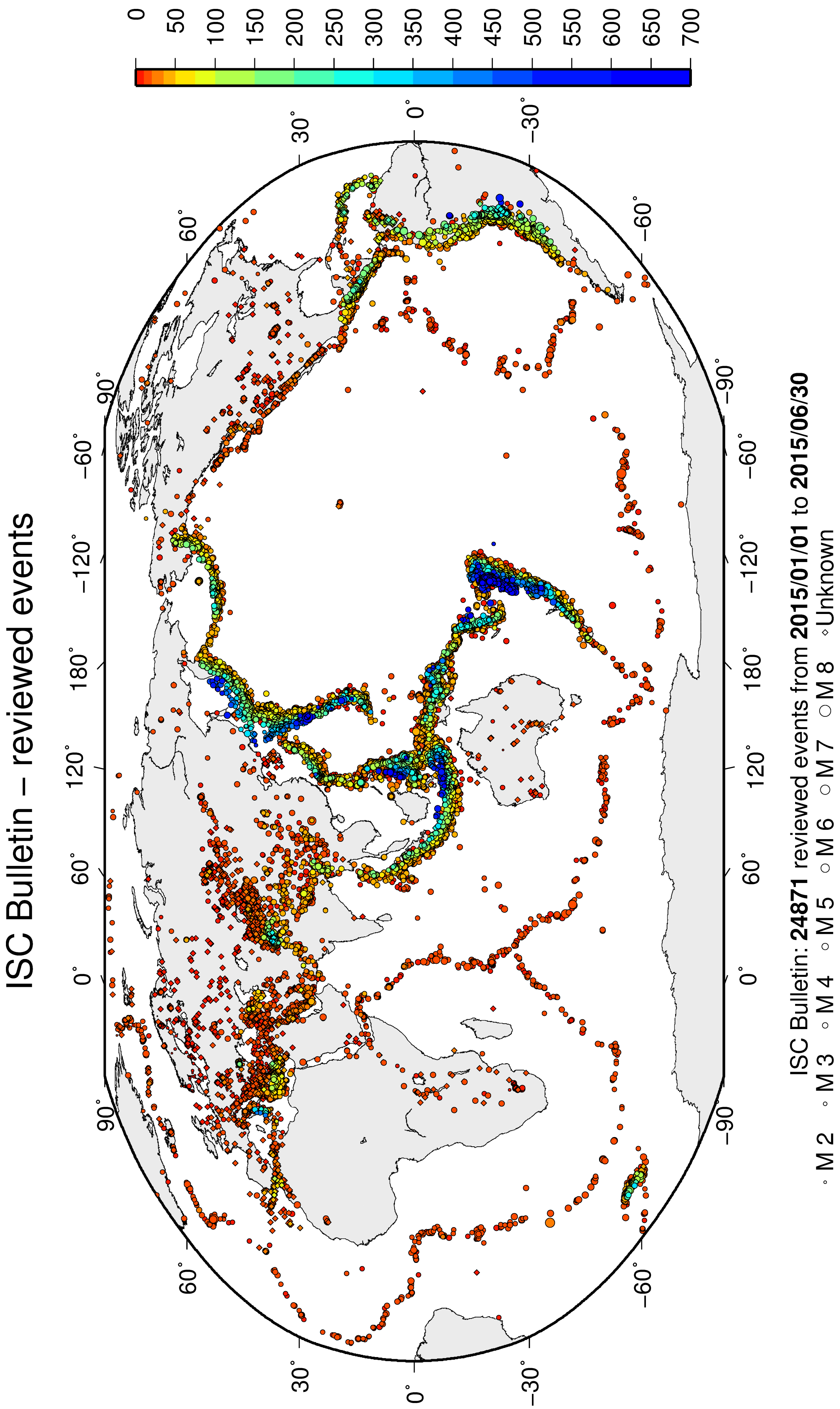

Figure 9.3: *Map of all events reviewed by the ISC for this time period. Prime hypocentre locations are shown.*

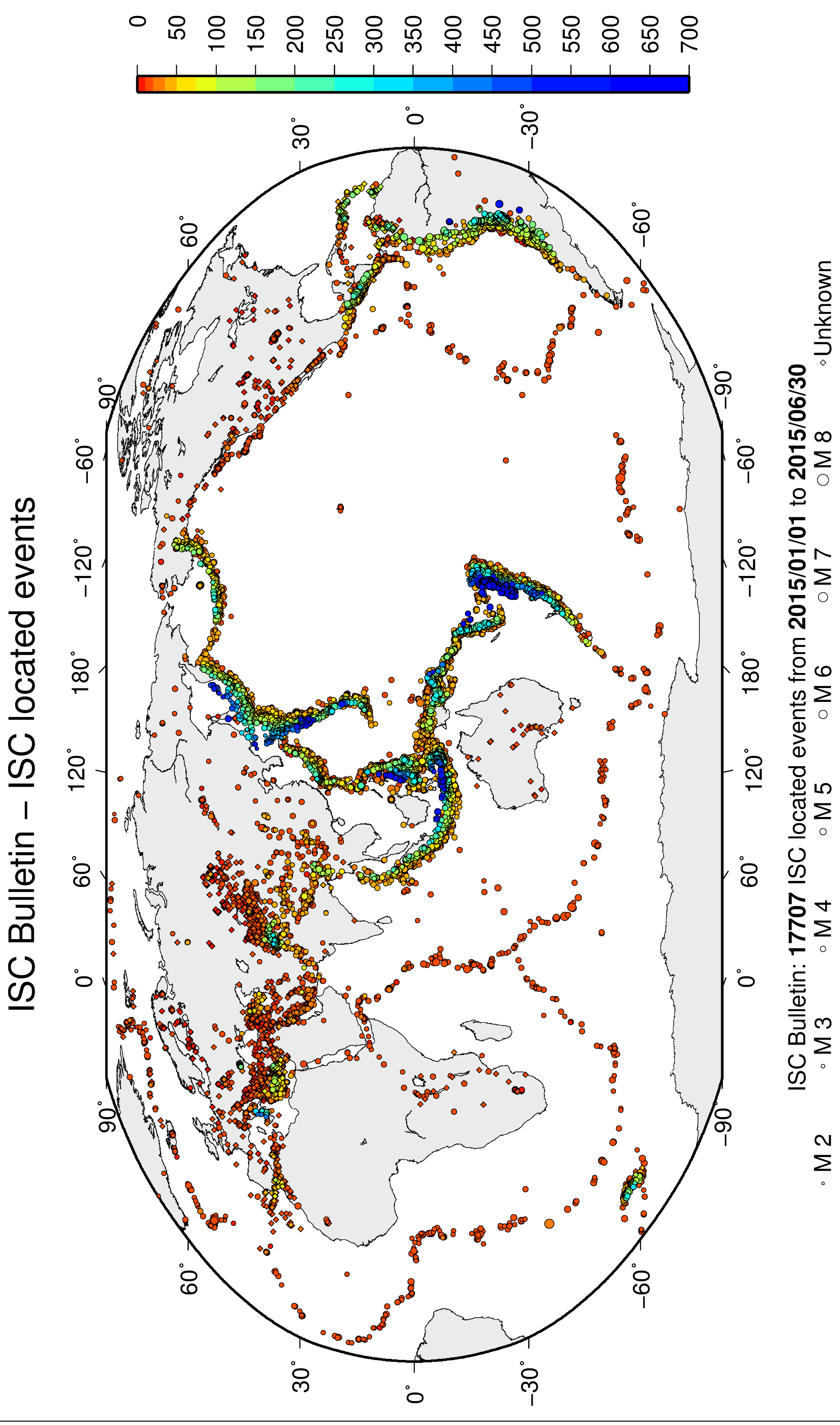

Figure 9.4: *Map of all events located by the ISC for this time period. ISC determined hypocentre locations are shown.*

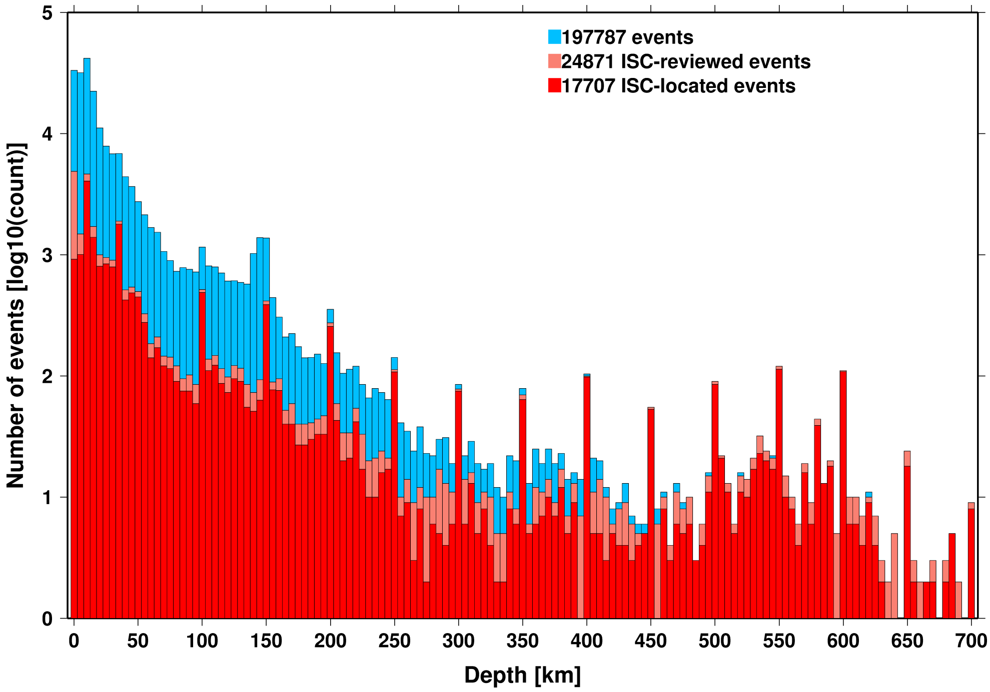

Figure 9.5: *Distribution of event depths in the ISC Bulletin (blue) and for the ISC-reviewed (pink) and the ISC-located (red) events during the summary period. All ISC-located events are reviewed, but not all reviewed events are located by the ISC. The vertical scale is logarithmic.*

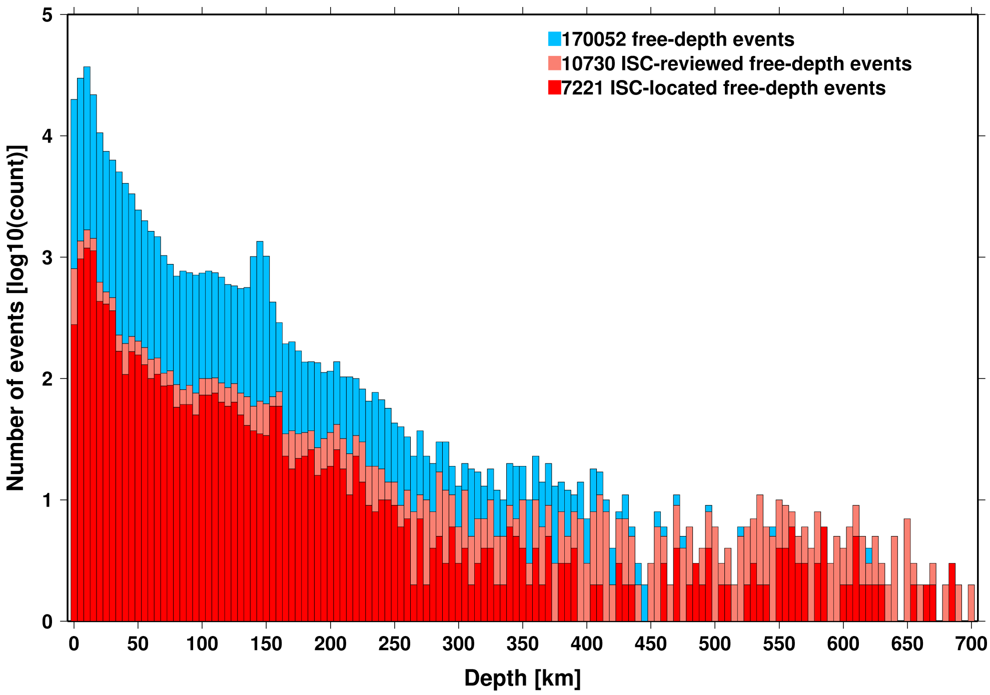

Figure 9.6: *Hypocentral depth distribution of events where the prime hypocentres are reported/located with a free-depth solution in the ISC Bulletin. The vertical scale is logarithmic.*

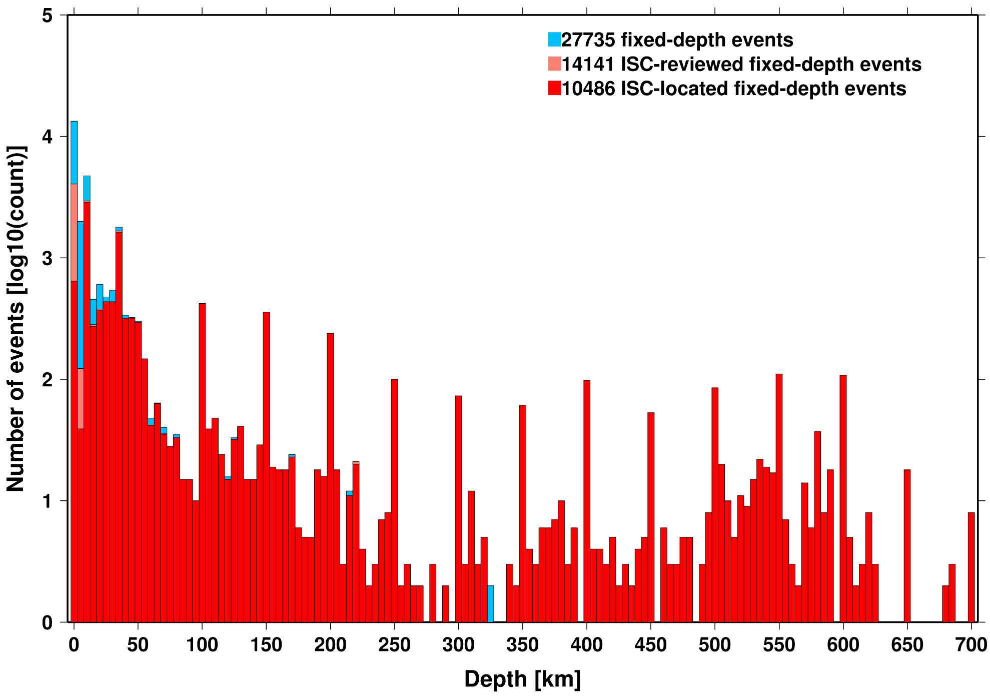

Figure 9.7: *Hypocentral depth distribution of events where the prime hypocentres are reported/located with a fixed-depth solution in the ISC Bulletin. The vertical scale is logarithmic.*

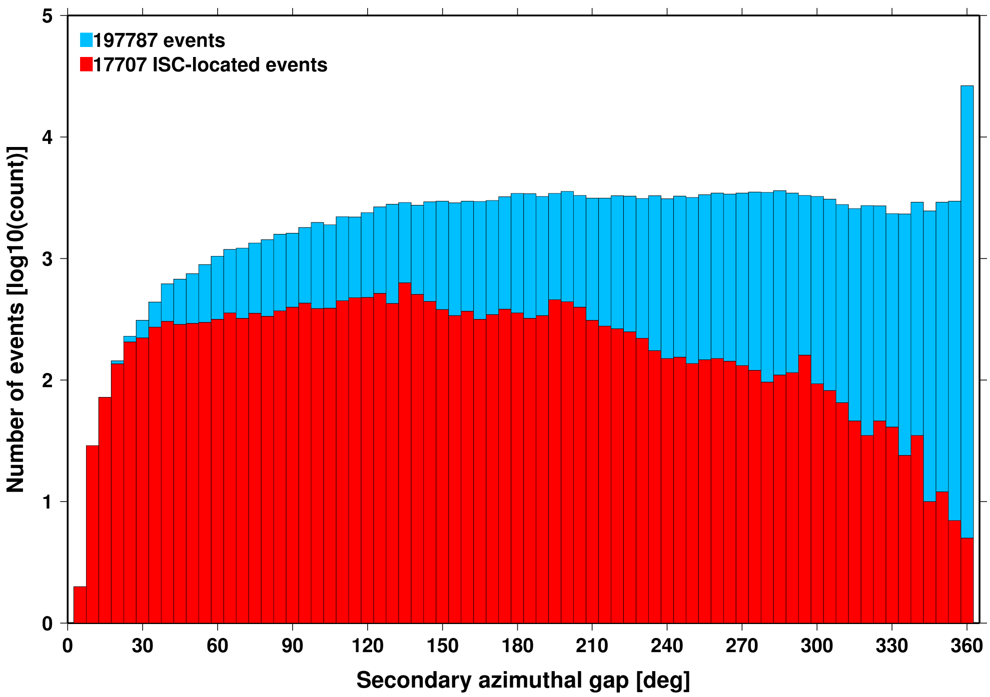

Figure 9.8: *Distribution of secondary azimuthal gap for events in the ISC Bulletin (blue) and those selected for ISC location (red). The vertical scale is logarithmic.*

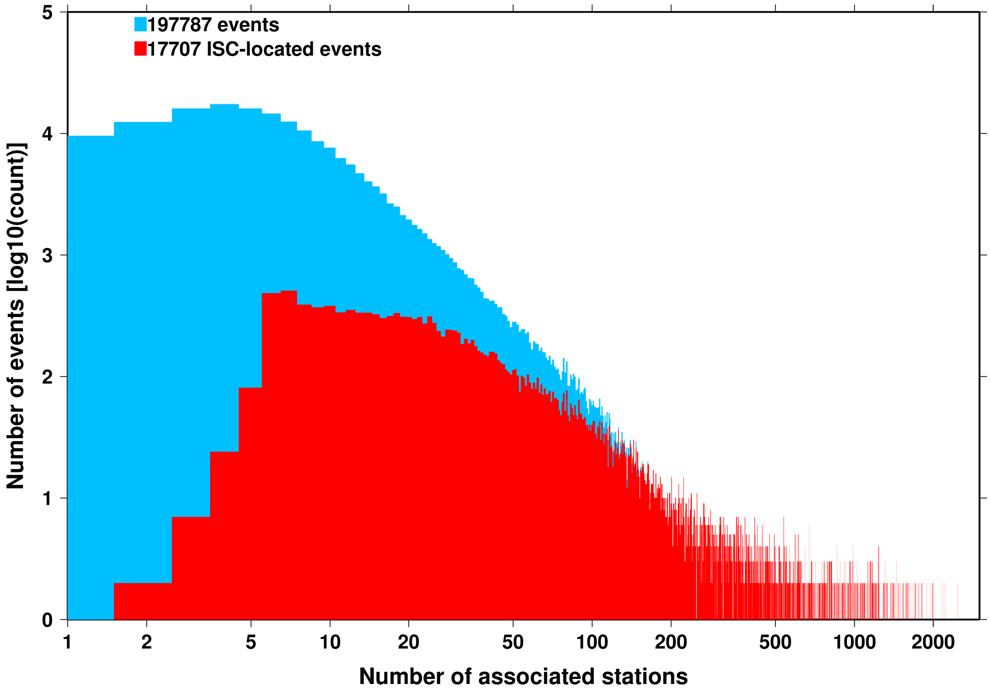

Figure 9.9: *Distribution of the number of associated stations for events in the ISC Bulletin (blue) and those selected for ISC location (red). The vertical scale is logarithmic.*

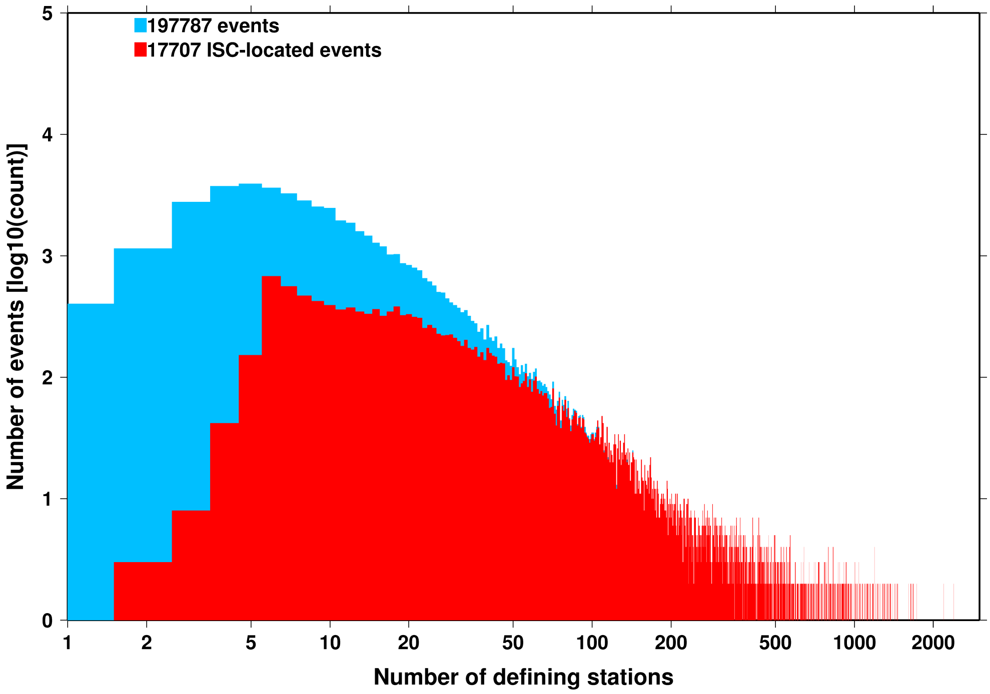

Figure 9.10: *Distribution of the number of defining stations for events in the ISC Bulletin (blue) and those selected for ISC location (red). The vertical scale is logarithmic.*

of the events have an error ellipse area less than 1597 km^2, and 95% of the events have an error ellipse area less than 2933 km^2.

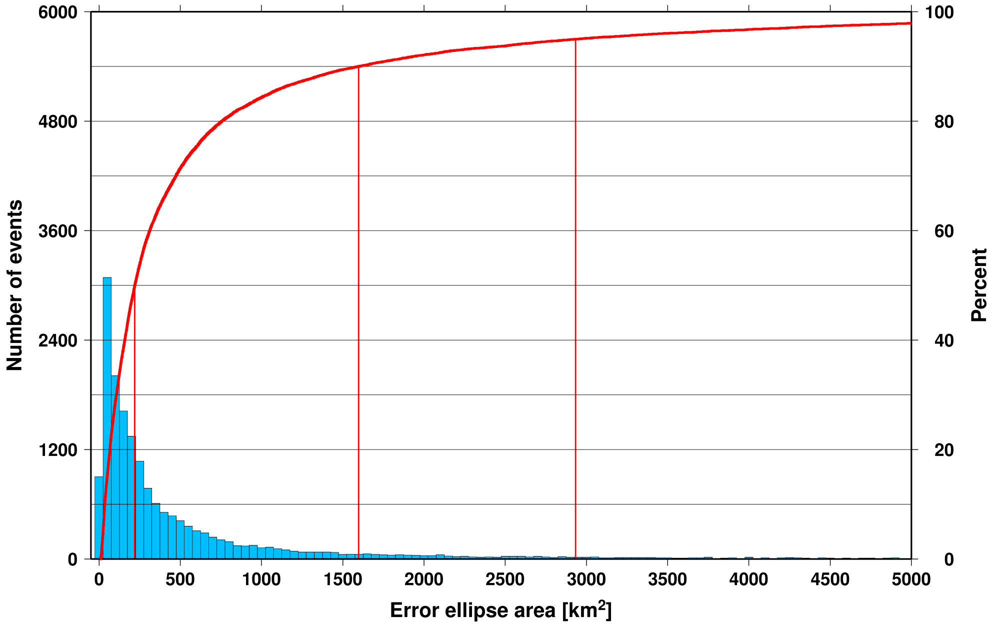

Figure 9.11: *Distribution of the area of the 90% confidence error ellipse of the ISC-located events. Vertical red lines indicate the 50th, 90th and 95th percentile values.*

Figure 9.12 shows one of the major characteristic features of the ISC location algorithm (Bondár and Storchak, 2011). Because the ISC locator accounts for correlated travel-time prediction errors due to unmodelled velocity heterogeneities along similar ray paths, the area of the 90% confidence error ellipse does not decrease indefinitely with increasing number of stations, but levels off once the information carried by the network geometry is exhausted, thus providing more realistic uncertainty estimates.

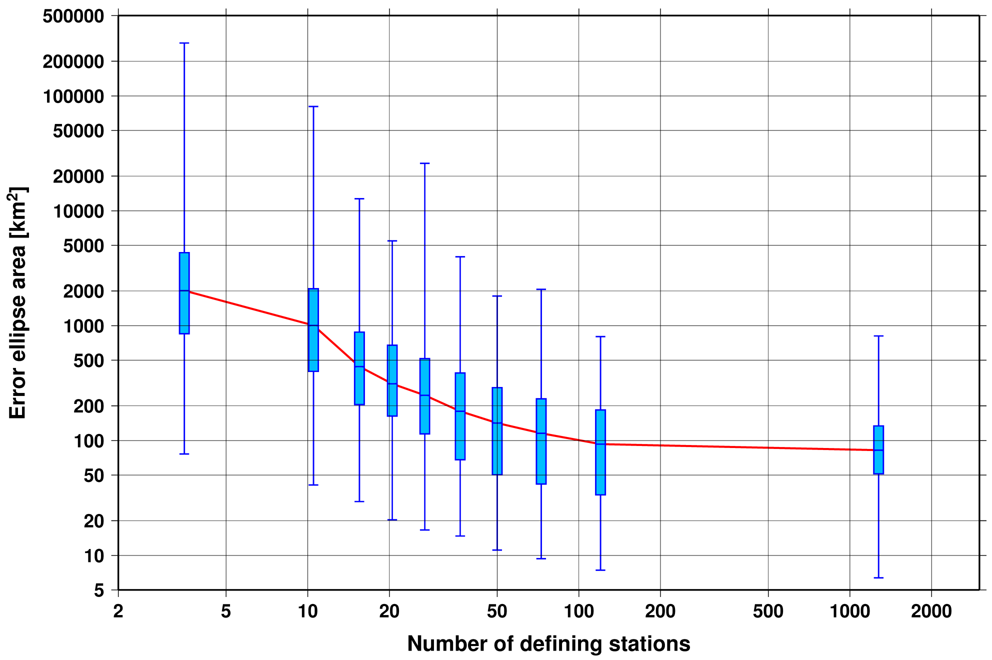

Figure 9.12: *Box-and-whisker plot of the area of the 90% confidence error ellipse of the ISC-located events as a function of the number of defining stations. Each box represents one-tenth-worth of the total number of data. The red line indicates the median 90% confidence error ellipse area.*

9.2 Seismic Phases and Travel-Time Residuals

The number of phases that are associated to events over the summary period in the ISC Bulletin is shown in Figure 9.13. Phase types and their total number in the ISC Bulletin is shown in the Appendix, Table 11.3. A summary of phase types is indicated in Figure 9.14.

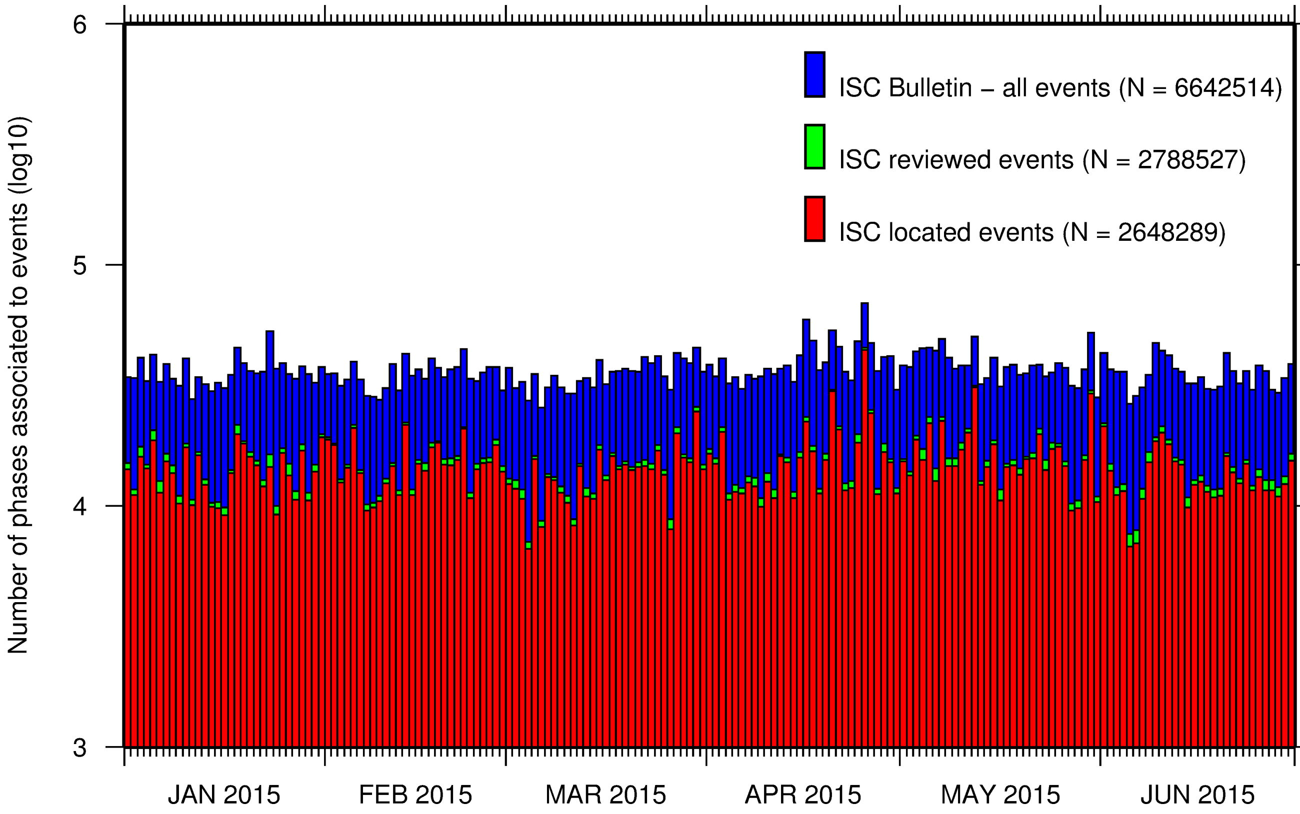

Figure 9.13: *Histogram showing the number of phases (N) that the ISC has associated to events within the ISC Bulletin for the current summary period.*

In computing ISC locations, the current (for events since 2009) ISC location algorithm (*Bondár and Storchak*, 2011) uses all *ak135* phases where possible. Within the Bulletin, the phases that contribute to an ISC location are labelled as *time defining*. In this section, we summarise these time defining phases.

In Figure 9.15, the number of defining phases is shown in a histogram over the summary period. Each defining phase is listed in Table 9.1, which also provides a summary of the number of defining phases per event. A pie chart showing the proportion of defining phases is shown in Figure 9.16. Figure 9.17 shows travel times of seismic waves. The distribution of residuals for these defining phases is shown for the top five phases in Figures 9.18 through 9.22.

Table 9.1: *Numbers of 'time defining' phases (N) within the ISC Bulletin for 17707 ISC located events.*

Phase	Number of 'defining' phases	Number of events	Max per event	Median per event
P	815706	13625	2777	14
Pn	488744	16138	820	15
Sn	149889	13523	211	5
Pb	77170	6652	121	6
Pg	58188	5338	209	6
PKPdf	54685	3807	735	2
Sb	50315	6270	99	4
Sg	45876	4957	142	6

Table 9.1: *(continued)*

Phase	Number of 'defining' phases	Number of events	Max per event	Median per event
PKiKP	36124	3352	390	2
S	33493	3381	404	3
PKPbc	23229	3619	285	2
PKPab	15788	2510	175	2
PcP	11783	3424	134	2
PP	7682	1329	113	2
pP	7575	1238	162	3
Pdif	6408	991	276	2
SS	3809	1002	59	2
ScP	3612	1147	57	2
sP	2408	796	85	2
PKKPbc	2261	427	82	2
SKSac	2252	419	91	1
pPKPdf	1168	377	55	1
pwP	1137	431	40	1
SnSn	1001	548	8	1
SKPbc	960	293	66	2
ScS	943	446	52	1
PnPn	941	542	10	1
SKiKP	624	297	57	1
sS	589	338	15	1
pPKPab	494	151	39	1
P'P'df	474	159	22	2
PKKPab	473	219	17	1
pPKPbc	462	199	23	1
PKKPdf	435	207	16	1
PS	395	189	18	1
sPKPdf	305	180	17	1
SKSdf	301	205	9	1
SKPab	264	138	16	1
SKKSac	247	135	18	1
PcS	205	178	10	1
SKKPbc	169	39	31	1
Sdif	169	54	30	1
SKPdf	168	62	15	1
PnS	148	103	9	1
SP	145	62	27	1
sPKPbc	143	90	20	1
PKSdf	136	108	5	1
sPKPab	126	53	20	1
SKKSdf	124	119	2	1
pPdif	79	31	28	1
pS	65	61	2	1
PbPb	57	43	6	1
SPn	38	15	24	1
pPKiKP	26	19	4	1
P'P'ab	21	2	13	10
SKKPdf	18	9	4	1
SbSb	16	14	2	1
P'P'bc	15	5	11	1
sPdif	11	10	2	1
SKKPab	8	8	1	1
pPn	7	3	4	2
sPKiKP	6	3	4	1
PKSbc	5	1	5	5
PKKSbc	5	1	5	5
sPn	5	4	2	1
PgPg	4	3	2	1
sSdif	4	3	2	1
sSKSac	3	2	2	2
SgSg	2	2	1	1
sPb	2	1	2	2
pPb	2	2	1	1
S'S'ac	1	1	1	1
PgS	1	1	1	1
pSKSdf	1	1	1	1
sSb	1	1	1	1

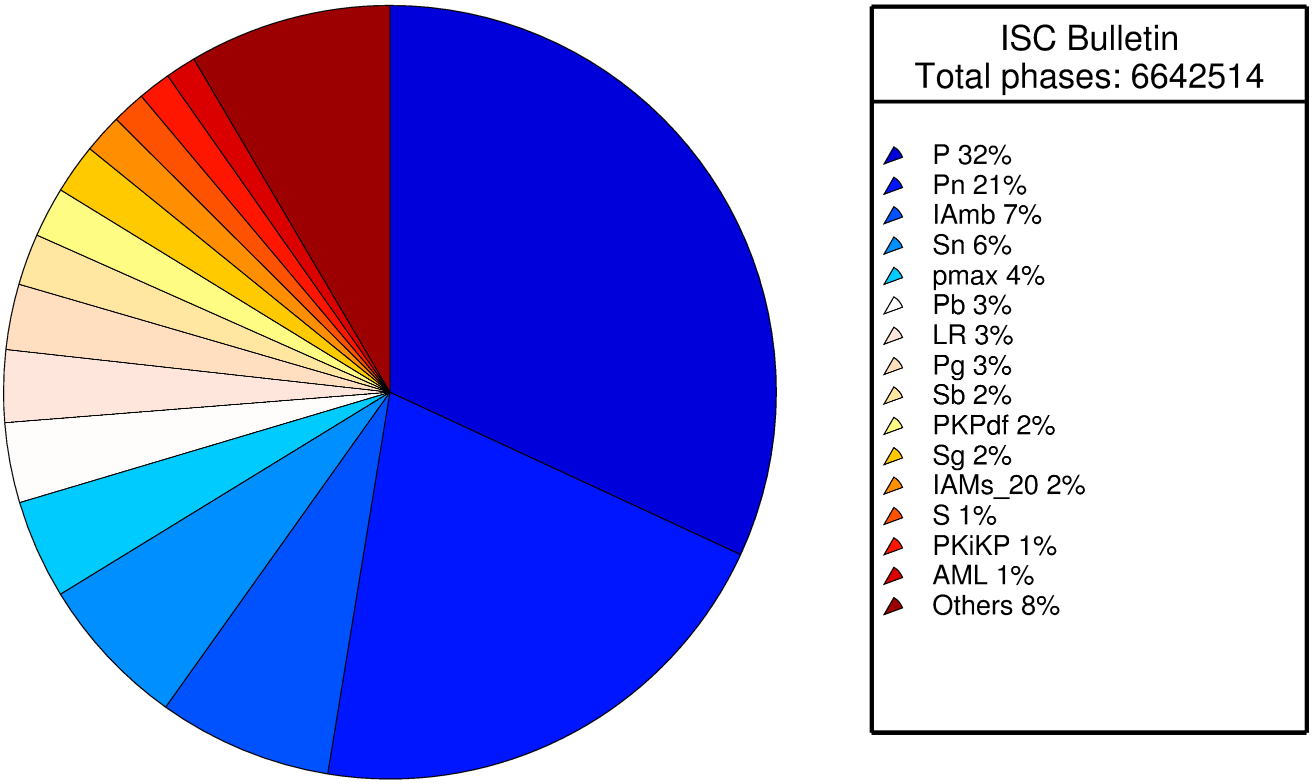

Figure 9.14: *Pie chart showing the fraction of various phase types in the ISC Bulletin for this summary period.*

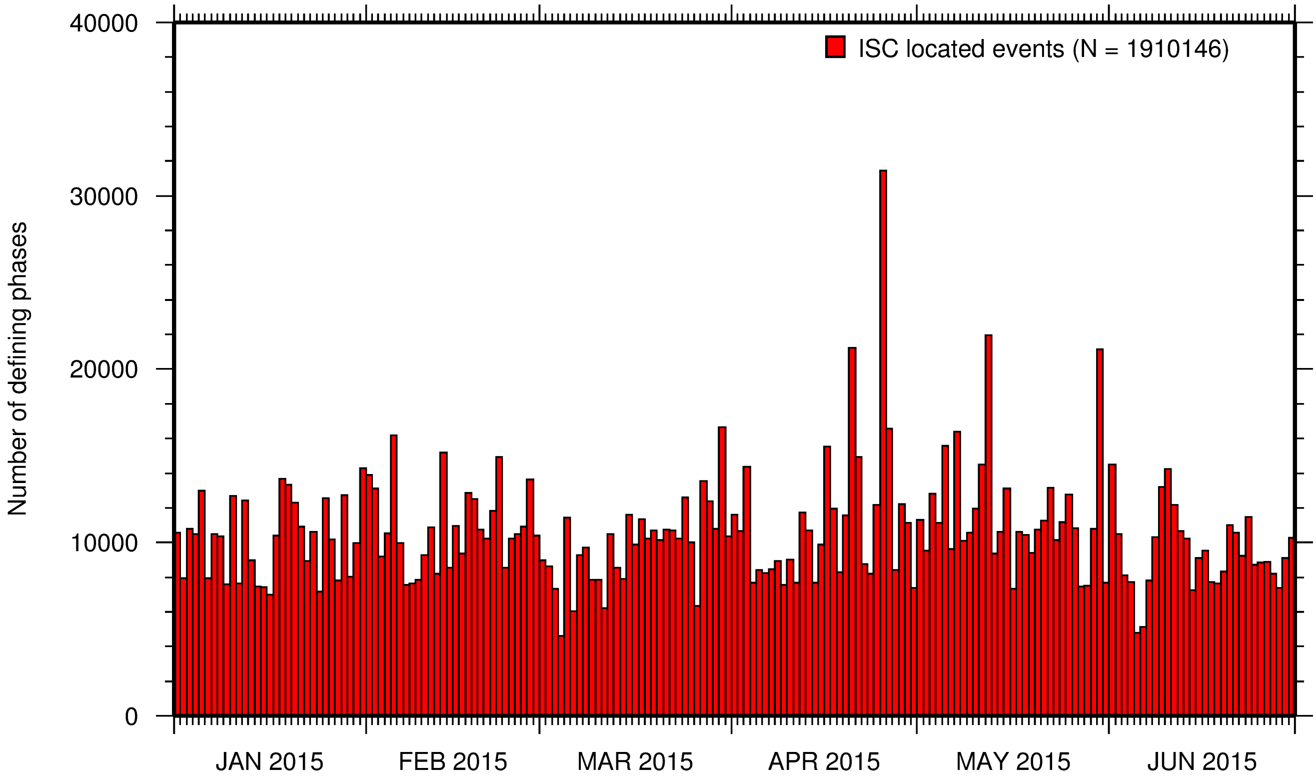

Figure 9.15: *Histogram showing the number of defining phases in the ISC Bulletin, for events located by the ISC.*

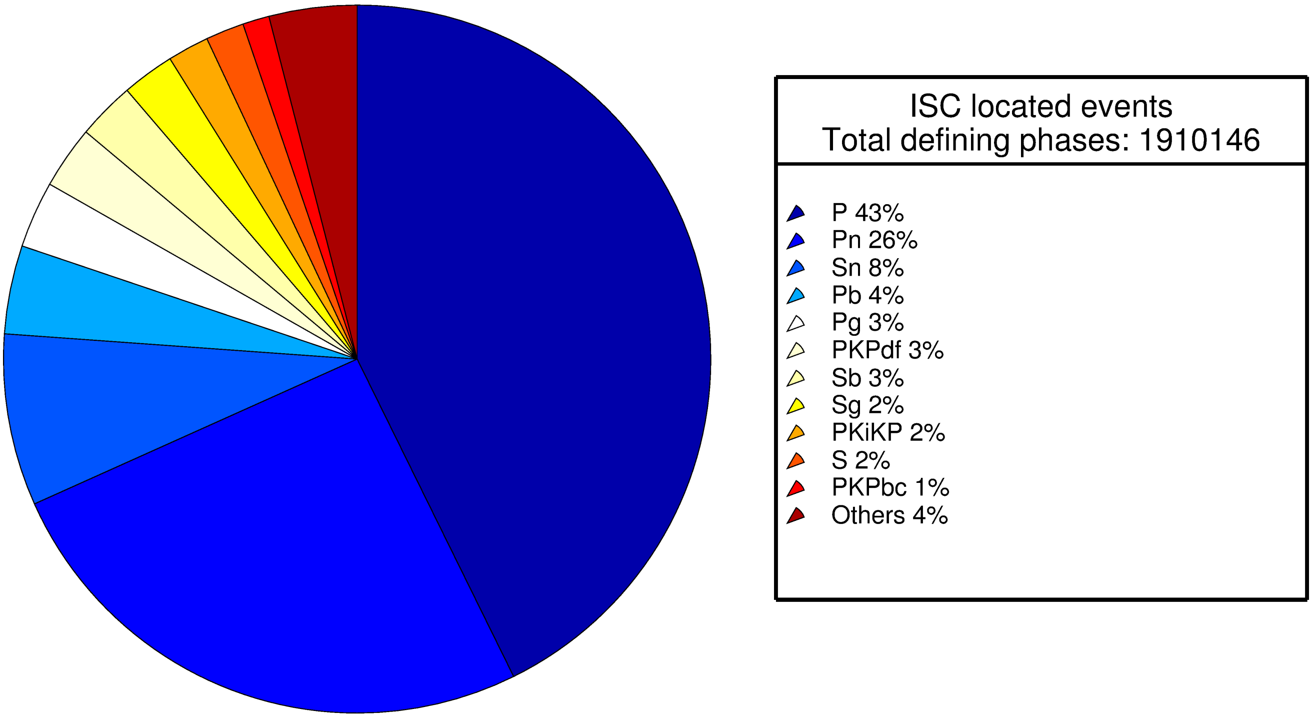

Figure 9.16: *Pie chart showing the defining phases in the ISC Bulletin, for events located by the ISC. A complete list of defining phases is shown in Table 9.1.*

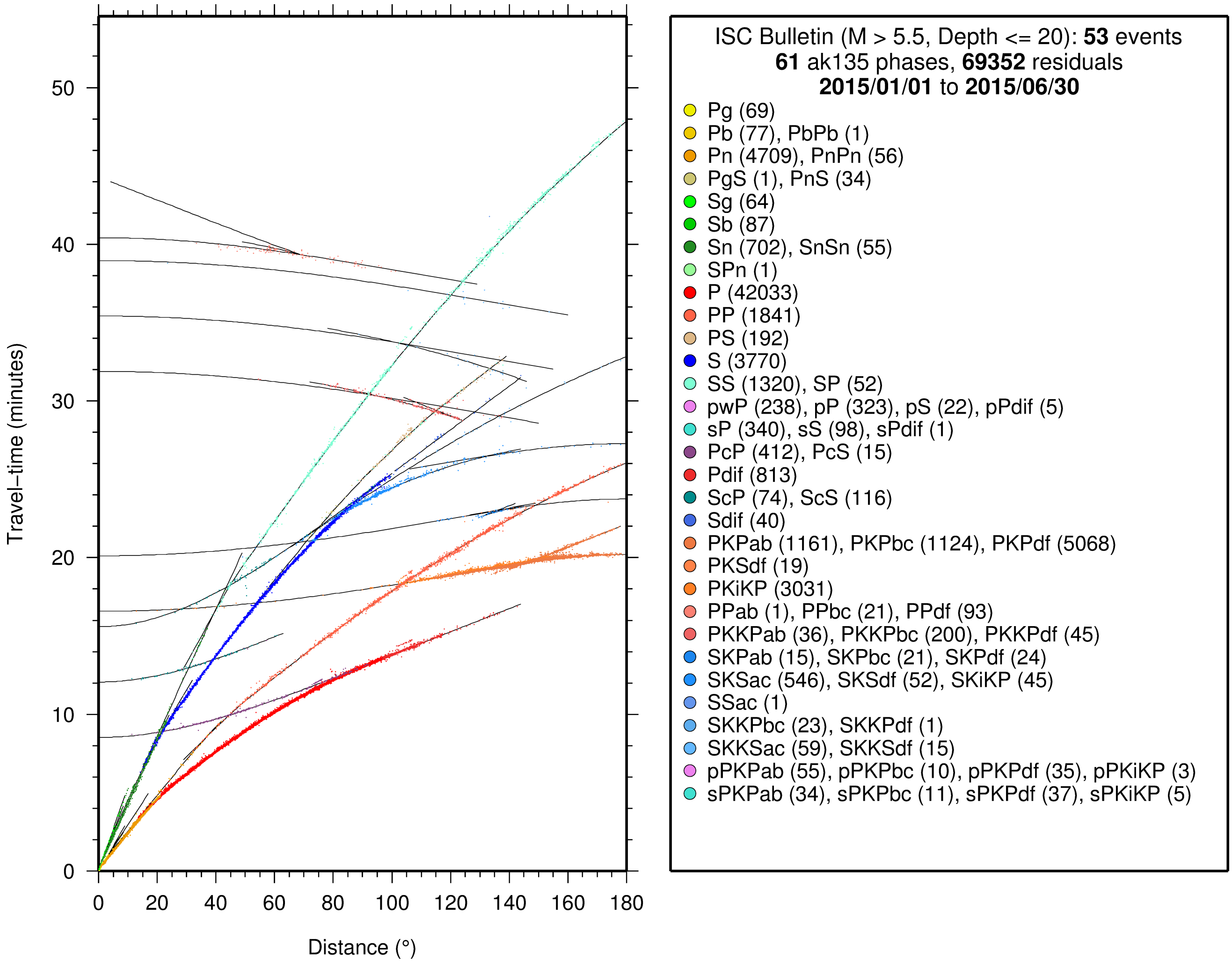

Figure 9.17: *Distribution of travel-time observations in the ISC Bulletin for events with M > 5.5 and depth less than 20 km. The travel-time observations are shown relative to a 0 km source and compared with the theoretical ak135 travel-time curves (solid lines). The legend lists the number of each phase plotted.*

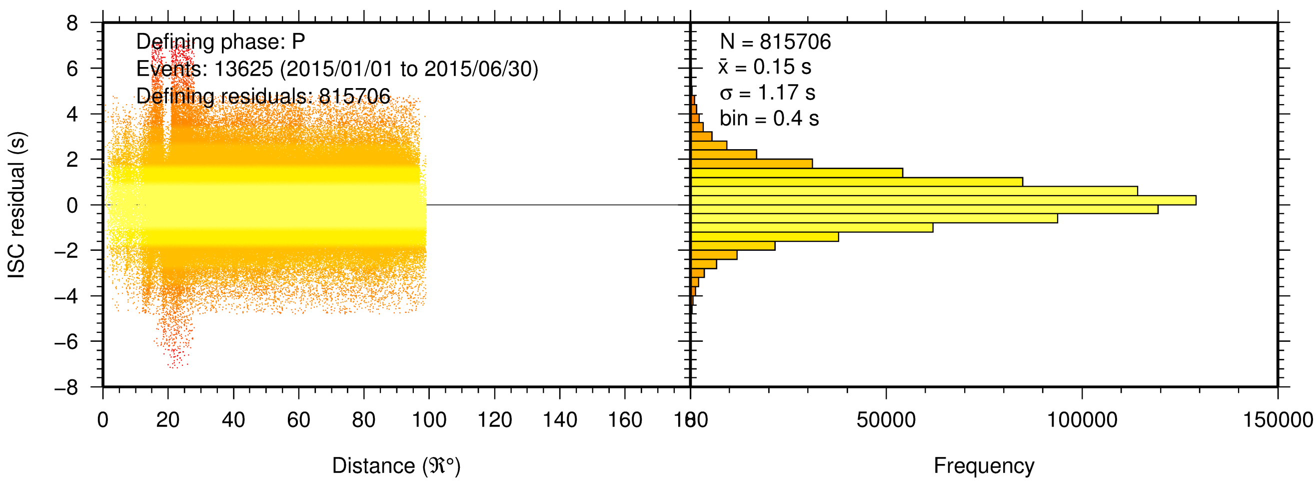

Figure 9.18: *Distribution of travel-time residuals for the defining P phases used in the computation of ISC located events in the Bulletin.*

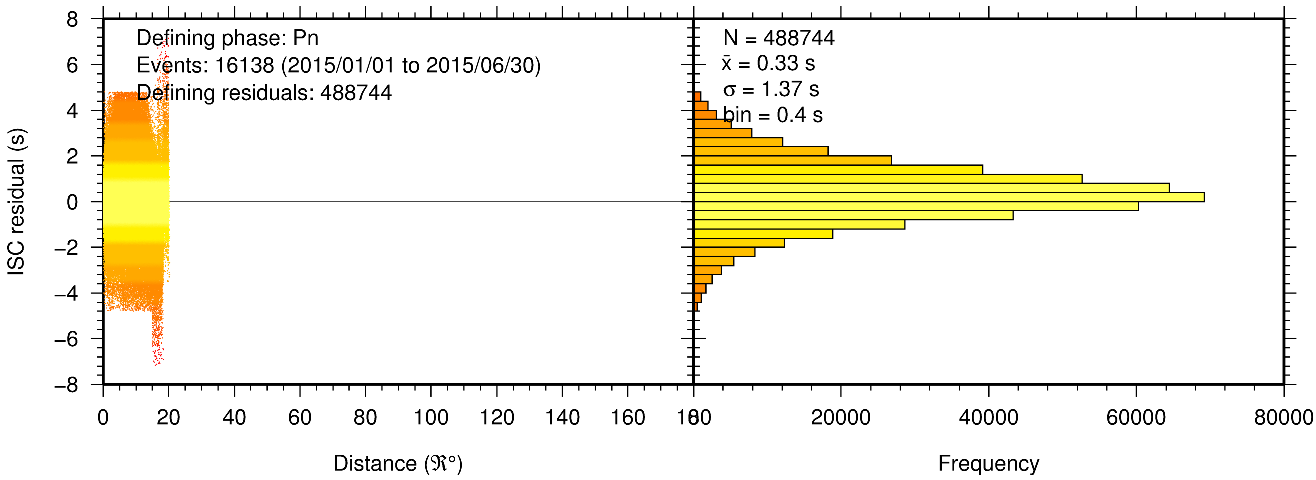

Figure 9.19: *Distribution of travel-time residuals for the defining Pn phases used in the computation of ISC located events in the Bulletin.*

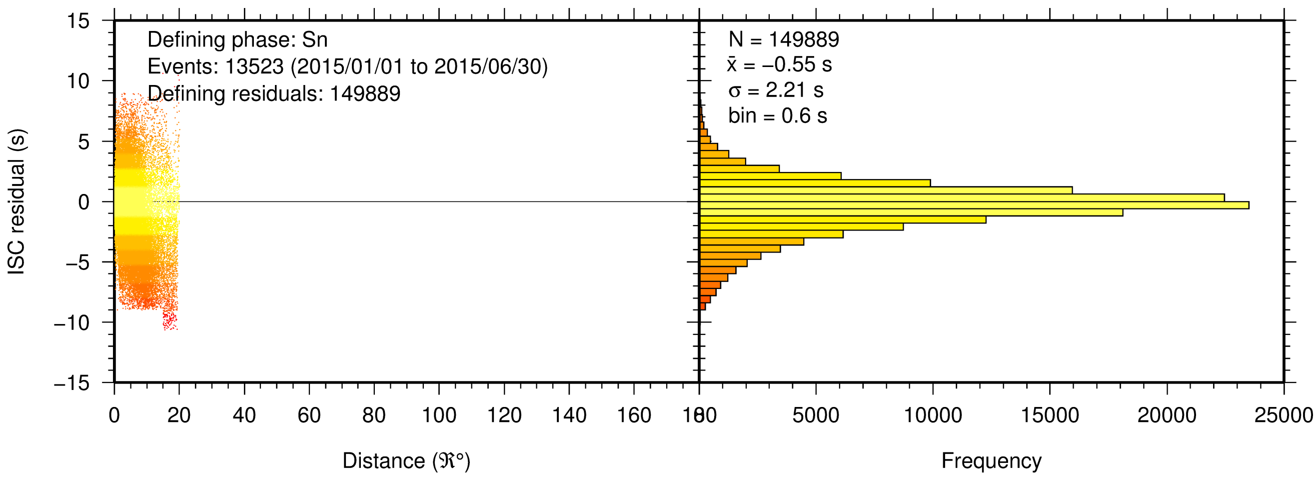

Figure 9.20: *Distribution of travel-time residuals for the defining Sn phases used in the computation of ISC located events in the Bulletin.*

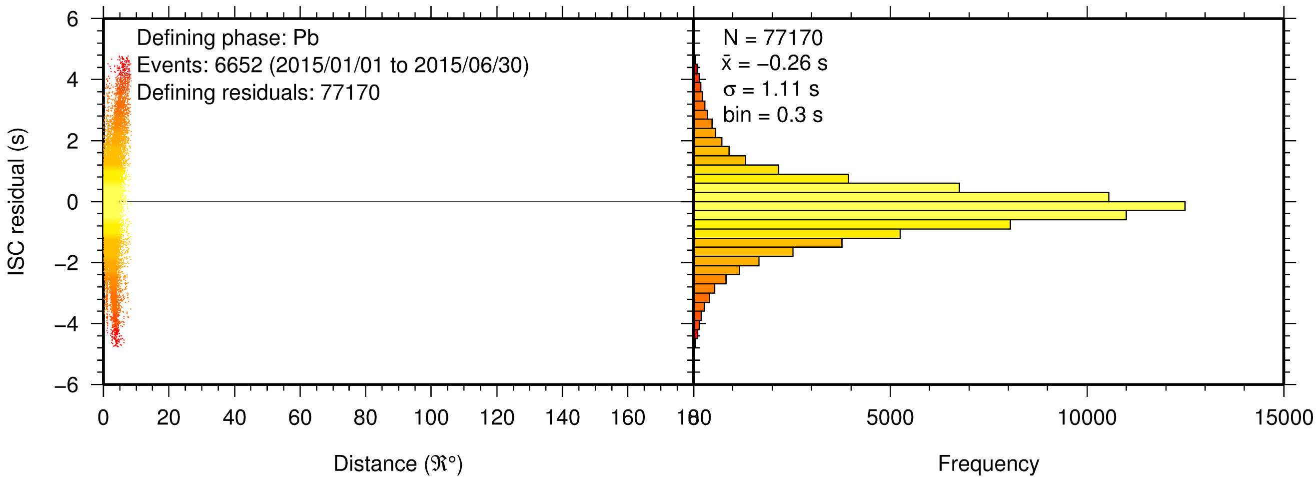

Figure 9.21: *Distribution of travel-time residuals for the defining Pb phases used in the computation of ISC located events in the Bulletin.*

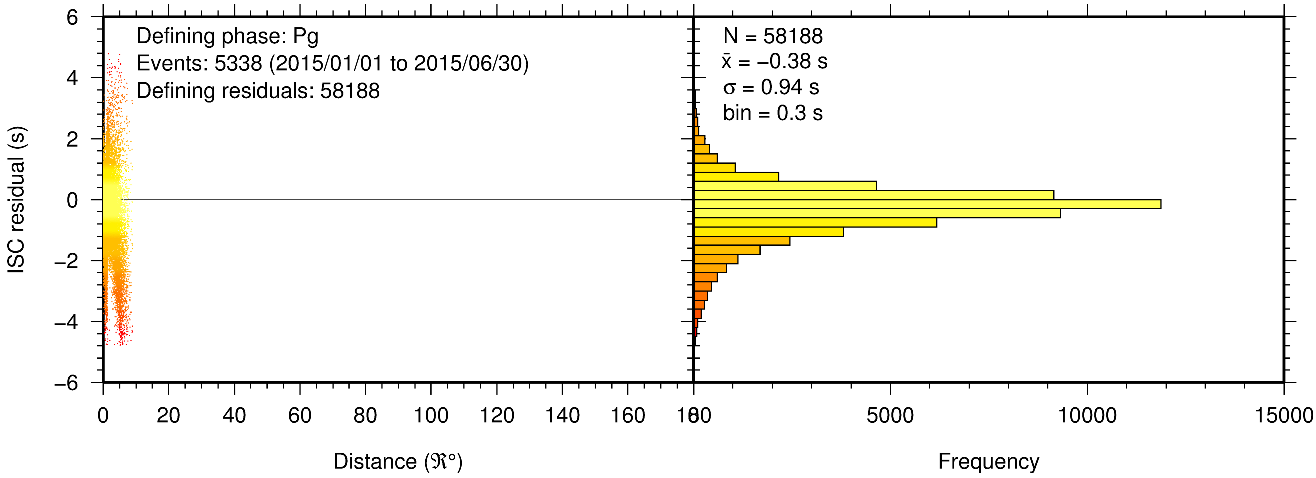

Figure 9.22: Distribution of travel-time residuals for the defining Pg phases used in the computation of ISC located events in the Bulletin.

9.3 Seismic Wave Amplitudes and Periods

The ISC Bulletin contains a variety of seismic wave amplitudes and periods measured by reporting agencies. For this Bulletin Summary, the total of collected amplitudes and periods is 2706746 (see Section 8.3). For the determination of the ISC magnitudes MS and mb, only a fraction of such data can be used. Indeed, the ISC network magnitudes are computed only for ISC located events. Here we recall the main features of the ISC procedure for MS and mb computation (see detailed description in Section 11.1.4). For each amplitude-period pair in a reading the ISC algorithm computes the magnitude (a reading can include several amplitude-period measurements) and the reading magnitude is assigned to the maximum A/T in the reading. If more than one reading magnitude is available for a station, the station magnitude is the median of the reading magnitudes. The network magnitude is computed then as the 20% alpha-trimmed median of the station magnitudes (at least three required). MS is computed for shallow earthquakes (depth $\leq$ 60 km) only and using amplitudes and periods on all three components (when available) if the period is within 10-60 s and the epicentral distance is between 20° and 160°. mb is computed also for deep earthquakes (depth down to 700 km) but only with amplitudes on the vertical component measured at periods $\leq$ 3 s in the distance range 21°-100°.

Table 9.2 is a summary of the amplitude and period data that contributed to the computation of station and ISC MS and mb network magnitudes for this Bulletin Summary.

***Table 9.2:** Summary of the amplitude-period data used by the ISC Locator to compute MS and mb.*

	MS	mb
Number of amplitude-period data	145172	442604
Number of readings	130292	438487
Percentage of readings in the ISC located events with qualifying data for magnitude computation	15.3	43.8
Number of station magnitudes	124787	395161
Number of network magnitudes	3295	11795

A small percentage of the readings with qualifying data for MS and mb calculation have more than one amplitude-period pair. Notably, only 15% of the readings for the ISC located (shallow) events included qualifying data for MS computation, whereas for mb the percentage is much higher at 44%. This is due to the seismological practice of reporting agencies. Agencies contributing systematic reports of amplitude and period data are listed in Appendix Table 11.4. Obviously the ISC Bulletin would benefit if more agencies included surface wave amplitude-period data in their reports.

Figure 9.23 shows the distribution of the number of station magnitudes versus distance. For mb there is a significant increase in the distance range 70°-90°, whereas for MS most of the contributing stations are below 100°. The increase in number of station magnitude between 70°-90° for mb is partly due to the very dense distribution of seismic stations in North America and Europe with respect to earthquake occurring in various subduction zones around the Pacific Ocean.

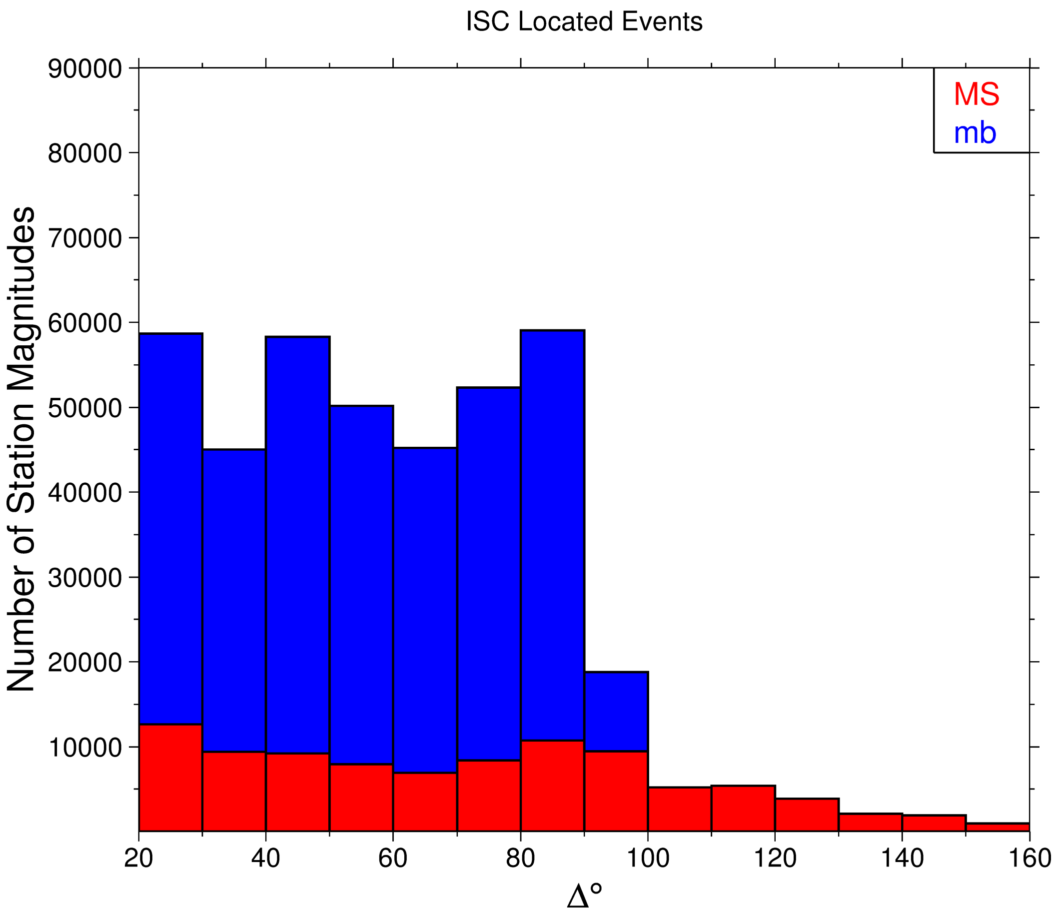

Figure 9.23: *Distribution of the number of station magnitudes computed by the ISC Locator for mb (blue) and MS (red) versus distance.*

Finally, Figure 9.24 shows the distribution of network MS and mb as well as the median number of stations for magnitude bins of 0.2. Clearly with increasing magnitude the number of events is smaller but with a general tendency of having more stations contributing to the network magnitude.

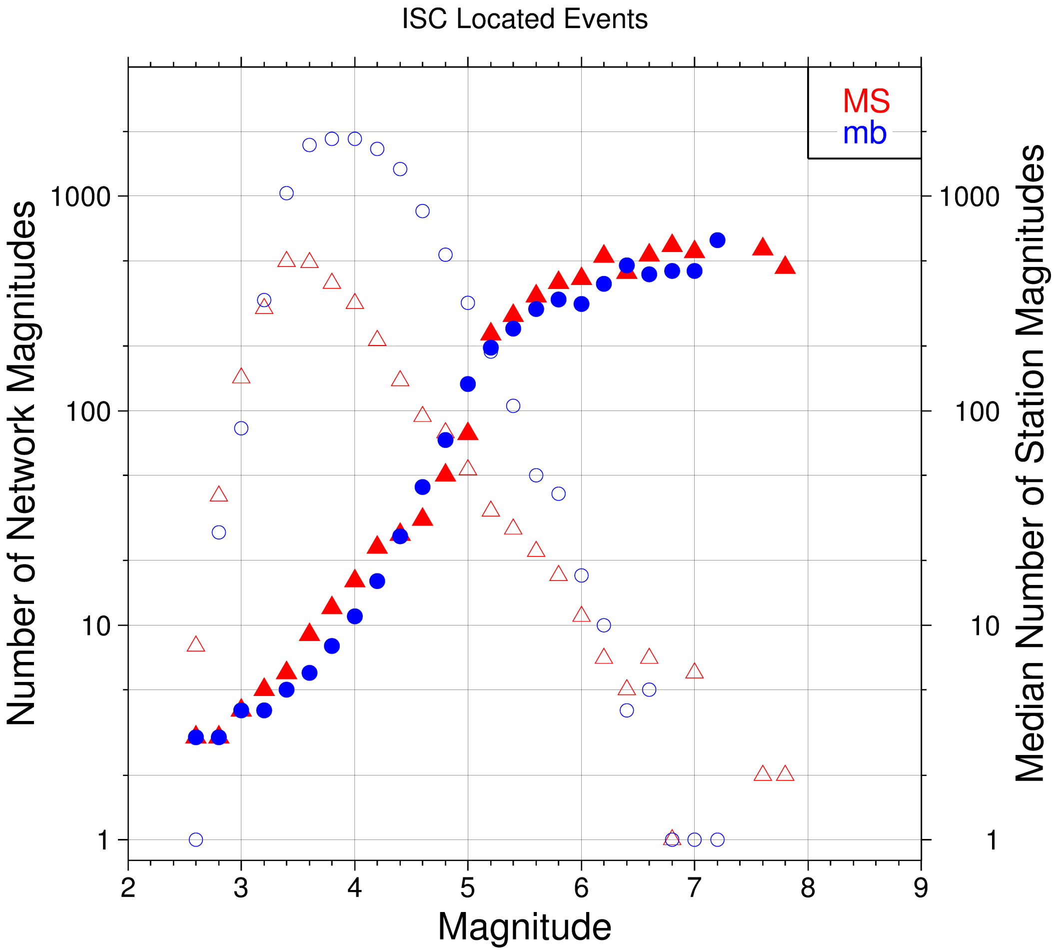

Figure 9.24: *Number of network magnitudes (open symbols) and median number of stations magnitudes (filled symbols). Blue circles refer to mb and red triangles to MS. The width of the magnitude interval δM is 0.2, and each symbol includes data with magnitude in $M \pm \delta M/2$.*

9.4 Completeness of the ISC Bulletin

The completeness of the ISC Bulletin can be expressed as a magnitude value, above which we expect the Bulletin to contain 100% of events. This magnitude of completeness, M_C can be measured as the point where the seismicity no longer follows the Gutenberg-Richter relationship. We compute an estimate of M_C using the maximum curvature technique of *Woessner and Wiemer* (2005).

The completeness of the ISC Bulletin for this summary period is shown in Figure 9.25. A history of completeness for the ISC Bulletin is shown in Figure 9.26. The step change in 1996 corresponds with the inclusion of the Prototype IDC (EIDC) Bulletin, followed by the Reviewed Event Bulletin (REB) of the IDC.

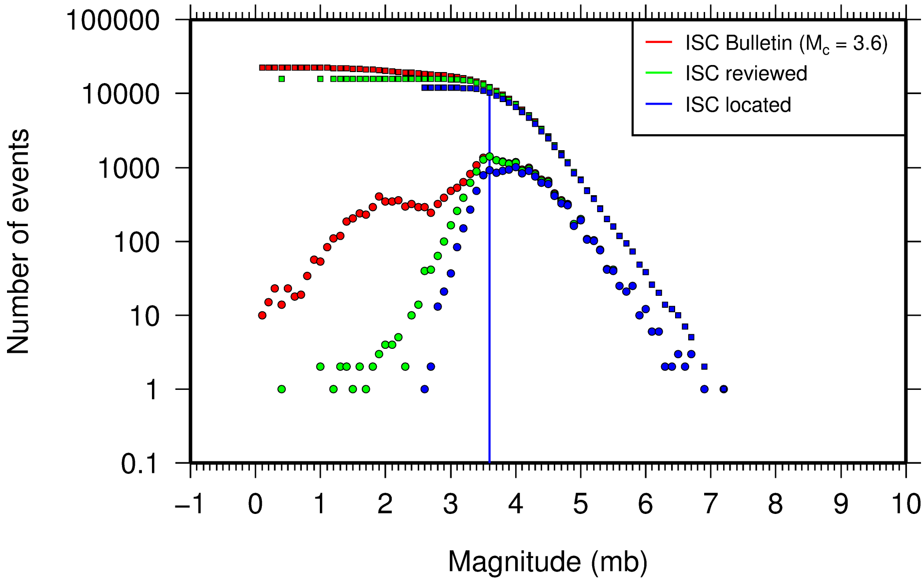

Figure 9.25: Frequency and cumulative frequency magnitude distribution for all events in the ISC Bulletin, ISC reviewed events and events located by the ISC. The magnitude of completeness (M_C) is shown for the ISC Bulletin. Note: only events with values of mb are represented in the figure.

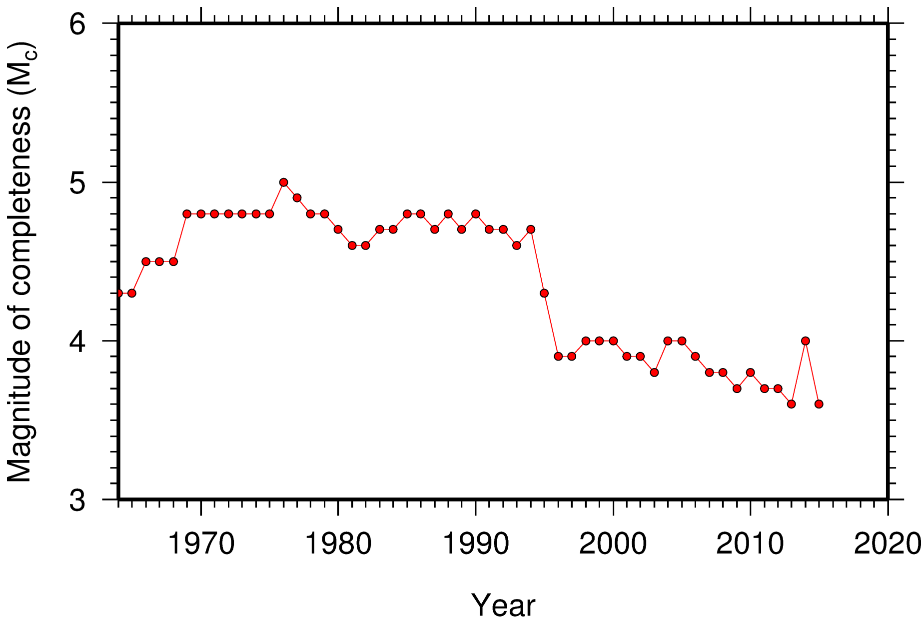

Figure 9.26: Variation of magnitude of completeness (M_C) for each year in the ISC Bulletin. Note: M_C is calculated only using those events with values of mb.

9.5 Magnitude Comparisons

The ISC Bulletin publishes network magnitudes reported by multiple agencies to the ISC. For events that have been located by the ISC, where enough amplitude data has been collected, the MS and mb magnitudes are calculated by the ISC (MS is computed only for depths $\leq$ 60 km). In this section, ISC magnitudes and some other reported magnitudes in the ISC Bulletin are compared.

The comparison between MS and mb computed by the ISC locator for events in this summary period is shown in Figure 9.27, where the large number of data pairs allows a colour coding of the data density. The scatter in the data reflects the fundamental differences between these magnitude scales.

Similar plots are shown in Figure 9.28 and 9.29, respectively, for comparisons of ISC mb and ISC MS with M_W from the GCMT catalogue. Since M_W is not often available below magnitude 5, these distributions are mostly for larger, global events. Not surprisingly, the scatter between mb and M_W is larger than the scatter between MS and M_W. Also, the saturation effect of mb is clearly visible for earthquakes with

$M_W > 6.5$. In contrast, MS scales well with $M_W > 6$, whereas for smaller magnitudes MS appears to be systematically smaller than M_W.

In Figure 9.30 ISC values of mb are compared with all reported values of mb, values of mb reported by NEIC and values of mb reported by IDC. Similarly in Figure 9.31, ISC values of MS are compared with all reported values of MS, values of MS reported by NEIC and values of MS reported by IDC. There is a large scatter between the ISC magnitudes and the mb and MS reported by all other agencies.

The scatter decreases both for mb and MS when ISC magnitudes are compared just with NEIC and IDC magnitudes. This is not surprising as the latter two agencies provide most of the amplitudes and periods used by the ISC locator to compute MS and mb. However, ISC mb appears to be smaller than NEIC mb for $mb < 4$ and larger than IDC mb for $mb > 4$. Since NEIC does not include IDC amplitudes, it seems these features originate from observations at the high-gain, low-noise sites reported by the IDC. For the MS comparisons between ISC and NEIC a similar but smaller effect is observed for $MS < 4.5$, whereas a good scaling is generally observed for the MS comparisons between ISC and IDC.

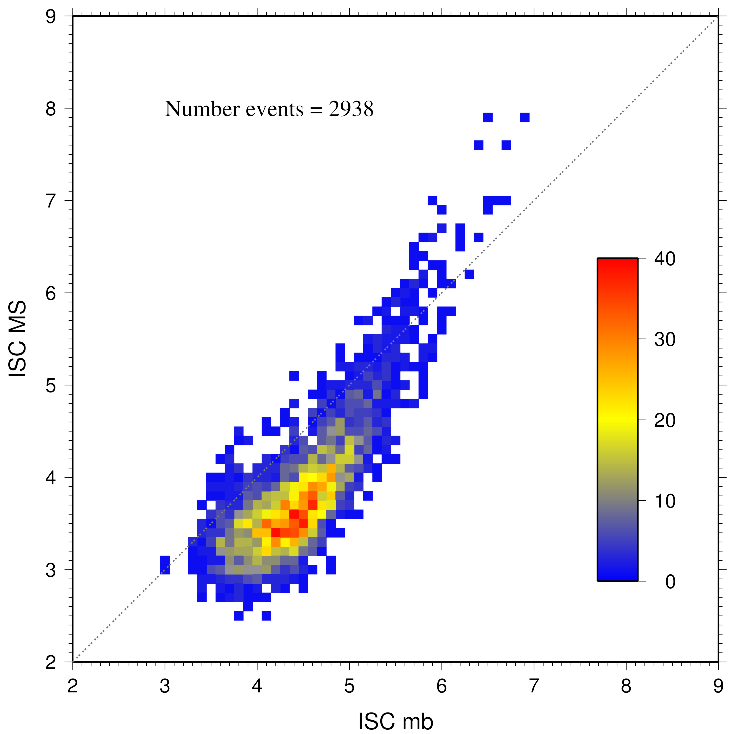

Figure 9.27: *Comparison of ISC values of MS with mb for common event pairs.*

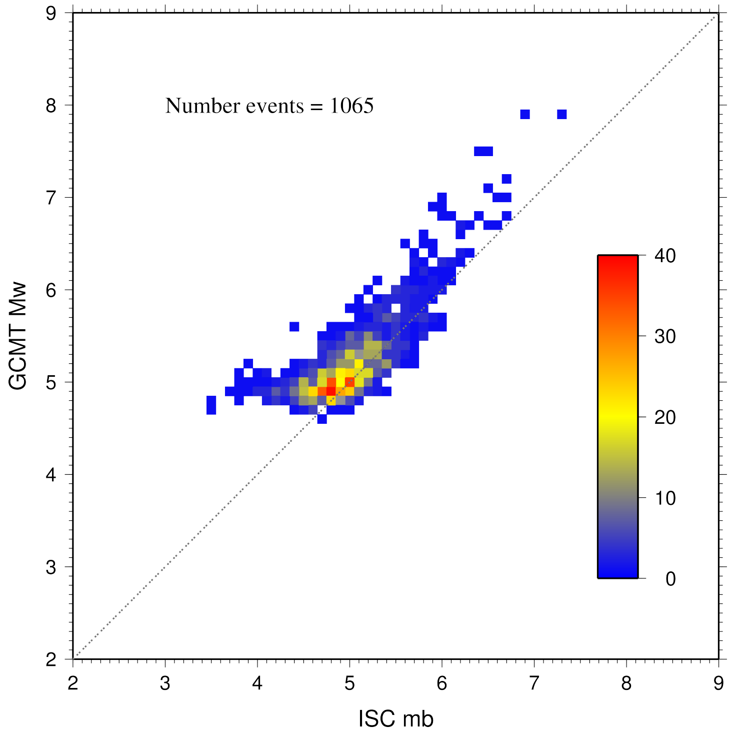

Figure 9.28: *Comparison of ISC values of mb with GCMT M_W for common event pairs.*

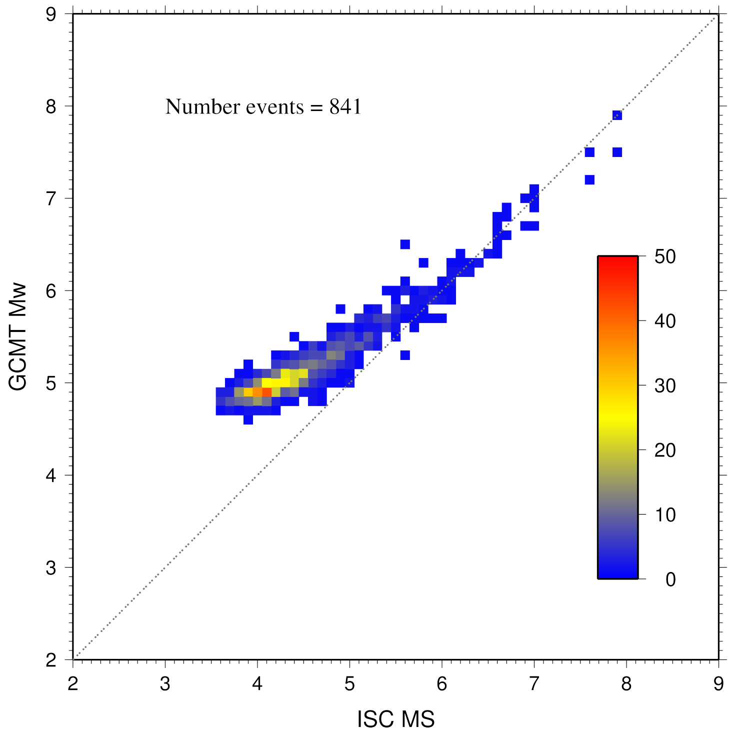

Figure 9.29: *Comparison of ISC values of MS with GCMT M_W for common event pairs.*

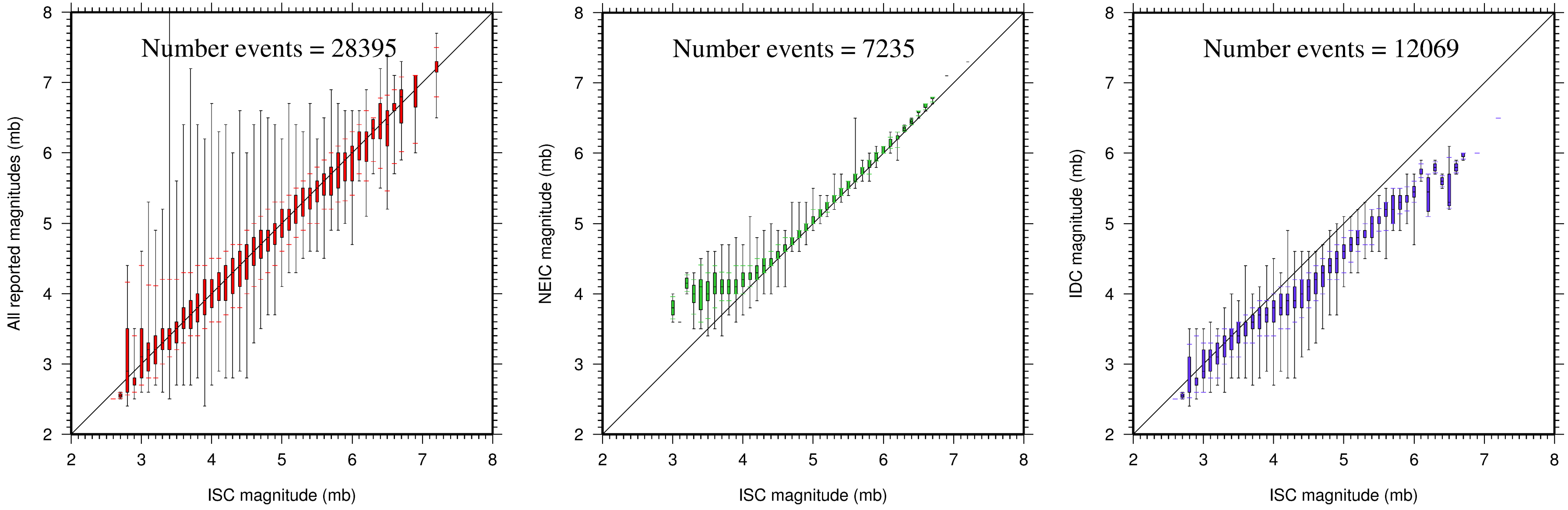

(a) (b) (c)

Figure 9.30: *Comparison of ISC magnitude data (mb) with additional agency magnitudes (mb). The statistical summary is shown in box-and-whisker plots where the 10th and 90th percentiles are shown in addition to the max and min values. (a): All magnitudes reported; (b): NEIC magnitudes; (c): IDC magnitudes.*

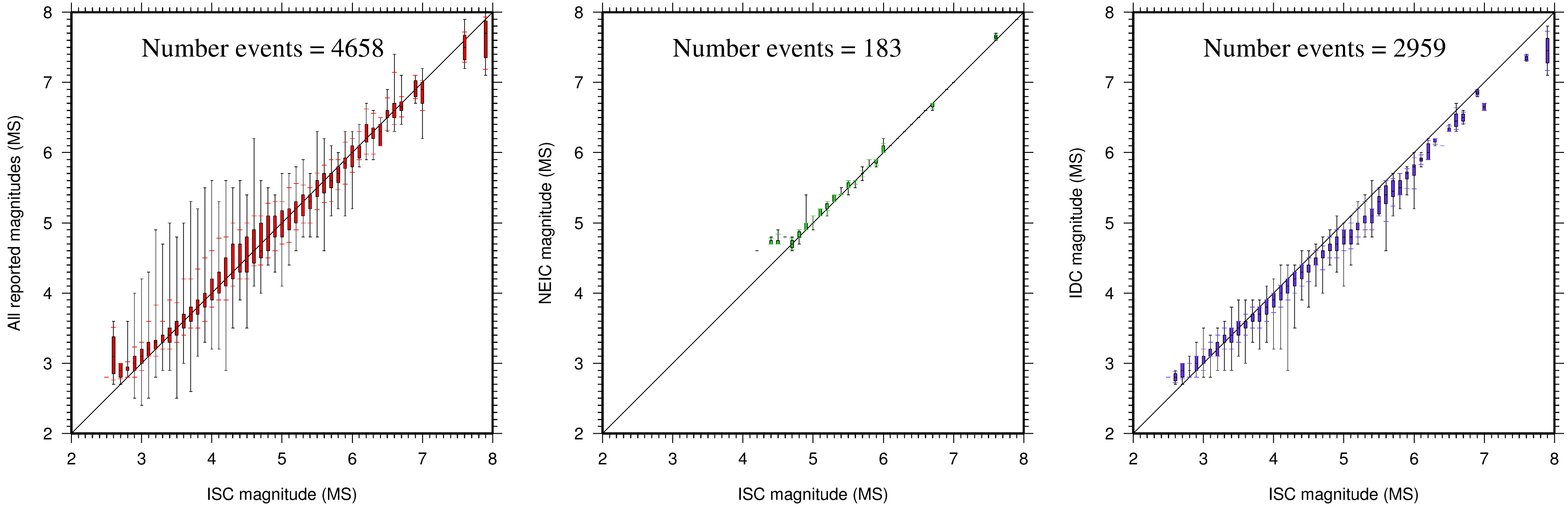

(a) (b) (c)

Figure 9.31: *Comparison of ISC magnitude data (MS) with additional agency magnitudes (MS). The statistical summary is shown in the box-and-whisker plots where the 10th and 90th percentiles are shown in addition to the max and min values. (a): All magnitudes reported; (b): NEIC magnitudes; (c): IDC magnitudes.*

10

The Leading Data Contributors

For the current six-month period, 148 agencies reported related bulletin data. Although we are grateful for every report, we nevertheless would like to acknowledge those agencies that made the most useful or distinct contributions to the contents of the ISC Bulletin. Here we note those agencies that:

- provided a comparatively large volume of parametric data (see Section 10.1),
- reported data that helped quite considerably to improve the quality of the ISC locations or magnitude determinations (see Section 10.2),
- helped the ISC by consistently reporting data in one of the standard recognised formats and in-line with the ISC data collection schedule (see Section 10.3).

We do not aim to discourage those numerous small networks who provide comparatively smaller yet still most essential volumes of regional data regularly, consistently and accurately. Without these reports the ISC Bulletin would not be as comprehensive and complete as it is today.

10.1 The Largest Data Contributors

We acknowledge the contribution of IDC, NEIC, BJI, MOS, DJA, CLL and a few others (Figure 10.1) that reported the majority of moderate to large events recorded at teleseismic distances. The contributions of NEIC, IDC, MEX, JMA, and several others are also acknowledged with respect to smaller seismic events. The contributions of JMA, NEIC, IDC, TAP, ATH, DDA and a number of others are also acknowledged with respect to small seismic events. Note that the NEIC bulletin accumulates a contribution of all regional networks in the USA. Several agencies monitoring highly seismic regions routinely report large volumes of small to moderate magnitude events, such as those in Japan, Chinese Taipei, Turkey, Italy, Greece, New Zealand, Mexico and Columbia. Contributions of small magnitude events by agencies in regions of low seismicity, such as Finland are also gratefully received.

We also would like to acknowledge contributions of those agencies that report a large portion of arrival time and amplitude data (Figure 10.2). For small magnitude events, these are local agencies in charge of monitoring local and regional seismicity. For moderate to large events, contributions of IDC, USArray, NEIC, MOS are especially acknowledged. Notably, three agencies (IDC, NEIC and MOS) together reported over 77% of all amplitude measurements made for teleseismically recorded events. We hope that other agencies would also be able to update their monitoring routines in the future to include the amplitude reports for teleseismic events compliant with the IASPEI standards.

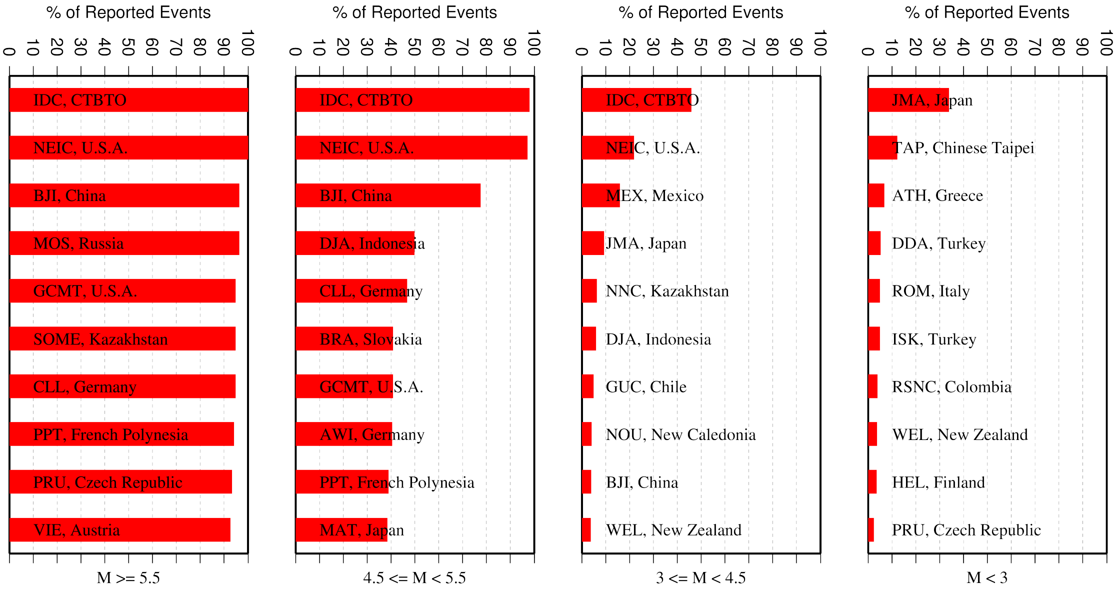

Figure 10.1: *Frequency of events in the ISC Bulletin for which an agency reported at least one item of data: a moment tensor, a hypocentre, a station arrival time or an amplitude. The top ten agencies are shown for four magnitude intervals.*

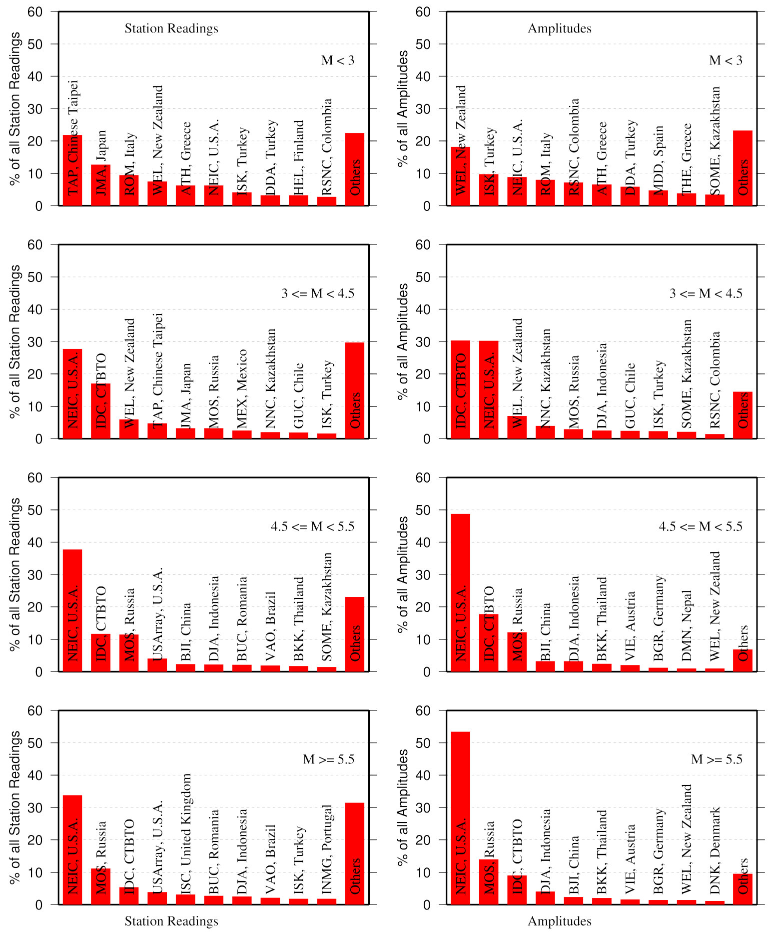

Figure 10.2: *Contributions of station arrival time readings (left) and amplitudes (right) of agencies to the ISC Bulletin. Top ten agencies are shown for four magnitude intervals.*

10.2 Contributors Reporting the Most Valuable Parameters

One of the main ISC duties is to re-calculate hypocentre estimates for those seismic events where a collective wealth of all station reports received from all agencies is likely to improve either the event location or depth compared to the hypocentre solution from each single agency. For areas with a sparse local seismic network or an unfavourable station configuration, readings made by other networks at teleseismic distances are very important. All events near mid-oceanic ridges as well as those in the majority of subduction zones around the world fall into this category. Hence we greatly appreciate the effort made by many agencies that report data for remote earthquakes (Figure 10.3). For some agencies, such as the IDC and the NEIC, it is part of their mission. For instance, the IDC reports almost every seismic event that is large enough to be recorded at teleseismic distance (20 degrees and beyond). This is largely because the International Monitoring System of primary arrays and broadband instruments is distributed at quiet sites around the world in order to be able to detect possible violations of the Comprehensive Nuclear-Test-Ban Treaty. The NEIC reported over 43% of those events as their mission requires them to report events above magnitude 4.5 outside the United States of America. For other agencies reporting distant events it is an extra effort that they undertake to notify their governments and relief agencies as well as to help the ISC and academic research in general. Hence these agencies usually report on the larger magnitude events. BJI, CLL, MOS, AWI, PRU, BRA, DJA and VIE each reported individual station arrivals for several percent of all relevant events. We encourage other agencies to report distant events to us.

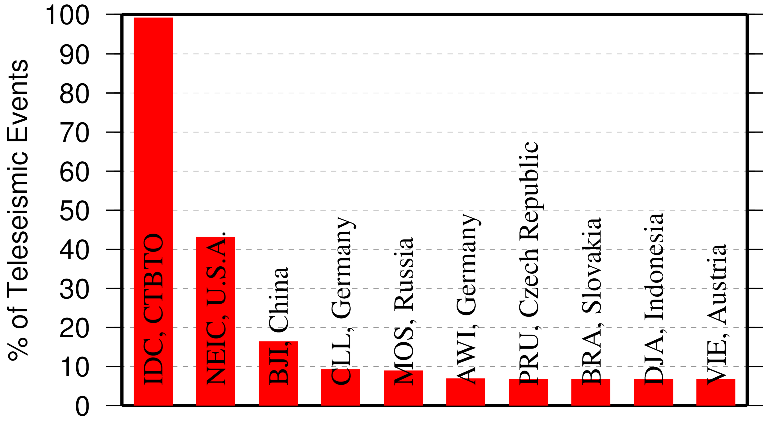

Figure 10.3: *Top ten agencies that reported teleseismic phase arrivals for a large portion of ISC events.*

In addition to the first arriving phase we encourage reporters to contribute observations of secondary seismic phases that help constrain the event location and depth: S, Sn, Sg and pP, sP, PcP (Figure 10.4). We expect though that these observations are actually made from waveforms, rather than just predicted by standard velocity models and modern software programs. It is especially important that these arrivals are manually reviewed by an operator (as we know takes place at the IDC and NEIC), as opposed to some lesser attempts to provide automatic phase readings that are later rejected by the ISC due to a generally poor quality of unreviewed picking.

Another important long-term task that the ISC performs is to compute the most definitive values of MS and mb network magnitudes that are considered reliable due to removal of outliers and consequent averaging (using alpha-trimmed median) across the largest network of stations, generally not feasible

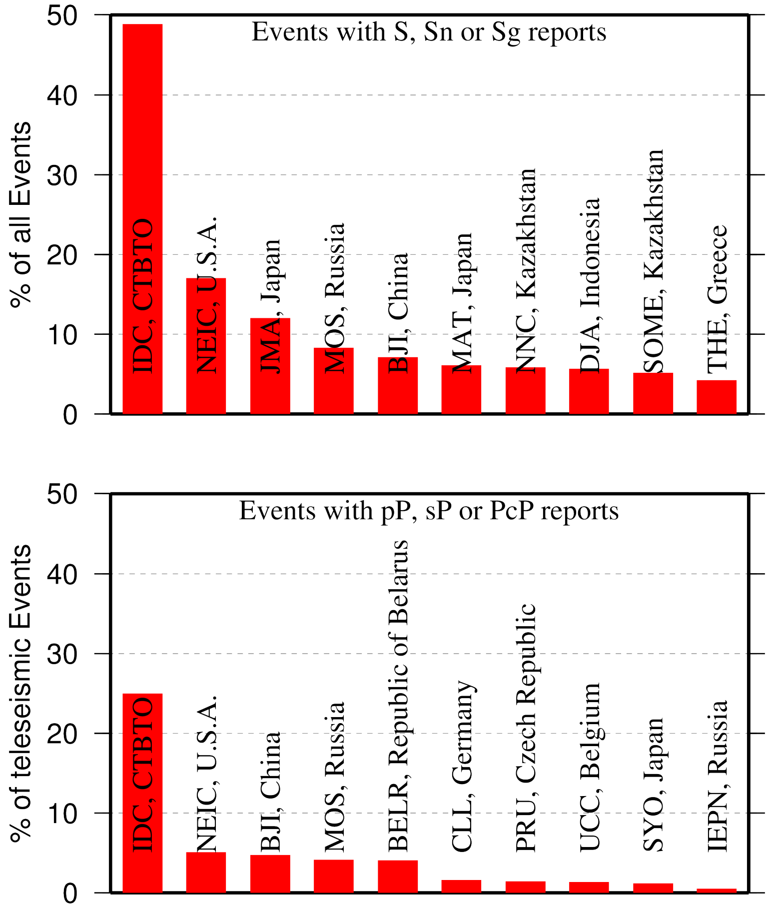

Figure 10.4: *Top ten agencies that reported secondary phases important for an accurate epicentre location (top) and focal depth determination (bottom).*

for a single agency. Despite concern over the bias at the lower end of mb introduced by the body wave amplitude data from the IDC, other agencies are also known to bias the results. This topic is further discussed in Section 9.5.

Notably, the IDC reports almost 100% of all events for which MS and mb are estimated. This is due to the standard routine that requires determination of body and surface wave magnitudes useful for discrimination purposes. NEIC, BJI, MOS, PPT, DJA, BELR and a few other agencies (Figure 10.5) are also responsible for the majority of the amplitude and period reports that contribute towards the ISC magnitudes.

Since the ISC does not routinely process waveforms, we rely on other agencies to report moment magnitudes as well as moment tensor determinations (Figure 10.6).

Among other event parameters the ISC Bulletin also contains information on event type. We cannot independently verify the type of each event in the Bulletin and thus rely on other agencies to report the event type to us. Practices of reporting non-tectonic events vary greatly from country to country. Many agencies do not include anthropogenic events in their reports. Suppression of such events from reports to the ISC may lead to a situation where a neighbouring agency reports the anthropogenic event as an earthquake for which expected data are missing. This in turn is detrimental to ISC Bulletin users studying natural seismic hazard. Hence we encourage all agencies to join the agencies listed on Figure 10.7 and several others in reporting both natural and anthropogenic events to the ISC.

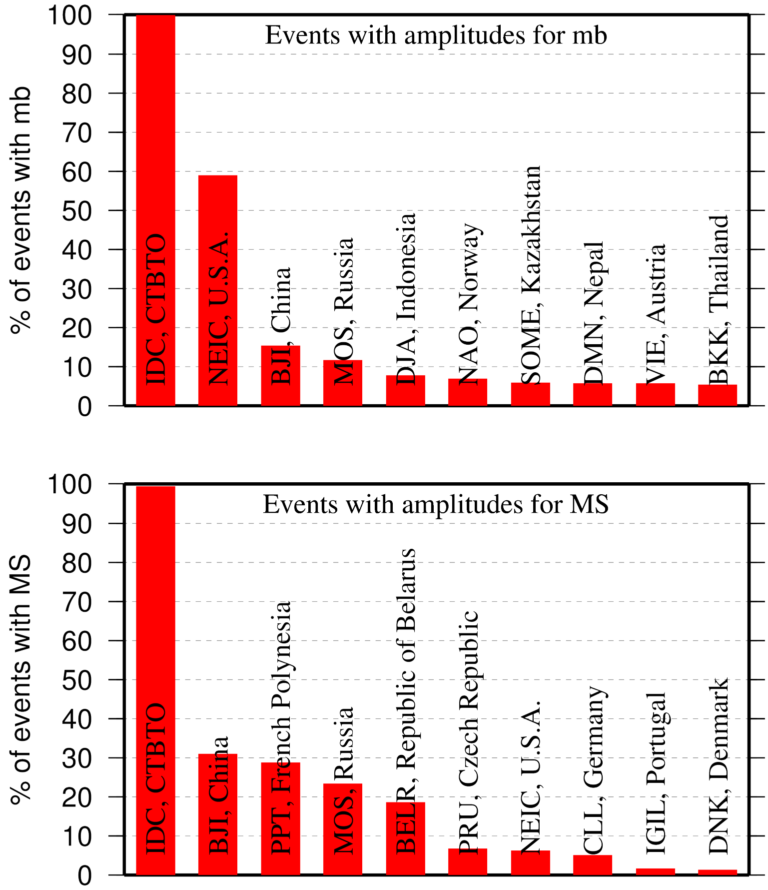

Figure 10.5: *Agencies that report defining body (top) and surface (bottom) wave amplitudes and periods for the largest fraction of those ISC Bulletin events with MS/mb determinations.*

The ISC Bulletin also contains felt and damaging information when local agencies have reported it to us. Agencies listed on Figure 10.8 provide such information for the majority of all felt or damaging events in the ISC Bulletin.

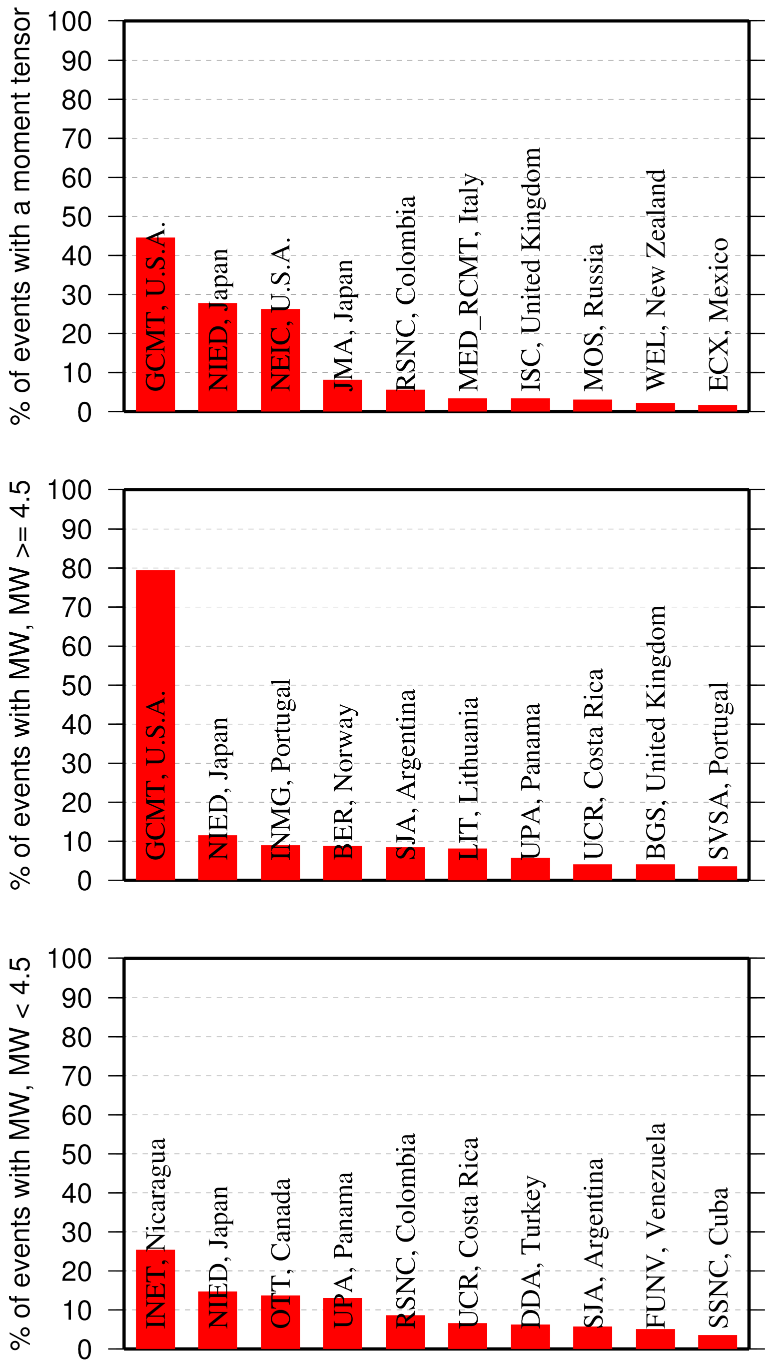

Figure 10.6: *Top ten agencies that most frequently report determinations of seismic moment tensor (top) and moment magnitude (middle/bottom for M greater/smaller than 4.5).*

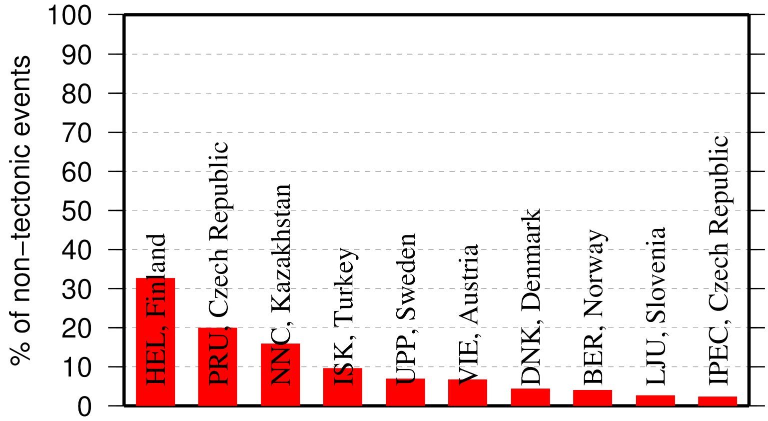

Figure 10.7: *Top ten agencies that most frequently report non-tectonic seismic events to the ISC.*

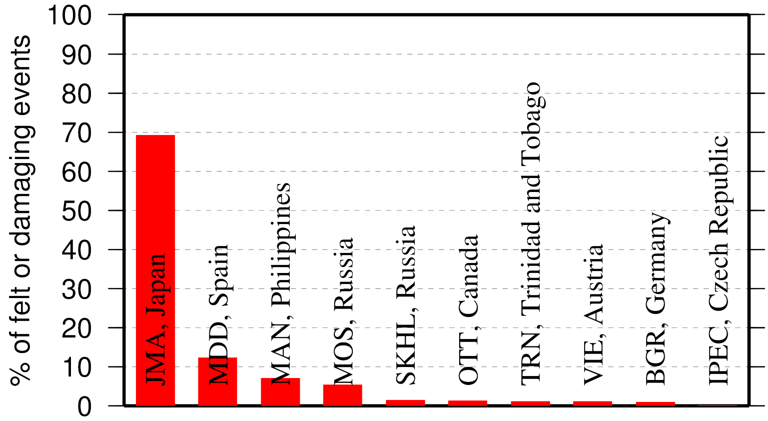

Figure 10.8: *Top ten agencies that most frequently report macroseismic information to the ISC.*

10.3 The Most Consistent and Punctual Contributors

During this six-month period, 29 agencies reported their bulletin data in one of the standard seismic formats (ISF, IMS, GSE, Nordic or QuakeML) and within the current 12-month deadline. Here we must reiterate that the ISC accepts reviewed bulletin data after a final analysis as soon as they are ready. These data, even if they arrive before the deadline, are immediately parsed into the ISC database, grouped with other data and become available to the ISC users on-line as part of the preliminary ISC Bulletin. There is no reason to wait until the deadline to send the data to the ISC. Table 10.1 lists all agencies that have been helpful to the ISC in this respect during the six-month period.

Table 10.1: *Agencies that contributed reviewed bulletin data to the ISC in one of the standard international formats before the submission deadline.*

Agency Code	Country	Average Delay from real time (days)
ZUR	Switzerland	14
PPT	French Polynesia	22
NAO	Norway	25
LIC	Ivory Coast	28
IGIL	Portugal	31
ATH	Greece	36
BUC	Romania	46
IDC	Austria	48
ISN	Iraq	55
ISK	Turkey	59
NAM	Namibia	63
SVSA	Portugal	71
KRSC	Russia	77
INMG	Portugal	79
BELR	Republic of Belarus	79
AUST	Australia	83
THE	Greece	101
BJI	China	136
DMN	Nepal	138
PRE	South Africa	150
IRIS	U.S.A.	181
LVSN	Latvia	188
ECX	Mexico	197
BEO	Serbia	211
BGS	United Kingdom	216
VIE	Austria	311
UCR	Costa Rica	323
INET	Nicaragua	356
IPEC	Czech Republic	358

11

Appendix

11.1 ISC Operational Procedures

11.1.1 Introduction

The relational database at the ISC is the primary source for the ISC Bulletin. This database is also the source for the ISC web-based search, the ISC CD-ROMs and this printed Summary. The ISC database is also mirrored at several institutions such as the Data Management Center of the Incorporated Research Institutions for Seismology (IRIS DMC), Earthquake Research Institute (ERI) of the University of Tokyo and a few others.

The database holds information about ISC events, both natural and anthropogenic. Information on each event may include hypocentre estimates, moment tensors, event type, felt and damaging reports and associated station observations reported by different agencies and grouped together per physical event.

The majority of the ISC events (∼80%) are small and are not reviewed by the ISC analysts. Those that are reviewed (∼20%, usually magnitude greater than 3.5) may or may not include an ISC hypocentre solution and magnitude estimates. The decision depends on whether the wealth of combined information from several agencies as compared to the data of each single agency alone warrants the ISC location. The events are called ISC events regardless of whether they have been reviewed or located by the ISC or not.

All events located by the ISC are reviewed by the ISC analysts but not the other way round. Analyst review involves an examination of the integrity of all reported parametric information. It does not involve review of waveforms. Even if waveforms from all of the ∼6,000 stations included in a typical recent month of the ISC Bulletin were freely available, it would be an unmanageable task to inspect them all.

We shall now describe briefly current processes and procedures involved in producing the Bulletin of the International Seismological Centre. These have been developed from former practices described in the Introduction to earlier issues of the ISC Bulletin to account for modern methods and technologies of data collection and analysis.

11.1.2 Data Collection

Parametric data, mainly comprising seismic event hypocentre solutions, phase arrival observations and associated magnitude data, are now mostly emailed to the ISC (seismo@isc.ac.uk) by agencies around the world. Other macroseismic and source information associated with seismic events may also be incorporated in accordance with modern standards. The process of data collection at the ISC involves the automatic parsing of these data into the ISC relational database. The ISC now has over 200 individual parsers to account for legacy and current bulletin data formats used by data reporters.

Figure 11.1 shows the 313 agencies that have reported bulletin data to the ISC, directly or via regional data centres, during the entire period of the ISC existence: these agencies are also listed in Table 11.2 of the Appendix. In Figure 11.1, corresponding countries are shown shaded in red. Please note that the continent of Antarctica appears white on the map despite a steady stream of bulletin data from Antarctic stations: the agencies that run these stations are based elsewhere.

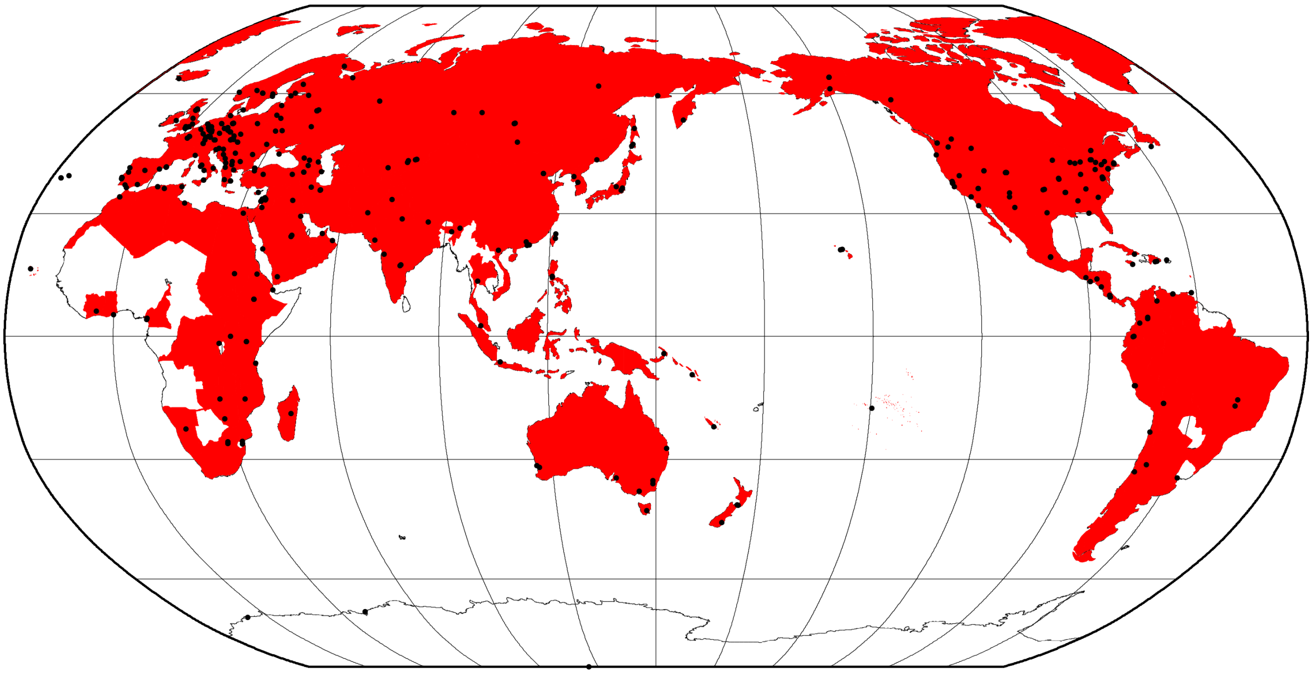

Figure 11.1: *Map of 313 agencies and corresponding countries that have reported seismic bulletin data to the ISC at least once during the entire period of the ISC operations, either directly or via regional data centres. Corresponding countries are shaded in red.*

11.1.3 ISC Automatic Procedures

Grouping

Grouping is the automatic process by which the many hypocentre solutions sent by the agencies reporting to the ISC for the same physical event are merged together into a single ISC event. This process possibly begins with an alert message and ends before a final review by ISC analysts. The process periodically runs through a set time interval of the input data stream, typically one day, looking for hypocentres in newly received data that are not yet grouped into an ISC event. Thus it considers only data more recent than the last data month reviewed by the ISC analysts. Immediately after grouping the seismic arrival associator is run on the same time interval, dealing with new phase arrival data not associated with any hypocentre.

The first stage of grouping gets a score where possible for each hypocentre to determine whether the reported hypocentre will be considered to be the primary estimate, or prime, for an ISC event. This score is based on the station arrival times reported in association with the hypocentre in four epicentral distance zones that characterise the networks of stations reporting:

1. Whole network
2. Local, 0 - 150 km
3. Near-regional, 3° - 10°
4. Teleseismic, 28° - 180°

For each distance zone, the azimuthal gap, the secondary azimuthal gap (the largest azimuthal gap filled by a single station), the minimum and maximum epicentral distance and number of stations are all used to calculate the value of dU, the normalised absolute deviation from best fitting uniformly distributed stations (*Bondár and McLaughlin*, 2009a). Clearly, this procedure can only use:

1. Bulletin data with hypocentres and sufficient associated seismic arrivals
2. Data for stations that are in the International Registry (IR)
3. Station data that are actually reported to ISC: CENC (China), for example, reports at most 24 stations, whilst many more may have been used to determine the hypocentre.

The hypocentres are then each considered in turn for grouping using one of two methods, the first by searching for a similar hypocentre, and the second by searching for the best fit of the reported phase arrival data that are associated with the candidate hypocentre. The method chosen for a reporter is based on feedback gained from ISC analysts.

For finding similar hypocentres, three sets of limits for origin-time difference and epicentral separation are used according to the type of bulletin data, be it alert, provisional or final: these limits are, respectively:

- ± 2 minutes and 10°
- ± 2 minutes and 4°
- ± 1 minutes and 2°

If there is no overlap with the hypocentre of an existing ISC event, a new event is formed. For each candidate hypocentre, a proximity score is otherwise calculated based on differences in time, t, and distance, s, between the candidate hypocentre and a hypocentre in an event with which it could potentially be grouped.

Proximity score $= 2 - (dt/dt_{max}) - (ds/ds_{max})$

where ds_{max} is the maximum distance between hypocentres and dt_{max} the maximum difference in origin time.

As long as there is no duplication of hypocentre (with the same author, origin time and location within tight limits) the candidate hypocentre together with the associated phase data is grouped with the prime hypocentre of the event and the initial dU score is used to reassess the prime hypocentre designation. Apparent duplicated hypocentre estimations, including preliminary solutions relayed by other agencies, need to be assessed to determine whether they should really be split between different events. Should there be two or more equally valid events, these can be assessed in turn and may eventually be merged together.

Grouping by fit of the associated phase arrival data is simpler. The residuals of the arrival data are calculated using ak135 travel times for all suitable prime hypocentres within the widest proximity limits given above for similar hypocentres. The hypocentre and associated phase arrival data is then grouped with the event with the best fitting prime hypocentre, which may similarly be re-designated according to the dU scores. Associations of phase arrival data are updated to be with the prime hypocentre estimate of each ISC event.

It follows that a hypocentre and associated phase arrival data submitted by a reporter will have the reported hypocentre set as the prime hypocentre in the ISC event if no other submitted hypocentre estimate is a closer match. It follows also that a hypocentre submitted without phase data can only be grouped with a similar hypocentre. Generally, early arriving data may be superseded by later arriving data: the data will still be in the ISC database but be deprecated, that is, marked as being no longer useful for further processes.

Association

Association is the automatic procedure, run routinely after grouping, that links reported phase arrivals at IR stations with the prime hypocentres of ISC events. As grouping took care of those phases associated with reported hypocentres, by associating the phases to the respective prime hypocentres of the ISC events without further checks, this procedure is only required for phase arrival observations that were sent without any association of event made for them by the reporter. Currently only 5% of arrival data is sent unassociated compared with 25% ten years ago.

If a phase arrival is found to be very similar to another already reported, it is placed in the same event, otherwise the procedure below is followed.

For associating a phase arrival, suitable events are sought with prime hypocentre origin-times in the window 40 minutes before and 100 s after the arrival time. For each phase arrival and prime hypocentre an ak135 travel-time residual is calculated for either the reported arrival phase name or an alternative from a default list if appropriate. Possible timing errors that are multiples of 60 s (a minute) are considered if the phase arrival is at a station not known to be digitally recording. A reporting likelihood is then determined based on the reported event magnitude: a magnitude default of 3.0 is used if no magnitude is given.

A final score is calculated from the residuals, from the likelihood of the phase observations for the magnitude of the event and from the S-P misfit. A phase arrival along with all other phase arrivals in that reading for the station is then associated with the prime hypocentre with the best score. If no suitable match is found, the reading remains unassociated but may be used at some later stage.

Thresholding

Thresholding is the process determining which events are to be reviewed by the ISC analysts. In former times, before email transmission of data was convenient, all events were reviewed, with magnitudes nearly always 3.5 or above. Nowadays, data contributors are encouraged to send all their data, which are stored in the ISC database. The overwhelming amount of data, including that for many more smaller events and from many more seismograph stations, led to the advent of ISC Comprehensive Bulletin, for all events, and the ISC Reviewed Bulletin, for selected events reviewed by ISC analysts. Thresholding has been under constant review since the start of the 1999 data year.

Several criteria are considered to decide which events merit review. Once a decision is made, whether or not an event is to be reviewed, further criteria are not considered.

In this section, M is the maximum magnitude reported by any agency for the event. The sequence of tests in the automatic decision process for reviewing events is currently:

- All events reported by the International Data Centre (IDC) of the Comprehensive Nuclear-Test-Ban Treaty Organization (CTBTO) are reviewed.
- If M is greater than or equal to 3.5, the event is reviewed.
- If M is less than 2.5, the event is not reviewed.
- If M is unknown, the number of data sources of hypocentres and phase arrivals is used. Care is taken here to avoid counting indirect reports arriving via agencies such as NEIC, CSEM and CASC, which compile regional and global data:
  - If the number of hypocentre authors is greater than two and the maximum epicentral distance of arrival data is greater than 10°, the event is reviewed.
  - If the number of arrival authors is greater than two and the maximum epicentral distance of arrival data is greater than 10°, the event is reviewed.
  - Otherwise the event is not reviewed.
- If M is between 2.5 and 3.5:
  - If the number of hypocentre and seismic arrival authors is less than two, the event is not reviewed.
  - If any bulletin contributing to the event has at least ten stations within 3° and the secondary azimuthal gap (the largest azimuthal gap filled by a single station) is less than 135°, the event is not reviewed.

Location by the ISC

The automatic processes group and associate incoming data into ISC events as indicated above. These data are available to users before review by the ISC analysts but there will be no ISC hypocentre solutions for any of the events. The candidate events due for review by the ISC analysts are determined by the thresholding process, which is why many smaller events remain without an ISC hypocentre solution even after the analyst review.

Several further checks of the data are made in preparation for the analyst review, and initial trial estimates for ISC hypocentres are then generated using the accumulated data. If sufficiently robust, the ISC hypocentre estimation will be retained and be made the prime solution for the event, but this, of course, will itself be subject to the analyst review.

It is important to note that not all reviewed events will have an ISC hypocentre. For the reviewed events certain criteria must be met for an initial ISC location of an event to be made. These criteria are shown below:

- All events with an IDC hypocentre, unless IDC is the only hypocentre author and there are less than six associated phases.
- Two or more reporters of data
- Phase data at epicentral distance $\geq 20°$

The ISC locator also needs an intial seed location; in all events except those with eight or more reporters of data where the existing prime is used, this is calculated using a Neighbourhood Algorithm (NA) (*Sambridge*, 1999; *Sambridge and Kennett*, 2001). More information about the ISC location algorithm and initial seed is given in the next section.

11.1.4 ISC Location Algorithm

The new ISC location algorithm is described in detail in *Bondár and Storchak* (2011) (doi: 10.1111/j.1365-246X.2011.05107.x, Manual www.isc.ac.uk/iscbulletin/iscloc/); here we give a short summary of the major features. Ever since the ISC came into existence in 1964, it has been committed to providing a homogeneous bulletin that benefits scientific research. Hence the location algorithm used by the ISC, except for some minor modifications, has remained largely unchanged for the past 40 years (*Adams et al.*, 1982; *Bolt*, 1960). While the ISC location procedures have served the scientific community well in the past, they can certainly be improved.

Linearised location algorithms are very sensitive to the initial starting point for the location. The old procedures made the assumption that a good initial hypocentre is available among the reported hypocentres. However, there is no guarantee that any of the reported hypocentres are close to the global minimum in the search space. Furthermore, attempting to find a free-depth solution was futile when the data had no resolving power for depth (e.g. when the first arrival is not within the inflection point of the P travel-time curve). When there was no depth resolution, the algorithm would simply pick a point on the origin time – depth trade-off curve. The old ISC locator assumed that the observational errors are independent. The recent years have seen a phenomenal growth both in the number of reported events and phases, owing to the ever-increasing number of stations worldwide. Similar ray paths will produce correlated travel-time prediction errors due to unmodelled heterogeneities in the Earth, resulting in underestimated location uncertainties and for unfavourable network geometries, location bias. Hence, accounting for correlated travel-time prediction errors becomes imperative if we want to improve (or simply maintain) location accuracy as station networks become progressively denser. Finally, publishing network magnitudes that may have been derived from a single station measurement was rather prone to producing erroneous event magnitude estimates.

To meet the challenge imposed by the ever-increasing data volume from heavily unbalanced networks we introduced a new ISC location algorithm to ensure the efficient handling of data and to further improve the location accuracy of events reviewed by the ISC. The new ISC location algorithm

- Uses all ak135 (*Kennett et al.*, 1995) predicted phases (including depth phases) in the location;
- Obtains the initial hypocentre guess via the Neighbourhood Algorithm (NA) (*Sambridge*, 1999; *Sambridge and Kennett*, 2001);
- Performs iterative linearised inversion using an *a priori* estimate of the full data covariance matrix to account for correlated model errors (*Bondár and McLaughlin*, 2009b);
- Attempts a free-depth solution if and only if there is depth resolution, otherwise it fixes the depth to a region-dependent default depth;
- Scales uncertainties to 90% confidence level and calculates location quality metrics for various distance ranges;
- Obtains a depth-phase depth estimate based on reported surface reflections via depth-phase stacking (*Murphy and Barker*, 2006);
- Provides robust network magnitude estimates with uncertainties.

Seismic Phases

One of the major advantages of using the ak135 travel-time predictions (*Kennett et al.*, 1995) is that they do not suffer from the baseline difference between P, S and PKP phases compared with the Jeffreys-Bullen tables (*Jeffreys and Bullen*, 1940). Furthermore, ak135 offers an abundance of phases from the IASPEI Standard Seismic List (*Storchak et al.*, 2003; 2011) that can be used in the location, most notably the PKP branches and depth-sensitive phases. Elevation and ellipticity corrections (*Dziewonski and Gilbert*, 1976; *Engdahl et al.*, 1998; *Kennett et al.*, 1996), using the WG84 ellipsoid parameters, are added to the ak135 predictions. For depth phases, bounce point (elevation correction at the surface reflection point) and water depth (for pwP) corrections are calculated using the algorithm of *Engdahl et al.* (1998). We use the ETOPO1 global relief model (*Amante and Eakins*, 2009) to obtain the elevation or the water depth at the bounce point.

Phase picking errors are described by *a priori* measurement error estimates derived from the inspection of the distribution of ground truth residuals (residuals calculated with respect to the ground truth location) from the IASPEI Reference Event List (*Bondár and McLaughlin*, 2009a). For phases that do not have a sufficient number of observations in the ground truth database we establish *a priori* measurement errors so that the consistency of the relative weighting schema is maintained. First-arriving P-type phases (P, Pn, Pb, Pg) are picked more accurately than later phases, so their measurement error estimates are the smallest, 0.8 s. The measurement error for first-arriving S-phases (S, Sn, Sb, Sg) is set to 1.5 s. Phases traversing through or reflecting from the inner/outer core of the Earth have somewhat larger (1.3 s for PKP, PKS, PKKP, PKKS and P'P' branches as well as PKiKP, PcP and PcS, and 1.8 s for SKP, SKS, SKKP, SKKS and S'S' branches as well as SKiKP, ScP and ScS) measurement error estimates to account for possible identification errors among the various branches. Free-surface reflections and conversions (PnPn, PbPb, PgPg, PS, PnS, PgS and SnSn, SbSb, SgSg, SP, SPn, SPg) are observed less frequently and with larger uncertainty, and therefore suffer from large, 2.5 s, measurement errors. Similarly, a measurement error of 2.8 s is assigned to the longer period and typically emergent diffracted phases (Pdif, Sdif, PKPdif). The *a priori* measurement error for the commonly observed depth phases (pP, sP, pS, sS and pwP) is set to 1.3 s, while the remaining depth phases (pPKP, sPKP, pSKS, sSKS branches and pPb, sPb, sSb, pPn, sPn, sSn) have the measurement error estimate set to 1.8 s. We set the measurement error estimate to 2.5 s for the less reliable depth phases (pPg, sPg, sSg, pPdif, pSdif, sPdif and sSdif). Note that we also allow for distance-dependent measurement errors. For instance, to account for possible phase identification errors at far-regional distances the *a priori* measurement error for Pn and P is increased from 0.8 s to 1.2 s and for Sn and S from 1.5 s to 1.8 s between 15° and 28°. The measurement errors between 40° and 180° are set to 1.3 s and 1.8 s for the prominent PP and SS arrivals respectively, but they are increased to 1.8 s and 2.5 s between 25° and 40°.

The relative weighting scheme (Figure 11.2) described above ensures that arrivals picked less reliably or prone to phase identification errors are down-weighted in the location algorithm. Since the ISC works with reported parametric data with wildly varying quality, we opted for a rather conservative set of *a priori* measurement error estimates.

Correlated Travel-Time Prediction Error Structure

Most location algorithms, either linearised or non-linear, assume that all observational errors are independent. This assumption is violated when the separation between stations is less than the scale length of local velocity heterogeneities. When correlated travel-time prediction errors are present, the data covariance matrix is no longer diagonal, and the redundancy in the observations reduces the effective number of degrees of freedom. Thus, ignoring the correlated error structure inevitably results in underestimated location uncertainty estimates. For events located by an unbalanced seismic network this may also lead to a biased location estimate. *Chang et al.* (1983) demonstrated that accounting for correlated error structure in a linearised location algorithm is relatively straightforward once an estimate of the non-diagonal data covariance matrix is available. To determine the data covariance matrix we follow the approach described by *Bondár and McLaughlin* (2009b). They assume that the similarity between ray paths is well approximated by the station separation. This simplifying assumption allows for the estimation of covariances between station pairs from a generic P variogram model derived from ground truth residuals. Because the overwhelming number of phases in the ISC Bulletin is teleseismic P, we expect that the generic variogram model will perform reasonably well anywhere on the globe.

Since in this representation the covariances depend only on station separations, the covariance matrix (and its inverse) needs to be calculated only once. We assume that different phases owing to the different ray paths they travel along as well as station pairs with a separation larger than 1000 km are uncorrelated. Hence, the data covariance matrix is a sparse, block-diagonal matrix. Furthermore, if the stations in

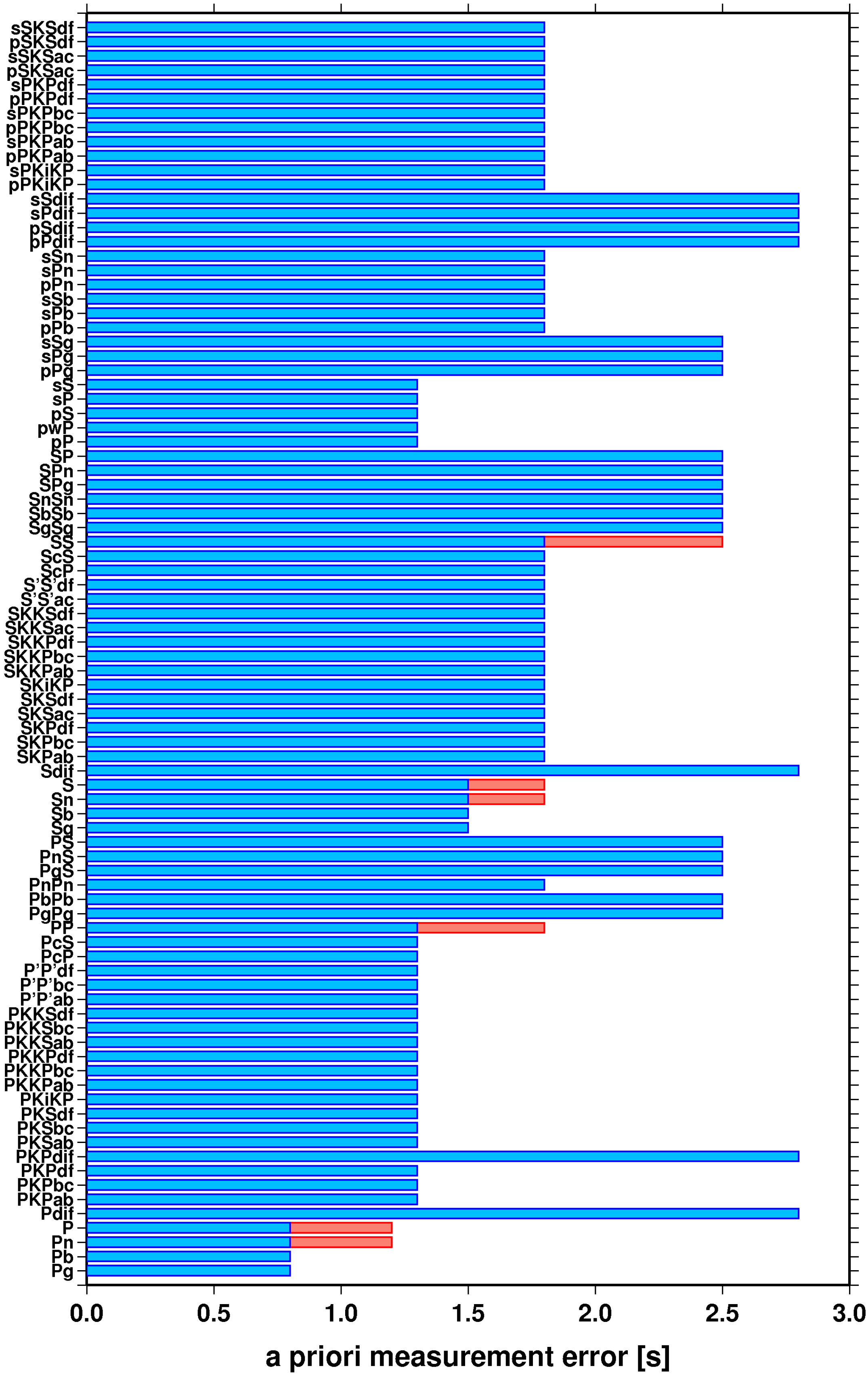

Figure 11.2: A priori *measurement error estimates for phases used in the location algorithm. The red coloured errors are distance-dependent, which are applied for distances when phase identification errors may occur (see text).*

each phase block are ordered by their nearest neighbour distance, the phase blocks themselves become block-diagonal. To reduce the computational time of inverting large matrices we exploit the inherent block-diagonal structure by inverting the covariance matrix block-by-block. The *a priori* measurement error variances are added to the diagonal of the data covariance matrix.

Depth Resolution

In principle, depth can be resolved if there is a mixture of upgoing and downgoing waves emanating from the source, that is, if there are stations covering the distance range where the vertical partial derivative of the travel-time of the first-arriving phase changes sign (local networks), or if there are phases with vertical slowness of opposite sign (depth phases). Core reflections, such as PcP, and to a lesser extent, secondary phases (S in particular) could also help in resolving the depth.

We developed a number of criteria to test whether the reported data for an event have sufficient depth resolution:

- local network: one or more stations within 0.2° with time-defining phases
- depth phases: five or more time-defining depth phases reported by at least two agencies (to reduce a chance of misinterpretation by a single inexperienced analyst)
- core reflections: five or more time-defining core reflections (PcP, ScS) reported by at least two agencies
- local/near regional S: five or more time-defining S and P pairs within 3°

We attempt a free-depth solution if any of the above criteria are satisfied; otherwise we fix the depth to a default depth dependent on the epicentre location. The default depth grid was derived from the EHB (*Engdahl et al.*, 1998) free-depth solutions, including the fixed-depth EHB earthquakes that were flagged as having reliable depth estimate (personal communication with Bob Engdahl), as well as from free-depth solutions obtained by the new locator when locating the entire ISC Bulletin data-set. As Figure 11.3 indicates, the default depth grid provides a reasonable depth estimate where seismicity is well established. Note that the depths of known anthropogenic events and landslides are fixed to the surface.

Depth-Phase Stack

While we use depth phases directly in the location, the depth-phase stacking method (*Murphy and Barker*, 2006) provides an independent means to obtain robust depth estimates. Because the depth obtained from the depth-phase stacking method implicitly depends on the epicentre itself, we perform the depth-phase stack only twice: first, with respect to the initial location in order to obtain a reasonable starting point for the depth in the grid search described in the following section; second, with respect to the final location to obtain the final estimate for the depth-phase constrained depth.

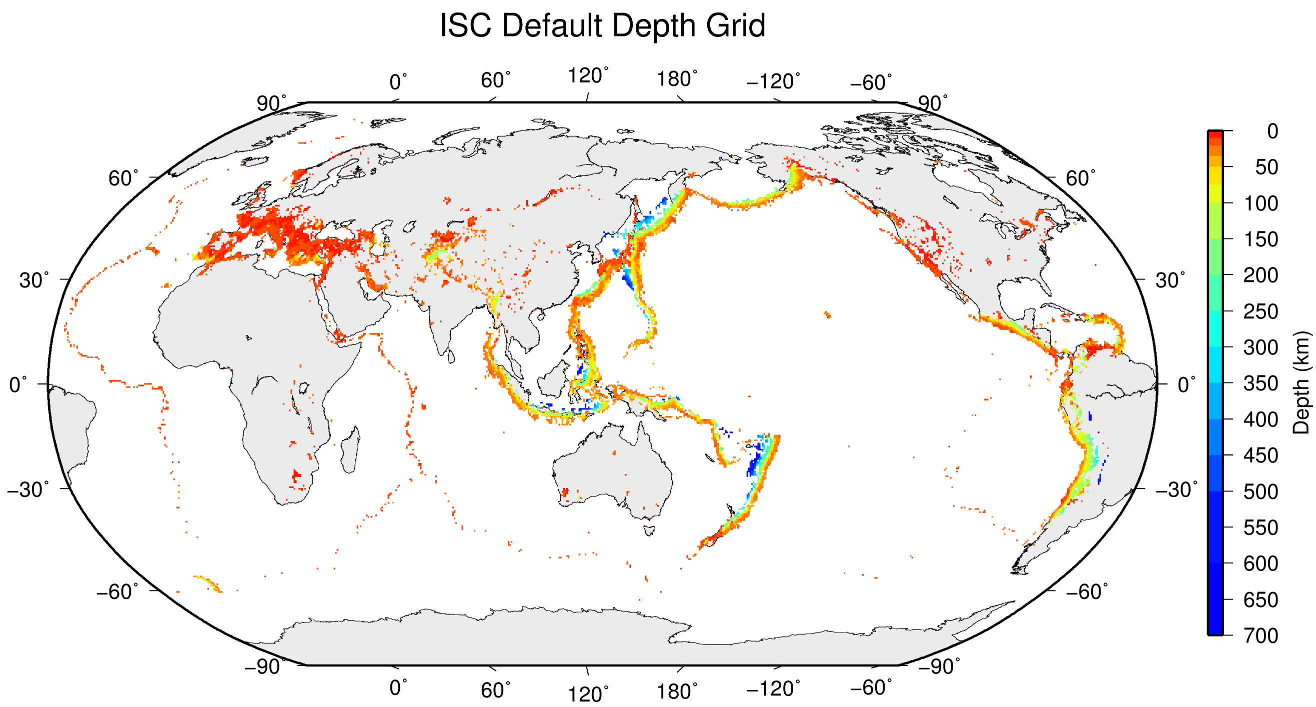

Figure 11.3: *Default depths on a 0.5×0.5 degree grid derived from EHB free-depth solutions and EHB events flagged as reliable depth, as well as free-depth solutions from the entire ISC Bulletin located with the new locator.*

Initial Hypocentre

For poorly recorded events the reported hypocentres may exhibit a large scatter and they could suffer from large location errors, especially if they are only recorded teleseismically. In order to obtain a good initial hypocentre guess for the linearised location algorithm we employ the Neighbourhood Algorithm (NA) (*Sambridge*, 1999; *Sambridge and Kennett*, 2001). NA is a nonlinear grid search method capable of exploring a large search space and rapidly closing in on the global optimum. *Kennett* (2006) discusses in detail the NA algorithm and its use for locating earthquakes.

We perform a search around the median of reported hypocentre parameters with a generously defined search region – within a 2° radius circle around the median epicentre, 10 s around the median origin time and 150 km around the median reported depth. These default search parameters were obtained by trial-and-error runs to achieve a compromise between execution time and allowance for gross errors in the median reported hypocentre parameters. Note that if our test for depth resolution fails, we fix the depth to the region-dependent default depth. The initial hypocentre estimate will be the one with the smallest L1-norm misfit among the NA trial hypocentres. Once close to the global optimum, we proceed with the linearised location algorithm to obtain the final solution and corresponding formal uncertainties.

Iterative Linearised Location Algorithm

We adopt the location algorithm described in detail in *Bondár and McLaughlin* (2009b). Recall that in the presence of correlated travel-time prediction errors the data covariance matrix is no longer diagonal. Using the singular value decomposition of the data covariance matrix we construct a projection matrix that orthogonalises the data set and projects redundant observations into the null space. In other words, we solve the inversion problem in the eigen coordinate system in which the transformed observations are independent.

The model covariance matrix yields the four-dimensional error ellipsoid whose projections provide the two-dimensional error ellipse and one-dimensional errors for depth and origin time. These uncertainties are scaled to the 90% confidence level. Note that since we projected the system of equations into the eigen coordinate system, the number of independent observations is less than the total number of observations. Hence, the estimated location error ellipses necessarily become larger, providing a more realistic representation of the location uncertainties. The major advantage of this approach is that the projection matrix is calculated only once for each event location.

Validation Tests

To demonstrate improvements due to the new location procedures, we located some 7,200 GT0-5 events in the IASPEI Reference Event List (*Bondár and McLaughlin*, 2009a) both with the old ISC locator (which constitutes the baseline) and with the new location algorithm. We also located the entire (1960-2010) ISC Bulletin, including four years of the International Seismological Summary (ISS, the predecessor of the ISC) catalogue (*Villaseñor and Engdahl*, 2005; 2007).

The location of GT events demonstrated that the new ISC location algorithm provides small but consistent location improvements, considerable improvements in depth determination and significantly more accurate formal uncertainty estimates. Even using a 1-D model and a variogram model that fits teleseismic observations we could achieve realistic uncertainty estimates, as the 90% confidence error ellipses cover the true locations 80-85% of the time. The default depth grid provides reasonable depth estimates where there is seismicity. We have shown that the location and depth accuracy obtained by the new algorithm matches or surpasses the EHB accuracy.

We noted above that the location improvements for the ground truth events are consistent, but minor. This is not surprising as most of the events in the IASPEI Reference Event List are very well-recorded with a small azimuthal gap and dominated by P-type phases. In these circumstances we could expect significant location improvements only for heavily unbalanced networks where large numbers of correlated ray paths conspire to introduce location bias. On the other hand, the ISC Bulletin represents a plethora of station configurations ranging from reasonable to the most unfavourable network geometries. Hence, we could expect more dramatic location improvements when locating the entire ISC Bulletin. Although in this case we cannot measure the improvement in location accuracy due to the lack of ground truth information, we show that with the new locator we obtain significantly better clustering of event locations (Figure 11.4), thus providing an improved view of the seismicity of the Earth.

Magnitude Calculation

Currently the ISC locator calculates body and surface wave magnitudes. MS is calculated for shallow events (depth $<$ 60 km) only. At least three station magnitudes are required for a network (mb or MS) magnitude. The network magnitude is defined as the median of the station magnitudes, and its

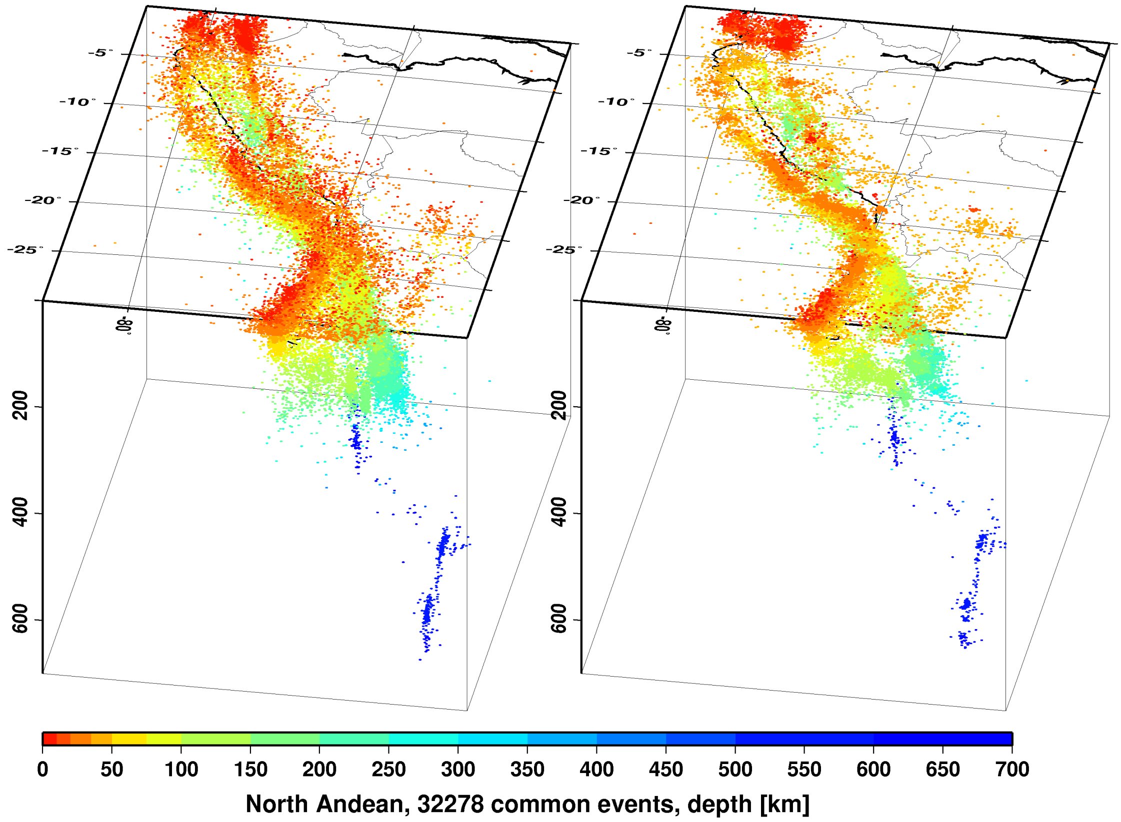

(a)

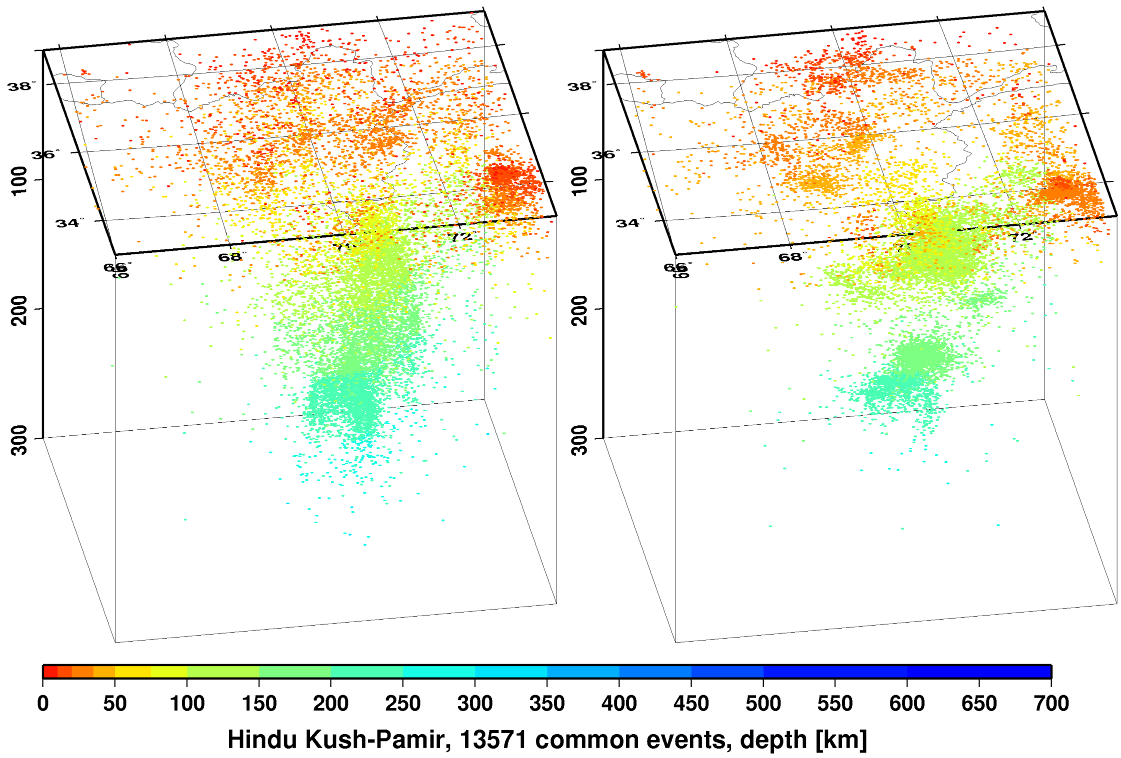

(b)

Figure 11.4: *Comparison of seismicity maps for common events in the reviewed ISC Bulletin (old locator, left) and the located ISC Bulletin (new locator, right) for the North Andean (a) and Hindu Kush - Pamir regions (b). The events are better clustered when located with the new locator.*

uncertainty is defined as the standard median absolute deviation (SMAD) of the alpha-trimmed (*alpha* = 20%) station magnitudes.

The station magnitude is defined as the median of reading magnitudes for a station. The reading magnitude is defined as the magnitude computed from the maximal log(A/T) in a reading. Amplitude magnitudes are calculated for each reported amplitude-period pair.

Body-Wave Magnitudes

Body-wave magnitudes are calculated for each reported amplitude-period pair, provided that the phase is in the list of phases that can contribute to *mb* (P, pP, sP, AMB, IAmb, pmax), the station is between the epicentral distances 21 − 100° and the period is less than 3 s.

A reading contains all parametric data reported by a single agency for an event at a station, and it may have several reported amplitude and periods. The amplitudes are measured as zero-to-peak values in nanometres. For each pair an amplitude *mb* is calculated.

$$mb_{amp} = log(A/T) + Q(\Delta, h) - 3 \tag{11.1}$$

If no amplitude-period pairs are reported for a reading, the body-wave magnitude is calculated using the reported logat values for $log(A/T)$.

$$mb_{amp} = logat + Q(\Delta, h) - 3 \tag{11.2}$$

where the magnitude attenuation $Q(\Delta, h)$ value is calculated using the Gutenberg-Richter tables (*Gutenberg and Richter*, 1956).

For each reading the ISC locator finds the reported amplitude-period pair for which A/T is maximal:

$$mb_{rd} = log(max(A/T)) + Q(\Delta, h) - 3 \tag{11.3}$$

Or, if no amplitude-period pairs were reported for the reading:

$$mb_{rd} = max(logat) + Q(\Delta, h) - 3 \tag{11.4}$$

Several agencies may report data from the same station. The station magnitude is defined as the median of the reading magnitudes for a station.

$$mb_{sta} = median(mb_{rd}) \tag{11.5}$$

Once all station *mb* values are determined, the station magnitudes are sorted and the lower and upper alpha percentiles are made non-defining. The network *mb* and its uncertainty are then calculated as the median and the standard median absolute deviation (SMAD) of the alpha-trimmed station magnitudes, respectively.

Surface-Wave Magnitudes

Surface-wave magnitudes are calculated for each reported amplitude-period pair, provided that the phase is in the list of phases that can contribute to MS (*AMS, IAMs_20, LR, MLR, M, L*), the station is between the epicentral distances $20 - 160°$ and the period is between $10 - 60$ s.

For each reported amplitude-period pair MS is calculated using the Prague formula (*Vaněk et al.*, 1962). Amplitude MS is calculated for each component (Z, E, N) separately.

$$MS_{amp} = log(A/T) + 1.66 * log(\Delta) + 0.3 \quad (11.6)$$

To calculate the reading MS, the ISC locator first finds the reported amplitude-period pair for which A/T is maximal on the vertical component.

$$MS_Z = log(max(A_Z/T_Z)) + 1.66 * log(\Delta) + 0.3 \quad (11.7)$$

Then it finds the max(A/T) for the E and N components for which the period measured on the horizontal components is within ±5s from the period measured on the vertical component.

$$MS_E = log(max(A_E/T_E)) + 1.66 * log(\Delta) + 0.3 \quad (11.8)$$

$$MS_N = log(max(A_N/T_N)) + 1.66 * log(\Delta) + 0.3 \quad (11.9)$$

The horizontal MS is calculated as

$$max(A/T)h = \begin{cases} \sqrt{2(max(A_E/T_E))^2} & \text{if } MS_N \text{ does not exist} \\ \sqrt{(max(A_E/T_E))^2 + (max(A_N/T_N))^2} & \text{if } MS_E \text{ and } MS_N \text{ exist} \\ \sqrt{2(max(A_N/T_N))^2} & \text{if } MS_E \text{ does not exist} \end{cases} \quad (11.10)$$

$$MS_H = log(max(A/T)_H) + 1.66 * log(\Delta) + 0.3 \quad (11.11)$$

The reading MS is defined as

$$MS = \begin{cases} (MS_Z + MS_H)/2 & \text{if } MS_Z \text{ and } MS_H \text{ exist} \\ MS_H & \text{if } MS_Z \text{ does not exist} \\ MS_Z & \text{if } MS_H \text{ does not exist} \end{cases} \quad (11.12)$$

Several agencies may report data from the same station. The station magnitude is defined as the median of the reading magnitudes for a station.

$$MS_{sta} = median(MS_{rd}) \quad (11.13)$$

Once all station MS values are determined, the station magnitudes are sorted and the lower and upper alpha percentiles are made non-defining. The network MS and its uncertainty are calculated as the median and the standard median absolute deviation (SMAD) of the alpha-trimmed station magnitudes, respectively.

11.1.5 Review Process

Typically, for each month, the ISC analysts now review approximately 20% of the events in the ISC database, currently 3,500-5,000 per data month. This review is done about 24 months behind real time to allow for the comprehensive collection of data from networks and data centres worldwide.

Users of the ISC Bulletin can be assured that all ISC Bulletin events with an ISC hypocentre solution have been reviewed by the ISC analysts. Not all reviewed events will end up having an ISC hypocentre solution, but events that have not been reviewed are flagged accordingly.

An automatic process creates a monthly listing of the events for the analysts to review. The analysis is performed in batches: thus, events are generally not finalised one at a time, and a completed month of events is published after all the analysis is finished.

The first batch of editing involves careful examination of all events selected for review for the month. The entire month is then reprocessed incorporating the editing changes deemed necessary by the analysts. The analysts next review the same events again in a second pass through the data, checking for each event where there is a change that the result was as could be expected by comparing the revised solution against the initial solution. When the analysts are satisfied with an event, it is no longer revised in a subsequent pass but analysis continues in several passes until all events are considered satisfactory.

The analysts initially print the entire monthly listing, which is split into sections each with about 150 events. Each event, uniquely identified in the monthly printout, shows the reported hypocentres, magnitudes and phase arrivals grouped and associated for the event, as well as an ISC solution of hypocentre, if there is one, along with quality metrics, error estimates, redetermined magnitudes and phase arrival-time residuals. Ancillary information including the geographic region and reported macroseismic observations is also present in the listing for each pass.

The analysts have the capability to execute a variety of commands that can be used to merge or split events, to move phase arrivals or hypocentres from one event to another or to modify the reported phase names. Each of these changes initiates a new revision of the relevant events and ISC hypocentre solutions. There are also several commands to change the starting depth or location in the location algorithm.

The main tasks in reviewing the ISC Bulletin are to:

1. Check that the grouping of hypocentres and association of phase arrivals is appropriate.
2. Check that the depth and location is appropriate for the region and reported phase arrivals.
3. Check that no data are missing for an event, given the region and magnitude, and that included data are appropriate.

4. Examine the phase arrival-time residuals to check that the ISC hypocentre solution is appropriate.
5. Look for outliers in the observations and for misassociated phases.

As well as examining each event closely, it is also important to scan the hypocentres and phase arrivals of adjacent events, close in time and space, to ensure that there is uniformity in the composition of the events. In some cases, two events should be merged into one event, as apparent in some other case. In other cases, one apparent event needs to be split into two events, when the automatic grouping has erroneously created one event with more than one reported hypocentre out of the observations for two real events that are distinct but closely occurring.

Misassociated phase arrivals are returned to the unassociated data stream, if not immediately placed by the analyst in another event where they belong, These unassociated phases are then available to be associated with some other event if the time and location is appropriate. The analysts also check that no phase is associated to more than one event.

Towards the end of the monthly analysis, the ISC 'Search' procedure runs, attempting to build events from the remaining set of unassociated phase arrivals. The algorithm is based on the methodology of *Engdahl and Gunst* (1966). Candidate events are validated or rejected by attempting to find ISC hypocentres for them using the ISC locator. The surviving events are then reviewed. Those events with phase arrival observations reported by stations from at least two networks are added to the ISC Bulletin if the solutions meet the standards set by the ISC analysts. These events have only an ISC determination of hypocentre.

At the end of analysis for a data month, a set of final checks is run for quality control, with the results reviewed by an analyst and the defects rectified. These are checks for inconsistencies and errors to ensure the general integrity of the ISC Bulletin.

11.1.6 History of Operational Changes

- From data-month January 2001 onwards, both P and S groups of arrival times are used in location.
- From data-month September 2002 onwards, the printed ISC Bulletins have been generated directly from the ISC Relational Database.
- From data-month October 2002, a new location program ISCloc has been used in operations. Also, the IASPEI standard phase list has now been adopted by the ISC. Please see Section 11.2.1 for details.
- From data-month January 2003 onwards, an updated regionalisation scheme has been adopted (*Young et al.*, 1996).
- From data-month January 2006 the ISC hypocentres are computed using the *ak135* earth velocity model (*Kennett et al.*, 1995) and then reviewed by ISC seismologists. The ISC still produces the hypocentre solutions based on Jeffreys-Bullen travel time tables (agency code ISCJB), yet these solutions are no longer reviewed.

Currently, the ISC is re-computing the entire ISC Bulletin as part of the Rebuild Project using *ak135* and the new location program (Section 11.1.4) in order to assure homogeneity and consistency of the data in the ISC Bulletin.

- From data-month January 2009, a new location program (*Bondár and Storchak*, 2011) has been used in operations. The new program uses all predicted *ak135* phases and accounts for correlated model errors. An overview of the location algorithm is provided in this volume (Section 11.1.4).

11.2 IASPEI Standards

11.2.1 Standard Nomenclature of Seismic Phases

The following list of seismic phases was approved by the IASPEI Commission on Seismological Observation and Interpretation (CoSOI) and adopted by IASPEI on 9th July 2003. More details can be found in *Storchak et al.* (2003) and *Storchak et al.* (2011). Ray paths for some of these phases are shown in Figures 11.5–11.10.

Crustal Phases	
Pg	At short distances, either an upgoing P wave from a source in the upper crust or a P wave bottoming in the upper crust. At larger distances also, arrivals caused by multiple P-wave reverberations inside the whole crust with a group velocity around 5.8 km/s.
Pb	Either an upgoing P wave from a source in the lower crust or a P wave bottoming in the lower crust (alt: P*)
Pn	Any P wave bottoming in the uppermost mantle or an upgoing P wave from a source in the uppermost mantle
PnPn	Pn free-surface reflection
PgPg	Pg free-surface reflection
PmP	P reflection from the outer side of the Moho
PmP*N*	PmP multiple free surface reflection; *N* is a positive integer. For example, PmP2 is PmPPmP.
PmS	P to S reflection/conversion from the outer side of the Moho
Sg	At short distances, either an upgoing S wave from a source in the upper crust or an S wave bottoming in the upper crust. At larger distances also, arrivals caused by superposition of multiple S-wave reverberations and SV to P and/or P to SV conversions inside the whole crust.
Sb	Either an upgoing S wave from a source in the lower crust or an S wave bottoming in the lower crust (alt: S*)
Sn	Any S wave bottoming in the uppermost mantle or an upgoing S wave from a source in the uppermost mantle
SnSn	Sn free-surface reflection
SgSg	Sg free-surface reflection
SmS	S reflection from the outer side of the Moho
SmS*N*	SmS multiple free-surface reflection; *N* is a positive integer. For example, SmS2 is SmSSmS.
SmP	S to P reflection/conversion from the outer side of the Moho
Lg	A wave group observed at larger regional distances and caused by superposition of multiple S-wave reverberations and SV to P and/or P to SV conversions inside the whole crust. The maximum energy travels with a group velocity of approximately 3.5 km/s
Rg	Short-period crustal Rayleigh wave

Mantle Phases

P	A longitudinal wave, bottoming below the uppermost mantle; also an upgoing longitudinal wave from a source below the uppermost mantle
PP	Free-surface reflection of P wave leaving a source downward
PS	P, leaving a source downward, reflected as an S at the free surface. At shorter distances the first leg is represented by a crustal P wave.
PPP	Analogous to PP
PPS	PP which is converted to S at the second reflection point on the free surface; travel time matches that of PSP
PSS	PS reflected at the free surface
PcP	P reflection from the core-mantle boundary (CMB)
PcS	P converted to S when reflected from the CMB
PcPN	PcP reflected from the free surface N - 1 times; N is a positive integer. For example PcP2 is PcPPcP.
Pz+P	(alt: PzP) P reflection from outer side of a discontinuity at depth z; z may be a positive numerical value in km. For example, P660+P is a P reflection from the top of the 660 km discontinuity.
Pz-P	P reflection from inner side of a discontinuity at depth z. For example, P660-P is a P reflection from below the 660 km discontinuity, which means it is precursory to PP.
Pz+S	(alt:PzS) P converted to S when reflected from outer side of discontinuity at depth z
Pz-S	P converted to S when reflected from inner side of discontinuity at depth z
PScS	P (leaving a source downward) to ScS reflection at the free surface
Pdif	P diffracted along the CMB in the mantle (old: Pdiff)
S	Shear wave, bottoming below the uppermost mantle; also an upgoing shear wave from a source below the uppermost mantle
SS	Free-surface reflection of an S wave leaving a source downward
SP	S, leaving a source downward, reflected as P at the free surface. At shorter distances the second leg is represented by a crustal P wave.
SSS	Analogous to SS
SSP	SS converted to P when reflected from the free surface; travel time matches that of SPS
SPP	SP reflected at the free surface
ScS	S reflection from the CMB
ScP	S converted to P when reflected from the CMB
ScSN	ScS multiple free-surface reflection; N is a positive integer. For example ScS2 is ScSScS.
Sz+S	S reflection from outer side of a discontinuity at depth z; z may be a positive numerical value in km. For example S660+S is an S reflection from the top of the 660 km discontinuity. (alt: SzS)
Sz-S	S reflection from inner side of discontinuity at depth z. For example, S660-S is an S reflection from below the 660 km discontinuity, which means it is precursory to SS.
Sz+P	(alt: SzP) S converted to P when reflected from outer side of discontinuity at depth z
Sz-P	S converted to P when reflected from inner side of discontinuity at depth z
ScSP	ScS to P reflection at the free surface
Sdif	S diffracted along the CMB in the mantle (old: Sdiff)

Core Phases

PKP	Unspecified P wave bottoming in the core (alt: P')
PKPab	P wave bottoming in the upper outer core; ab indicates the retrograde branch of the PKP caustic (old: PKP2)
PKPbc	P wave bottoming in the lower outer core; bc indicates the prograde branch of the PKP caustic (old: PKP1)
PKPdf	P wave bottoming in the inner core (alt: PKIKP)

PKPpre	A precursor to PKPdf due to scattering near or at the CMB (old: PKhKP)
PKPdif	P wave diffracted at the inner core boundary (ICB) in the outer core
PKS	Unspecified P wave bottoming in the core and converting to S at the CMB
PKSab	PKS bottoming in the upper outer core
PKSbc	PKS bottoming in the lower outer core
PKSdf	PKS bottoming in the inner core
P'P'	Free-surface reflection of PKP (alt: PKPPKP)
P'*N*	PKP reflected at the free surface *N* - 1 times; *N* is a positive integer. For example, P'3 is P'P'P'. (alt: PKP*N*)
P'*z*-P'	PKP reflected from inner side of a discontinuity at depth *z* outside the core, which means it is precursory to P'P'; *z* may be a positive numerical value in km
P'S'	(alt: PKPSKS) PKP converted to SKS when reflected from the free surface; other examples are P'PKS, P'SKP
PS'	P (leaving a source downward) to SKS reflection at the free surface (alt: PSKS)
PKKP	Unspecified P wave reflected once from the inner side of the CMB
PKKPab	PKKP bottoming in the upper outer core
PKKPbc	PKKP bottoming in the lower outer core
PKKPdf	PKKP bottoming in the inner core
P*N*KP	P wave reflected *N* - 1 times from inner side of the CMB; *N* is a positive integer.
PKKPpre	A precursor to PKKP due to scattering near the CMB
PKiKP	P wave reflected from the inner core boundary (ICB)
PK*N*IKP	P wave reflected *N* - 1 times from the inner side of the ICB
PKJKP	P wave traversing the outer core as P and the inner core as S
PKKS	P wave reflected once from inner side of the CMB and converted to S at the CMB
PKKSab	PKKS bottoming in the upper outer core
PKKSbc	PKKS bottoming in the lower outer core
PKKSdf	PKKS bottoming in the inner core
PcPP'	PcP to PKP reflection at the free surface; other examples are PcPS', PcSP', PcSS', PcPSKP, PcSSKP. (alt: PcPPKP)
SKS	unspecified S wave traversing the core as P (alt: S')
SKSac	SKS bottoming in the outer core
SKSdf	SKS bottoming in the inner core (alt: SKIKS)
SPdifKS	SKS wave with a segment of mantleside Pdif at the source and/or the receiver side of the ray path (alt: SKPdifS)
SKP	Unspecified S wave traversing the core and then the mantle as P
SKPab	SKP bottoming in the upper outer core
SKPbc	SKP bottoming in the lower outer core
SKPdf	SKP bottoming in the inner core
S'S'	Free-surface reflection of SKS (alt: SKSSKS)
S'*N*	SKS reflected at the free surface *N* - 1 times; *N* is a positive integer
S'*z*-S'	SKS reflected from inner side of discontinuity at depth *z* outside the core, which means it is precursory to S'S'; *z* may be a positive numerical value in km.
S'P'	(alt: SKSPKP) SKS converted to PKP when reflected from the free surface; other examples are S'SKP, S'PKS.
S'P	(alt: SKSP) SKS to P reflection at the free surface
SKKS	Unspecified S wave reflected once from inner side of the CMB
SKKSac	SKKS bottoming in the outer core
SKKSdf	SKKS bottoming in the inner core
S*N*KS	S wave reflected *N* - 1 times from inner side of the CMB; *N* is a positive integer.
SKiKS	S wave traversing the outer core as P and reflected from the ICB
SKJKS	S wave traversing the outer core as P and the inner core as S
SKKP	S wave traversing the core as P with one reflection from the inner side of the CMB and then continuing as P in the mantle

SKKPab	SKKP bottoming in the upper outer core
SKKPbc	SKKP bottoming in the lower outer core
SKKPdf	SKKP bottoming in the inner core
ScSS'	ScS to SKS reflection at the free surface; other examples are ScPS', ScSP', ScPP', ScSSKP, ScPSKP. (alt: ScSSKS)

Near-source Surface reflections (Depth Phases)

pPy	All P-type onsets (Py), as defined above, which resulted from reflection of an upgoing P wave at the free surface or an ocean bottom. WARNING: The character y is only a wild card for any seismic phase, which could be generated at the free surface. Examples are pP, pPKP, pPP, pPcP, etc.
sPy	All Py resulting from reflection of an upgoing S wave at the free surface or an ocean bottom; for example, sP, sPKP, sPP, sPcP, etc.
pSy	All S-type onsets (Sy), as defined above, which resulted from reflection of an upgoing P wave at the free surface or an ocean bottom; for example, pS, pSKS, pSS, pScP, etc.
sSy	All Sy resulting from reflection of an upgoing S wave at the free surface or an ocean bottom; for example, sSn, sSS, sScS, sSdif, etc.
pwPy	All Py resulting from reflection of an upgoing P wave at the ocean's free surface
pmPy	All Py resulting from reflection of an upgoing P wave from the inner side of the Moho

Surface Waves

L	Unspecified long-period surface wave
LQ	Love wave
LR	Rayleigh wave
G	Mantle wave of Love type
GN	Mantle wave of Love type; N is integer and indicates wave packets traveling along the minor arcs (odd numbers) or major arc (even numbers) of the great circle
R	Mantle wave of Rayleigh type
RN	Mantle wave of Rayleigh type; N is integer and indicates wave packets traveling along the minor arcs (odd numbers) or major arc (even numbers) of the great circle
PL	Fundamental leaking mode following P onsets generated by coupling of P energy into the waveguide formed by the crust and upper mantle SPL S wave coupling into the PL waveguide; other examples are SSPL, SSSPL.

Acoustic Phases

H	A hydroacoustic wave from a source in the water, which couples in the ground
HPg	H phase converted to Pg at the receiver side
HSg	H phase converted to Sg at the receiver side
HRg	H phase converted to Rg at the receiver side
I	An atmospheric sound arrival which couples in the ground
IPg	I phase converted to Pg at the receiver side
ISg	I phase converted to Sg at the receiver side
IRg	I phase converted to Rg at the receiver side
T	A tertiary wave. This is an acoustic wave from a source in the solid earth, usually trapped in a low-velocity oceanic water layer called the SOFAR channel (SOund Fixing And Ranging).
TPg	T phase converted to Pg at the receiver side
TSg	T phase converted to Sg at the receiver side
TRg	T phase converted to Rg at the receiver side

Amplitude Measurement Phases

The following set of amplitude measurement names refers to the IASPEI Magnitude Standard (see www.iaspei.org/commissions/CSOI/Summary_of_WG_recommendations.pdf) compliance to which is indicated by the presence of leading letter I. The absence of leading letter I indicates that a measurement is non-standard. Letter A indicates a measurement in nm made on a displacement seismogram, whereas letter V indicates a measurement in nm/s made on a velocity seismogram.

IAML	Displacement amplitude measured according to the IASPEI standard for local magnitude ML
IAMs_20	Displacement amplitude measured according to IASPEI standard for surface-wave magnitude $MS(20)$
IVMs_BB	Velocity amplitude measured according to IASPEI standard for broadband surface-wave magnitude $MS(BB)$
IAmb	Displacement amplitude measured according to IASPEI standard for short-period teleseismic body-wave magnitude mb
IVmB_BB	Velocity amplitude measured according to IASPEI standard for broadband teleseismic body-wave magnitude $mB(BB)$
AX_IN	Displacement amplitude of phase of type X (e.g., PP, S, etc), measured on an instrument of type IN (e.g., SP - short-period, LP - long-period, BB - broadband)
VX_IN	Velocity amplitude of phase of type X and instrument of type IN (as above)
A	Unspecified displacement amplitude measurement
V	Unspecified velocity amplitude measurement
AML	Displacement amplitude measurement for nonstandard local magnitude
AMs	Displacement amplitude measurement for nonstandard surface-wave magnitude
Amb	Displacement amplitude measurement for nonstandard short-period body-wave magnitude
AmB	Displacement amplitude measurement for nonstandard medium to long-period body-wave magnitude
END	Time of visible end of record for duration magnitude

Unidentified Arrivals

x	unidentified arrival (old: i, e, NULL)
rx	unidentified regional arrival (old: i, e, NULL)
tx	unidentified teleseismic arrival (old: i, e, NULL)
Px	unidentified arrival of P type (old: i, e, NULL, (P), P?)
Sx	unidentified arrival of S type (old: i, e, NULL, (S), S?)

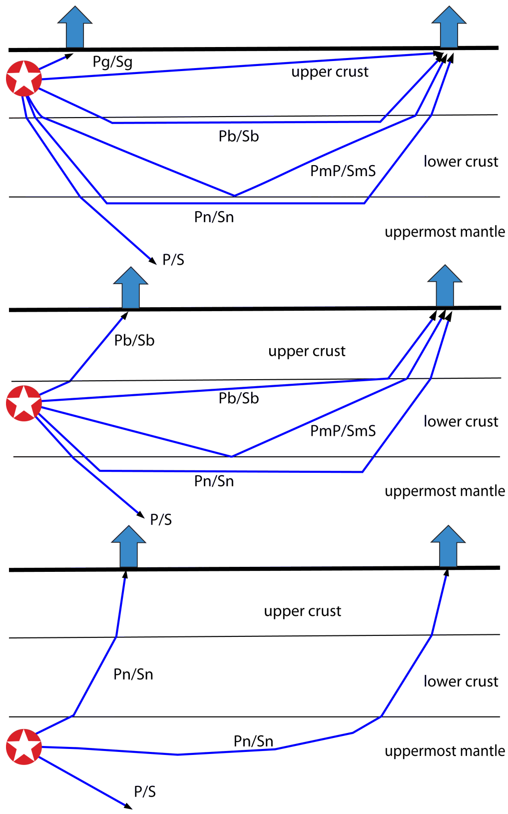

Figure 11.5: *Seismic 'crustal phases' observed in the case of a two-layer crust in local and regional distance ranges (0°<D< about 20°) from the seismic source in the: upper crust (top); lower crust (middle); and uppermost mantle (bottom).*

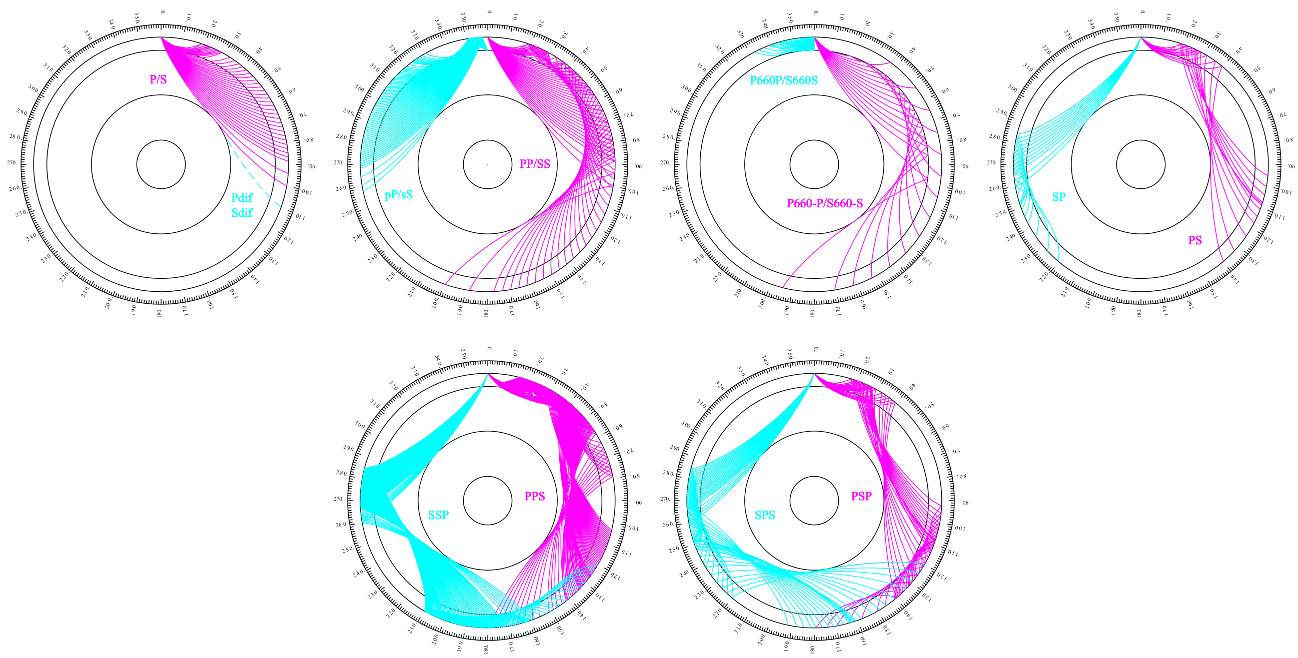

Figure 11.6: *Mantle phases observed at the teleseismic distance range D > about 20°.*

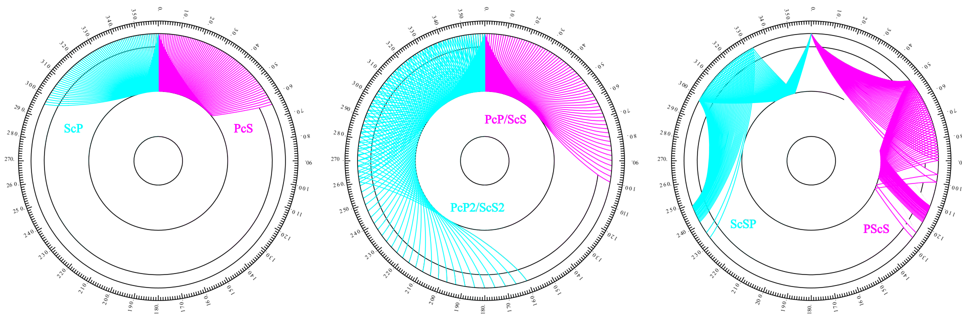

Figure 11.7: *Reflections from the Earth's core.*

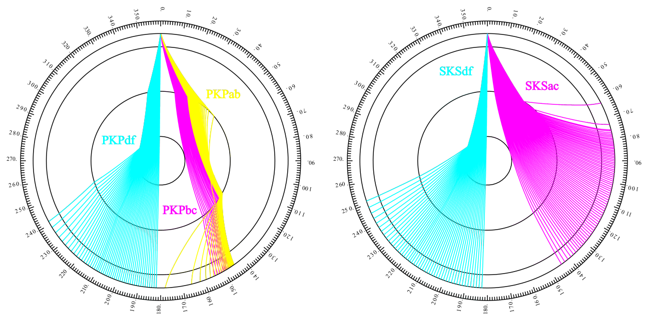

Figure 11.8: *Seismic rays of direct core phases.*

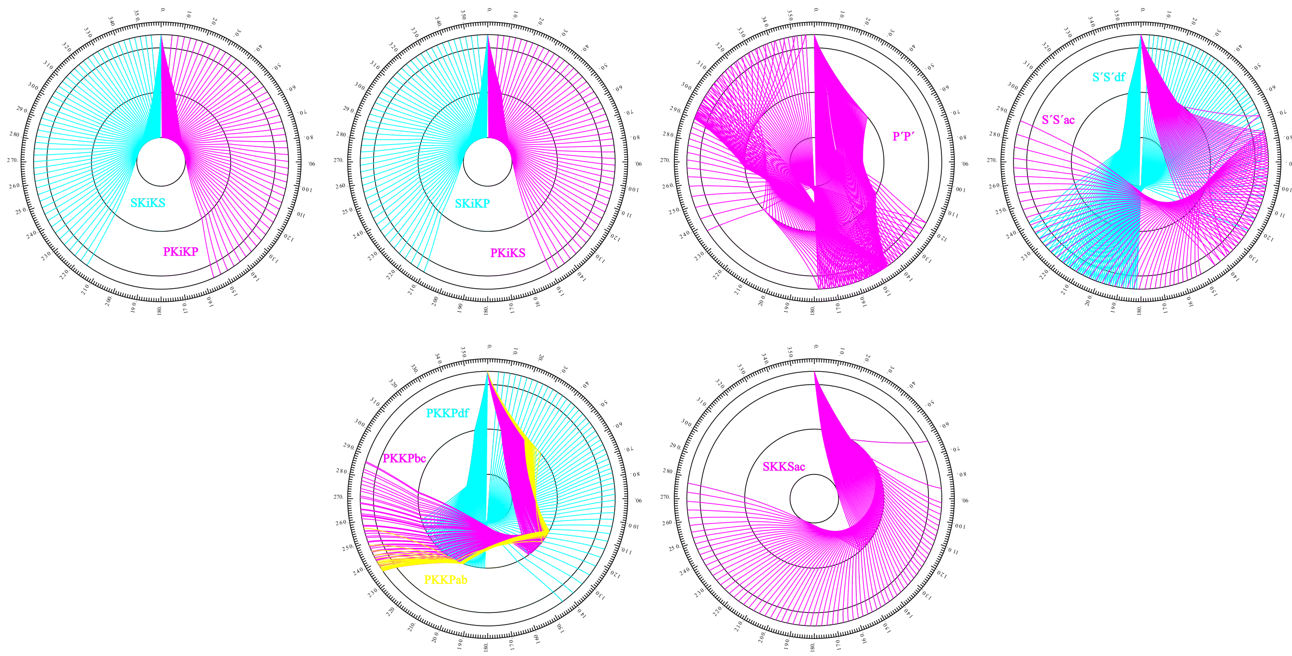

Figure 11.9: *Seismic rays of single-reflected core phases.*

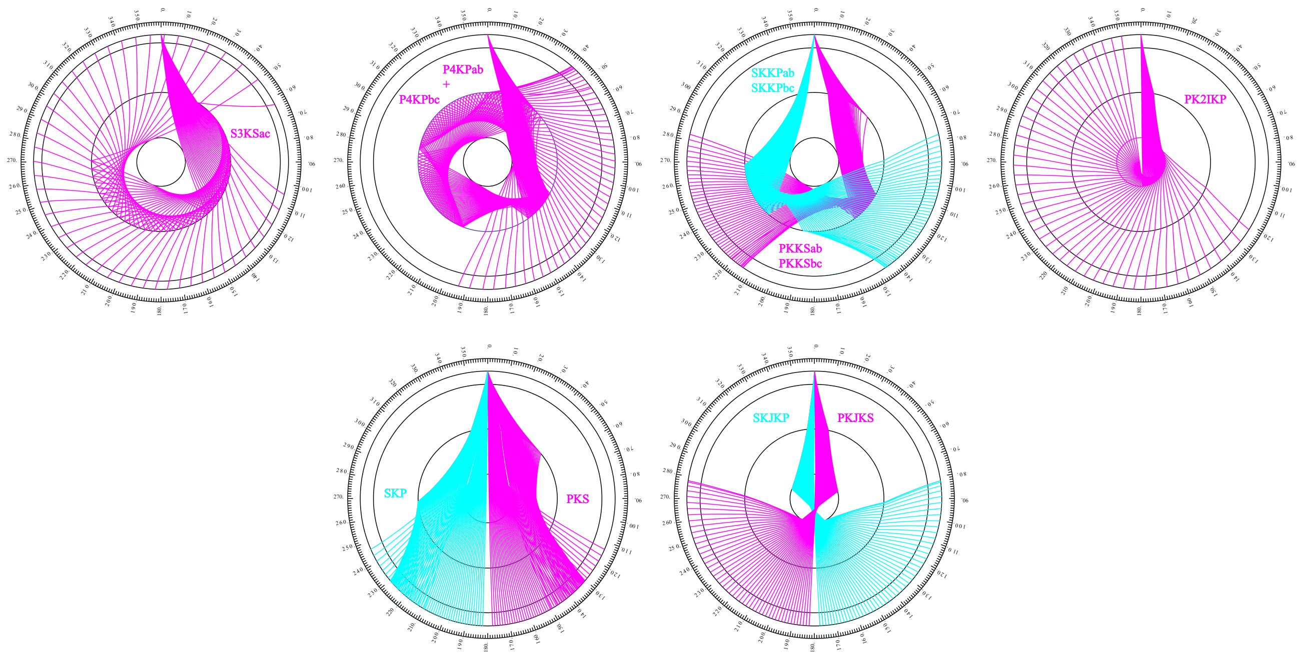

Figure 11.10: *Seismic rays of multiple-reflected and converted core phases.*

11.2.2 Flinn-Engdahl Regions

The Flinn-Engdahl regions were first proposed by *Flinn and Engdahl* (1965), with the standard defined by *Flinn et al.* (1974). The latest version of the schema, published by *Young et al.* (1996), divides the Earth into 50 seismic regions (Figure 11.11), which are further subdivided producing a total of 754 geographical regions (listed below). The geographic regions are numbered 1 to 757 with regions 172, 299 and 550 no longer in use. The boundaries of these regions are defined at one-degree intervals.

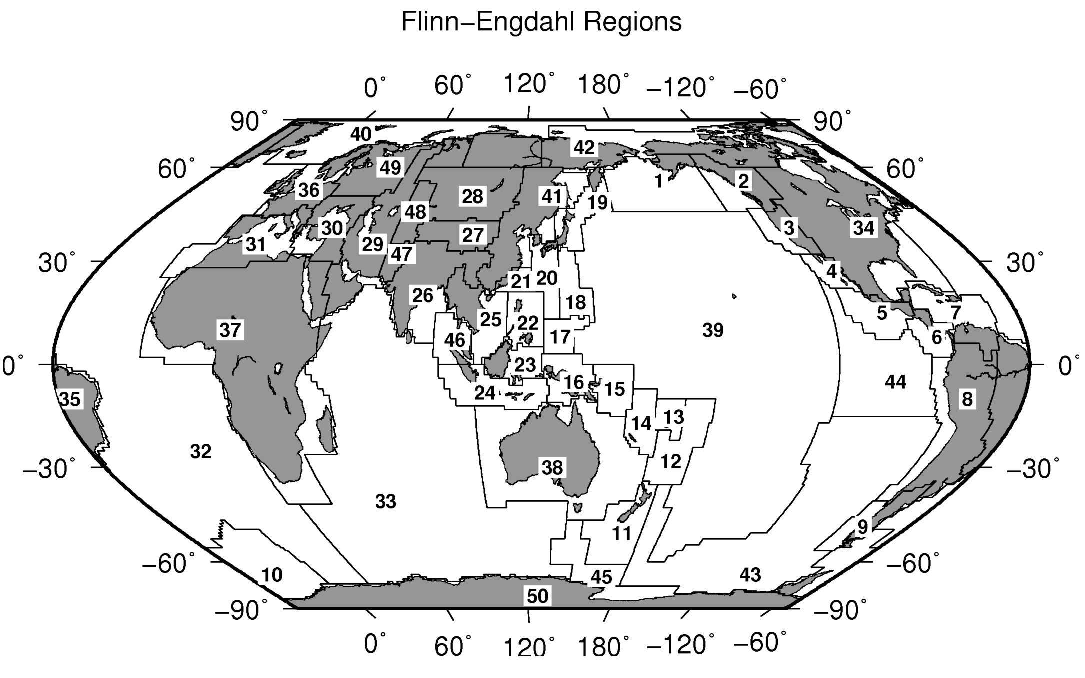

Figure 11.11: *Map of all Flinn-Engdahl seismic regions.*

Seismic Region 1
Alaska-Aleutian Arc
1. Central Alaska
2. Southern Alaska
3. Bering Sea
4. Komandorsky Islands region
5. Near Islands
6. Rat Islands
7. Andreanof Islands
8. Pribilof Islands
9. Fox Islands
10. Unimak Island region
11. Bristol Bay
12. Alaska Peninsula
13. Kodiak Island region
14. Kenai Peninsula
15. Gulf of Alaska
16. South of Aleutian Islands
17. South of Alaska

Seismic Region 2
Eastern Alaska to Vancouver Island
18. Southern Yukon Territory
19. Southeastern Alaska
20. Off coast of southeastern Alaska
21. West of Vancouver Island
22. Queen Charlotte Islands region
23. British Columbia
24. Alberta
25. Vancouver Island region
26. Off coast of Washington
27. Near coast of Washington
28. Washington-Oregon border region
29. Washington

Seismic Region 3
California-Nevada Region
30. Off coast of Oregon
31. Near coast of Oregon
32. Oregon
33. Western Idaho
34. Off coast of northern California
35. Near coast of northern California
36. Northern California
37. Nevada
38. Off coast of California
39. Central California
40. California-Nevada border region
41. Southern Nevada
42. Western Arizona
43. Southern California
44. California-Arizona border region
45. California-Baja California border region
46. Western Arizona-Sonora border region

Seismic Region 4
Lower California and Gulf of California
47. Off west coast of Baja California
48. Baja California
49. Gulf of California
50. Sonora
51. Off coast of central Mexico
52. Near coast of central Mexico

Seismic Region 5
Mexico-Guatemala Area
53. Revilla Gigedo Islands region
54. Off coast of Jalisco
55. Near coast of Jalisco
56. Near coast of Michoacan
57. Michoacan
58. Near coast of Guerrero
59. Guerrero
60. Oaxaca
61. Chiapas
62. Mexico-Guatemala border region
63. Off coast of Mexico
64. Off coast of Michoacan
65. Off coast of Guerrero
66. Near coast of Oaxaca
67. Off coast of Oaxaca
68. Off coast of Chiapas
69. Near coast of Chiapas
70. Guatemala
71. Near coast of Guatemala
730. Northern East Pacific Rise

Seismic Region 6
Central America
72. Honduras
73. El Salvador
74. Near coast of Nicaragua
75. Nicaragua
76. Off coast of central America
77. Off coast of Costa Rica
78. Costa Rica
79. North of Panama
80. Panama-Costa Rica border region
81. Panama
82. Panama-Colombia border region
83. South of Panama

Seismic Region 7
Caribbean Loop
84. Yucatan Peninsula
85. Cuba region
86. Jamaica region
87. Haiti region
88. Dominican Republic region
89. Mona Passage
90. Puerto Rico region
91. Virgin Islands
92. Leeward Islands
93. Belize
94. Caribbean Sea
95. Windward Islands
96. Near north coast of Colombia
97. Near coast of Venezuela
98. Trinidad
99. Northern Colombia
100. Lake Maracaibo
101. Venezuela
731. North of Honduras

Seismic Region 8
Andean South America
102. Near west coast of Colombia
103. Colombia
104. Off coast of Ecuador
105. Near coast of Ecuador
106. Colombia-Ecuador border region
107. Ecuador
108. Off coast of northern Peru
109. Near coast of northern Peru
110. Peru-Ecuador border region
111. Northern Peru
112. Peru-Brazil border region
113. Western Brazil
114. Off coast of Peru
115. Near coast of Peru
116. Central Peru
117. Southern Peru
118. Peru-Bolivia border region
119. Northern Bolivia
120. Central Bolivia
121. Off coast of northern Chile
122. Near coast of northern Chile
123. Northern Chile
124. Chile-Bolivia border region
125. Southern Bolivia
126. Paraguay
127. Chile-Argentina border region
128. Jujuy Province
129. Salta Province
130. Catamarca Province
131. Tucuman Province
132. Santiago del Estero Province
133. Northeastern Argentina
134. Off coast of central Chile
135. Near coast of central Chile
136. Central Chile
137. San Juan Province
138. La Rioja Province
139. Mendoza Province

140. San Luis Province
141. Cordoba Province
142. Uruguay

Seismic Region 9
Extreme South America
143. Off coast of southern Chile
144. Southern Chile
145. Southern Chile-Argentina border region
146. Southern Argentina

Seismic Region 10
Southern Antilles
147. Tierra del Fuego
148. Falkland Islands region
149. Drake Passage
150. Scotia Sea
151. South Georgia Island region
152. South Georgia Rise
153. South Sandwich Islands region
154. South Shetland Islands
155. Antarctic Peninsula
156. Southwestern Atlantic Ocean
157. Weddell Sea
732. East of South Sandwich Islands

Seismic Region 11
New Zealand Region
158. Off west coast of North Island
159. North Island
160. Off east coast of North Island
161. Off west coast of South Island
162. South Island
163. Cook Strait
164. Off east coast of South Island
165. North of Macquarie Island
166. Auckland Islands region
167. Macquarie Island region
168. South of New Zealand

Seismic Region 12
Kermadec-Tonga-Samoa Area
169. Samoa Islands region
170. Samoa Islands
171. South of Fiji Islands
172. West of Tonga Islands (REGION NOT IN USE)
173. Tonga Islands
174. Tonga Islands region
175. South of Tonga Islands
176. North of New Zealand
177. Kermadec Islands region
178. Kermadec Islands
179. South of Kermadec Islands

Seismic Region 13
Fiji Area
180. North of Fiji Islands
181. Fiji Islands region
182. Fiji Islands

Seismic Region 14
Vanuatu (New Hebrides)
183. Santa Cruz Islands region
184. Santa Cruz Islands
185. Vanuatu Islands region
186. Vanuatu Islands
187. New Caledonia
188. Loyalty Islands
189. Southeast of Loyalty Islands

Seismic Region 15
Bismarck and Solomon Islands
190. New Ireland region
191. North of Solomon Islands
192. New Britain region
193. Bougainville-Solomon Islands region
194. D'Entrecasteaux Islands region
195. South of Solomon Islands

Seismic Region 16
New Guinea
196. Irian Jaya region
197. Near north coast of Irian Jaya
198. Ninigo Islands region
199. Admiralty Islands region
200. Near north coast of New Guinea
201. Irian Jaya
202. New Guinea
203. Bismarck Sea
204. Aru Islands region
205. Near south coast of Irian Jaya
206. Near south coast of New Guinea
207. Eastern New Guinea region
208. Arafura Sea

Seismic Region 17
Caroline Islands to Guam
209. Western Caroline Islands
210. South of Mariana Islands

Seismic Region 18
Guam to Japan
211. Southeast of Honshu
212. Bonin Islands region
213. Volcano Islands region
214. West of Mariana Islands
215. Mariana Islands region
216. Mariana Islands

Seismic Region 19
Japan-Kurils-Kamchatka
217. Kamchatka Peninsula
218. Near east coast of Kamchatka Peninsula
219. Off east coast of Kamchatka Peninsula
220. Northwest of Kuril Islands
221. Kuril Islands
222. East of Kuril Islands
223. Eastern Sea of Japan
224. Hokkaido region
225. Off southeast coast of Hokkaido
226. Near west coast of eastern Honshu
227. Eastern Honshu
228. Near east coast of eastern Honshu
229. Off east coast of Honshu
230. Near south coast of eastern Honshu

Seismic Region 20
Southwestern Japan and Ryukyu Islands
231. South Korea
232. Western Honshu
233. Near south coast of western Honshu
234. Northwest of Ryukyu Islands
235. Kyushu
236. Shikoku
237. Southeast of Shikoku
238. Ryukyu Islands
239. Southeast of Ryukyu Islands
240. West of Bonin Islands
241. Philippine Sea

Seismic Region 21
Taiwan
242. Near coast of southeastern China
243. Taiwan region
244. Taiwan
245. Northeast of Taiwan
246. Southwestern Ryukyu Islands
247. Southeast of Taiwan

Seismic Region 22
Philippines
248. Philippine Islands region
249. Luzon
250. Mindoro
251. Samar
252. Palawan
253. Sulu Sea
254. Panay

255. Cebu
256. Leyte
257. Negros
258. Sulu Archipelago
259. Mindanao
260. East of Philippine Islands

Seismic Region 23
Borneo-Sulawesi
261. Borneo
262. Celebes Sea
263. Talaud Islands
264. North of Halmahera
265. Minahassa Peninsula, Sulawesi
266. Northern Molucca Sea
267. Halmahera
268. Sulawesi
269. Southern Molucca Sea
270. Ceram Sea
271. Buru
272. Seram

Seismic Region 24
Sunda Arc
273. Southwest of Sumatera
274. Southern Sumatera
275. Java Sea
276. Sunda Strait
277. Jawa
278. Bali Sea
279. Flores Sea
280. Banda Sea
281. Tanimbar Islands region
282. South of Jawa
283. Bali region
284. South of Bali
285. Sumbawa region
286. Flores region
287. Sumba region
288. Savu Sea
289. Timor region
290. Timor Sea
291. South of Sumbawa
292. South of Sumba
293. South of Timor

Seismic Region 25
Myanmar and Southeast Asia
294. Myanmar-India border region
295. Myanmar-Bangladesh border region
296. Myanmar
297. Myanmar-China border region
298. Near south coast of Myanmar
299. Southeast Asia (REGION NOT IN USE)
300. Hainan Island
301. South China Sea
733. Thailand
734. Laos
735. Kampuchea
736. Vietnam
737. Gulf of Tongking

Seismic Region 26
India-Xizang-Szechwan-Yunnan
302. Eastern Kashmir
303. Kashmir-India border region
304. Kashmir-Xizang border region
305. Western Xizang-India border region
306. Xizang
307. Sichuan
308. Northern India
309. Nepal-India border region
310. Nepal
311. Sikkim
312. Bhutan
313. Eastern Xizang-India border region
314. Southern India
315. India-Bangladesh border region
316. Bangladesh
317. Northeastern India
318. Yunnan
319. Bay of Bengal

Seismic Region 27
Southern Xinjiang to Gansu
320. Kyrgyzstan-Xinjiang border region
321. Southern Xinjiang
322. Gansu
323. Western Nei Mongol
324. Kashmir-Xinjiang border region
325. Qinghai

Seismic Region 28
Alma-Ata to Lake Baikal
326. Southwestern Siberia
327. Lake Baykal region
328. East of Lake Baykal
329. Eastern Kazakhstan
330. Lake Issyk-Kul region
331. Kazakhstan-Xinjiang border region
332. Northern Xinjiang
333. Tuva-Buryatia-Mongolia border region
334. Mongolia

Seismic Region 29
Western Asia
335. Ural Mountains region
336. Western Kazakhstan
337. Eastern Caucasus
338. Caspian Sea
339. Northwestern Uzbekistan
340. Turkmenistan
341. Iran-Turkmenistan border region
342. Turkmenistan-Afghanistan border region
343. Turkey-Iran border region
344. Iran-Armenia-Azerbaijan border region
345. Northwestern Iran
346. Iran-Iraq border region
347. Western Iran
348. Northern and central Iran
349. Northwestern Afghanistan
350. Southwestern Afghanistan
351. Eastern Arabian Peninsula
352. Persian Gulf
353. Southern Iran
354. Southwestern Pakistan
355. Gulf of Oman
356. Off coast of Pakistan

Seismic Region 30
Middle East-Crimea-Eastern Balkans
357. Ukraine-Moldova-Southwestern Russia region
358. Romania
359. Bulgaria
360. Black Sea
361. Crimea region
362. Western Caucasus
363. Greece-Bulgaria border region
364. Greece
365. Aegean Sea
366. Turkey
367. Turkey-Georgia-Armenia border region
368. Southern Greece
369. Dodecanese Islands
370. Crete
371. Eastern Mediterranean Sea
372. Cyprus region
373. Dead Sea region
374. Jordan-Syria region
375. Iraq

Seismic Region 31
Western Mediterranean Area
376. Portugal
377. Spain

378. Pyrenees
379. Near south coast of France
380. Corsica
381. Central Italy
382. Adriatic Sea
383. Northwestern Balkan Peninsula
384. West of Gibraltar
385. Strait of Gibraltar
386. Balearic Islands
387. Western Mediterranean Sea
388. Sardinia
389. Tyrrhenian Sea
390. Southern Italy
391. Albania
392. Greece-Albania border region
393. Madeira Islands region
394. Canary Islands region
395. Morocco
396. Northern Algeria
397. Tunisia
398. Sicily
399. Ionian Sea
400. Central Mediterranean Sea
401. Near coast of Libya

Seismic Region 32
Atlantic Ocean

402. North Atlantic Ocean
403. Northern Mid-Atlantic Ridge
404. Azores Islands region
405. Azores Islands
406. Central Mid-Atlantic Ridge
407. North of Ascension Island
408. Ascension Island region
409. South Atlantic Ocean
410. Southern Mid-Atlantic Ridge
411. Tristan da Cunha region
412. Bouvet Island region
413. Southwest of Africa
414. Southeastern Atlantic Ocean
738. Reykjanes Ridge
739. Azores-Cape St. Vincent Ridge

Seismic Region 33
Indian Ocean

415. Eastern Gulf of Aden
416. Socotra region
417. Arabian Sea
418. Lakshadweep region
419. Northeastern Somalia
420. North Indian Ocean
421. Carlsberg Ridge
422. Maldive Islands region
423. Laccadive Sea
424. Sri Lanka
425. South Indian Ocean
426. Chagos Archipelago region
427. Mauritius-Reunion region
428. Southwest Indian Ridge
429. Mid-Indian Ridge
430. South of Africa
431. Prince Edward Islands region
432. Crozet Islands region
433. Kerguelen Islands region
434. Broken Ridge
435. Southeast Indian Ridge
436. Southern Kerguelen Plateau
437. South of Australia
740. Owen Fracture Zone region
741. Indian Ocean Triple Junction
742. Western Indian-Antarctic Ridge

Seismic Region 34
Eastern North America

438. Saskatchewan
439. Manitoba
440. Hudson Bay
441. Ontario
442. Hudson Strait region
443. Northern Quebec
444. Davis Strait
445. Labrador
446. Labrador Sea
447. Southern Quebec
448. Gaspe Peninsula
449. Eastern Quebec
450. Anticosti Island
451. New Brunswick
452. Nova Scotia
453. Prince Edward Island
454. Gulf of St. Lawrence
455. Newfoundland
456. Montana
457. Eastern Idaho
458. Hebgen Lake region, Montana
459. Yellowstone region
460. Wyoming
461. North Dakota
462. South Dakota
463. Nebraska
464. Minnesota
465. Iowa
466. Wisconsin
467. Illinois
468. Michigan
469. Indiana
470. Southern Ontario
471. Ohio
472. New York
473. Pennsylvania
474. Vermont-New Hampshire region
475. Maine
476. Southern New England
477. Gulf of Maine
478. Utah
479. Colorado
480. Kansas
481. Iowa-Missouri border region
482. Missouri-Kansas border region
483. Missouri
484. Missouri-Arkansas border region
485. Missouri-Illinois border region
486. New Madrid region, Missouri
487. Cape Girardeau region, Missouri
488. Southern Illinois
489. Southern Indiana
490. Kentucky
491. West Virginia
492. Virginia
493. Chesapeake Bay region
494. New Jersey
495. Eastern Arizona
496. New Mexico
497. Northwestern Texas-Oklahoma border region
498. Western Texas
499. Oklahoma
500. Central Texas
501. Arkansas-Oklahoma border region
502. Arkansas
503. Louisiana-Texas border region
504. Louisiana
505. Mississippi
506. Tennessee
507. Alabama
508. Western Florida
509. Georgia
510. Florida-Georgia border region
511. South Carolina
512. North Carolina
513. Off east coast of United States
514. Florida Peninsula
515. Bahama Islands
516. Eastern Arizona-Sonora border region
517. New Mexico-Chihuahua border region
518. Texas-Mexico border region
519. Southern Texas
520. Near coast of Texas
521. Chihuahua
522. Northern Mexico
523. Central Mexico
524. Jalisco
525. Veracruz
526. Gulf of Mexico
527. Bay of Campeche

Seismic Region 35
Eastern South America
528. Brazil
529. Guyana
530. Suriname
531. French Guiana

Seismic Region 36
Northwestern Europe
532. Eire
533. United Kingdom
534. North Sea
535. Southern Norway
536. Sweden
537. Baltic Sea
538. France
539. Bay of Biscay
540. The Netherlands
541. Belgium
542. Denmark
543. Germany
544. Switzerland
545. Northern Italy
546. Austria
547. Czech and Slovak Republics
548. Poland
549. Hungary

Seismic Region 37
Africa
550. Northwest Africa (REGION NOT IN USE)
551. Southern Algeria
552. Libya
553. Egypt
554. Red Sea
555. Western Arabian Peninsula
556. Chad region
557. Sudan
558. Ethiopia
559. Western Gulf of Aden
560. Northwestern Somalia
561. Off south coast of northwest Africa
562. Cameroon
563. Equatorial Guinea
564. Central African Republic
565. Gabon
566. Congo
567. Zaire
568. Uganda
569. Lake Victoria region
570. Kenya
571. Southern Somalia
572. Lake Tanganyika region
573. Tanzania
574. Northwest of Madagascar
575. Angola
576. Zambia
577. Malawi
578. Namibia
579. Botswana
580. Zimbabwe
581. Mozambique
582. Mozambique Channel
583. Madagascar
584. South Africa
585. Lesotho
586. Swaziland
587. Off coast of South Africa
743. Western Sahara
744. Mauritania
745. Mali
746. Senegal-Gambia region
747. Guinea region
748. Sierra Leone
749. Liberia region
750. Cote d'Ivoire
751. Burkina Faso
752. Ghana
753. Benin-Togo region
754. Niger
755. Nigeria

Seismic Region 38
Australia
588. Northwest of Australia
589. West of Australia
590. Western Australia
591. Northern Territory
592. South Australia
593. Gulf of Carpentaria
594. Queensland
595. Coral Sea
596. Northwest of New Caledonia
597. New Caledonia region
598. Southwest of Australia
599. Off south coast of Australia
600. Near coast of South Australia
601. New South Wales
602. Victoria
603. Near southeast coast of Australia
604. Near east coast of Australia
605. East of Australia
606. Norfolk Island region
607. Northwest of New Zealand
608. Bass Strait
609. Tasmania region
610. Southeast of Australia

Seismic Region 39
Pacific Basin
611. North Pacific Ocean
612. Hawaiian Islands region
613. Hawaiian Islands
614. Eastern Caroline Islands region
615. Marshall Islands region
616. Enewetak Atoll region
617. Bikini Atoll region
618. Gilbert Islands region
619. Johnston Island region
620. Line Islands region
621. Palmyra Island region
622. Kiritimati region
623. Tuvalu region
624. Phoenix Islands region
625. Tokelau Islands region
626. Northern Cook Islands
627. Cook Islands region
628. Society Islands region
629. Tubuai Islands region
630. Marquesas Islands region
631. Tuamotu Archipelago region
632. South Pacific Ocean

Seismic Region 40
Arctic Zone
633. Lomonosov Ridge
634. Arctic Ocean
635. Near north coast of Kalaallit Nunaat
636. Eastern Kalaallit Nunaat
637. Iceland region
638. Iceland
639. Jan Mayen Island region
640. Greenland Sea
641. North of Svalbard
642. Norwegian Sea
643. Svalbard region
644. North of Franz Josef Land
645. Franz Josef Land
646. Northern Norway
647. Barents Sea
648. Novaya Zemlya
649. Kara Sea
650. Near coast of northwestern Siberia
651. North of Severnaya Zemlya
652. Severnaya Zemlya
653. Near coast of northern Siberia
654. East of Severnaya Zemlya
655. Laptev Sea

Seismic Region 41
Eastern Asia
656. Southeastern Siberia
657. Priamurye-Northeastern China border region
658. Northeastern China
659. North Korea

660. Sea of Japan
661. Primorye
662. Sakhalin Island
663. Sea of Okhotsk
664. Southeastern China
665. Yellow Sea
666. Off east coast of southeastern China

Seismic Region 42
Northeastern Asia, Northern Alaska to Greenland
667. North of New Siberian Islands
668. New Siberian Islands
669. Eastern Siberian Sea
670. Near north coast of eastern Siberia
671. Eastern Siberia
672. Chukchi Sea
673. Bering Strait
674. St. Lawrence Island region
675. Beaufort Sea
676. Northern Alaska
677. Northern Yukon Territory
678. Queen Elizabeth Islands
679. Northwest Territories
680. Western Kalaallit Nunaat
681. Baffin Bay
682. Baffin Island region

Seismic Region 43
Southeastern and Antarctic Pacific Ocean
683. Southeastcentral Pacific Ocean
684. Southern East Pacific Rise
685. Easter Island region
686. West Chile Rise
687. Juan Fernandez Islands region
688. East of North Island
689. Chatham Islands region
690. South of Chatham Islands
691. Pacific-Antarctic Ridge
692. Southern Pacific Ocean
756. Southeast of Easter Island

Seismic Region 44
Galapagos Area
693. Eastcentral Pacific Ocean
694. Central East Pacific Rise
695. West of Galapagos Islands
696. Galapagos Islands region
697. Galapagos Islands
698. Southwest of Galapagos Islands
699. Southeast of Galapagos Islands
757. Galapagos Triple Junction region

Seismic Region 45
Macquarie Loop
700. South of Tasmania
701. West of Macquarie Island
702. Balleny Islands region

Seismic Region 46
Andaman Islands to Sumatera
703. Andaman Islands region
704. Nicobar Islands region
705. Off west coast of northern Sumatera
706. Northern Sumatera
707. Malay Peninsula
708. Gulf of Thailand

Seismic Region 47
Baluchistan
709. Southeastern Afghanistan
710. Pakistan
711. Southwestern Kashmir
712. India-Pakistan border region

Seismic Region 48
Hindu Kush and Pamir
713. Central Kazakhstan
714. Southeastern Uzbekistan
715. Tajikistan
716. Kyrgyzstan
717. Afghanistan-Tajikistan border region
718. Hindu Kush region
719. Tajikistan-Xinjiang border region
720. Northwestern Kashmir

Seismic Region 49
Northern Eurasia
721. Finland
722. Norway-Murmansk border region
723. Finland-Karelia border region
724. Baltic States-Belarus-Northwestern Russia
725. Northwestern Siberia
726. Northern and central Siberia

Seismic Region 50
Antarctica
727. Victoria Land
728. Ross Sea
729. Antarctica

11.2.3 IASPEI Magnitudes

The ISC publishes a diversity of magnitude data. Although trying to be as complete and specific as possible, preference is now given to magnitudes determined according to standard procedures recommended by the Working Group on Magnitude Measurements of the IASPEI Commission on Seismological Observation and Interpretation (CoSOI). So far, such standards have been agreed upon for the local magnitude ML, the local-regional mb_Lg, and for two types each of body-wave (*mb* and mB_BB) and surface-wave magnitudes (Ms_20 and Ms_BB). With the exception of ML, all other standard magnitudes are measured on vertical-component records only. BB stands for direct measurement on unfiltered velocity broadband records in a wide range of periods, provided that their passband covers at least the period range within which mB_BB and Ms_BB are supposed to be measured. Otherwise, a deconvolution has to be applied prior to the amplitude and period measurement so as to assure that this specification is met. In contrast, mb_Lg, *mb* and Ms_20 are based on narrowband amplitude measurements around periods of 1 s and 20 s, respectively.

ML is consistent with the original definition of the local magnitude by *Richter* (1935) and mB_BB in close agreement with the original definition of medium-period body-wave magnitude mB measured in a wide range of periods between some 2 to 20 s and calibrated with the *Gutenberg and Richter* (1956) Q-function for vertical-component P waves. Similarly, Ms_BB is best tuned to the unbiased use of the IASPEI (1967) recommended standard magnitude formula for surface-wave amplitudes in a wide range of periods and distances, as proposed by its authors *Vaněk et al.* (1962). In contrast, *mb* and Ms_20 are chiefly based on measurement standards defined by US agencies in the 1960s in conjunction with the global deployment of the World-Wide Standard Seismograph Network (WWSSN), which did not include medium or broadband recordings. Some modifications were made in the 1970s to account for IASPEI recommendations on extended measurement time windows for *mb*. Although not optimal for calibrating narrow-band spectral amplitudes measured around 1 s and 20 s only, *mb* and Ms_20 use the same original calibrations functions as mB_BB and Ms_BB. But *mb* and Ms_20 data constitute by far the largest available magnitude data sets. Therefore they continue to be used, with appreciation for their advantages (e.g., *mb* is by far the most frequently measured teleseismic magnitude and often the only available and reasonably good magnitude estimator for small earthquakes) and their shortcomings (see section 3.2.5.2 of Chapter 3 in NMSOP-2).

Abbreviated descriptions of the standard procedures for ML, mb_Lg, *mb*, mB_BB and Ms_BB are summarised below. For more details, including also the transfer functions of the simulation filters to be used, see www.iaspei.org/commissions/CSOI/Summary_WG-Recommendations_20130327.pdf.

All amplitudes used in the magnitude formulas below are in most circumstances to be measured as one-half the maximum deflection of the seismogram trace, peak-to-adjacent-trough or trough-to-adjacent-peak, where the peak and trough are separated by one crossing of the zero-line: this measurement is sometimes described as "one-half peak-to-peak amplitude." The periods are to be measured as twice the time-intervals separating the peak and adjacent-trough from which the amplitudes are measured. The amplitude-phase arrival-times are to be measured and reported too as the time of the zero-crossing between the peak and adjacent-trough from which the amplitudes are measured. The issue of amplitude and period measuring procedures, and circumstances under which alternative procedures are acceptable or preferable, is discussed further in Section 5 of IS 3.3 and in section 3.2.3.3 of Chapter 3 of NMSOP-2.

Amplitudes measured according to recommended IASPEI standard procedures should be reported with the following ISF amplitude "phase names": IAML, IAmb_Lg, IAmb, IAMs_20, IVmB_BB and IVMs_BB. "I" stands for "International" or "IASPEI", "A" for displacement amplitude, measured in nm, and "V" for velocity amplitude, measured in nm/s. Although the ISC will calculate standard surface-wave magnitudes only for earthquakes shallower than 60 km, contributing agencies or stations are encouraged to report standard amplitude measurements of IAMs_20 and IVMs_BB for deeper earthquakes as well.

Note that the commonly known classical calibration relationships have been modified in the following to be consistent with displacements measured in nm, and velocities in nm/s, which is now common with high-resolution digital data and analysis tools. With these general definitions of the measurement parameters, where R is hypocentral distance in km (typically less than 1000 km), Δ is epicentral distance in degrees and h is hypocentre depth in km, the standard formulas and procedures read as follows:

ML:

$$ML = \log_{10}(A) + 1.11 \log_{10} R + 0.00189R - 2.09 \tag{11.14}$$

for crustal earthquakes in regions with attenuative properties similar to those of southern California, and with A being the maximum trace amplitude in nm that is measured on output from a horizontal-component instrument that is filtered so that the response of the seismograph/filter system replicates that of a Wood-Anderson standard seismograph (but with a static magnification of 1). For the normalised simulated response curve and related poles and zeros see Figure 1 and Table 1 in IS 3.3 of NMSOP-2.

Equation (11.14) is an expansion of that of *Hutton and Boore* (1987). The constant term in equation (11.14), −2.09, is based on an experimentally determined static magnification of the Wood-Anderson of 2080 (see *Uhrhammer and Collins* (1990)), rather than the theoretical magnification of 2800 that was specified by the seismograph´s manufacturer. The formulation of equation (11.14) assures that reported ML amplitude data are not affected by uncertainty in the static magnification of the Wood-Anderson seismograph.

For seismographic stations containing two horizontal components, amplitudes are measured independently from each horizontal component and each amplitude is treated as a single datum. There is no effort to measure the two observations at the same time, and there is no attempt to compute a vector average. For crustal earthquakes in regions with attenuative properties that are different from those of coastal California and for measuring magnitudes with vertical-component seismographs the constants in the above equation have to be re-determined to adjust for the different regional attenuation and travel paths as well as for systematic differences between amplitudes measured on horizontal and vertical seismographs.

mb_Lg:

$$mb\_Lg = \log_{10}(A) + 0.833 \log_{10} R + 0.434\gamma(R - 10) - 0.87 \tag{11.15}$$

where A = "sustained ground-motion amplitude" in nm, defined as the third largest amplitude in the time window corresponding to group velocities of 3.6 to 3.2 km/s, in the period (T) range 0.7 s to 1.3

s; R = epicentral distance in km, γ = coefficient of attenuation in km^{-1}. γ is related to the quality factor Q through the equation $\gamma = \pi/(QUT)$, where U is group velocity and T is the wave period of the L_g wave. γ is a strong function of crustal structure and should be determined specifically for the region in which the mb_Lg is to be used. A and T are measured on output from a vertical-component instrument that is filtered so that the frequency response of the seismograph/filter system replicates that of a WWSSN short-period seismograph (see Figure 1 and Table 1 in IS 3.3 of NMSOP-2). Arrival times with respect to the origin of the seismic disturbance are used, along with epicentral distance, to compute group velocity U.

mb:

$$mb = \log_{10}(A/T) + Q(\Delta, h) - 3.0 \tag{11.16}$$

where A = vertical component P-wave ground amplitude in nm measured at distances $20° \leq \Delta \leq 100°$ and calculated from the maximum trace-amplitude with $T < 3$ s in the entire P-phase train (time spanned by P, pP, sP, and possibly PcP and their codas, and ending preferably before PP). A and T are measured on output from an instrument that is filtered so that the frequency response of the seismograph/filter system replicates that of a WWSSN short-period seismograph (see Figure 1 and Table 1 in IS 3.3 of NMSOP-2). A is determined by dividing the maximum trace amplitude by the magnification of the simulated WWSSN-SP response at period T.

$Q(\Delta, h)$ = attenuation function for PZ (P-waves recorded on vertical component seismographs) established by *Gutenberg and Richter* (1956) in the tabulated or algorithmic form as used by the U.S. Geological Survey/National Earthquake Information Center (USGS/NEIC) (see Table 2 in IS 3.3 and program description PD 3.1 in NMSOP-2);

mB_BB:

$$mB\_BB = \log_{10}(Vmax/2\pi) + Q(\Delta, h) - 3.0 \tag{11.17}$$

where $Vmax$ = vertical component ground velocity in nm/s at periods between 0.2 s $< T <$ 30 s, measured in the range $20° \leq \Delta \leq 100°$. $Vmax$ is calculated from the maximum trace-amplitude in the entire P-phase train (see mb), as recorded on a seismogram that is proportional to velocity at least in the period range of measurements. $Q(\Delta, h)$ = attenuation function for PZ established by *Gutenberg and Richter* (1956) (see 11.16). Equation (11.16) differs from the equation for mB of *Gutenberg and Richter* (1956) by virtue of the $log_{10}(Vmax/2\pi)$ term, which replaces the classical $\log_{10}(A/T)_{max}$ term. Contributors should continue to send observations of A and T to ISC.

Ms_20:

$$Ms\_20 = \log_{10}(A/T) + 1.66\log_{10}\Delta + 0.3 \tag{11.18}$$

where A = vertical-component ground displacement in nm at $20° \leq \Delta \leq 160°$ epicentral distance measured from the maximum trace amplitude of a surface-wave phase having a period T between 18 s and 22 s on a waveform that has been filtered so that the frequency response of the seismograph/filter replicates that of a WWSSN long-period seismograph (see Figure 1 and Table 1 in IS 3.3 of NMSOP-2). A is determined by dividing the maximum trace amplitude by the magnification of the simulated WWSSN-LP response at period T. Equation (11.18) is formally equivalent to the Ms equation proposed by *Vaněk et al.* (1962) but is here applied to vertical motion measurements in a narrow range of periods.

Ms_BB:

$$Ms\_BB = \log_{10}(Vmax/2\pi) + 1.66\log_{10}\Delta + 0.3 \quad (11.19)$$

where $Vmax$ = vertical-component ground velocity in nm/s associated with the maximum trace-amplitude in the surface-wave train at periods between 3 s $< T <$ 60 s as recorded at distances $2^\circ \leq \Delta \leq 160^\circ$ on a seismogram that is proportional to velocity in that range of considered periods. Equation (11.19) is based on the Ms equation proposed by *Vaněk et al.* (1962), but is here applied to vertical motion measurements and is used with the $\log_{10}(Vmax/2\pi)$ term replacing the $\log_{10}(A/T)_{max}$ term of the original. As for mB_BB, observations of A and T should be reported to ISC.

Mw:

$$Mw = (\log_{10} M_0 - 9.1)/1.5 \quad (11.20)$$

Moment magnitude Mw is calculated from data of the scalar seismic moment M_0 (when given in Nm), or

$$Mw = (\log_{10} M_0 - 16.1)/1.5 \quad (11.21)$$

its CGS equivalent when M_0 is in dyne·cm.

Please note that the magnitude nomenclature used in this Section uses the IASPEI standards as the reference. However, the magnitude type is typically written in plain text in most typical data reports and so it is in this document. Moreover, writing magnitude types in plain text allows us to reproduce the magnitude type as stored in the database and provides a more direct identification of the magnitude type reported by different agencies. A short description of the common magnitude types available in this Summary is given in table 8.6.

11.2.4 The IASPEI Seismic Format (ISF)

The ISF is the IASPEI approved standard format for the exchange of parametric seismological data (hypocentres, magnitudes, phase arrivals, moment tensors etc.) and is one of the formats used by the ISC. It was adopted as standard in August 2001 and is an extension of the International Monitoring System 1.0 (IMS1.0) standard, which was developed for exchanging data used to monitor the Comprehensive Nuclear-Test-Ban Treaty. An example of the ISF is shown in Listing 11.1.

Bulletins which use the ISF are comprised of origin and arrival information, provided in a series of data blocks. These include: a bulletin title block; an event title block; an origin block; a magnitude sub-block; an effect block; a reference block; and a phase block.

Within these blocks an important extension of the IMS1.0 standard is the ability to add additional comments and thus provide further parametric information. The ISF comments are distinguishable within the open parentheses required for IMS1.0 comments by beginning with a hash mark (#) followed by a keyword identifying the type of formatted comment. Each additional line required in the ISF comment begins with the hash (within the comment parentheses) followed by blank spaces at least as long as the keyword. Optional lines within the comment are signified with a plus sign (+) instead of a hash mark. The keywords include `PRIME` (to designate a prime origin of a hypocentre); `CENTROID` (to indicate the centroid origin); `MOMTENS` (moment tensor solution); `FAULT_PLANE` (fault plane solution); `PRINAX` (principal axes); `PARAM` (an origin parameter e.g. hypocentre depth given by a depth phase).

The full documentation for the ISF is maintained at the ISC and can be downloaded from:
www.isc.ac.uk/doc/code/isf/isf.pdf

The documentation for the IMS1.0 standard can be downloaded from:
www.isc.ac.uk/doc/code/isf/ims1_0.pdf

Listing 11.1: *Example of an ISF formatted event*

```
Event 15146084 Near east coast of eastern Honshu
   Date       Time        Err   RMS Latitude Longitude  Smaj  Smin  Az Depth   Err Ndef Nsta Gap  mdist  Mdist Qual   Author      OrigID
2010/09/01 07:32:00                  37.9000  141.9000f                  44.0                                           NIED      17047453
 (#MOMTENS sc    M0 fCLVD    MRR    MTT    MPP    MRT    MTP    MPR NST1 NST2 Author   )
 (#             eM0 eCLVD    eRR    eTT    ePP    eRT    eTP    ePR NCO1 NCO2 Duration )
 (#          16 5.760                                                 NIED     )
 (#                                                                            )
 (#FAULT_PLANE Typ Strike   Dip    Rake  NP  NS Plane Author   )
 (#            BDC 199.00 19.00   86.00                NIED     )
 (+                23.00 71.00   91.00                         )
 (Epicenter information from JMA Focal Mechanism Solution Determined Manually Variance reduction = 96.98%)
2010/09/01 07:32:47.50        1.470  37.8300  142.2400                   37.0         71       281  11.00  51.10     uk BJI       15275482
2010/09/01 07:32:52.20   0.92         38.0320  141.8090   6.7   4.5 110  44.0        114                               MOS       16741494
2010/09/01 07:32:52.53   0.35 0.889  37.9202  141.8229 4.090 2.740 145  49.7  2.76  490  478 122   0.65  92.01 m i fe ISCJB     01631732
 (#PARAM pP_DEPTH=41.11021)
2010/09/01 07:32:52.60   0.10         37.9100  141.8700   1.1   0.9  -1  43.0   1.0                                  fe JMA       16271222
 (Felt I=III-III J1)
2010/09/01 07:32:53.66   0.42 0.770  37.9250  141.7880   5.1   3.4 140  44.4   3.9  102       127   3.17 127.67      fe NEIC      01134459
 (#MOMTENS sc    M0 fCLVD    MRR    MTT    MPP    MRT    MTP    MPR NST1 NST2 Author   )
 (#             eM0 eCLVD    eRR    eTT    ePP    eRT    eTP    ePR NCO1 NCO2 Duration )
 (#          16 5.800         3.600 -0.550 -3.040  1.850 -1.140  4.150           NIED     )
 (#                                                                            )
 (#FAULT_PLANE Typ Strike   Dip    Rake  NP  NS Plane Author   )
 (#            BDC 199.00 19.00   86.00                NIED     )
 (+                23.00 71.00   91.00                         )
 (Recorded [3 JMA] in Miyagi; [2 JMA] in Fukushima and Iwate; [1 JMA] in Akita, Aomori, Ibaraki, Tochigi and Yamagata.)
2010/09/01 07:32:53.70   0.20         37.9300  142.0600 2.224 1.112  -1  50.3   1.0  262   89                                  GCMT      00124877
 (#CENTROID)
 (#MOMTENS sc    M0 fCLVD    MRR    MTT    MPP    MRT    MTP    MPR NST1 NST2 Author   )
 (#             eM0 eCLVD    eRR    eTT    ePP    eRT    eTP    ePR NCO1 NCO2 Duration )
 (#          16 6.891         5.430 -0.440 -4.990  1.500 -2.070  3.710   64   89 GCMT     )
 (#                           0.173  0.118  0.120  0.100  0.094  0.110  102  160      0.90 )
 (#FAULT_PLANE Typ Strike   Dip    Rake  NP  NS Plane Author   )
 (#            BDC  22.00 63.00   91.00                GCMT     )
 (+               201.00 27.00   89.00                         )
 (#PRINAX sc  T_val T_azim  T_pl  B_val B_azim  B_pl  P_val P_azim  P_pl Author    )
 (#       16  6.711 293.00 72.00  0.360 201.00  0.00 -7.072 111.00 18.00 GCMT      )
 (nsta1 refers to body waves, cutoff=40s. nsta2 refers to surface waves, cutoff=50s.)
2010/09/01 07:32:55.05   1.77 1.070  37.8692  141.9450  12.9  10.4 100  63.6  16.8   36       127   3.24 117.04      uk IDC       16680924
2010/09/01 07:32:52.23   0.30 1.333  37.8836  141.9148 5.558 4.001 142  38.9  2.33  542  478  61   0.72 141.68 m i se ISC       01237353
 (#PRIME)
 (#PARAM pP_DEPTH=39.00000)

Magnitude  Err Nsta Author      OrigID
Mw      5.1          NIED      17047453
Ms      4.8        61 BJI       15275482
Ms7     4.6        58 BJI       15275482
mB      5.1        48 BJI       15275482
mb      5.0        63 BJI       15275482
MS      4.7        19 MOS       16741494
mb      5.2        49 MOS       16741494
MS      4.6        43 ISCJB     01631732
mb      4.9       138 ISCJB     01631732
        5.0           JMA       16271222
mb      5.0        55 NEIC      01134459
MW      5.1           NIED      01134459
MW      5.2        89 GCMT      00124877
MS      4.4 0.1    28 IDC       16680924
Ms1     4.4 0.1    28 IDC       16680924
mb      4.4 0.1    27 IDC       16680924
mb1     4.5 0.0    33 IDC       16680924
mb1mx   4.4 0.0    37 IDC       16680924
mbtmp   4.7 0.1    33 IDC       16680924
ms1mx   4.3 0.1    31 IDC       16680924
MS      4.7 0.2    43 ISC       01237353
mb      4.9 0.2   145 ISC       01237353

Sta     Dist  EvAz Phase           Time  TRes  Azim AzRes   Slow   SRes Def   SNR       Amp   Per Qual Magnitude       ArrID
JIO     0.72 322.1 Pn       07:33:05.9   -0.06                           T__                       d_               49540510
JIO     0.72 322.1 Sn       07:33:15.0   -0.82                           T__                       __               49540511
JMM     0.89 269.2 Pn       07:33:08.4     0.2                           T__                       d_               49540512
JMM     0.89 269.2 Sn       07:33:19.2   -0.68                           T__                       __               49540513
JFK     0.97 238.3 Pn       07:33:09.5     0.1                           T__                       d_               49540514
JFK     0.97 238.3 Sn       07:33:21.5   -0.54                           T__                       __               49540515
JOU     1.10 296.4 Pn       07:33:11.5     0.4                           T__                       d_               49540516
JOU     1.10 296.4 Sn       07:33:25.4     0.3                           T__                       _e               49540517
ONAJ    1.18 229.0 Pn       07:33:12.4     0.1                           T__                       d_               49540530
JMK     1.20 333.1 Pn       07:33:12.5     0.0                           T__                       d_               49540518
JMK     1.20 333.1 Sn       07:33:27.1   -0.39                           T__                       _e               49540519
OFUJ    1.21 350.9 Pn       07:33:12.3   -0.34                           T__                       d_               49540531
.
.
.
532A   91.05  49.8 P        07:45:52.799 -0.00  90.9                     T__                       __               05504129
334A   91.18  47.9 P        07:45:54.012   0.7  91.0                     T__                       __               05504128
H06N1  91.36  64.9 T        09:27:33.559                                 ___   6.0                 __               58438458
MIAR   91.43  42.9 P        07:45:54.85    0.5  91.2                     T__                       __               05504179
Y39A   91.60  43.6 P        07:45:55.543   0.4  91.4                     T__                       __               05504214
534A   91.98  49.0 P        07:45:57.308   0.2  91.8                     T__                       __               05504130
KEST   94.59 323.1 LR       08:33:52.432       320.5        38.70        ___           466.5 18.65 __               58438480
ESDC   96.70 334.2 LR       08:34:40.011       345.0        38.30        ___           375.8 20.18 __               58438449
TORD  117.01 315.6 PKPdf    07:51:32.55  -0.82  17.7         2.30        T__   5.1       0.4  0.70 __               58438504
TORD  117.01 315.6 PP       07:52:39.3   -2.90  31.2         6.30        T__   6.5       1.3  0.68 __               58438505
QSPA  127.62 180.0 PKPdf    07:51:52.02  -0.16                           T__                       _e               23535420
SNAA  141.68 197.1 PKPdf    07:52:13.751 -4.52                           T__                       __               20375340
VNA2  143.24 196.3 PKPbc    07:52:18.562   0.4 122.0         2.31        ___                       __               20375338
VNA1  143.64 196.2 PKPbc    07:52:19.77    0.6                           ___                       __               20375339
```

11.2.5 Ground Truth (GT) Events

Accurate locations are crucial in testing Earth models derived from body and surface wave tomography as well as in location calibration studies. 'Ground Truth' (GT) events are well-established source locations and origin times. A database of IASPEI reference events (GT earthquakes and explosions) is hosted at the ISC (www.isc.ac.uk). A full description of GT selection criteria can be found in *Bondár and McLaughlin* (2009a).

The events are coded by category GT0, GT1, GT2 or GT5, where the epicentre of a GTX event is known to within X km to a 95% confidence level. A map of all IASPEI reference events is shown in Figure 11.12 and the types of event are categorised in Figure 11.13. GT0 are explosions with announced locations and origin times. GT1 and GT2 are typically explosions, mine blasts or rock bursts either associated to explosion phenomenology located upon overhead imagery with seismically determined origin times, or precisely located by in-mine seismic networks. GT1-2 events are assumed to be shallow, but depth is unknown.

The database consists of nuclear explosions of GT0–5 quality, adopted from the Nuclear Explosion Database (*Bennett et al.*, 2010); GT0–5 chemical explosions, rock bursts, mine-induced events, as well as a few earthquakes, inherited from the reference event set by *Bondár et al.* (2004); GT5 events (typically earthquakes with crustal depths) which have been identified using either the method of *Bondár et al.* (2008) (2,275 events) or *Bondár and McLaughlin* (2009a) (updated regularly from the EHB catalogue (*Engdahl et al.*, 1998)), which uses the following criteria:

- 10 or more stations within 150 km from the epicentre
- one or more stations within 10 km
- $\Delta U \leq 0.35$
- a secondary azimuthal gap $\leq 160°$

where ΔU is the network quality metric defined as the mean absolute deviation between the best-fitting uniformly distributed network of stations and the actual network:

$$\Delta U = \frac{4 \sum |esaz_i - (unif_i + b)|}{360N}, 0 \leq \Delta U \leq 1 \qquad (11.22)$$

where N is the number of stations, $esaz_i$ is the ith event-to-station azimuth, $unif_i = 360i/N$ for $i = 0$, ..., $N - 1$, and $b = avg\,(esaz_i) - avg\,(unif_i)$. ΔU is normalised so that it is 0 when the stations are uniformly distributed in azimuth and 1 when all the stations are at the same azimuth.

The seismological community is invited to participate in this project by nominating seismic events for the reference event database. Submitters may be contacted for further confirmation and for arrival time data. The IASPEI Reference Event List will be periodically published both in written and electronic form with proper acknowledgement of all submitters.

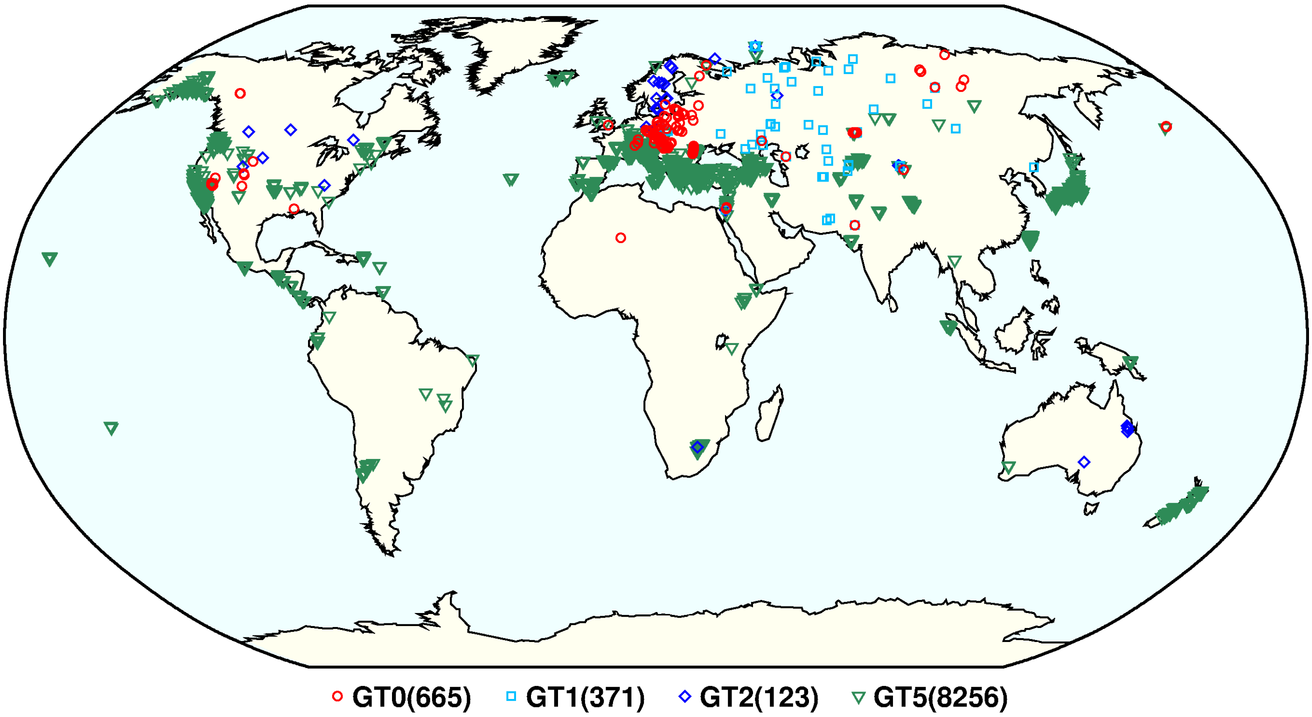

Figure 11.12: *Map of all IASPEI Reference Events as of May 2018.*

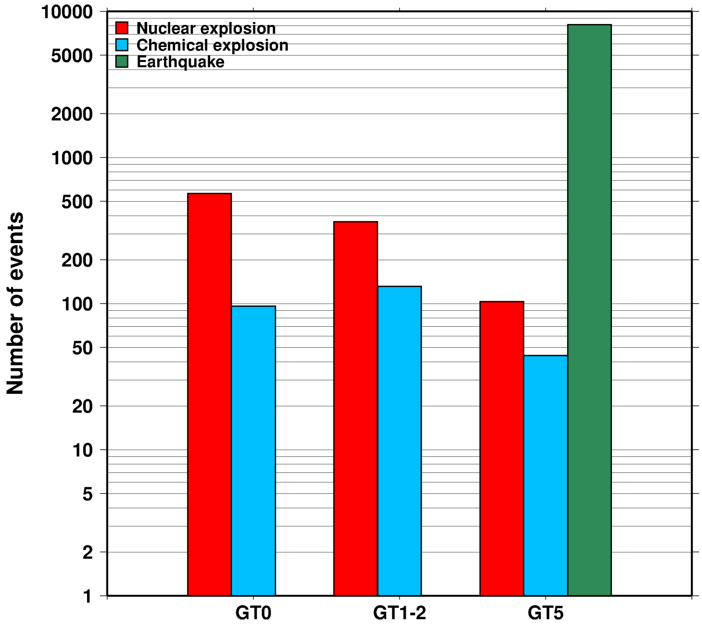

Figure 11.13: *Histogram showing the event types within the IASPEI Reference Event list as of May 2018.*

11.2.6 Nomenclature of Event Types

The nomenclature of event types currently used in the ISC Bulletin takes its origin from the IASPEI International Seismic Format (ISF).

Event type codes are composed of a leading character that generally indicates the confidence with which the type of the event is asserted and a trailing character that generally gives the type of the event. The leading and trailing characters may be used in any combination.

The **leading** characters are:

- s = suspected
- k = known
- f = felt (implies known)
- d = damaging (implies felt and known)

The **trailing** characters are:

- c = meteoritic event
- e = earthquake
- h = chemical explosion
- i = induced event
- l = landslide
- m = mining explosion
- n = nuclear explosion
- r = rock burst
- x = experimental explosion

A chemical explosion might be for mining or experimental purposes, and it is conceivable that other types of event might be assigned two or more different event type codes. This is deliberate, and matches the ambiguous identification of events in existing databases.

In addition, the code `uk` is used for events of unknown type and `ls` is used for known landslides.

The frequency of the different event types designated in the ISC Bulletin since 1964 is indicated in Figure 11.14.

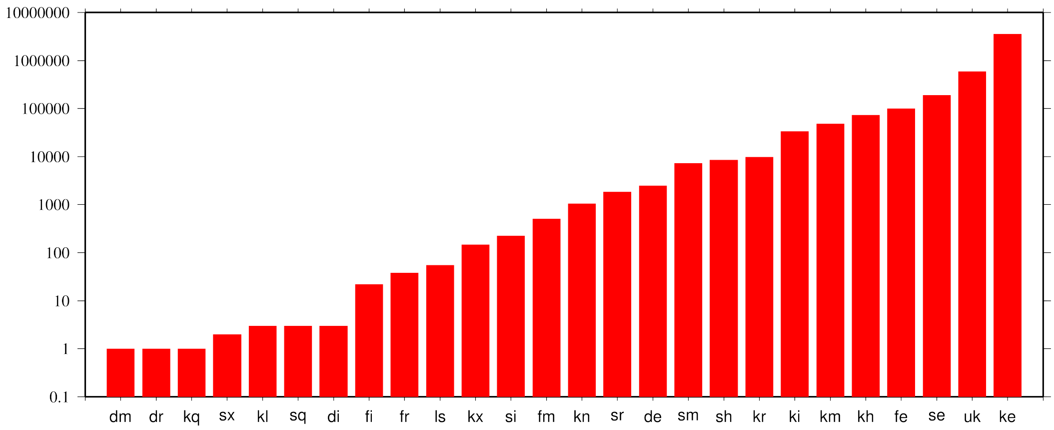

Figure 11.14: *Event types in the ISC Bulletin*

There are currently plans to revise this nomenclature as part of the coordination process between the National Earthquake Information Center (NEIC/USGS), European-Mediterranean Seismological Centre (CSEM) and the ISC.

11.3 Tables

Table 11.2: *Listing of all 373 agencies that have directly reported to the ISC. The 148 agencies highlighted in bold have reported data to the ISC Bulletin for the period of this Bulletin Summary.*

Agency Code	Agency Name
AAA	Alma-ata, Kazakhstan
AAE	**University of Addis Ababa, Ethiopia**
AAM	University of Michigan, USA
ADE	Primary Industries and Resources SA, Australia
ADH	Observatorio Afonso Chaves, Portugal
AEIC	Alaska Earthquake Information Center, USA
AFAR	The Afar Depression: Interpretation of the 1960-2000 Earthquakes, Israel
AFUA	University of Alabama, USA
ALG	Algiers University, Algeria
ANDRE	, USSR
ANF	USArray Array Network Facility, USA
ANT	Antofagasta, Chile
ARE	Instituto Geofisico del Peru, Peru
ARO	Observatoire Géophysique d'Arta, Djibouti
ASIES	**Institute of Earth Sciences, Academia Sinica, Chinese Taipei**
ASL	Albuquerque Seismological Laboratory, USA
ASM	University of Asmara, Eritrea
ASRS	**Altai-Sayan Seismological Centre, GS SB RAS, Russia**
ATA	The Earthquake Research Center Ataturk University, Turkey
ATH	**National Observatory of Athens, Greece**
AUST	**Geoscience Australia, Australia**
AVETI	, USSR
AWI	**Alfred Wegener Institute for Polar and Marine Research, Germany**
AZER	**Republic Center of Seismic Survey, Azerbaijan**

Table 11.2: Continued.

Agency Code	Agency Name
BCIS	Bureau Central International de Sismologie, France
BDF	Observatório Sismológico da Universidade de Brasília, Brazil
BELR	**Centre of Geophysical Monitoring of the National Academy of Sciences of Belarus, Republic of Belarus**
BEO	**Seismological Survey of Serbia, Serbia**
BER	**University of Bergen, Norway**
BERK	Berkheimer H, Germany
BGR	**Bundesanstalt für Geowissenschaften und Rohstoffe, Germany**
BGS	**British Geological Survey, United Kingdom**
BHUJ2	Study of Aftershocks of the Bhuj Earthquake by Japanese Research Team, Japan
BIAK	Biak earthquake aftershocks (17-Feb-1996), USA
BJI	**China Earthquake Networks Center, China**
BKK	**Thai Meteorological Department, Thailand**
BNS	Erdbebenstation, Geologisches Institut der Universität, Köl, Germany
BOG	Universidad Javeriana, Colombia
BRA	**Geophysical Institute, Slovak Academy of Sciences, Slovakia**
BRG	**Seismological Observatory Berggießhübel, TU Bergakademie Freiberg, Germany**
BRK	Berkeley Seismological Laboratory, USA
BRS	Brisbane Seismograph Station, Australia
BUC	**National Institute for Earth Physics, Romania**
BUD	**Geodetic and Geophysical Research Institute, Hungary**
BUEE	Earth & Environment, USA
BUG	Institute of Geology, Mineralogy & Geophysics, Germany
BUL	**Goetz Observatory, Zimbabwe**
BUT	Montana Bureau of Mines and Geology, USA
BYKL	**Baykal Regional Seismological Centre, GS SB RAS, Russia**
CADCG	Central America Data Centre, Costa Rica
CAN	Australian National University, Australia
CANSK	Canadian and Scandinavian Networks, Sweden
CAR	Instituto Sismologico de Caracas, Venezuela
CASC	Central American Seismic Center, Costa Rica
CENT	Centennial Earthquake Catalog, USA
CERI	Center for Earthquake Research and Information, USA
CFUSG	**Inst. of Seismology and Geodynamics, V.I. Vernadsky Crimean Federal University, Republic of Crimea**
CLL	**Geophysikalisches Observatorium Collm, Germany**
CMWS	Laboratory of Seismic Monitoring of Caucasus Mineral Water Region, GSRAS, Russia
CNG	Seismographic Station Changalane, Mozambique
CNRM	Centre National de Recherche, Morocco
COSMOS	Consortium of Organizations for Strong Motion Observations, USA
CRAAG	**Centre de Recherche en Astronomie, Astrophysique et Géophysique, Algeria**
CSC	University of South Carolina, USA
CSEM	Centre Sismologique Euro-Méditerranéen (CSEM/EMSC), France

Table 11.2: Continued.

Agency Code	Agency Name
CUPWA	**Curtin University, Australia**
DASA	Defense Atomic Support Agency, USA
DBN	Koninklijk Nederlands Meteorologisch Instituut, Netherlands
DDA	**Disaster and Emergency Management Presidency, Turkey**
DHMR	Yemen National Seismological Center, Yemen
DIAS	Dublin Institute for Advanced Studies, Ireland
DJA	**Badan Meteorologi, Klimatologi dan Geofisika, Indonesia**
DMN	**National Seismological Centre, Nepal, Nepal**
DNAG	, USA
DNK	**Geological Survey of Denmark and Greenland, Denmark**
DRS	Dagestan Branch, Geophysical Survey, Russian Academy of Sciences, Russia
DSN	**Dubai Seismic Network, United Arab Emirates**
DUSS	Damascus University, Syria, Syria
EAF	**East African Network, Unknown**
EAGLE	Ethiopia-Afar Geoscientific Lithospheric Experiment, Unknown
EBR	Observatori de l'Ebre, Spain
EBSE	Ethiopian Broadband Seismic Experiment, Unknown
ECGS	**European Center for Geodynamics and Seismology, Luxembourg**
ECX	**Centro de Investigación Científica y de Educación Superior de Ensenada, Mexico**
EFATE	OBS Experiment near Efate, Vanuatu, USA
EHB	Engdahl, van der Hilst and Buland, USA
EIDC	Experimental (GSETT3) International Data Center, USA
EKA	Eskdalemuir Array Station, United Kingdom
ENT	Geological Survey and Mines Department, Uganda
EPSI	Reference events computed by the ISC for EPSI project, United Kingdom
ERDA	Energy Research and Development Administration, USA
EST	Geological Survey of Estonia, Estonia
EVBIB	Data from publications listed in the ISC Event Bibliography, Unknown
FBR	Fabra Observatory, Spain
FDF	Fort de France, Martinique
FIA0	Finessa Array, Finland
FOR	Unknown Historical Agency, Unknown - historical agency
FUBES	Earth Science Dept., Geophysics Section, Germany
FUNV	**Fundación Venezolana de Investigaciones Sismológicas, Venezuela**
FUR	Geophysikalisches Observatorium der Universität München, Germany
GBZT	Marmara Research Center, Turkey
GCG	**INSIVUMEH, Guatemala**
GCMT	**The Global CMT Project, USA**
GDNRW	Geologischer Dienst Nordrhein-Westfalen, Germany
GEN	**Dipartimento per lo Studio del Territorio e delle sue Risorse (RSNI), Italy**
GEOMR	GEOMAR, Germany

Table 11.2: *Continued.*

Agency Code	Agency Name
GFZ	Helmholtz Centre Potsdam GFZ German Research Centre For Geosciences, Germany
GII	**The Geophysical Institute of Israel**, **Israel**
GOM	Observatoire Volcanologique de Goma, Democratic Republic of the Congo
GRAL	**National Council for Scientific Research**, **Lebanon**
GSDM	**Geological Survey Department Malawi**, **Malawi**
GTFE	German Task Force for Earthquakes, Germany
GUC	**Centro Sismológico Nacional, Universidad de Chile**, **Chile**
HAN	Hannover, Germany
HDC	Observatorio Vulcanológico y Sismológico de Costa Rica, Costa Rica
HEL	**Institute of Seismology, University of Helsinki**, **Finland**
HFS	Hagfors Observatory, Sweden
HFS1	Hagfors Observatory, Sweden
HFS2	Hagfors Observatory, Sweden
HIMNT	Himalayan Nepal Tibet Experiment, USA
HKC	**Hong Kong Observatory**, **Hong Kong**
HLUG	Hessisches Landesamt für Umwelt und Geologie, Germany
HLW	**National Research Institute of Astronomy and Geophysics**, **Egypt**
HNR	**Ministry of Mines, Energy and Rural Electrification**, **Solomon Islands**
HON	Pacific Tsunami Warning Center - NOAA, USA
HRVD	Harvard University, USA
HRVD_LR	Department of Geological Sciences, Harvard University, USA
HVO	Hawaiian Volcano Observatory, USA
HYB	**National Geophysical Research Institute**, **India**
HYD	National Geophysical Research Institute, India
IAG	Instituto Andaluz de Geofisica, Spain
IASBS	Institute for Advanced Studies in Basic Sciences, Iran
IASPEI	IASPEI Working Group on Reference Events, USA
ICE	Instituto Costarricense de Electricidad, Costa Rica
IDC	**International Data Centre, CTBTO**, **Austria**
IDG	Institute of Dynamics of Geosphere, Russian Academy of Sciences, Russia
IEC	Institute of the Earth Crust, SB RAS, Russia
IEPN	**Institute of Environmental Problems of the North, Russian Academy of Sciences**, **Russia**
IGIL	**Instituto Geofisico do Infante Dom Luiz**, **Portugal**
IGQ	**Servicio Nacional de Sismología y Vulcanología**, **Ecuador**
IGS	Institute of Geological Sciences, United Kingdom
INDEPTH3	International Deep Profiling of Tibet and the Himalayas, USA
INET	**Instituto Nicaraguense de Estudios Territoriales - INETER**, **Nicaragua**
INMG	**Instituto Português do Mar e da Atmosfera, I.P.**, **Portugal**
INMGC	Instituto Nacional de Meteorologia e Geofísica, Cape Verde
IPEC	**The Institute of Physics of the Earth (IPEC)**, **Czech Republic**

Table 11.2: Continued.

Agency Code	Agency Name
IPER	Institute of Physics of the Earth, Academy of Sciences, Moscow, Russia
IPGP	Institut de Physique du Globe de Paris, France
IPRG	Institute for Petroleum Research and Geophysics, Israel
IRIS	**IRIS Data Management Center**, **USA**
IRSM	Institute of Rock Structure and Mechanics, Czech Republic
ISK	**Kandilli Observatory and Research Institute**, **Turkey**
ISN	**Iraqi Meteorological and Seismology Organisation**, **Iraq**
ISS	International Seismological Summary, United Kingdom
IST	Institute of Physics of the Earth, Technical University of Istanbul, Turkey
ISU	**Institute of Seismology, Academy of Sciences, Republic of Uzbekistan**, **Uzbekistan**
ITU	Faculty of Mines, Department of Geophysical Engineering, Turkey
JEN	Geodynamisches Observatorium Moxa, Germany
JMA	**Japan Meteorological Agency**, **Japan**
JOH	Bernard Price Institute of Geophysics, South Africa
JSN	**Jamaica Seismic Network**, **Jamaica**
JSO	**Jordan Seismological Observatory**, **Jordan**
KBC	Institut de Recherches Géologiques et Minières, Cameroon
KEA	Korea Earthquake Administration, Democratic People's Republic of Korea
KEW	Kew Observatory, United Kingdom
KHC	Geofysikalni Ustav, Ceske Akademie Ved, Czech Republic
KISR	**Kuwait Institute for Scientific Research**, **Kuwait**
KLM	**Malaysian Meteorological Service**, **Malaysia**
KMA	**Korea Meteorological Administration**, **Republic of Korea**
KNET	**Kyrgyz Seismic Network**, **Kyrgyzstan**
KOLA	**Kola Regional Seismic Centre, GS RAS**, **Russia**
KRAR	Krasnoyarsk Scientific Research Inst. of Geology and Mineral Resources, Russia, Russia
KRL	Geodätisches Institut der Universität Karlsruhe, Germany
KRNET	**Institute of Seismology, Academy of Sciences of Kyrgyz Republic**, **Kyrgyzstan**
KRSC	**Kamchatkan Experimental and Methodical Seismological Department, GS RAS**, **Russia**
KRSZO	**Geodetic and Geophysical Reasearch Institute, Hungarian Academy of Sciences**, **Hungary**
KSA	Observatoire de Ksara, Lebanon
KUK	Geological Survey Department of Ghana, Ghana
LAO	Large Aperture Seismic Array, USA
LDG	**Laboratoire de Détection et de Géophysique/CEA**, **France**
LDN	University of Western Ontario, Canada
LDO	Lamont-Doherty Earth Observatory, USA
LED	Landeserdbebendienst Baden-Württemberg, Germany
LEDBW	Landeserdbebendienst Baden-Württemberg, Germany
LER	Besucherbergwerk Binweide Station, Germany
LIB	Tripoli, Libya
LIC	**Station Géophysique de Lamto**, **Ivory Coast**

Table 11.2: Continued.

Agency Code	Agency Name
LIM	Lima, Peru
LIS	Instituto de Meteorologia, Portugal
LIT	**Geological Survey of Lithuania**, **Lithuania**
LJU	**Slovenian Environment Agency**, **Slovenia**
LPA	**Universidad Nacional de La Plata**, **Argentina**
LPZ	Observatorio San Calixto, Bolivia
LRSM	Long Range Seismic Measurements Project, Unknown
LSZ	**Geological Survey Department of Zambia**, **Zambia**
LVSN	**Latvian Seismic Network**, **Latvia**
MAN	**Philippine Institute of Volcanology and Seismology**, **Philippines**
MAT	**The Matsushiro Seismological Observatory**, **Japan**
MATSS	, USSR
MCO	**Macao Meteorological and Geophysical Bureau**, **Macao, China**
MCSM	**Main Centre for Special Monitoring**, **Ukraine**
MDD	**Instituto Geográfico Nacional**, **Spain**
MED_RCMT	**MedNet Regional Centroid - Moment Tensors**, **Italy**
MERI	Maharashta Engineering Research Institute, India
MES	Messina Seismological Observatory, Italy
MEX	**Instituto de Geofísica de la UNAM**, **Mexico**
MIRAS	**Mining Institute of the Ural Branch of the Russian Academy of Sciences**, **Russia**
MNH	Institut für Angewandte Geophysik der Universitat Munchen, Germany
MOLD	**Institute of Geophysics and Geology**, **Moldova**
MOS	**Geophysical Survey of Russian Academy of Sciences**, **Russia**
MOZ	Direccao Nacional de Geologia, Mozambique
MOZAR	, Mozambique
MRB	**Institut Cartogràfic i Geològic de Catalunya**, **Spain**
MSI	Messina Seismological Observatory, Italy
MSSP	**Micro Seismic Studies Programme, PINSTECH**, **Pakistan**
MSUGS	Michigan State University, Department of Geological Sciences, USA
MUN	Mundaring Observatory, Australia
NAI	University of Nairobi, Kenya
NAM	**The Geological Survey of Namibia**, **Namibia**
NAO	**Stiftelsen NORSAR**, **Norway**
NCEDC	Northern California Earthquake Data Center, USA
NDI	**National Centre for Seismology of the Ministry of Earth Sciences of India**, **India**
NEIC	**National Earthquake Information Center**, **USA**
NEIS	National Earthquake Information Service, USA
NERS	**North Eastern Regional Seismological Centre, GS RAS**, **Russia**
NIC	**Cyprus Geological Survey Department**, **Cyprus**
NIED	**National Research Institute for Earth Science and Disaster Prevention**, **Japan**
NKSZ	, USSR
NNC	**National Nuclear Center**, **Kazakhstan**
NORS	North Ossetia (Alania) Branch, Geophysical Survey, Russian Academy of Sciences, Russia

Table 11.2: Continued.

Agency Code	Agency Name
NOU	**IRD Centre de Nouméa, New Caledonia**
NSSC	National Syrian Seismological Center, Syria
NSSP	**National Survey of Seismic Protection, Armenia**
OBM	Research Centre of Astronomy and Geophysics, Mongolia
OGAUC	Centro de Investigação da Terra e do Espaço da Universidade de Coimbra, Portugal
OGSO	Ohio Geological Survey, USA
OMAN	**Sultan Qaboos University, Oman**
ORF	Orfeus Data Center, Netherlands
OSPL	**Observatorio Sismologico Politecnico Loyola, Dominican Republic**
OSUB	Osservatorio Sismologico Universita di Bari, Italy
OTT	**Canadian Hazards Information Service, Natural Resources Canada, Canada**
PAL	Palisades, USA
PAS	California Institute of Technology, USA
PDA	Universidade dos Açores, Portugal
PDG	**Seismological Institute of Montenegro, Montenegro**
PEK	Peking, China
PGC	Pacific Geoscience Centre, Canada
PLV	**National Center for Scientific Research, Vietnam**
PMEL	Pacific seismicity from hydrophones, USA
PMR	Alaska Tsunami Warning Center,, USA
PNNL	Pacific Northwest National Laboratory, USA
PNSN	**Pacific Northwest Seismic Network, USA**
PPT	**Laboratoire de Géophysique/CEA, French Polynesia**
PRE	**Council for Geoscience, South Africa**
PRU	**Geophysical Institute, Academy of Sciences of the Czech Republic, Czech Republic**
PTO	Instituto Geofísico da Universidade do Porto, Portugal
PTWC	Pacific Tsunami Warning Center, USA
QCP	**Manila Observatory, Philippines**
QUE	Pakistan Meteorological Department, Pakistan
QUI	Escuela Politécnica Nacional, Ecuador
RAB	Rabaul Volcanological Observatory, Papua New Guinea
RBA	Université Mohammed V, Morocco
REN	MacKay School of Mines, USA
REY	**Icelandic Meteorological Office, Iceland**
RHSSO	**Republic Hydrometeorological Service, Seismological Observatory, Banja Luka, Bosnia-Herzegovina**
RISSC	**Laboratory of Research on Experimental and Computational Seimology, Italy**
RMIT	Royal Melbourne Institute of Technology, Australia
ROC	Odenbach Seismic Observatory, USA
ROM	**Istituto Nazionale di Geofisica e Vulcanologia, Italy**
RRLJ	Regional Research Laboratory Jorhat, India
RSMAC	Red Sísmica Mexicana de Apertura Continental, Mexico

Table 11.2: Continued.

Agency Code	Agency Name
RSNC	**Red Sismológica Nacional de Colombia, Colombia**
RSPR	**Red Sísmica de Puerto Rico, USA**
RYD	King Saud University, Saudi Arabia
SAPSE	Southern Alps Passive Seismic Experiment, New Zealand
SAR	Sarajevo Seismological Station, Bosnia and Herzegovina
SBDV	, USSR
SCB	**Observatorio San Calixto, Bolivia**
SCEDC	Southern California Earthquake Data Center, USA
SCSIO	Key Laboratory of Ocean and Marginal Sea Geology, South China Sea, China
SDD	Universidad Autonoma de Santo Domingo, Dominican Republic
SEA	Geophysics Program AK-50, USA
SET	Setif Observatory, Algeria
SFS	**Real Instituto y Observatorio de la Armada, Spain**
SGS	**Saudi Geological Survey, Saudi Arabia**
SHL	Central Seismological Observatory, India
SIGU	**Subbotin Institute of Geophysics, National Academy of Sciences, Ukraine**
SIK	Seismic Institute of Kosovo, Unknown
SIO	Scripps Institution of Oceanography, USA
SJA	**Instituto Nacional de Prevención Sísmica, Argentina**
SJS	Instituto Costarricense de Electricidad, Costa Rica
SKHL	**Sakhalin Experimental and Methodological Seismological Expedition, GS RAS, Russia**
SKL	Sakhalin Complex Scientific Research Institute, Russia
SKO	**Seismological Observatory Skopje, FYR Macedonia**
SLC	Salt Lake City, USA
SLM	Saint Louis University, USA
SNET	**Servicio Nacional de Estudios Territoriales, El Salvador**
SNM	New Mexico Institute of Mining and Technology, USA
SNSN	Saudi National Seismic Network, Saudi Arabia
SOF	**Geophysical Institute, Bulgarian Academy of Sciences, Bulgaria**
SOMC	**Seismological Observatory of Mount Cameroon, Cameroon**
SOME	**Seismological Experimental Methodological Expedition, Kazakhstan**
SPA	USGS - South Pole, Antarctica
SPGM	Service de Physique du Globe, Morocco
SPITAK	, Armenia
SRI	Stanford Research Institute, USA
SSN	Sudan Seismic Network, Sudan
SSNC	**Servicio Sismológico Nacional Cubano, Cuba**
SSS	Centro de Estudios y Investigaciones Geotecnicas del San Salvador, El Salvador
STK	Stockholm Seismological Station, Sweden
STR	**EOST / RéNaSS, France**
STU	Stuttgart Seismological Station, Germany
SVSA	**Sistema de Vigilância Sismológica dos Açores, Portugal**

Table 11.2: *Continued.*

Agency Code	Agency Name
SYO	**National Institute of Polar Research, Japan**
SZGRF	Seismologisches Zentralobservatorium Gräfenberg, Germany
TAC	Estación Central de Tacubaya, Mexico
TAN	Antananarivo, Madagascar
TANZANIA	Tanzania Broadband Seismic Experiment, USA
TAP	**CWB, Chinese Taipei**
TAU	University of Tasmania, Australia
TEH	**Tehran University, Iran**
TEIC	Center for Earthquake Research and Information, USA
THE	**Department of Geophysics, Aristotle University of Thessaloniki, Greece**
THR	**International Institute of Earthquake Engineering and Seismology (IIEES), Iran**
TIF	**Institute of Earth Sciences/ National Seismic Monitoring Center, Georgia**
TIR	**The Institute of Seismology, Academy of Sciences of Albania, Albania**
TRI	**Istituto Nazionale di Oceanografia e di Geofisica Sperimentale (OGS), Italy**
TRN	**The Seismic Research Centre, Trinidad and Tobago**
TTG	Titograd Seismological Station, Montenegro
TUL	Oklahoma Geological Survey, USA
TUN	**Institut National de la Météorologie, Tunisia**
TVA	Tennessee Valley Authority, USA
TZN	University of Dar Es Salaam, Tanzania
UAF	Department of Geosciences, USA
UAV	Red Sismológica de Los Andes Venezolanos, Venezuela
UCB	University of Colorado, Boulder, USA
UCC	**Royal Observatory of Belgium, Belgium**
UCDES	Department of Earth Sciences, United Kingdom
UCR	**Sección de Sismología, Vulcanología y Exploración Geofísica, Costa Rica**
UCSC	Earth & Planetary Sciences, USA
UESG	School of Geosciences, United Kingdom
UGN	Institute of Geonics AS CR, Czech Republic
ULE	University of Leeds, United Kingdom
UNAH	Universidad Nacional Autonoma de Honduras, Honduras
UPA	**Universidad de Panama, Panama**
UPIES	Institute of Earth- and Environmental Science, Germany
UPP	**University of Uppsala, Sweden**
UPSL	**University of Patras, Department of Geology, Greece**
UREES	Department of Earth and Environmental Science, USA
USAEC	United States Atomic Energy Commission, USA
USCGS	United States Coast and Geodetic Survey, USA
USGS	United States Geological Survey, USA
UTEP	Department of Geological Sciences, USA
UUSS	The University of Utah Seismograph Stations, USA

Table 11.2: *Continued.*

Agency Code	Agency Name
UVC	Universidad del Valle, Colombia
UWMDG	University of Wisconsin-Madison, Department of Geoscience, USA
VAO	**Instituto Astronomico e Geofísico**, **Brazil**
VIE	**Zentralanstalt für Meteorologie und Geodynamik (ZAMG)**, **Austria**
VKMS	Lab. of Seismic Monitoring, Voronezh region, GSRAS & Voronezh State University, Russia
VLA	Vladivostok Seismological Station, Russia
VSI	University of Athens, Greece
VUW	Victoria University of Wellington, New Zealand
WAR	**Institute of Geophysics, Polish Academy of Sciences**, **Poland**
WASN	, USA
WBNET	West Bohemia Seismic Network, Czech Republic
WEL	**Institute of Geological and Nuclear Sciences**, **New Zealand**
WES	Weston Observatory, USA
WUSTL	Washington University Earth and Planentary Sciences, USA
YARS	**Yakutiya Regional Seismological Center, GS SB RAS**, **Russia**
ZAG	**Seismological Survey of the Republic of Croatia**, **Croatia**
ZEMSU	, USSR
ZUR	**Swiss Seismological Service (SED)**, **Switzerland**
ZUR_RMT	Zurich Moment Tensors, Switzerland

Table 11.3: *Phases reported to the ISC. These include phases that could not be matched to an appropriate* ak135 *phases. Those agencies that reported at least 10% of a particular phase are also shown.*

Reported Phase	Total	Agencies reporting
P	3016800	TAP (14%), NEIC (11%)
S	1422759	TAP (28%), JMA (16%)
AML	448226	ROM (76%), ATH (21%)
IAmb	382052	NEIC (98%)
NULL	306582	NEIC (39%), AEIC (18%), RSNC (17%)
IAML	226092	NEIC (44%), DDA (30%)
Pn	224292	NEIC (44%)
Pg	179017	NNC (13%)
Sg	137290	NEIC (12%)
pmax	112522	MOS (79%), BJI (21%)
PG	90028	ISK (52%), HEL (18%), PRU (14%)
IAMs_20	86999	NEIC (98%)
LR	81844	IDC (68%), BJI (23%)
SG	76152	ISK (34%), HEL (25%), PRU (22%), IPEC (11%)
IAmb_Lg	74933	NEIC (100%)
Sn	73860	IDC (14%), LDG (13%)
PN	72865	ISK (69%), MOS (14%)
Lg	62542	NNC (45%), MDD (35%)
PKP	27176	IDC (53%)
A	25980	SVSA (51%), INMG (34%), SKHL (14%)
T	23251	IDC (93%)
PKPbc	16846	IDC (61%), BGR (18%), NEIC (11%)
MSG	16442	HEL (99%)
SN	15356	HEL (45%), ISK (28%), BRA (11%)
PKIKP	14964	MOS (97%)
pP	14753	BJI (49%), IDC (23%)
MLR	14566	MOS (100%)
PKPdf	13971	NEIC (56%)
PcP	11131	IDC (67%), NEIC (11%)
PP	10363	IDC (25%), BJI (21%), BELR (18%)
SS	8032	MOS (31%), BELR (23%), BJI (21%)
PB	7944	HEL (100%)
smax	6917	MOS (86%), BJI (14%)
SB	6880	HEL (100%)
sP	6815	BJI (83%)
PKPab	6504	IDC (41%), NEIC (21%), INMG (12%), BGR (12%)
L	5980	BJI (81%), BGR (11%)
PMZ	5933	BJI (100%)
Smax	5429	BYKL (100%)
x	5091	NDI (32%), PRU (22%), UCC (17%), BRG (16%), KRSZO (11%)
Pmax	4506	BYKL (99%)
Sb	4151	IRIS (61%), BELR (24%), BYKL (13%)
Pb	3643	IRIS (37%), BELR (29%), BYKL (19%), KRSZO (14%)
Amp	3578	BRG (100%)
ScP	3437	IDC (84%)
END	3390	ROM (100%)
LQ	3123	BELR (47%), PPT (26%), INMG (13%), IEPN (12%)
PKiKP	3088	IDC (54%), UCC (14%)
AMB	3085	SKHL (88%), BJI (11%)
PPP	3069	BELR (54%), MOS (39%)
LRM	2947	BELR (97%)
SSS	2807	BELR (61%), MOS (27%)
AMS	2804	PRU (86%), SKHL (11%)
LG	2777	BRA (84%), OTT (15%)
max	2764	BYKL (100%)
PKP2	2730	MOS (92%)
AMP	2562	IEPN (48%), TIR (33%), HLW (15%)
PKKPbc	2390	IDC (97%)
Trac	2275	OTT (100%)
LE	2176	BJI (100%)
LN	2173	BJI (100%)
*PP	2143	MOS (100%)
LZ	2098	BJI (100%)
sS	1840	BJI (83%), BELR (13%)
PKhKP	1588	IDC (100%)

Table 11.3: (continued)

Reported Phase	Total	Agencies reporting
PS	1448	BELR (38%), MOS (27%)
SKS	1254	BELR (39%), BJI (28%), PRU (16%)
pPKP	1218	IDC (35%), BJI (24%), PRU (12%)
SKPbc	1208	IDC (90%)
Pdiff	1151	IDC (53%), AWI (18%)
X	998	JMA (82%), SYO (16%)
ScS	952	BJI (47%), BELR (32%), IDC (11%)
IVMs_BB	858	BER (66%), ISC (34%)
Pdif	838	BER (40%), NEIC (25%)
PKPPKP	767	IDC (98%)
PKHKP	711	MOS (99%)
PKPDF	707	PRU (100%)
pPKPbc	648	IDC (55%), BGR (38%)
SP	566	BER (34%), MOS (19%)
SKKS	561	BELR (64%), BJI (27%)
SKSac	539	BER (54%), CLL (12%)
pPKPdf	517	NEIC (42%), BGR (24%)
SKP	505	IDC (51%), BELR (22%), PRU (16%)
PKKP	492	IDC (66%)
E	484	ZAG (99%)
PKPAB	483	PRU (100%)
IVmB_BB	468	BER (97%)
*SP	458	MOS (100%)
PDIFF	432	BRA (49%), PRU (38%), IPEC (13%)
PKP1	429	LIC (98%)
sPKP	423	BJI (72%), BELR (14%)
Sm	407	SIGU (62%), CFUSG (38%)
Lm	379	CLL (100%)
Pm	319	SIGU (76%), CFUSG (24%)
PKKPab	318	IDC (80%), BGR (11%)
*SS	301	MOS (100%)
PKP2bc	301	IDC (100%)
p	276	ROM (100%)
SMN	259	BJI (100%)
SME	259	BJI (100%)
Sgmax	250	NERS (100%)
PPS	235	CLL (60%), MOS (19%), BELR (12%)
PKS	231	BELR (50%), BJI (29%)
s	225	ROM (97%)
SKKPbc	219	IDC (84%)
LmV	215	CLL (100%)
PcS	214	BJI (71%), BELR (25%)
PPMZ	198	BJI (100%)
Rg	198	NAO (33%), NNC (31%), IDC (30%)
P3KPbc	186	IDC (100%)
PmP	166	BGR (84%), ZUR (16%)
LmH	157	CLL (100%)
MSN	151	HEL (68%), BER (32%)
pPKPab	140	IDC (49%), CLL (21%)
SgSg	136	BYKL (100%)
SKPdf	133	BER (54%), CLL (26%), AWI (11%)
PgPg	132	BYKL (95%)
P4KPbc	132	IDC (100%)
SSSS	130	CLL (100%)
PnPn	125	UCC (97%)
SmS	124	BGR (94%)
m	111	SIGU (100%)
Pgmax	104	NERS (99%)
PKPpre	87	NEIC (76%), CLL (13%), PRU (11%)
PCP	86	PRU (57%), LPA (24%), IPEC (12%)
RG	85	IPEC (94%)
(P)	82	CLL (59%), BRG (41%)
IVmBBB	75	BER (99%)
PKP2ab	69	IDC (100%)
pPcP	63	IDC (97%)
H	63	IDC (100%)
pPP	60	CLL (43%), LPA (40%)

Table 11.3: (continued)

Reported Phase	Total	Agencies reporting
SKKSac	58	CLL (57%), IEPN (21%), LJU (14%)
Sdif	56	CLL (62%), PPT (21%), WAR (12%)
MPN	54	HEL (74%), BER (26%)
-	54	INMG (100%)
AMb	53	IGIL (98%)
SKKP	53	IDC (45%), BELR (21%), PRU (11%)
pPKiKP	52	UCC (44%), SYO (23%), CLL (17%)
SKPab	50	IDC (92%)
AMSG	47	BER (98%)
pPdiff	46	SYO (80%), LJU (13%)
PKSdf	46	CLL (61%), BER (35%)
SDIF	43	PRU (100%)
Lmax	42	CLL (100%)
SDIFF	33	BRA (36%), IPEC (33%), LPA (30%)
PSKS	32	CLL (100%)
SCS	32	LPA (84%), IPEC (16%)
sPP	31	CLL (97%)
SPP	31	BELR (71%), MOS (16%), CLL (13%)
sPKPab	30	UCC (70%), CLL (20%)
Amb	30	KRSZO (100%)
pPdif	28	INMG (79%), CLL (18%)
SKIKS	28	LPA (100%)
ASSG	27	BER (74%), OSPL (26%)
ASPG	27	BER (74%), OSPL (26%)
ATSG	26	BER (77%), OSPL (23%)
ATPG	26	BER (77%), OSPL (23%)
pwP	25	NEIC (100%)
PKPf	25	BRG (100%)
P3KP	24	IDC (100%)
PPPP	24	CLL (100%)
SKSdf	24	BER (83%)
sPKiKP	23	UCC (74%), CLL (26%)
sSS	23	CLL (100%)
PbPb	23	UCC (96%)
AMPG	23	BER (96%)
pPn	22	UCC (95%)
Sgm	22	CFUSG (100%)
LQM	22	MOLD (100%)
(PP)	20	CLL (95%)
sPKPdf	20	CLL (85%)
SKIKP	19	LPA (100%)
AMl	18	NIC (100%)
Piff	18	BRG (100%)
(sP)	17	CLL (100%)
sPKPbc	16	BGR (44%), CLL (31%), UCC (25%)
P'P'bc	16	PPT (81%), NEIC (19%)
rx	16	SKHL (100%)
AMd	16	NIC (100%)
P*	16	BGR (69%), MOS (25%)
(pP)	15	CLL (100%)
SKPDF	15	BRA (100%)
SnSn	14	UCC (71%), KRSZO (29%)
Sdiff	13	LJU (54%), IDC (46%)
PKKPdf	13	CLL (46%), AWI (46%)
(SS)	13	CLL (100%)
PKIKS	12	LPA (100%)
SKSp	12	BRA (83%), WAR (17%)
PKPlp	12	CLL (100%)
PSP	12	LPA (100%)
SKiKP	12	IDC (67%), AWI (33%)
sSSS	11	CLL (100%)
(PKPdf)	11	CLL (100%)
(PcP)	11	CLL (100%)
S*	11	BGR (91%)
sSKS	11	BELR (64%), IPEC (36%)
Plp	11	CLL (100%)
pS	10	BELR (70%), IEPN (20%)

Table 11.3: *(continued)*

Reported Phase	Total	Agencies reporting
Cod	10	SFS (100%)
LMZ	10	WAR (100%)
Siff	9	BRG (100%)
(PKP)	9	CLL (67%), BRG (33%)
SCP	9	PRU (100%)
IVMsBB	9	BER (78%), ISC (11%), NDI (11%)
SKSP	9	CLL (100%)
(PKiKP)	9	CLL (100%)
Pgm	9	CFUSG (100%)
sPn	9	UCC (78%), OMAN (22%)
PKPdif	9	NEIC (67%), LJU (22%), CLL (11%)
(SSSS)	9	CLL (100%)
(SSS)	9	CLL (100%)
PPPrev	9	CLL (100%)
EP	8	SFS (100%)
PKPPKPdf	8	CLL (100%)
SH	8	SYO (100%)
(pPKPdf)	7	CLL (100%)
dur	7	MOLD (100%)
P4KP	7	IDC (100%)
(Sg)	7	CLL (57%), BRG (43%)
(Pg)	7	CLL (100%)
(PPP)	7	CLL (100%)
PPlp	7	CLL (100%)
sSdiff	7	CLL (86%), LJU (14%)
PKKS	7	BELR (71%), IEPN (29%)
(PKPab)	7	CLL (100%)
pPKKPbc	7	CLL (100%)
sPdiff	7	SYO (86%), LJU (14%)
PKPdiff	6	CLL (100%)
PSS	6	CLL (100%)
PSPS	6	CLL (100%)
PKPbcd	6	WAR (100%)
SKKPdf	6	CLL (83%), WAR (17%)
R	6	LDG (100%)
PsP	5	MOLD (100%)
sPPP	5	CLL (100%)
PKPc	5	WAR (100%)
SKKPab	5	LIT (60%), IDC (40%)
(Sn)	5	CLL (100%)
P(2)	5	CLL (100%)
PA	5	ISC (100%)
(S)	5	CLL (100%)
SbSb	4	UCC (75%), KRSZO (25%)
(SP)	4	CLL (100%)
sPS	4	CLL (100%)
M	4	MOLD (100%)
pPiff	4	BRG (100%)
(Pdif)	4	CLL (100%)
Snm	4	CFUSG (100%)
sSSSS	4	CLL (100%)
pPDIFF	4	IPEC (100%)
sSKSac	4	CLL (100%)
(PPPP)	3	CLL (100%)
sPg	3	UCC (100%)
PKKPb	3	BRG (100%)
LV	3	CLL (100%)
PKKSbc	3	CLL (100%)
(SKPdf)	3	CLL (100%)
PPmax	3	CLL (100%)
pPPP	3	CLL (100%)
PDIF	3	PRU (100%)
P9	3	UPA (67%), SNET (33%)
SKSSKSac	3	CLL (100%)
Li	3	MOLD (100%)
sPKKPbc	3	CLL (100%)
SKKSa	3	BRG (100%)

Table 11.3: *(continued)*

Reported Phase	Total	Agencies reporting
Lm(360	3	CLL (100%)
pPKPPKPd	3	CLL (100%)
(SKSac)	3	CLL (100%)
PKPbc(2)	3	CLL (100%)
sPcP	3	CLL (100%)
sSKKSac	3	CLL (100%)
sSKKPbc	3	CLL (100%)
pPb	2	UCC (100%)
PKPM	2	MOLD (100%)
SKKSacre	2	CLL (100%)
PKKPf	2	BRG (100%)
sPb	2	UCC (100%)
AMSN	2	NDI (100%)
pPPS	2	CLL (100%)
SM	2	MOLD (100%)
(pPP)	2	CLL (100%)
X2	2	BGR (100%)
(SKS)	2	BRG (100%)
(pPKiKP)	2	CLL (100%)
PcPPKPre	2	CLL (100%)
(Pn)	2	CLL (100%)
LmV(360	2	CLL (100%)
sPKKPdf	2	CLL (100%)
X1	2	BGR (100%)
PKSbc	2	CLL (100%)
SKKSdf	2	CLL (50%), WAR (50%)
sSb	2	UCC (100%)
PM	2	MOLD (100%)
(PS)	2	CLL (100%)
(sPKiKP)	2	CLL (100%)
(PKSdf)	2	CLL (100%)
PSSrev	2	CLL (100%)
(pPKPab)	2	CLL (100%)
sPPS	2	CLL (100%)
pPKKSbc	1	CLL (100%)
sPKPPKPd	1	CLL (100%)
SKPd	1	BER (100%)
sPSKS	1	CLL (100%)
Coda	1	SFS (100%)
sPSS	1	CLL (100%)
AP	1	MOS (100%)
(PKPbc)	1	CLL (100%)
PKPPKPab	1	CLL (100%)
PSPS(2)	1	CLL (100%)
pSKKPbc	1	CLL (100%)
PPM	1	MOLD (100%)
tx	1	IEPN (100%)
XS	1	PRU (100%)
SSmax	1	CLL (100%)
(sSSS)	1	CLL (100%)
dPdiff	1	SYO (100%)
SKPPKPdf	1	CLL (100%)
sSN	1	IPEC (100%)
(sSS)	1	CLL (100%)
sSKKPbc2	1	CLL (100%)
(PPS)	1	CLL (100%)
(SPP)	1	CLL (100%)
(sSP)	1	CLL (100%)
SKac	1	SYO (100%)
(PPPrev)	1	CLL (100%)
SZ	1	MEX (100%)
n	1	INMG (100%)
-MS	1	INMG (100%)
pPKKPdf	1	CLL (100%)
SKPa	1	NAO (100%)
PKPmax	1	CLL (100%)
SKPb	1	NAO (100%)

Table 11.3: *(continued)*

Reported Phase	Total	Agencies reporting
(PKKPdf)	1	CLL (100%)
sPKKPbc2	1	CLL (100%)
(pPPP)	1	CLL (100%)
SPS	1	CLL (100%)
pPPPP	1	CLL (100%)
PKPdf(2)	1	CLL (100%)
N	1	SFS (100%)
pPLPdf	1	SYO (100%)
En	1	INMG (100%)
sPPPPrev	1	CLL (100%)
P'P'df	1	NEIC (100%)
pPKS	1	LPA (100%)
Pd1	1	ATH (100%)
pScP	1	IDC (100%)
PPS(2)	1	CLL (100%)
(PcS)	1	CLL (100%)
del	1	AUST (100%)
pSKS	1	BELR (100%)
(sPcP)	1	CLL (100%)
Lq	1	MOLD (100%)
SKKSac2	1	CLL (100%)
pSKSac	1	CLL (100%)
pPKSdf	1	CLL (100%)
3PKPdf	1	CLL (100%)
sSn	1	UCC (100%)
pSP	1	CLL (100%)
PKKPbc2	1	CLL (100%)
Pdiff(2)	1	CLL (100%)
pSKPbc	1	CLL (100%)
pPPPrev	1	CLL (100%)
sSP	1	CLL (100%)
PKKSdf	1	CLL (100%)
pPmax	1	CLL (100%)
RM	1	MOLD (100%)
sSPP	1	CLL (100%)
(Sdif)	1	CLL (100%)
PP(2)	1	CLL (100%)
(pPKPbc)	1	CLL (100%)
(SKSdf)	1	CLL (100%)
Sj	1	DNK (100%)
(sPP)	1	CLL (100%)
S(2)	1	CLL (100%)
Ex	1	ZAG (100%)
PPP(2)	1	CLL (100%)
S5	1	INMG (100%)
sPKP2	1	BJI (100%)
(sSKSac)	1	CLL (100%)
KP	1	INMG (100%)
(PSPS)	1	CLL (100%)
PS(2)	1	CLL (100%)
SS(2)	1	LPA (100%)
sPdif	1	CLL (100%)
PKPab(2)	1	CLL (100%)
PKKbc	1	BGR (100%)
St	1	MEX (100%)
pSKKPdf	1	CLL (100%)
pPP(2)	1	LPA (100%)
Pd2	1	ATH (100%)
(sPKPdf)	1	CLL (100%)
(PSKS)	1	CLL (100%)
Sq	1	MOLD (100%)
pSKSP	1	CLL (100%)
pPKPdiff	1	CLL (100%)
-ML	1	INMG (100%)
Pq	1	MOLD (100%)
pPS	1	CLL (100%)
PPPPrev	1	CLL (100%)

Table 11.3: (continued)

Reported Phase	Total	Agencies reporting
LQR	1	MOLD (100%)
sPKKSbc	1	CLL (100%)
SKKPbc2	1	CLL (100%)

Table 11.4: Reporters of amplitude data

Agency	Number of reported amplitudes	Number of amplitudes in ISC located events	Number used for ISC mb	Number used for ISC MS
NEIC	634534	262417	168027	40609
ROM	342190	9195	0	0
IDC	329396	309741	134301	33663
WEL	260844	23218	0	0
MOS	111792	109504	56256	9894
ATH	94479	11700	0	0
NNC	93232	29799	76	0
DJA	79945	49827	10882	0
ISK	73724	12862	0	0
SOME	70416	22257	4514	0
DDA	68517	8518	0	0
BJI	61435	59800	12025	14142
MDD	56015	9077	0	0
RSNC	52707	4231	0	0
VIE	35578	19960	7737	0
BKK	34122	23290	7765	0
THE	29200	5359	0	0
LDG	20682	4035	10	0
GUC	19196	4154	2	0
HEL	16506	739	0	0
SVSA	13560	441	183	0
BYKL	12671	3672	0	0
INMG	12582	5478	2800	0
BER	10953	2392	5	1
PRU	10710	3335	0	1937
DNK	10469	5403	3235	357
PPT	9980	8520	906	2722
DMN	9044	8636	5288	0
BUC	8318	2081	0	0
NIC	7740	3042	0	0
BELR	7484	5477	633	1461
BGR	7480	7258	5837	0
SKHL	6795	4920	0	0
MAN	6341	1488	0	0
NDI	5767	5405	1619	184
LJU	5416	196	58	0
ZUR	5059	785	0	0
YARS	4850	234	0	0
MRB	4250	77	0	0
PDG	4212	2633	0	0
PRE	4192	219	0	0
TEH	4144	2779	0	0
SNET	4039	1591	0	0
KRSZO	4019	1857	58	0

Table 11.4: *Continued.*

Agency	Number of reported amplitudes	Number of amplitudes in ISC located events	Number used for ISC mb	Number used for ISC MS
BRG	3576	2219	0	0
SKO	3261	383	0	0
BGS	3259	1888	859	390
SJA	2944	2936	0	0
CLL	2519	2291	393	273
OTT	2273	360	0	0
ECX	2200	394	0	0
KNET	1647	539	0	0
LVSN	1585	297	0	0
IPEC	1491	202	0	0
IEPN	1477	1341	22	0
LIC	1473	1190	603	0
ASRS	1333	738	0	0
NAO	1149	1146	836	0
SSNC	995	134	0	0
OSPL	976	253	0	0
ISC	934	804	101	1
UCR	903	864	0	0
UCC	857	650	557	0
TIR	844	471	0	0
SIGU	815	489	0	0
IGIL	808	333	93	99
ISN	751	297	0	0
THR	603	438	2	0
NOU	584	470	237	0
MOLD	417	247	14	0
NERS	368	116	0	0
MIRAS	366	20	0	0
CFUSG	352	275	0	0
KISR	332	107	5	0
WAR	314	290	0	211
LIT	277	224	29	0
MCSM	145	145	0	0
SCB	109	107	0	0
HYB	99	99	69	0
UPA	52	5	0	0
JSO	50	50	0	0
EAF	17	5	0	0
PLV	4	4	0	0
LSZ	2	1	0	0

12

Glossary of ISC Terminology

- Agency/ISC data contributor

  An academic or government institute, seismological organisation or company, geological/meteorological survey, station operator or author that reports or contributed data in the past to the ISC or one of its predecessors. Agencies may contribute data to the ISC directly, or indirectly through other ISC data contributors.

- Agency code

  A unique, maximum eight-character code for a data reporting agency (e.g. NEIC, GFZ, BUD) or author (e.g. ISC, EHB, IASPEI). Often the agency code is the commonly used acronym of the reporting institute.

- Arrival

  A phase pick at a station is characterised by a phase name and an arrival time.

- Associated phase

  Associated phase arrival or amplitude measurements represent a collection of observations belonging to (i.e. generated by) an event. The complete set of observations are associated to the prime hypocentre.

- Azimuthal gap/Secondary azimuthal gap

  The azimuthal gap for an event is defined as the largest angle between two stations with defining phases when the stations are ordered by their event-to-station azimuths. The secondary azimuthal gap is the largest azimuthal gap a single station closes.

- BAAS

  Seismological bulletins published by the British Association for the Advancement of Science (1913-1917) under the leadership of H.H. Turner. These bulletins are the predecessors of the ISS Bulletins and include reports from stations distributed worldwide.

- Bulletin

  An ordered list of event hypocentres, uncertainties, focal mechanisms, network magnitudes, as well as phase arrival and amplitude observations associated to each event. An event bulletin may list all the reported hypocentres for an event. The convention in the ISC Bulletin is that the preferred (prime) hypocentre appears last in the list of reported hypocentres for an event.

- Catalogue

  An ordered list of event hypocentres, uncertainties and magnitudes. An event catalogue typically lists only the preferred (prime) hypocentres and network magnitudes.

- CoSOI/IASPEI

  Commission on Seismological Observation and Interpretation, a commission of IASPEI that prepares and discusses international standards and procedures in seismological observation and interpretation.

- Defining/Non-defining phase

  A defining phase is used in the location of the event (time-defining) or in the calculation of the network magnitude (magnitude-defining). Non-defining phases are not used in the calculations because they suffer from large residuals or could not be identified.

- Direct/Indirect report

  A data report sent (e-mailed) directly to the ISC, or indirectly through another ISC data contributor.

- Duplicates

  Nearly identical phase arrival time data reported by one or more agencies for the same station. Duplicates may be created by agencies reporting observations from other agencies, or several agencies independently analysing the waveforms from the same station.

- Event

  A natural (e.g. earthquake, landslide, asteroid impact) or anthropogenic (e.g. explosion) phenomenon that generates seismic waves and its source can be identified by an event location algorithm.

- Grouping

  The ISC algorithm that organises reported hypocentres into groups of events. Phases associated to any of the reported hypocentres will also be associated to the preferred (prime) hypocentre. The grouping algorithm also attempts to associate phases that were reported without an accompanying hypocentre to events.

- Ground Truth

  An event with a hypocentre known to certain accuracy at a high confidence level. For instance, GT0 stands for events with exactly known location, depth and origin time (typically explosions); GT5 stands for events with their epicentre known to 5 km accuracy at the 95% confidence level, while their depth and origin time may be known with less accuracy.

- Ground Truth database

  On behalf of IASPEI, the ISC hosts and maintains the IASPEI Reference Event List, a bulletin of ground truth events.

- IASPEI

  International Association of Seismology and Physics of the Earth Interior, www.iaspei.org.

- International Registry of Seismograph Stations (IR)

  Registry of seismographic stations, jointly run by the ISC and the World Data Center for Seismology, Denver (NEIC). The registry provides and maintains unique five-letter codes for stations participating in the international parametric and waveform data exchange.

- ISC Bulletin

  The comprehensive bulletin of the seismicity of the Earth stored in the ISC database and accessible through the ISC website. The bulletin contains both natural and anthropogenic events. Currently the ISC Bulletin spans more than 50 years (1960-to date) and it is constantly extended by adding both recent and past data. Eventually the ISC Bulletin will contain all instrumentally recorded events since 1900.

- ISC Governing Council

  According to the ISC Working Statutes the Governing Council is the governing body of the ISC, comprising one representative for each ISC Member.

- ISC-located events

  A subset of the events selected for ISC review are located by the ISC. The rules for selecting an event for location are described in Section 11.1.3; ISC-located events are denoted by the author ISC.

- ISC Member

  An academic or government institute, seismological organisation or company, geological/meteorological survey, station operator, national/international scientific organisation that contribute to the ISC budget by paying membership fees. ISC members have voting rights in the ISC Governing Council.

- ISC-reviewed events

  A subset of the events reported to the ISC are selected for ISC analyst review. These events may or may not be located by the ISC. The rules for selecting an event for review are described in Section 11.1.3. Non-reviewed events are explicitly marked in the ISC Bulletin by the comment following the prime hypocentre "Event not reviewed by the ISC".

- ISF

  International Seismic Format (www.isc.ac.uk/standards/isf). A standard bulletin format approved by IASPEI. The ISC Bulletin is presented in this format at the ISC website.

- ISS

  International Seismological Summary (1918-1963). These bulletins are the predecessors of the ISC Bulletin and represent the major source of instrumental seismological data before the digital era. The ISS contains regionally and teleseismically recorded events from several hundreds of globally distributed stations.

- Network magnitude

The event magnitude reported by an agency or computed by the ISC locator. An agency can report several network magnitudes for the same event and also several values for the same magnitude type. The network magnitude obtained with the ISC locator is defined as the median of station magnitudes of the same magnitude type.

- Phase

  A maximum eight-character code for a seismic, infrasonic, or hydroacoustic phase. During the ISC processing, reported phases are mapped to standard IASPEI phase names. Amplitude measurements are identified by specific phase names to facilitate the computation of body-wave and surface-wave magnitudes.

- Prime hypocentre

  The preferred hypocentre solution for an event from a list of hypocentres reported by various agencies or calculated by the ISC.

- Reading

  Parametric data that are associated to a single event and reported by a single agency from a single station. A reading typically includes one or more phase names, arrival time and/or amplitude/period measurements.

- Report/Data report

  All data that are reported to the ISC are parsed and stored in the ISC database. These may include event bulletins, focal mechanisms, moment tensor solutions, macroseismic descriptions and other event comments, as well as phase arrival data that are not associated to events. Every single report sent to the ISC can be traced back in the ISC database via its unique report identifier.

- Shide Circulars

  Collections of station reports for large earthquakes occurring in the period 1899-1912. These reports were compiled through the efforts of J. Milne. The reports are mainly for stations of the British Empire equipped with Milne seismographs. After Milne's death, the Shide Circulars were replaced by the Seismological Bulletins of the BAAS.

- Station code

  A unique, maximum six-character code for a station. The ISC Bulletin contains data exclusively from stations registered in the International Registry of Seismograph Stations.

13

Acknowledgements

We thank our colleagues at the University of Bergen and the University of Helsinki for kindly accepting our invitation and submitting the articles on their seismic network's history, current status and operational procedures for this issue of the Summary.

We are also grateful to the developers of the Generic Mapping Tools (GMT) suite of software (Wessel and Smith, 1998) that was used extensively for producing the graphical figures.

Finally, we thank the ISC Member Institutions, Data Contributors, Funding Agencies (including NSF Award EAR-1417970 and USGS Award G15AC00202) and Sponsors for supporting the long-term operation of the ISC.

References

Adams, R. D., A. A. Hughes, and D. M. McGregor (1982), Analysis procedures at the International Seismological Centre, *Physics of the Earth and Planetary Interiors*, *30*, 85–93.

Amante, C., and B. W. Eakins (2009), ETOPO1 1 arc-minute global relief model: procedures, data sources and analysis, *NOAA Technical Memorandum NESDIS NGDC-24*, NOAA.

Balfour, N., R. Baldwin, and A. Bird (2008), Magnitude calculations in Antelope 4.10, *Analysis Group Note of Geological Survey of Canada*, pp. 1–13.

Bennett, T. J., V. Oancea, B. W. Barker, Y.-L. Kung, M. Bahavar, B. C. Kohl, J. . Murphy, and I. K. Bondár (2010), The nuclear explosion database NEDB: a new database and web site for accessing nuclear explosion source information and waveforms, *Seismological Research Letters*, *81*, doi:10.1785/gssrl.81.1.12.

Bisztricsany, E. A. (1958), A new method for the determination of the magnitude of earthquakes, *Geofiz. Kozl*, pp. 69–76.

Bolt, B. A. (1960), The revision of earthquake epicentres, focal depths and origin time using a high-speed computer, *Geophysical Journal of the Royal Astronomical Society*, *3*, 434–440.

Bondár, I., and K. McLaughlin (2009a), A new ground truth data set for seismic studies, *Seismological Research Letters*, *80*, 465–472.

Bondár, I., and K. McLaughlin (2009b), Seismic location bias and uncertainty in the presence of correlated and non-Gaussian travel-time errors, *Bulletin of the Seismological Society of America*, *99*, 172–193.

Bondár, I., and D. Storchak (2011), Improved location procedures at the International Seismological Centre, *Geophysical Journal International*, *186*, 1220–1244.

Bondár, I., E. R. Engdahl, X. Yang, H. A. A. Ghalib, A. Hofstetter, V. Kirchenko, R. Wagner, I. Gupta, G. Ekström, E. Bergman, H. Israelsson, and K. McLaughlin (2004), Collection of a reference event set for regional and teleseismic location calibration, *Bulletin of the Seismological Society of America*, *94*, 1528–1545.

Bondár, I., E. Bergman, E. R. Engdahl, B. Kohl, Y.-L. Kung, and K. McLaughlin (2008), A hybrid multiple event location technique to obtain ground truth event locations, *Geophysical Journal International*, *175*, doi:10.1111/j.1365,246X.2008.03,867x.

Bormann, P., and J. W. Dewey (2012), The new iaspei standards for determining magnitudes from digital data and their relation to classical magnitudes, is 3.3, *New Manual of Seismological Observatory Practice 2 (NMSOP-2), P. Bormann (Ed.)*, pp. 1–44, doi:10.2312/GFZ.NMSOP-2_IS_3.3,10.2312/GFZ.NMSOP-2, `http://nmsop.gfz-postsdam.de`.

Bormann, P., and J. Saul (2008), The new IASPEI standard broadband magnitude mB, *Seism. Res. Lett*, *79*(5), 698–705.

Bormann, P., R. Liu, X. Ren, R. Gutdeutsch, D. Kaiser, and S. Castellaro (2007), Chinese national network magnitudes, their relation to NEIC magnitudes and recommendations for new IASPEI magnitude standards, *Bulletin of the Seismological Society of America*, *97*(1B), 114–127, doi:10.1785/012006007835.

Bormann, P., R. Liu, Z. Xu, R. Ren, and S. Wendt (2009), First application of the new IASPEI teleseismic magnitude standards to data of the China National Seismographic Network, *Bulletin of the Seismological Society of America*, *99*, 1868–1891, doi:10.1785/0120080010.

Chang, A. C., R. H. Shumway, R. R. Blandford, and B. W. Barker (1983), Two methods to improve location estimates - preliminary results, *Bulletin of the Seismological Society of America*, *73*, 281–295.

Choy, G. L., and J. L. Boatwright (1995), Global patterns of readiated seismic energy and apparent stress, *J. Geophys. Res.*, *100*(B9), 18,205–18,228.

Dziewonski, A. M., and F. Gilbert (1976), The effect of small, aspherical perturbations on travel times and a re-examination of the correction for ellipticity, *Geophysical Journal of the Royal Astronomical Society*, *44*, 7–17.

Dziewonski, A. M., T.-A. Chou, and J. H. Woodhouse (1981), Determination of earthquake source parameters from waveform data for studies of global and regional seismicity, *J. Geophys. Res.*, *86*, 2825–2852.

Engdahl, E. R., and R. H. Gunst (1966), Use of a high speed computer for the preliminary determination of earthquake hypocentres, *Bulletin of the Seismological Society of America*, *56*, 325–336.

Engdahl, E. R., and A. Villaseñor (2002), Global seismicity: 1900-1999, *International Handbook of Earthquake Engineering and Seismology, International Geophysics series*, *81A*, 665–690.

Engdahl, E. R., R. van der Hilst, and R. Buland (1998), Global teleseismic earthquake relocation with improved travel times and procedures for depth determination, *Bulletin of the Seismological Society of America*, *88*, 722–743.

Flinn, E. A., and E. R. Engdahl (1965), Proposed basis for geographical and seismic regionalization, *Reviews of Geophysics*, *3*(1), 123–149.

Flinn, E. A., E. R. Engdahl, and A. R. Hill (1974), Seismic and geographical regionalization, *Bulletin of the Seismological Society of America*, *64*, 771–993.

Gutenberg, B. (1945a), Amplitudes of P, PP and S and magnitude of shallow earthquakes, *Bulletin of the Seismological Society of America*, *35*, 57–69.

Gutenberg, B. (1945b), Magnitude determination of deep-focus earthquakes, *Bulletin of the Seismological Society of America*, *35*, 117–130.

Gutenberg, B. (1945c), Amplitudes of surface waves and magnitudes of shallow earthquakes, *Bulletin of the Seismological Society of America*, *35*, 3–12.

Gutenberg, B., and C. F. Richter (1956), Magnitude and Energy of earthquakes, *Ann. Geof.*, *9*, 1–5.

Hutton, L. K., and D. M. Boore (1987), The ML scale in southern California, *Bulletin of the Seismological Society of America*, *77*, 2074–2094.

IASPEI (2005), Summary of magnitude working group recommendations on standard procedures for determining earthquake magnitudes from digital data, `http://www.iaspei.org/commissions/CSOI.html#wgmm,http://www.iaspei.org/commissions/CSOI/summary_of_WG_recommendations_2005.pdf`.

IASPEI (2013), Summary of magnitude working group recommendations on standard procedures for determining earthquake magnitudes from digital data, `http://www.iaspei.org/commissions/CSOI/Summary_of_WG_recommendations_20130327.pdf`.

IDC (1999), IDC processing of seismic, hydroacoustic and infrasonic data, *IDC Documentation*.

Jeffreys, H., and K. E. Bullen (1940), *Seismological Tables*, British Association for the Advancement of Science.

Kanamori, H. (1977), The energy release in great earthquakes, *J. Geophys. Res.*, *82*, 2981–2987.

Kennett, B. L. N. (2006), Non-linear methods for event location in a global context, *Physics of the Earth and Planetary Interiors*, *158*, 45–64.

Kennett, B. L. N., E. R. Engdahl, and R. Buland (1995), Constraints on seismic velocities in the Earth from traveltimes, *Geophysical Journal International*, *122*, 108–124.

Kennett, B. L. N., E. R. Engdahl, and R. Buland (1996), Ellipticity corrections for seismic phases, *Geophysical Journal International*, *127*, 40–48.

Lee, W. H. K., R. Bennet, and K. Meagher (1972), A method of estimating magnitude of local earthquakes from signal duration, *U.S. Geol. Surv.*, Open-File Rep.

Murphy, J. R., and B. W. Barker (2006), Improved focal-depth determination through automated identication of the seismic depth phases pP and sP, *Bulletin of the Seismological Society of America*, *96*, 1213–1229.

NMSOP-2 (2012), *New Manual of Seismological Observatory Practice (NMSOP-2)*, IASPEI, GFZ, German Research Centre for Geosciences, Potsdam, doi:10.2312/GFZ.NMSOP-2, `http://nmsop.gfz-potsdam.de`, urn:nbn:de:kobv:b103-NMSOP-2.

Nuttli, O. W. (1973), Seismic wave attenuation and magnitude relations for eastern North America, *J. Geophys. Res.*, *78*, 876–885.

Richter, C. F. (1935), An instrumental earthquake magnitude scale, *Bulletin of the Seismological Society of America*, *25*, 1–32.

Ringdal, F. (1976), Maximum-likelihood estimation of seismic magnitude, *Bulletin of the Seismological Society of America*, *66*(3), 789–802.

Sambridge, M. (1999), Geophysical inversion with a neighbourhood algorithm, *Geophysical Journal International*, *138*, 479–494.

Sambridge, M., and B. L. N. Kennett (2001), Seismic event location: non-linear inversion using a neighbourhood algorithm, *Pure and Applied Geophysics*, *158*, 241–257.

Storchak, D. A., J. Schweitzer, and P. Bormann (2003), The IASPEI standard seismic phases list, *Seismological Research Letters*, *74*(6), 761–772.

Storchak, D. A., J. Schweitzer, and P. Bormann (2011), Seismic phase names: IASPEI standard, in *Encyclopedia of Solid Earth Geophysics*, edited by H. Gupta, pp. 1162–1173, Springer.

Tsuboi, C. (1954), Determination of the Gutenberg-Richter's magnitude of earthquakes occurring in and near Japan, *Zisin (J. Seism. Soc. Japan)*, *Ser. II*(7), 185–193.

Tsuboi, S., K. Abe, K. Takano, and Y. Yamanaka (1995), Rapid determination of Mw from broadband P waveforms, *Bulletin of the Seismological Society of America*, *85*(2), 606–613.

Uhrhammer, R. A., and E. R. Collins (1990), Synthesis of Wood-Anderson Seismograms from Broadband Digital Records, *Bulletin of the Seismological Society of America*, *80*(3), 702–716.

Vaněk, J., A. Zapotek, V. Karnik, N. V. Kondorskaya, Y. V. Riznichenko, E. F. Savarensky, S. L. Solov'yov, and N. V. Shebalin (1962), Standardization of magnitude scales, *Izvestiya Akad. SSSR.*, *Ser. Geofiz.*(2), 153–158, pages 108–111 in the English translation.

Villaseñor, A., and E. R. Engdahl (2005), A digital hypocenter catalog for the International Seismological Summary, *Seismological Research Letters*, *76*, 554–559.

Villaseñor, A., and E. R. Engdahl (2007), Systematic relocation of early instrumental seismicity: Earthquakes in the International Seismological Summary for 1960–1963, *Bulletin of the Seismological Society of America*, *97*, 1820–1832.

Woessner, J., and S. Wiemer (2005), Assessing the quality of earthquake catalogues: estimating the magnitude of completeness and its uncertainty, *Bulletin of the Seismological Society of America*, *95*(2), doi:10/1785/012040,007.

Young, J. B., B. W. Presgrave, H. Aichele, D. A. Wiens, and E. A. Flinn (1996), The Flinn-Engdahl regionalisation scheme: the 1995 revision, *Physics of the Earth and Planetary Interiors*, *96*, 223–297.

Case Study

Structural Monitoring
Natural Caverns
Brazil

GeoSIG
swiss made to measure

In Cooperation With GeoSIG Partner

FUGRO

Background

People have been using metals for more than 9,000 years when they first discovered how to get copper from its ore. We use metals in every facet of our lives, from the pipes and fasteners in our homes to the vehicles we use to travel to the tools used by surgeons or mechanics or artists. We wear jewelry. We build computers. Metals are an intrinsic part of our everyday lives. Because metals are found in the earth, they must be mined.

Vale SA is a multinational corporation that is engaged in metals and mining; it is one of the largest logistics operators in Brazil. Vale is the largest producer of iron ore and nickel in the world, but it also produces manganese, ferroalloys, copper, bauxite, potash, kaolin, and cobalt.

Challenge

The objective of the project was to monitor the stability and impact of nearby mining activities on a series of small natural caverns located in Brazil, which are protected by Brazil environmental regulations. Vale wanted to present to the authorities real data to ensure their mining activities would not impact the protected caverns.

Solution

Our Partner, Fugro Brazil, won a contract with Vale to do the monitoring project for several natural caverns. Fugro is the world's largest integrator of geotechnical, survey, subsea and geosciences services. Its services are specifically designed to support engineering design and large structure building projects.

In one cavern, they placed a GMSplus6, which was attached to two LVDT-100 transducers and a temperature and humidity sensor. In two further caverns they placed two GMSplus6 (for a total of four), which were attached to four LVDT-100 transducers and two temperature and humidity sensors, as well as a power controller and battery. Due to the remoteness of the mines, satellite communication and solar panels were used for monitoring the mines as well as providing state of health information about the equipment/instrument for near online monitoring. Fugro through their cloud servers and their monitoring team are able to provide continuous monitoring and provide alerts, as may be the case, as well as periodical management reports.

Another Solution using GeoSIG instruments demonstrating that quality and reliability can also be cost effective.

Product links

GMSplus seismic recorders

GMSplus6 seismic recorders

The mining site was located near some protected natural caverns in Brazil.

Satellite communication and solar panels were used due to the remote location.

The instruments are accessible in the control cabinet.

The GMSplus6 in situ.

If It Moves, You'll Know It. Immediately.

For over 40 years REF TEK®, a Trimble brand, has been the trusted partner for seismologists around the globe. If it shakes, sinks or shifts our reliable sensors and recorders will know about it instantaneously. And you will too, anytime, as sophisticated application software informs you immediately. Always on the job, offering some peace of mind in an unstable world.

REF TEK 130S-01 High Resolution Seismic Recorder

A compact and lightweight seismic recorder, with IP Communications, ultra-low latency data transmission and removeable data storage. Meets the requirements for earthquake early warning (EEW) systems.

REF TEK 147A Strong Motion Accelerometer

With high sensitivity, large linear range, high resolution and dynamic range the 147A is suitable for free field applications such as microzonation, site response, earthquake monitoring and more.

REF TEK 151B-120 Observer, High Performance Broadband Seismometer

The low self-noise performance makes the Observer an ideal seismometer for seismicity studies in different installation configurations, including observatory and portable, surface and posthole applications.

For more information visit
www.reftek.com

REF TEK®
A TRIMBLE BRAND

SEISMOLOGY RESEARCH CENTRE

GECKO

7th Generation Kelunji Seismograph

Seismic Recorders, Seismographs and Accelerographs
Designed by seismologists for ease of use and portability
Engineered for reliable continuous recording & telemetry

Connect any brand and model of seismic sensor to the Gecko Compact or Gecko Rugged 3-channel data loggers. The in-built LCD and 4-button keypad allows you to completely configure the device without a laptop, with minimal settings to get you recording within minutes.
The Gecko consumes less than 1W of power while recording continuous MiniSEED data to a removable SD card. Data telemetry options include Ethernet or cellular modems for streaming to a PC for a live data display.

Gecko Compact

Gecko Rugged

Model	Features *(applies to all models)*	Price
Compact	40Vpp, 142dB RMS-FS, 32-bit ADC	★½
Rugged	gain x1 to x256, 40sps to 4000sps	★★
- comparative price of leading-brand competitors:		★★★

Model	Sensitivity	Frequency	Price
Blast	28.8V/m/s	4.5Hz to 1kHz+	★★
SMA	2g to 400g full scale	DC to 400Hz+	★★½
Blast-HR	78.74V/m/s	2Hz to 1kHz+	★★★
SMA-HR	2g or 4g full scale	DC to 100Hz	★★★½
Helix	400V/m/s	1Hz to 100Hz	★★★★½
Prism	868V/m/s	30sec to 80Hz	★★★★★

Educational and Research Discounts of up to 30% available to ISC Members

Gecko SMA or Blast

For more information visit www.src.com.au
email sales@src.com.au or call +61 3 8420 8940

MADE IN AUSTRALIA

Actual size of Gecko Prism or Helix (A4)

The IP67-rated waterproof Gecko Rugged seismic recorder is the basis for our range of seismographs and accelerographs with integrated sensors. The all-in-one design improves portability and allows for rapid installation, removing the need for inter-connecting cables, and simplifying setup.
The Gecko SMA and SMA-HR accelerographs are perfects for structural monitoring applications. The Gecko Prism, Helix, Blast-HR and Blast models integrate more sensitive velocity sensors, suited to local and regional earthquake monitoring networks, aftershock monitoring, blast compliance, and other vibration monitoring applications.

Gecko SMA-HR

Gecko Prism, Helix or Blast-HR